UNIVERSITY OF THESSALY
School of Engineering
Department of Civil Engineering

Flood Hazard and Risk Modelling Framework for Ungauged Streams and Watersheds

George Papaioannou

PhD dissertation submitted for the Degree of Doctor of Philosophy at the Department of Civil Engineering, University of Thessaly.

Volos, November 2017

UNIVERSITY OF THESSALY
School of Engineering
Department of Civil Engineering

Flood Hazard and Risk Modelling Framework for Ungauged Streams and Watersheds

George Papaioannou

PhD dissertation submitted for the Degree of Doctor of Philosophy at the Department of Civil Engineering, University of Thessaly.

Volos, November 2017

This dissertation has been approved by the advisory committee

Prof. A. Loukas	UTH, Greece, Supervisor
Prof. N. Mylopoylos	UTH, Greece, Member of the Advisory Committee
Assoc. Prof. F. Maris	DUTH, Greece, Member of the Advisory Committee

Members of the Ph.D. Examination Committee:

Prof. A. Loukas	UTH, Greece, Supervisor
Prof. N. Mylopoylos	UTH, Greece, Member of the Advisory Committee
Assoc. Prof. F. Maris	DUTH, Greece, Member of the Advisory Committee
Prof. G. Tsakiris	NTUA, Greece
Prof. G. Karatzas	TUC, Greece
Assoc. Prof. G.T. Aronica	UNIME, Italy
Assoc. Prof. E. Farsirotou	TEI of Thessaly, Greece

PROLEGOMENA

Prolegomena

The present dissertation "Flood Hazard and Risk Modelling Framework for Ungauged Streams and Watersheds" has been submitted as a requirement for the Ph.D. degree at the University of Thessaly (UTH). The main supervisor was Professor Athanasios Loukas (UTH), and co-supervisors were Professor Nikitas Mylopoulos (UTH) and Associate Professor Fotis Marris (DUTH).

The dissertation contains an introduction with the objectives, study area, field survey, flood hazards mapping framework, sensitivity analysis framework, uncertainty analysis framework, and finally conclusions and perspectives. The study has taken place at the Department of Civil Engineering from October 2008 to September 2016.

An external research stay of three months was spent at the Department of Civil, Computer, Construction and Environmental Engineering and of Applied Mathematics, University of Messina, Italy (UNIME) with Professor Giuseppe Tito Aronica as the Host (supervisor). The research was supported by LLP/ERASMUS Exchange Program (spring semester of academic year 2011/2012). Another, external research stay of one month was spent at Department of Land and Water Resources Management (FCE), Slovak University of Technology in Bratislava, Slovakia (STU) with Professor Ján Szolgay and Professor Silvia Kohnová as the Hosts (supervisor and co-supervisor respectively). The research was supported by STSM COST ES0901: "European Procedure for Flood Frequency Estimation (FLOODFREQ)". Furthermore, this dissertation funded by undergraduate scholarships awarded by the Department of Civil Engineering, University of Thessaly (Academic years 2010-2013). The dissertation has been financially supported by the following two scientific research programs:

- "Sustainable Use of Irrigation Water in the Mediterranean Region (SIRRIMED)" – FP7-KBBE-2009-3 – Proposal Reference Number: FP7-245159. Scientific Responsible: Dr. Juan José Alarcón (2010-2013).

- "Development of an Integrated System for the Water Resources Quality and Quantity Monitoring and Management of Agricultural Watersheds Under Climate Change Conditions. Application to Lake Karla Watershed (HYDROMENTOR)", General Secretariat for Research and Technology. National Action "Cooperation", Coordinator: Prof. A. Loukas (2011-2014).

Mr. Papaioannou participated during his doctoral study, as member of the Laboratory of Hydrology and Aquatic Systems Analysis, and financed by the following professional projects:

- "Reconnaissance Study of Dam and Reservoir Development in the Position of Gavroneri Stomiou". Municipality of Evrimenon. Scientific Responsible: Assoc. Prof. N. Mylopoulos (2009).

- "Climate Change Effects Estimation on Hydrometeorological Data in Thessaly, Epirus and West Sterea Ellada", Special Secretariat of Water, Ministry of Environment and Climate Change, Consortium J. Karavokyris and Associates Consulting Engineers S.A. Scientific Responsible: Assoc. Prof. N. Mylopoulos (2011).

- "Investigation of the surface runoff routing of the subwatershed of Velestino area through a technical project and conjunction with ground water modeling". Management body of ecodevelopment area of Karla-Maurovouniou-Kefalovrisou-Velestinou, Magnesia, Greece. Scientific supervisor: Prof. N. Mylopoulos (2013-2014).

- "Evaluation of Alternative Scenarios of Irrigation Withdrawals from Pinios River for the LALR Pinios-Pumping Station B", Region of Thessaly, Coordinator: K. Iakovakis, Scientific Responsible: Prof. A. Loukas (2014).

- "Management Plans of Flood Risks for River Basins in Thessaly, Epirus and Western Sterea Ellada Regions, Greece", Special Secretariat of Water, Ministry of Environment and Climate Change, Consortium J. Karavokyris and Associates Consulting Engineers S.A. Scientific Responsible: Prof. A. Loukas (2015-2017).

Volos, November 2017

George Papaioannou

Declaration

The material contained in this dissertation has not been previously submitted by the candidate for a degree in this or any other University.

Acknowledgments

First of all I would like to thank my supervisor, Prof. Athanasios Loukas, for his endless support as a supervisor, tutor, “father” and an appreciated friend. With his experience, ideas and guidance he accurately spearheaded the hard work involved behind this dissertation and helped me master my scientific knowledge throughout my research. Also, I would like to thank Prof. Nikitas Mylopoulos, and Prof. Fotis Marris for their valuable guidance and advice. I would also like to thank Prof. G.T. Aronica for all these years of cooperation, as well as Prof. G. Tsakiris, Prof. G. Karatzas, and Prof. E. Farsirotou for their kind support and participation in my dissertation examination committee. Many thanks also go to Dr. Lampros Vasilliades and PhD candidate Eleftherios Gkilimanakis for their never-ending support and their valued friendship.

I would like to cordially acknowledge the great assistance provided by Prof. P. Patias, Assist. Prof. H. Georgiadis and the personnel of the Laboratory of Photogrammetry and Remote Sensing (AUTH). Prof. P. Patias provided the Terrestrial Laser Scanner ILRIS 3D which has been used in the field measurements of this dissertation. Furthermore, he provided the resources and the personnel of his Laboratory, especially the Assist. Prof. H. Georgiadis, who offered his kind assistance on the post-processing of the data. Moreover, the author would like to acknowledge the valuable assistance provided by E. Mousoulis and the DHI-group. DHI-group provided free of charge the following software and licenses for academic purposes: MIKE11, MIKE21 and MIKE FLOOD. Also, I would like to acknowledge the valuable assistance provided by the head of the Administration of Technical works / Decentralized Administration of Thessaly Region, Flampouris Konstantinos. Many thanks go, also, to my colleagues and friends Dr. Marios Spiliotopoulos, Dr. Chrysostomos Fafoutis, Dr. Pantelis Sidiropoulos, PhD candidate George Giatzios, PhD candidate Popi Michailidou-Notara, PhD candidate Aggelos Alamanos and PhD candidate John Tzabiras, on providing me with significant reports, documents and files as well as for their friendship and the “brain storming” coffee breaks.

Finally, I would like to make a special reference to some people that have a great influence in my life. First of all, I would like to thank my parents, my brother’s family and my uncle, Konstantinos-Eleni, Spyros-Ritsa-Konstantinos and Vassilis for their endless love, care, support and encouragement throughout these long years of studies. Without their support I would have never enjoyed the opportunities to fulfill my aspirations. Also, I would like to thank my wife Nikoletta Syrtadioti, whose love, understanding and contribution in many aspects have assisted substantially to complete this work. Also, my daughter Eleni who was born during the last two years of this dissertation filled me with unending joy and love. Nikoletta and Eleni are a source of courage and inspiration for me to become better as a person and as a scientist. Unfortunately, my words of appreciation cannot compensate their contribution, yet I thank them from the bottom of my heart.

ABOUT THE AUTHOR

ABOUT THE AUTHOR

George Papaioannou is a registered professional Forest Engineer in Greece and is member of the Geotechnical Chamber of Greece. He was awarded a BSc from the Forest and Water Engineering Sector, Department of Forestry and Management of the Environment and Natural Resources, Democritus University of Thrace, Greece in 2006, and a MSc in Sustainable Management of the Environment and Natural Resources with specialization at the sector of Sustainable Management of Mountainous Watersheds with Intelligent Information Systems and Geographical Information Systems in 2008 from Democritus University of Thrace. Since July 2008 he has been at Department of Civil Engineering, University of Thessaly as a PhD student; involved in the following two research programs and many other projects as a professional Forest Engineer.

Scientific Research Programs

- "Sustainable Use of Irrigation Water in the Mediterranean Region (SIRRIMED)" – FP7-KBBE-2009-3 – Proposal Reference Number: FP7-245159. Scientific Responsible: Dr. Juan José Alarcón (**2010-2013**).

- "Development of an Integrated System for the Water Resources Quality and Quantity Monitoring and Management of Agricultural Watersheds Under Climate Change Conditions. Application to Lake Karla Watershed (HYDROMENTOR)", General Secretariat for Research and Technology. National Action "Cooperation", Coordinator: Prof. A. Loukas (**2011-2014**).

Professional Experience

- "Reconnaissance Study of Dam and Reservoir Development in the Position of Gavroneri Stomiou". Municipality of Evrimenon. Scientific Responsible: Assoc. Prof. N. Mylopoulos (**2009**).

- "Climate Change Effects Estimation on Hydrometeorological Data in Thessaly, Epirus and West Sterea Ellada ", Special Secretariat of Water, Ministry of Environment and Climate Change, Consortium J. Karavokyris and Associates Consulting Engineers S.A. Scientific Responsible: Assoc. Prof. N. Mylopoulos (**2011**).

- "Investigation of the surface runoff routing of the subwatershed of Velestino area through a technical project and conjunction with ground water modeling". Management body of ecodevelopment area of Karla-Maurovouniou-Kefalovrisou-

Velestinou, Magnesia, Greece. Scientific supervisor: Prof. N. Mylopoulos (**2013-2014**).

- "Evaluation of Alternative Scenarios of Irrigation Withdrawals from Pinios River for the LALR Pinios-Pumping Station B", Region of Thessaly, Coordinator: K. Iakovakis, Scientific Responsible: Prof. A. Loukas (**2014**).

- "Management Plans of Flood Risks for River Basins in Thessaly, Epirus and Western Sterea Ellada Regions, Greece", Special Secretariat of Water, Ministry of Environment and Climate Change, Consortium J. Karavokyris and Associates Consulting Engineers S.A. Scientific Responsible: Prof. A. Loukas (**2015-2017**).

George Papaioannou assisted in various ways as a collaborator at the Laboratory of Hydrology and aquatic systems analysis, Department of Civil Engineering, University of Thessaly (2008-today). Specifically, he participated as teaching assistant at the course of "Hydrology" (2009-2014, Undergraduate Program, Department of Civil Engineering, University of Thessaly), at the course "Aquatic systems simulation applications" (2010-2012, Postgraduate Program - Applied Mechanics and Systems Modelling and Simulation, Department of Civil Engineering, University of Thessaly) and at the courses of "Floods" and "Hydrohazard Forecasting" (2010-2012, Common Greek-French MSc program, Management of Hydrometeorological Hazards - Hydrohasards. .Department of Civil Engineering, University of Thessaly) and at the courses of "Planning for HydroHazard Prevention and Management" and "GIS and Remote Sensing Applications in Hydrohazards Analysis" (2010-2016, Common Greek-French MSc program, Management of Hydrometeorological Hazards - Hydrohasards. .Department of Civil Engineering, University of Thessaly).
Finally, Mr. Papaioannou is the author and co-author of four (4) published scientific articles in refereed journals (one article in press) and twenty nine (29) scientific articles in conference proceedings. Finally, he is a reviewer at the journal "European Water" (EWRA), "Water" journal (MDPI) and a member of the European Geosciences Union (EGU).

Publications List (related to this dissertation)

Peer Reviewed International Journals

1. **Papaioannou, G.**, Vasiliades, L., Loukas, A., (2015). "Multi-criteria analysis framework for potential flood prone areas", Water Resour Manag .29(2): 399-418, doi 10.1007/s11269-014-0817-6

2. **Papaioannou, G.,** Loukas, A., Vasiliades, L. and Aronica, G.T. (2016). "Flood inundation mapping sensitivity to riverine spatial resolution and modelling approach", Nat Haz. 83(1):117-132. doi: 10.1007/s11069-016-2382-1

3. **Papaioannou, G.**, Vasiliades, L., Loukas, A., and Aronica, G.T. (2017) "Probabilistic flood inundation mapping at ungauged streams due to roughness coefficient uncertainty in hydraulic modelling", Adv. Geosci., 44, 23-34, doi:10.5194/adgeo-44-23-2017

4. **Papaioannou, G.**, Vasiliades, L., Loukas, A., and Aronica, G.T. (2017) "Sensitivity analysis of a probabilistic flood inundation mapping framework for ungauged catchments", European Water (Article in press).

Referred Conferences (full paper review):

1. **Papaioannou, G.,** A. Loukas, and L. Vasiliades, (2013). "Multi-criteria analysis framework for potential flood mapping areas", 8th International Conference of EWRA: Water Resources Management in an Interdisciplinary and Changing Context, 26-29 June 2013, Porto, Portugal.

2. **Papaioannou, G.**, Loukas, A., Georgiadis, Ch., (2013). "The effect of riverine terrain spatial resolution on flood modeling and mapping". First International Conference on Remote Sensing and Geoinformation of the Environment , 8-10 April 2013, Paphos, Cyprus, SPIE Proceedings Vol. 8795, doi: 10.1117/12.2028218.

3. **Papaioannou, G.,** Loukas, A., Vasiliades, L., and Aronica, T.G. (2017), "Sensitivity analysis of a probabilistic flood inundation mapping framework for ungauged catchments", 10th World Congress of EWRA: Panta Rhei, 5 – 9 July 2017, Athens, Greece.

Referred Presentations (abstract review):

1. **Papaioannou, G.**, Loukas, A., (2010). "Flood inundation mapping uncertainty introduced by topographic data accuracy, geometric configuration and modeling approach", EGU General Assembly, 02-07 May 2010, Vienna, Austria (Geophysical Research Abstracts, Vol. 12)

2. **Papaioannou, G.**, Loukas, A., Vasiliades, L., Aronica, G.T., (2011). "Flood prone areas mapping through GIS and Multi-Criteria Analysis", EGU Leonardo Conference: Floods in 3D: Processes, Patterns, Predictions, 23-25 November 2011, Bratislava, Slovakia.

3. **Papaioannou, G.**, Loukas, A., Vasiliades, L., (2013). "An evaluation of clustering techniques in flood prone areas mapping using Multicriteria Analysis", EGU Leonardo Conference, 17-19 October 2013, Kos Island, Greece.

4. **Papaioannou, G.**, Aronica, G.T., Loukas, A., Vasiliades, L., (2014). " The impact of DEM accuracy and hydraulic modeling performance for flood inundation mapping", European Symposium on Flood Frequency Estimation and Implications for Risk Management, FLOODFREQ COST ACTION ES0901, 6-7 March 2014, Potsdam, Germany.

5. **Papaioannou, G.**, Aronica, G.T., Loukas, A., Vasiliades, L., (2014). "A sensitivity analysis using different spatial resolution terrain models and flood inundation models", EGU General Assembly, 27 April – 02 May 2014, Vienna, Austria.

6. **Papaioannou, G.,** Loukas, A., Aronica, T.G. and Vasiliades, L., (2014), "Sensitivity analysis of flooded areas for the combination of hydraulic modeling and DEM spatial resolution", EGU Topical Meeting: Validation in flood risk modeling, 9 – 10 December 2014, Delft, Netherland.

7. **Papaioannou, G.,** Loukas, A., Vasiliades, L., and Aronica, T.G., (2016), "Evaluation of various modelling approaches in flood routing simulation and flood area mapping", EGU General Assembly, 17-22 April 2016, Vienna, Austria (Geophysical Research Abstracts, Vol. 18, EGU2016-16208).

8. **Papaioannou, G.,** Loukas, A., Vasiliades, L., and Aronica, T.G. (2016), "Floodplain mapping uncertainty framework for ungauged streams", EGU Plinius Topical Conferences: 15th Plinius Conference on Mediterranean Risks, 8 – 11 June 2016, Taormina, Italy (Plinius Conference Abstracts, Vol. 15, Plinius15-28).

List of Non-Referred Presentations:

1. **Papaioannou**, **G.**, (2011). "Sensitivity analysis on flood inundation mapping introduced by different DEM and modeling approaches", "Hydromedon" - Third meeting of PhD students, National Technical University of Athens, 11-12 July 2011, Athens, Greece (in Greek).

2. **Papaioannou**, **G.**, (2015). "Sensitivity analysis on flood hazard mapping introduced by different hydrodynamic modelling approaches" , Scientific lectures of summer semester, Department of Civil Engineering, University of Thessaly,29 March 2015, Volos, Greece (in Greek)

Publications List (relevant to this dissertation)

Peer Reviewed International Journals

1. **Papaioannou, G.**, Bacigal, T., Jeneiova, K., Kohnova, S., Szolgay, J., Hlavcova,K. and Loukas, A., (2016) "Joint modelling of flood peaks and volumes. A copula application for Danube River", J. Hydrol. Hydromech. 64(1):382-392. doi: 10.1515/johh-2016-0049

Referred Conferences (full paper review):

1. **Papaioannou, G.**, Drosos, V., (2007). "Materials and construction methods for earth and rockfill dams: Past – Present - Future "**,** 13th National forestry conference, Hellenic forestry society, 7-10 October 2007, Kastoria, Greece (in Greek).

2. **Papaioannou, G.**, Maris, F., Loukas, A., (2009). "Estimation of the erosion of the mountainous watershed of river Kosynthos"**,** Joint Conference Hellenic Hydrotechnical Union - Greek Committee for Water Resources Management, Volos, 27-30 May 2009 (in Greek).

4. Jabiras, J., Vasiliades, L., Sidiropoulos, P., **Papaioannou, G.**, Loukas, A., Mylopoulos, N., (2015) "Climate change impacts on hydrometeorological variables at Lake Karla watershed", 14th International Conference on Environmental Science and Technology CEST2015, 3-5 September 2015, Rhodes, Greece.

5. Vasiliades, L., Sidiropoulos, P., Jabiras, J., **Papaioannou, G.**, Kokkinos, K., Loukas, A., Mylopoulos, N., (2015). "An integrated modelling system for assessing water resources management practices", 9th World Congress of EWRA: Water resources management in a changing World: Challenges and Opportunities, 10 – 13 June 2015, Istanbul, Turkey.

6. Vasiliades, L., Sidiropoulos, P., Jabiras, J., Kokkinos, K., Spiliotopoulos, M., **Papaioannou, G.**, Fafoutis, C., Michailidou, K.,Tziatzios, G., Loukas, A., Mylopoulos, N., (2015). "An integrated monitoring and management system for quantity and quality assessment of water resources in rural basins", 9th World Congress of EWRA: Water resources management in a changing World: Challenges and Opportunities, 10 – 13 June 2015, Istanbul, Turkey.

7. Jabiras, J., Loukas, A., Fafoutis, Ch., Spiliotopoulos, M., Sidiropoulos, P., Kokkinos, K., Vasiliades, L., **Papaioannou, G.**, Mylopoulos, N. (2015), "Development of an

integrated information system for the planning and management of water resources of agricultural watersheds and strategic decision making", Honor book for Prof. Yannopoulos, S., AUTH (in Greek).

8. Alamanos, A., Fafoutis, C., **Papaioannou, G.**, Mylopoulos, N. (2017) "Extension of an integrated hydroeconomic model of Lake Karla watershed, under management, climate and pricing scenario analysis." Sixth International Conference on Environmental Management, Engineering, Planning and Economics (CEMEPE) and SECOTOX Conference, 25-30 Jun, 2017, Thessaloniki, Greece.

Referred Presentations (abstract review):

1. Loukas, A., G. Aronica, G. Brigandì, L. Vasiliades, and **Papaioannou**, **G**., (2011). "Probabilistic forecasting of antecedent soil moisture conditions as flash flood precursor variables", EGU General Assembly 2011, 3-8 April 2011, Vienna, Austria, Geophysical Research Abstracts, Vol. 13, EGU2011-12200.

2. Loukas, A., Vasiliades, L., **Papaioannou, G.**, Aronica, G.T., (2011). "Estimation of flood frequency curves in poorly gauged Mediterranean watersheds using a derived distribution procedure", EGU Leonardo Conference: Floods in 3D: Processes, Patterns, Predictions, 23-25 November 2011, Bratislava, Slovakia.

3. Brigandi, G., Aronica, G.T., Loukas, A., Vasiliades, L., **Papaioannou, G.**, (2011). "Probabilistic forecasting of antecedent soil moisture condition as flash flood precursor variables", EGU Leonardo Conference: Floods in 3D: Processes, Patterns, Predictions, 23-25 November 2011, Bratislava, Slovakia.

4. **Papaioannou, G.**, Bacigal, T., Jeneiova, K., Kohnová, S., Szolgay, J., Loukas, A., (2014). "Analysis of suitability of copula families for joint modeling of flood peaks and volumes along the Danube River" , European Symposium on Flood Frequency Estimation and Implications for Risk Management, FLOODFREQ COST ACTION ES0901, 6-7 March 2014, Potsdam, Germany.

5. **Papaioannou, G.**, Bacigal, T., Jeneiova, K., Kohnová, S., Szolgay, J., Loukas, A., (2014). "Bivariate analysis of flood peaks and volumes using copulas. An application to the Danube River", EGU General Assembly, 27 April – 02 May 2014, Vienna, Austria.

6. Tzabiras, J., Spiliotopoulos, M., Kokkinos, K., Fafoutis, Ch., Sidiropoulos, P., Vasiliades, L., **Papaioannou, G.,** Loukas, A. and Mylopoulos, N., (2015), "A GIS based watershed information system for water resources management and planning in

semi-arid areas", EGU General Assembly, 12-17 April 2015, Vienna, Austria (Geophysical Research Abstracts, Vol. 17, EGU2015-14150).

7. Vasiliades, L., Sidiropoulos, P., Tzabiras, J., Kokkinos, K., Spiliotopoulos, M., **Papaioannou, G.,** Fafoutis, Ch., Michailidou, K., Tziatzios, G., Loukas, A. and Mylopoulos, N., (2015), "Hydromentor: An integrated water resources monitoring and management system at modified semi-arid watersheds", EGU General Assembly, 12-17 April 2015, Vienna, Austria (Geophysical Research Abstracts, Vol. 17, EGU2015- 14138).

8. Kohnová, S., **Papaioannou, G.,** Bacigal, T., Jeneiova, K., Szolgay, J., Loukas, A., (2016), "Joint modelling of flood peaks and volumes along the Danube River", EGU General Assembly, 17-22 April 2016, Vienna, Austria (Geophysical Research Abstracts, Vol. 18, EGU2016-12121).

9. Efstratiadis, A., Papalexiou, S-M., Markonis, Y., Koukouvinos, A., Vasiliades, L., **Papaioannou, G.,** and Loukas, A., (2016), "Flood risk assessment at the regional scale: Computational challenges and the monster of uncertainty", EGU General Assembly, 17-22 April 2016, Vienna, Austria (Geophysical Research Abstracts, Vol. 18, EGU2016-12218).

10. Kohnová, S., **Papaioannou, G.,** Bacigal, T., Szolgay, J., Hlavcova, K., Loukas, A., and Vyleta, R., (2017), "On the suitability of the copula types for the joint modelling of flood peaks and volumes along the Danube River", EGU General Assembly, 23–28 April 2017, Vienna, Austria (Geophysical Research Abstracts, Vol. 19, EGU2017-7114).

Dedicated to my beloved parents,
my lovely wife and little daughter

TABLE OF CONTENTS

Table of contents

Notations

Symbol	Definition
A	Cross-sectional area (m^2)
A(t)	Time-area curve (Aw/Δt)
A_s	Upslope contributing area (km^2)
$A_{s,m}$	Modified version of upslope contributing area (km^2)
Aw	Area of the watershed (km^2)
A_c	Hit - event simulated to occur, and did occur (pixels or m^2 or km^2)
a_1,a_2	Velocity weighting coefficients
B_c	False alarm - event simulated to occur, but did not occur (pixels or m^2 or km^2)
C	Expansion or contraction loss coefficient
C_c	Miss - event simulated not to occur, but did occur (pixels or m^2 or km^2)
CI	Consistency index
CNI	Curve number for dry soil moisture conditions
CNII	Curve number for average soil moisture conditions
CNIII	Curve number for wetter soil moisture conditions
CR	Consistency ratio
D_c	Correct rejections - event simulated not to occur and did not occur (pixels or m^2 or km^2)
D_i	Characteristic size of bed material which is larger than i% of particles (m)
FI	Fournier Index
Fr	Froude number
F_t	Simulated flood extent for all cross-sections (pixels or m^2 or km^2)
g	Acceleration due to gravity (m/s^2)
h, h_{flow}	Flow depth (m)
h_e	Energy head loss (m)
H_{mref}	Mean elevation of the watershed (m)
H_{ref}	Minimum elevation of the watershed (m)
I_e	Effective intensity (mm/Δt)
$I_e(\tau)$	The effective rainfall intensity over the block of rainfall at time τ
IUH(t–τ)	The ordinate of the Instantaneous Unit Hydrograph (IUH) at time $t–\tau$
K	Measure of the carrying capacity of the channel ($m^{1/3}/s$)
Lmax	Maximum main channel length (km)
L	Length of channel reach (m)
L_{dl}	Discharge-weighted reach length (m)
L_{lob},L_{ch},L_{rob}	Cross section reach lengths specified for flow in the left overbank, main channel, and right overbank, respectively (m)
m	Number of steps Unit Hydrograph (UH)
MFI	Modified Fournier Index
MdAPE	Median Absolute Percentage Error
n	Manning's n roughness coefficient
N_m, N_d	Numbers of points in the model, set M and data set D, respectively
P_a	Accumulated rainfall depth at time *t*
P	Average annual rainfall amount (mm)

p	Average monthly rainfall (mm)
P_e	Accumulated precipitation excess at time *t*
p_{max}	Average monthly rainfall of the wettest month of the year (mm)
Pw	Wetted perimeter of the flow (m)
Q,q	Discharge / Channel flow (m^3/s)
Q_{lob}, Q_{ch}, Q_{rob}	Arithmetic average of the flows between sections for the left overbank, main channel, and right overbank, respectively (m^3/s)
R	Hydraulic radius (m)
RI	Random consistency index
S	Slope or energy gradient (m/m or %)
S_f	Slope of the channel (m/m or %)
$\bar{S}_f$	Representative friction slope between two sections (m/m or %)
S_{fr}	Slope of the energy gradeline (m/m or %)
Sk	Potential maximum retention (mm)
S_W	Water surface slope (m/m or %)
S_0	Bed slope (m/m or %)
t_c	Concentration time (hr)
TWI	Topographic Wetness Index
UH	Unit Hydrograph
v	Velocity (m/s)
V_1	Mean velocity at section 1 (m/s)
V_2	Mean velocity at section 2 (m/s)
w	The number of steps I_e
$w_{i,j}$	weights for a point match
x	Retardance class
Y_t	Observed flood extent (pixels or m^2 or km^2)
Y_1,Y_2	Water depth at cross sections (m)
z	Size of the comparison matrix
Z_1	Elevation of water surface at section 1 above a common datum (m)
Z_2	Elevation of water surface at section 2 above a common datum (m)
β	Slope gradient (m/m or (%))
Δt	Time interval (hr/min/s)
λ_{max}	Principal eigenvalue
τ	Dummy time variable of integration

LIST OF TABLES

LIST OF FIGURES

EXTENDED ABSTRACT

ABSTRACT

The aim of this dissertation is to investigate, produce and propose new methodologies for ungauged streams and watershed in order to a) improve flood hazard mapping; b) investigate the sensitivity of specific factors that affect the process of flood modelling and mapping and; c) investigate the uncertainty introduced in flood inundation modelling due to roughness coefficient. Therefore, a framework has been developed for flood hazard and risk modelling for ungauged streams and watersheds. The framework has been separated in the following components: 1) Identification and mapping of flood prone areas component; 2) Sensitivity analysis component; and 3) Uncertainty analysis component.

Typical methods and techniques have been used for flood data collection and the hydrometeorological analysis at ungauged catchments. Hence, the collection of historical flood records has been based on data retrieved by several authorities such as the Administration of Technical works (Decentralized Administration of Thessaly), the Welfare Department of Volos municipality, the Fire Department of Volos city, newspapers, records from local amateur meteorologists and local interviews and testimonies of flood victims. All historical flood data have been digitized, classified and evaluated within GIS environment. Moreover, common hydrologic techniques have been followed for the generation of the study flash-flood event hydrograph due to the ungauged nature of the study area.

Several field measurements have been implemented in order to collect high resolution stream geomorphology data, accurate topographic data for specific river cross sections and data concerning the river bed particle size. Specifically the field surveys conducted in this dissertation are:

1. LIDAR field survey with TLS instrument and processed LIDAR DEM creation. This field survey has been conducted using the high resolution Optech ILRIS 3D laser scanner with variable resolution that depended on the distance of the scanned objects. The collected point cloud data has been merged using a best fit analysis process (Iterative Closest Point algorithm). Finally, for the generation of the high-resolution “bare earth” DEM, several processes have been used such as Geomorphologic filters, GIS operations and expert knowledge.
2. Post flood analysis was based on field surveying data measured using typical topographical techniques. The entire post flood analysis has been based on a photograph taken during the study flood event (water depth is visible inside the channel). Based on the flood event photograph, a topographical survey was conducted in specific cross sections of the river for the estimation of the water depth. Then, the typical Manning formula, the slope-area method, and the hydraulic-hydrodynamic model HEC-RAS have been used for the Manning

roughness coefficient determination and the validation of the estimated discharge.

3. Wolman Pebble Count field survey for the estimation of stream bed roughness. Wolman pebble count method was conducted by using a zig-zag pattern and by selecting 958 particles with a step-toe procedure. Then, based on the bed particle size several predefined diameters such as d_{50}, d_{65}, d_{75}, d_{84}, and d_{94}, have been estimated. Finally, the Manning's roughness coefficient (*n*) has been estimated using several empirical formulas that developed mainly for gravel and cobble-bed streams.

The methodologies have been applied at Xerias Watershed, at the upper Xerias Watershed and a specified flood routing stream reach of Xerias that is located in Magnesia, Greece. The study areas are characterized by insufficient records of various hydrometeorological observations regarding both quantity and quality (ungauged watershed/stream). The climate is typical Mediterranean with hot and dry summers and severe precipitation incidents in autumn, winter and spring. The floods occurred in the study area are categorized as flash floods which are the common type of flooding in the Mediterranean region. The methodologies that have been developed, examined and validated in this dissertation are based on the extreme flash flood event occurred in 09 October 2006. During this flood event the entire city of Volos experienced several damages in local infrastructure, transportation networks, and agricultural areas. Based on previous analysis of Intensity-Duration-Frequency curves in the greater area, the current event return period has been approximately estimated to 100 years.

The generation of the study event flood hydrograph has been based on Clark Instantaneous Unit Hydrograph (CIUH) that uses the Kinematic wave approximation. The rainfall data from Volos-Fytoko meteorological station has been used in this analysis. The effective rainfall has been estimated using the Soil Conservation Service – Curve Number (SCS-CN). Finally, the runoff routing has been computed using a linear convolution that is based on estimated time-area curves according to Giandotti time of concentration formula. The following paragraphs summarize the three frameworks that have been developed according to the dissertation objectives.

Identification and mapping of flood prone areas component

The identification and mapping of flood-prone areas component is mainly based on the fusion of several GIS and Multi-Criteria analysis methodologies and the evaluation structure. The component has been applied at catchment scale for the flood hazard areas recognition at ungauged watersheds. The flood-prone areas recognition is based on the use of GIS data and techniques such as clustering/classification procedures and two Multi Criteria Decision Analysis (MCDA) methods the Analytical Hierarchy Process (AHP) and the Fuzzy Analytical Hierarchy Process (FAHP). The data (criteria) used in this analysis consists mainly of geomorphologic indices that are well associated with the

physical process of the flood generation mechanism. Moreover the selection of the final criteria used in the analysis has been based on an evaluation procedure that uses the correlation coefficient. Several sensitivity analysis tests have been conducted for the development of an objective and well-constructed component for the flood prone areas identification at ungauged watersheds. Therefore, the component has been separated in two different approaches where several different configurations have been applied. In both approaches there have been used five clustering/classification techniques (Natural Breaks classification method, K-mean clustering method using two distance approaches, Fuzzy c-mean, Gaussian Mixture Model Clustering, Clustering Large Applications method), AHP and FAHP and two approaches based on the number of the decision makers that involved in pairwise comparison process. In the first approach all criteria are normalized before the application of the MCA method and then, several clustering and classification techniques are applied to derive the final potential flood-prone areas. In the second approach all the criteria are clustered before and after the MCA process for the production of the potential flooded area maps, without normalization. Finally, the produced flood prone areas maps from both approaches are classified using the five proposed clustering techniques. The methodology is demonstrated to Xerias stream watershed that is located in the regions of Thessaly, Magnesia prefecture, Volos, Greece. The validation of the proposed framework has been based on a simulated flooded area derived from hydrologic - hydraulic modelling and historical flood inundation data of the study flood event (extreme flash flood event of 09/10/2006, Volos city, Greece). Results show that the proposed GIS-MCA component can be a valuable and low-cost tool for decision makers to access detection surveys and preliminary flood hazard maps. Despite the accurate flood prone areas estimation using the proposed component, for a more accurate investigation of flood hazard and risk characteristics (e.g., flood extent, water depth, etc.) the use of flood inundation modelling is mandatory.

Sensitivity analysis component

The sensitivity analysis component is based on several sensitivity analyses configurations that use different hydraulic-hydrodynamic modelling approaches in combination with several types of river and riparian areas spatial resolutions for floodplain mapping and flood inundation modelling at ungauged watersheds. The component has been separated in two different approaches where several different configurations have been applied. The first approach is referred as “First Level of Sensitivity Analysis”, while the second approach is referred as “Second Level of Sensitivity Analysis”.

The First Level of Sensitivity Analysis examined the flood inundation modelling sensitivity due to the accuracy of river and riverine topography data in combination with different modelling approaches. Four different types of riverine topography have been

used in this analysis are: a) Digital Elevation Model (DEM) created from TLS data, b) Digital Surface Model (DSM) created from TLS data, c) topographic land survey data and d) typical digitized contours from 1:5000 scale topographic maps. The hydraulic-hydrodynamic models used in this analysis are: a) One-dimensinall (1D) models: HEC-RAS and MIKE11 using two configurations (interpolated cross sections, DEM compilation), b) Two-dimensionall (2D) models: MIKE21 HD (Grid-based), MIKE21 HD FM (Flexible mesh), c) Coupled (1D/2D) models: MIKE11/MIKE21 HD (Grid-based) and MIKE11/MIKE21 HD FM (Flexible mesh) through MIKE FLOOD platform. Moreover, this analysis investigated the use of several different mesh/grid resolutions. The estimation of roughness coefficient factor has been based on the value estimated by post flood analysis.

The Second Level of Sensitivity Analysis examined the sensitivity introduced in flood inundation modelling due to the different modelling approaches used and the several modelling configurations. The riverine geomorphology used in this analysis is the Digital Elevation Model (DEM) created from TLS data. This configuration of riverine geomorphology derived as the best option from the First Level of Sensitivity Analysis. The models used in this analysis are: a) One dimension (1D) hydraulic models: HECRAS, MIKE11 (interpolated cross sections and DEM compilation approach), XPSTORM; b) Two dimension hydraulic models: HECRAS, LISFLOOD (Subgrid solver), MIKE21 (Grid-based and Flexible mesh), XPSTORM, FLO2D; c) Coupled (1D/2D) hydraulic models: HECRAS, LISFLOOD-FP (kinematic and diffusive wave approximation), MIKEFLOOD (Grid-based and Flexible mesh), XPSTORM. Moreover, this analysis investigated the use of different mesh/grid resolutions and the existence or not of inline hydraulic structures. An optimized rougness coefficient value has been used in this anlaysis that is based on an empirical formula, deterministic flood inundation analysis and the use of the objective evaluation metric Critical Success Index.

In both analyses, standard hydrological methods for ungauged watersheds have been used for both the hydrograph and the flood peak estimation. The methodology is demonstrated to a specific routing segment of Xerias stream, Volos, Greece. Specifically, the input hydrograph used in this analysis is the generated CIUH. The validation process of both sensitivity analysis levels is based on the use of 2x2 contingency tables and the Critical Success Index (CSI or Threat score)that compare the simulated flooded area with the observed flooded (historical extreme flash flood event of the year 2006). Results show that the sensitivity analysis should be a mandatory process followed in all flood risk modelling and mapping applications. The evidence from this analysis indicates that the input data uncertainty prevails over the model structure. Finally, the findings of this study indicate the use one dimensional hydraulic-hydrodynamic models for probabilistic approaches in flood inundation modelling and mapping for ungauged stream reaches.

Uncertainty analysis component

The uncertainty analysis component is based on an automated HEC-RAS probabilistic flood inundation system, GIS geoprocessing models, several sensitivity analysis configurations and the evaluation structure. The component has been applied at stream segment scale for roughness coefficient uncertainty analysis and calibration at ungauged watersheds. The core of the probabilistic flood inundation component is based on the use of Monte-Carlo simulations and the HEC-RAS 1D hydraulic-hydrodynamic model. The architecture of Monte-Carlo simulations has been established with existed and developed VBA routines and modules.

The initial ranges of Manning's *n* roughness coefficient have been generated with the use of the Wolman Pebble Count field survey process. Then, various theoretical probability distributions were fitted to the empirical distribution and were evaluated using several goodness-of-fit criteria. Moreover, the generation of different sets of Manning roughness coefficients were accomplished by using the Latin Hypercube sampling. Thus, the production of the flood probability maps has been based on several GIS geoprocessing models that developed in ArcGIS model builder environment using the outcomes of Monte-Carlo simulations. The uncertainty analysis was established using a calibration process that relied only on the flood extent. In this analysis the flood extent consisted of the observed flooded area derived from records of the historical extreme flash flood event of the year 2006. The derivation of acceptable solutions has been based on a validation process where the simulated flooded area is compared with the observed one using the proposed quantitative evaluation criterion of Median Absolute Percentage Error (MdAPE).

Furthermore, several sensitivity analysis configurations and a stability test have been conducted to strengthen the stability and reliability of the component and to extract the optimum component configuration. The factors that have been used for the sensitivity analysis of the component were: a) the interval distance between the cross sections, b) the number of acceptable realizations, c) the proposed threshold level in the validation process, and d) the distributions used for roughness coefficient generation. The stability test was based on the use of five setups that have been generated using the same (optimum) component configurations. Finally, deterministic and probabilistic approaches for flood inundation mapping at ungauged rivers were compared and evaluated in this study. The methodology is demonstrated to a specific routing segment of Xerias stream, Volos, Greece. Results show that probability flood inundation maps can provide better information on the inundation effect than a deterministic assessment. Therefore, an attractive way to visualize flooding likelihood and to increase estimation credibility is to use probability flood maps. Finally, the findings of this study indicate that the use of flood inundation prediction under different probabilistic scenarios can be a valuable tool in floodplain risk management and therefore, minimize the social and economic impacts of floods.

In summary, this dissertation has demonstrated a holistic study of flood hazard and risk modelling for ungauged streams and watersheds. This research has shown that typical methods for flood investigation are able to build a reasonably accurate and efficient framework for predicting flood prone areas, sensitivity and uncertainty analysis in floodplain modelling and mapping. Therefore, all the proposed methods and models may be valuable tools for decision makers in order to produce acceptable and accurate planning and implementing flood hazard and flood risk mitigation strategies at ungauged streams and watersheds.

ABSTRACT IN GREEK - ΕΚΤΕΤΑΜΕΝΗ ΠΕΡΙΛΗΨΗ

ΠΕΡΙΛΗΨΗ

Στην παρούσα διδακτορική διατριβή παρουσιάζεται ένα πλαίσιο προσομοίωσης για την εκτίμηση πλημμυρικού κινδύνου και επικινδυνότητας σε χειμαρρικά υδατορρεύματα και υδρολογικές λεκάνες με ελλιπή δεδομένα. Ο σκοπός της διατριβής είναι να εξεταστούν και να αναπτυχθούν τεχνικές και μεθοδολογίες που θα οδηγήσουν: α) Στην αναγνώριση πιθανών περιοχών πλημμυρικής κατάκλισης, β) Στην εκτίμηση και ποσοτικοποίηση των κύριων παραγόντων ευαισθησίας που υπεισέρχονται στην μοντελοποίηση και χαρτογράφηση των πλημμυρών, γ) Στην εκτίμηση και ποσοτικοποίηση της αβεβαιότητας που υπεισέρχεται στην μοντελοποίηση και χαρτογράφηση των πλημμυρών λόγω της μεταβλητότητας του συντελεστή τραχύτητας. Επομένως το γενικό πλαίσιο αποτελείται από τα εξής τρία συστήματα (δομικά στοιχεία): 1) Σύστημα εκτίμησης και χαρτογράφησης πιθανών περιοχών πλημμυρικής κατάκλισης, 2) Σύστημα ανάλυσης ευαισθησίας για την εκτίμηση και χαρτογράφηση πλημμυράς, 3) Σύστημα ανάλυσης αβεβαιότητας για την εκτίμηση και χαρτογράφηση πλημμυράς.

Η συλλογή και ανάλυση των απαραίτητων δεδομένων (υδρομετεωρολογικών, πλημμυρικής έκτασης, κτλ.) για την διερεύνηση ενός πλημμυρικού φαινομένου βασίστηκε σε κλασσικές τεχνικές που δημιουργήθηκαν και χρησιμοποιούνται για χειμαρρικά υδατορρεύματα και υδρολογικές λεκάνες με ελλιπή δεδομένα. Επομένως, η συλλογή των στοιχείων και πληροφοριών σχετικών με το υπό μελέτη ιστορικό πλημμυρικό γεγονός βασίστηκε σε καταγραφές από διάφορες υπηρεσίες και άλλες πηγές όπως: 1) Η Διεύθυνση Τεχνικών Έργων ΠΕ Μαγνησίας κ ΠΕ Σποράδων (Περιφέρεια Θεσσαλίας) 2) Το τμήμα της Πρόνοιας του Δήμου Βόλου, 3) Η Πυροσβεστική Υπηρεσία Βόλου, 4) Διάφορα μέσα μαζικής ενημέρωσης (Εφημερίδες), 5) Ερασιτέχνες Μετεωρολόγους, 6) Προσωπικές συνεντεύξεις με πληγέντες από την πλημμύρα. Όλα τα παραπάνω στοιχεία και οι πληροφορίες που συλλέχθησαν ψηφιοποιήθηκαν, κατηγοριοποιήθηκαν και αξιολογήθηκαν μέσα σε περιβάλλον Γεωγραφικών Συστημάτων Πληροφοριών ώστε να δημιουργηθεί μια χωρική βάση δεδομένων για το υπό μελέτη πλημμυρικό γεγονός. Επιπρόσθετα, έγινε χρήση τυπικών υδρολογικών μεθόδων, για περιοχές με ελλιπή δεδομένα, για την ανακατασκευή του πλημμυρογραφήματος της υπο μελέτης αιφνίδιας πλημμύρας.

Η χρήση επιτόπιων μετρήσεων πεδίου κρίθηκε αναγκαία λόγω των μεθοδολογιών που επιλέχθησαν να εφαρμοστούν και για τον καθορισμό απαραίτητων παραμέτρων που απαιτούνται για τις συγκεκριμένες αναλύσεις. Εν συνεχεία, διενεργήθησαν επιτόπιες μετρήσεις πεδίου κατά τις οποίες συλλέχθησαν δεδομένα γεωμετρίας ποταμού και πλημμυρικής ζώνης υψηλής ανάλυσης, έγινε ακριβή τοπογραφική αποτύπωση συγκεκριμένων διατομών και τέλος συλλέχθησαν δεδομένα μεγέθους φερτών υλών

από τον πυθμένα του χειμάρρου. Συγκεκριμένα οι μετρήσεις πεδίου που πραγματοποιήθηκαν στα πλαίσια της παρούσας διδακτορικής διατριβής είναι:

1. Η συλλογή δεδομένων υψηλής ανάλυσης γεωμετρίας ποταμού και πλημμυρικής ζώνης διενεργήθηκε με την χρήση επίγειου σαρωτή εδάφους. Στην συνέχεια τα συγκεκριμένα δεδομένα χρησιμοποιήθηκαν για την δημιουργία του επεξεργασμένου Ψηφιακού Μοντέλου Εδάφους (ΨΜΕ) υψηλής ακρίβειας (LIDAR DEM). Το μοντέλο του επίγειου σαρωτή εδάφους υψηλής ακρίβειας που χρησιμοποιήθηκε είναι το Optech ILRIS 3D. Η συλλογή των δεδομένων έγινε με την χρήση μοτίβου ζιγκ-ζακ σε όλη την εξεταζόμενη περιοχή μελέτης με διαφορετική ανάλυση (variable resolution) που καθοριζόταν σύμφωνα με την απόσταση των υπό μέτρηση αντικειμένων. Τα συλλεχθέντα νέφη σημείων (point cloud) συγχωνεύθηκαν με την χρήση του επαναληπτικού αλγόριθμου πλησιέστερων σημείων (Iterative Closest Point algorithm). Τέλος, η δημιουργία του ΨΜΕ υψηλής ακρίβειας γυμνού εδάφους (απαλλαγμένου από την βλάστηση και τα τεχνητά αντικείμενα) επιτεύχθηκε χρησιμοποιώντας διάφορες διαδικασίες όπως τα γεωμορφολογικά φίλτρα, εφαρμογές Γεωγραφικών Συστημάτων Πληροφοριών (ΓΣΠ) και την εμπειρία του χρήστη.
2. Σε περιπτώσεις όπου δεν υπάρχουν υδρομετρικά είναι απαραίτητο να γίνει η εκτίμηση αιχμής πλημμύρας, η οποία έχει περάσει από μια διατομή χωρίς να μετρηθεί. Στην παρούσα διατριβή χρησιμοποιήθηκαν κλασσικές τεχνικές εκ των υστέρων ανάλυσης πλημμύρας (post flood analysis) για τον υπολογισμό του συντελεστή τραχύτητας και την πιστοποίηση του εκτιμώμενου πλημμυρογραφήματος. Οι τεχνικές αυτές χρησιμοποιήθηκαν σε συγκεκριμένα τμήματα διατομών της κοίτης. Η μοναδική καταγραφή που εντοπίστηκε από το υπο-εξέταση πλημμυρικό γεγονός είναι μια φωτογραφία όπου φαίνεται η κεντρική κοίτη σχεδόν γεμάτη και μπορούν να εκτιμηθούν τα ίχνη της στάθμης του νερού. Έτσι, σύμφωνα με τα ίχνη της πλημμύρας που είναι εμφανή στην συγκεκριμένη φωτογραφία διενεργήθηκε κλασσική τοπογραφική αποτύπωση σε επιλεγμένα τμήματα του χειμάρρου και εκτιμήθηκε το ύψος στάθμης νερού. Αναλυτικότερα, οι τεχνικές που χρησιμοποιήθηκαν για τον υπολογισμό του συντελεστή τραχύτητας και την πιστοποίηση του εκτιμώμενου πλημμυρογραφήματος είναι η εξίσωση του Manning , η μέθοδος κλίσης επιφάνειας και το υδραυλικό μοντέλο HEC-RAS.
3. Η τελική εκτίμηση του συντελεστή τραχύτητας επιτεύχθηκε με την χρήση των μετρήσεων πεδίου Wolman Pebble Count. Η συλλογή δεδομένων, κατά την εφαρμογή της τεχνικής Wolman Pebble Count, έγινε με την χρήση μοτίβου ζιγκ-ζακ. Επιπλέον, η διαδικασία συλλογής δεδομένων επιτεύχθηκε με την χρήση δειγματοληψίας υλικού πυθμένα ανά βήμα με αποτέλεσμα την συλλογή και μέτρηση 958 δειγμάτων. Στην συνέχεια σύμφωνα με την στατιστική ανάλυση του συνολικού δείγματος εκτιμήθηκαν διάφορες τιμές καθορισμένων διαμέτρων όπως οι d_{50}, d_{65}, d_{75}, d_{84}, and d_{94}. Τέλος, υπολογίστηκε ο

συντελεστής τραχύτητας Manning (n) σύμφωνα με διάφορες εμπειρικές σχέσεις που αναπτύχθηκαν σε υδατορρέματα με υλικό πυθμένα που αποτελείται κυρίως από κροκάλες και μεγάλους λίθους.

Η περιοχή μελέτης της παρούσας διδακτορικής διατριβής είναι η λεκάνη απορροής του χειμάρρου Ξηρια που εντοπίζεται στο νομό Μαγνησίας, Ελλάδα. Συγκεκριμένα οι περιοχές μελέτης όπου εφαρμόστηκαν όλες οι προτεινόμενες μεθοδολογίες είναι η λεκάνη απορροής του χειμάρρου Ξηρια, η άνω λεκάνη απορροής του χειμάρρου Ξηρια και ένα επιλεγμένο τμήμα της κύριας κοίτης του Ξηριά. Όλες οι περιοχές μελέτης της παρούσας διδακτορικής διατριβής χαρακτηρίζονται από σοβαρή έλλειψη υδρομετεωρολογικών δεδομένων και καταγραφής πλημμύρας (ύψος στάθμης πλημμύρας, κτλ.) σε ποιότητα και ποσότητα (ungauged watershed/stream). Το κλίμα της ευρύτερης περιοχής μελέτης χαρακτηρίζεται ως τυπικό Μεσογειακό. Χαρακτηριστικό αυτού του κλίματος είναι το ξερό και θερμό καλοκαίρι, ο ψυχρός και υγρός χειμώνας και οι ισχυρές βροχοπτώσεις κατά την διάρκεια του φθινόπωρου, χειμώνα και της άνοιξης.

Τα πλημμυρικά φαινόμενα που έχουν παρατηρηθεί στην ευρύτερη περιοχή μελέτης οφείλονται κυρίως σε έντονες τοπικές βροχοπτώσεις με μικρό χρονικό διάστημα και κατατάσσονται στις στιγμιαίες πλημμύρες ή αιφνίδιες πλημμύρες ή πλημμύρες γρήγορης απόκρισης όπου είναι ο κοινός τύπος πλημμύρας των Μεσογειακών χωρών.

Το ακραίο πλημμυρικό γεγονός που βασίστηκε η παρούσα διατριβή είναι η πλημμύρα που έπληξε την πόλη του Βόλου στις 09/10/2006. Κατά την διάρκεια του συγκεκριμένου πλημμυρικού γεγονότος η πόλη του Βόλου υπέστη ανυπολόγιστες καταστροφές κυρίως λόγω τις υπερχείλισης των χειμάρρων με αποκορύφωμα την καταστροφή της γέφυρας του Οργανισμού Σιδηροδρόμων Ελλάδος (ΟΣΕ). Από την πλημμύρα κυρίως επλήγησαν διάφορες κτιριακές υποδομές (δημόσιες υπηρεσίες, οικίες και επιχειρήσεις), το οδικό δίκτυο και αρκετές αγροτικές περιοχές που βρίσκονται στα πέριξ της πόλης. Σύμφωνα με προηγούμενη ανάλυση των καμπυλών Έντασης-Διάρκειας-Συχνότητας Βροχόπτωσης της ευρύτερης περιοχής μελέτης, το συγκεκριμένο πλημμυρικό γεγονός εκτιμήθηκε ότι έχει περίοδο επαναφοράς περίπου 100 ετών.

Το εκτιμημένο πλημμυρογράφημα που χρησιμοποιήθηκε στην παρούσα διδακτορική διατριβή βασίζεται στο Συνθετικό Μοναδιαίο Υδρογράφημα του Clark με την χρήση της μεθόδου κινηματικού κύματος. Τα μετεωρολογικά δεδομένα που χρησιμοποιήθηκαν για την ανάλυση του πλημμυρικού γεγονότος προέρχονται από την καταγραφή του μετεωρολογικού σταθμού του Βόλου-Φυτόκο. Η εκτίμηση της απορροϊκής βροχής (ενεργή βροχόπτωση) έγινε με την χρήση της μέθοδού του απποροϊκού συντελεστή CN (Curve Number) της Soil Conservation Service (SCS). Τέλος, η όδευση της απορροής πραγματοποιήθηκε με χρήση γραμμικής συνέλιξης, η όποια βασίζεται στην μέθοδο ισόχρονων καμπυλών (καμπύλες χρόνου-έκτασης). Οι καμπύλες χρόνου-έκτασης εκτιμήθηκαν χρησιμοποιώντας την εξίσωση χρόνου συγκέντρωσης του Giandotti. Στις

επόμενες παραγράφους παρουσιάζονται συνοπτικά τα τρία μεθοδολογικά πλαίσια που αναπτύχθηκαν κατά την εκπόνηση της παρούσας διδακτορικής διατριβής.

Σύστημα εκτίμησης και χαρτογράφησης πιθανών περιοχών πλημμυρικής κατάκλισης

Το σύστημα εκτίμησης και χαρτογράφησης πιθανών περιοχών πλημμυρικής κατάκλισης (Identification of flood-prone areas component) στηρίζεται στην μίξη διαφορετικών μεθοδολογιών πολυκριτηριακής ανάλυσης (Multi-Criteria analysis) και διαφόρων τεχνικών με εφαρμογή σε περιβάλλον Γεωγραφικών Συστημάτων Πληροφοριών (ΓΣΠ) και στην μεθοδολογία πιστοποίησης. Το σύστημα εφαρμόστηκε σε επίπεδο λεκάνης απορροής για την εκτίμηση των εν δυνάμει πλημμυρικών περιοχών για λεκάνες με ελλιπή δεδομένα. Συγκεκριμένα, το σύστημα εκτίμησης πιθανών περιοχών πλημμυρικής κατάκλισης βασίζεται μόνο σε χωρικά δεδομένα με εφαρμογή σε ΓΣΠ, σε διάφορες μεθοδολογίες ομαδοποίησης (clustering techniques) και σε δύο (2) μεθόδους πολυκριτηριακής ανάλυσης (Multi Criteria Analysis), την η μεθοδολογία της Αναλυτικής Ιεράρχησης (Analytical Hierarchy Process) και την μεθοδολογία Ασαφής Αναλυτικής Ιεράρχησης (Fuzzy Analytical Hierarchy Process). Τα δεδομένα εισόδου του συστήματος αποτελούνται κυρίως από γεωμορφολογικούς δείκτες που σχετίζονται με την φυσική διαδικασία του μηχανισμού της πλημμυρογένεσης. Επιπλέον η επιλογή των τελικών κριτηρίων (χωρικά δεδομένα εισόδου) που χρησιμοποιήθηκαν στην συγκεκριμένη ανάλυση έγινε σύμφωνα με συγκριμένη διαδικασία αξιολόγησης μέσω του συντελεστή συσχέτισης (Correlation coefficient). Για την εξαγωγή της βέλτιστης δομής και την διασφάλιση της αντικειμενικότητας του συστήματος ώστε να καθοριστούν οι πιθανές πλημμυρικές περιοχές, διενεργήθηκαν διάφορα τεστ ευαισθησίας. Για αυτό τον λόγο το πλαίσιο χωρίστηκε σε δύο υποσυστήματα εφαρμογής όπου χρησιμοποιήθηκε διαφορετική δομή και ρυθμίσεις παραμέτρων.
Τα δύο υποσυστήματα εφαρμογής χρησιμοποιούν κάποιες κοινές τεχνικές όπως: α) πέντε μεθοδολογίες ομαδοποίησης (Natural Breaks classification method, K-mean clustering method using two distance approaches, Fuzzy c-mean, Gaussian Mixture Model Clustering , Clustering Large Applications method), β) την μεθοδολογία της Αναλυτικής Ιεράρχησης και την μεθοδολογία Ασαφής Αναλυτικής Ιεράρχησης, γ) δύο προσεγγίσεις που προκύπτουν από την διαδικασία των πινάκων σύγκρισης ζευγών και βασίζονται στην επιλογή του αριθμού των ατόμων που προσμετρούνται για την λήψη της απόφασης (και στις δύο προσεγγίσεις διενεργήθηκε έλεγχος τυχαιότητας (Consistency Ratio) . Στο πρώτο υποσυστήματα γίνεται κανονικοποίηση όλων των κριτηρίων πρίν από την εφαρμογή των μεθόδων πολυκριτηριακής ανάλυσης και έπειτα εφαρμόζεται η ομαδοποίηση τους κατά το τελικό στάδιο του συστήματος ώστε να καθοριστούν οι εν δυνάμει πλημμυριζουσες περιοχές. Στο δεύτερο υποσυστήματα γίνεται ομαδοποίηση των κριτηρίων πριν και μετά την εφαρμογή των μεθόδων πολυκριτηριακής ανάλυσης (δεν γίνεται κανονικοποίηση των κρητιρίων) με αποτέλεσμα να καθοριστούν οι εν δυνάμει πλημμυριζουσες περιοχές. Τέλος και στα

δύο υποσυστήματα η ομαδοποίηση των εν δυνάμει πλημμυρικών περιοχών γίνεται με την χρήση των πέντε μεθόδων ομαδοποίησης και ο πλημμυρικός κίνδυνος διακριτοποιείται σε πέντε κλάσεις (cluster). Το σύστημα εκτίμησης και χαρτογράφησης πιθανών περιοχών πλημμυρικής κατάκλισης εφαρμόστηκε στην λεκάνη απορροής του χειμάρρου Ξηριά, Μαγνησία, Θεσσαλία, Ελλάδα. Η πιστοποίηση του προτεινόμενου συστήματος βασίστηκε στην χρήση ιστορικών δεδομένων πλημμύρας και δεδομένων προσομοίωσης πλημμύρας του υπο εξέταση πλημμυρικού γεγονότος (ακραίο πλημμυρικό γεγονός στις 09/10/2006, Βόλος, Ελλάδα). Από τα αποτελέσματα προκύπτει ότι το προτεινόμενο σύστημα Πολυκριτηριακής Ανάλυσης – ΓΣΠ μπορεί να αποτελέσει ένα πολύτιμο εργαλείο για τους ιθύνοντες αποφάσεων όσον αφορά στην αναγνώριση των περιοχών οι οποίες υφίστανται κίνδυνους για ζημιές από πλημμύρες (δημιουργία προ-πλημμυρικών χαρτών) και στην λήψη αποφάσεων σχετικά με την ενημέρωση των πολιτών και την βελτιστοποίηση των στρατηγικών σχεδίων κατά των πλημμυρών. Παρόλο που το προτεινόμενο σύστημα εκτιμά με ακρίβεια τις πιθανές περιοχές πλημμυρικής κατάκλισης, για την καλύτερη και εγκυρότερη διερεύνηση των χαρακτηριστικών του πλημμυρικού κινδύνου και επικινδυνότητας (πχ: πλημμυρική έκταση, ύψος στάθμης πλημμύρας, ταχύτητα, κτλ) η χρήση υδραυλικού μοντέλου για προσομοίωση πλημμύρας θεωρείται απαραίτητη.

<u>Σύστημα ανάλυσης ευαισθησίας για την εκτίμηση και χαρτογράφηση πλημμυράς</u>

Το σύστημα ανάλυσης ευαισθησίας για την εκτίμηση και χαρτογράφηση πλημμυράς βασίζεται σε πληθώρα διαρθρώσεων συστήματος για ανάλυση ευαισθησίας παραμέτρων. Οι παράμετροι που εξετάστηκαν για την ανάλυση ευαισθησίας συστήματος είναι η χρήση διαφορετικών υδραυλικών-υδροδυναμικών μοντέλων και τύπου υδραυλικής - υδροδυναμικής προσομοίωσης (προσέγγισης) (1D, 2D, 1D/2D) σε συνδυασμό με διαφορετικούς τύπους ακρίβειας Ψηφιακών Μοντέλων Εδάφους (ΨΜΕ) και πλεγμάτων προσομοίωσης για την εκτίμηση και χαρτογράφηση πλημμύρας σε περιοχές με ελλιπή δεδομένα. Το σύστημα ανάλυσης ευαισθησίας για την εκτίμηση και χαρτογράφηση πλημμυράς χωρίστηκε σε δύο διαφορετικά υποσυστήματα όπου εξετάστηκαν διαφορετικές δομικές διαρθρώσεις. Το πρώτο υποσύστημα αναφέρεται ως «Ανάλυσης ευαισθησίας πρώτου επίπεδου», ενώ το δεύτερο υποσύστημα αναφέρεται ως «Ανάλυσης ευαισθησίας δεύτερου επίπεδου».

Οι παράμετροι που εμπλέκονται στην προσομοίωση πλημμύρας και εξετάστηκαν στο υποσύστημα «Ανάλυσης ευαισθησίας πρώτου επίπεδου» είναι η χρήση διαφορετικών υδραυλικών-υδροδυναμικών μοντέλων και προσεγγίσεων (1D, 2D, 1D/2D) σε συνδυασμό με διαφορετικούς τύπους ακρίβειας Ψηφιακών Μοντέλων Εδάφους (ΨΜΕ) και πλεγμάτων προσομοίωσης. Συνεπώς, οι τέσσερις (4) τύποι ΨΜΕ που χρησιμοποιήθηκαν στην παρούσα ανάλυση είναι οι εξής: α) ΨΜΕ που δημιουργήθηκε μετά από επεξεργασία δεδομένων επίγειου σαρωτή εδάφους, β) Ψηφιακό Μοντέλο Επιφάνειας που δημιουργήθηκε από τα ακατέργαστα δεδομένα του επίγειου σαρωτή

εδάφους, γ) ΨΜΕ που δημιουργήθηκε από δεδομένα κλασσικής τοπογραφικής αποτύπωσης, και δ) ΨΜΕ που δημιουργήθηκε με την χρήση ψηφιοποιημένων υσοιψών καμπυλών τοπογραφικού χάρτη κλίμακας 1:5000. Τα υδραυλικά-υδροδυναμικά μοντέλα που χρησιμοποιήθηκαν στην συγκεκριμένη ανάλυση είναι: α) Μονοδιάστατα μοντέλα (1D): HEC-RAS και MIKE11 χρησιμοποιώντας δύο δομές (πλήρωση κενών με παρεμβολή διατομών, πλήρωση κενών με χρήση του ΨΜΕ), b) Δισδιάστατα μοντέλα (2D): MIKE21 HD (βασισμένο σε κάναβο), MIKE21 HD FM (βασισμένο σε πλέγμα), c) Συζευγμένα μονοδιάστατα-δισδιάστατα μοντέλα (1D/2D): MIKE11/MIKE21 HD (βασισμένο σε κάναβο) and MIKE11/MIKE21 HD FM (βασισμένο σε πλέγμα) μέσω της πλατφόρμας MIKE FLOOD. Επιπλέον, στα πλαίσια της παρούσας ανάλυσης εξετάστηκε η χρήση διαφορετικής ανάλυσης φατνίου ή πλέγματος. Ο συντελεστής τραχύτητας εκτιμήθηκε σύμφωνα με την χρήση τεχνικών εκ των υστέρων ανάλυσης πλημμύρας.

Οι παράμετροι που εμπλέκονται στην προσομοίωση πλημμύρας και εξετάστηκαν στο υποσύστημα «Ανάλυσης ευαισθησίας δεύτερου επίπεδου» είναι η χρήση διαφορετικών υδραυλικών-υδροδυναμικών μοντέλων, προσεγγίσεων (1D, 2D, 1D/2D) και πλεγμάτων προσομοίωσης. Στην παρούσα ανάλυση χρησιμοποιήθηκε μονό ο τύπος ΨΜΕ που δημιουργήθηκε μετά από επεξεργασία δεδομένων επίγειου σαρωτή εδάφους (Processed LIDAR river geometry) όπου προέκυψε ως βέλτιστη λύση σύμφωνα με την προηγούμενη ανάλυση. Τα υδραυλικά-υδροδυναμικά μοντέλα που χρησιμοποιήθηκαν στην συγκεκριμένη ανάλυση είναι: α) Μονοδιάστατα μοντέλα (1D): HECRAS, MIKE11 χρησιμοποιώντας δύο δομές (πλήρωση κενών με παρεμβολή διατομών, πλήρωση κενών με χρήση του ΨΜΕ) και XPSTORM, β) Δισδιάστατα μοντέλα (2D): HECRAS, LISFLOOD-FP (επίλυση Subgrid), MIKE21 (βασισμένο σε κάναβο και βασισμένο σε πλέγμα), XPSTORM, FLO2D; γ) Συζευγμένα μονοδιάστατα-δισδιάστατα μοντέλα (1D/2D): HECRAS, MIKEFLOOD (βασισμένο σε κάναβο και βασισμένο σε πλέγμα), LISFLOOD-FP (μέθοδος κινιματικού κύματος και μέθοδος διάχυσης κύματος), XPSTORM. Επιπλέον, στα πλαίσια της παρούσας ανάλυσης εξετάστηκε η χρήση διαφορετικής ανάλυσης φατνίου ή πλέγματος και η χρήση ή όχι κατασκευών εντός της κοίτης (πχ: γέφυρες, κτλ.). Στην παρούσα ανάλυση χρησιμοποιήθηκε βελτιωμένη τιμή συντελεστή τραχύτητας που προέκυψε από την χρήση μιας εμπειρικής σχέσης, ντετερμινιστικής ανάλυσης πλημμύρας και του αντικειμενικού κριτηρίου πιστοποίησης αποτελεσμάτων CSI.

Και στα δύο (2) υποσύστημα ανάλυσης ευαισθησίας χρησιμοποιήθηκαν κλασσικές υδρολογικές τεχνικές που εφαρμόζονται σε λεκάνες απορροής με ελλιπή δεδομένα για την εκτίμησης της πλημμυρικής αιχμής και του πλημμυρογραφήματος. Η προτεινόμενη μεθοδολογία εφαρμόστηκε σε συγκεκριμένο τμήμα του χειμάρρου Ξηριά, Βόλος, Ελλάδα. Συγκεκριμένα, η πλημμυρική αιχμή και το πλημμυρογράφημα εισόδου υπολογίστηκαν σύμφωνα με την μέθοδο του Συνθετικού Μοναδιαίου Υδρογραφήματος τύπου Clark (ClUH). Η πιστοποίηση των αποτελεσμάτων των αναλύσεων ευαισθησίας χαρτογράφησης της πλημμυρικής ζώνης έγινε με την χρήση του κριτήριου αξιολόγησης αποτελεσμάτων Critical Success Index (CSI ή Threat score)

και των πινάκων συνάφειας 2 επί 2, όπου συγκρίθηκε η προσομοιωμένη πλημμυρικής έκταση με την παρατηρούμενη έκταση πλημμύρας (πλημμυρική έκταση σύμφωνα με τα ιστορικά δεδομένα πλημμύρας του 2006).
Από τα αποτελέσματα προκύπτει ότι η ανάλυση ευαισθησίας είναι ένα σημαντικό μεθοδολογικό στάδιο που πρέπει να ενσωματώνεται σε όλα τα πλαίσια την εκτίμησης και χαρτογράφησης της πλημμυρικής επικινδυνότητας. Επιπλέον, όπως προκύπτει από την παρούσα ανάλυση, η αβεβαιότητα των δεδομένων εισόδου επικρατεί έναντι της αβεβαιότητας της δομής του μοντέλου. Τέλος, σύμφωνα με τα αποτελέσματα της παρούσας έρευνας, προτείνεται η χρήση μονοδιάστατου υδραυλικού-υδροδυναμικού μοντέλου σε συνδυασμό με στοχαστικές διαδικασίες για την εκτίμηση και χαρτογράφηση πλημμυρών σε περιοχές με ελλιπή δεδομένα.

Σύστημα ανάλυσης αβεβαιότητας για την εκτίμηση και χαρτογράφηση πλημμυράς

Το σύστημα ανάλυσης αβεβαιότητας για την εκτίμηση και χαρτογράφηση πλημμυράς βασίζεται στο 1) αυτόματο υποσύστημα στοχαστικής εκτίμησης πλημμύρας με την χρήση του HEC-RAS (πυρήνας του κεντρικού συστήματος), 2) σε διάφορα μοντέλα χωρικής ανάλυση δεδομένων μέσω ΓΣΠ, 3) σε αρκετές διαφορετικές δομές ανάλυσης ευαισθησίας και 4) στο υποσύστημα αξιολόγησης αποτελεσμάτων. Το σύστημα εφαρμόστηκε σε επίπεδο τμήματος χειμάρρου για την εκτίμηση της αβεβαιότητας που υπεισέρχεται στο σύστημα λόγω του συντελεστή τραχύτητας και την βαθμονόμηση του για λεκάνες απορροής με ελλιπή δεδομένα. Το σύστημα στοχαστικών διαδικασιών για την εκτίμηση της πλημμυρικής έκτασης βασίζεται σε προσομοιώσεις Monte-Carlo και το μονοδιάστατο υδραυλικό-υδροδυναμικό μοντέλο HEC-RAS. Η αρχιτεκτονική του αυτόματου υποσυστήματος προσομοιώσεων Monte-Carlo βασίζεται στη γλώσσα προγραμματισμού Visual Basic for Applications (VBA) όπου χρησιμοποιήθηκαν προϋπάρχουσες και νέες ρουτίνες και δομοστοιχεία λογισμικού που αναπτύχθηκαν στα πλαίσια της παρούσας έρευνας.
Το αρχικό εύρος τιμών του συντελεστή τραχύτητας Manning's *n* εκτιμήθηκε με την χρήση των μετρήσεων πεδίου Wolman Pebble Count και διαφόρων εμπειρικών σχέσεων εκτίμησης του συντελεστή τραχύτητας που αναπτύχθηκαν σε υδατορρέματα με υλικό πυθμένα που αποτελείται κυρίως από κροκάλες και μεγάλους λίθους. Με αυτόν τον τρόπο δημιουργήθηκε η εμπειρική κατανομή για τον συντελεστή τραχύτητας. Ακολούθως, έγινε έλεγχος εφαρμογής διαφόρων θεωρητικών κατανομών στην εμπειρική κατανομή και αξιολογήθηκε η εφαρμογή τους χρησιμοποιώντας διάφορους δείκτες καλής προσαρμογής (goodness-of-fit criteria). Στην συνέχεια έγινε παραγωγή τυχαίων μεταβλητών συντελεστή τραχύτητας με την χρήση του αλγόριθμου Latin Hypercube Sampling σύμφωνα με τις θεωρητικές κατανομές που επιλέχθηκαν από το προηγούμενο στάδιο. Συνεπώς, η παραγωγή των τελικών πιθανοτικών χαρτών πλημμύρας βασίζεται στην εφαρμογή διαφόρων μοντέλων χωρικής ανάλυσης δεδομένων όπου δημιουργήθηκαν σε περιβάλλον ArcGIS model builder

χρησιμοποιώντας τα αποτελέσματα των προσομοιώσεων Monte-Carlo. Η εκτίμηση της αβεβαιότητας διενεργήθηκε με την χρήση της παραπάνω διαδικασίας βαθμονόμησης του συντελεστή τραχύτητας η οποία βασίζεται μόνο στην αξιολόγηση της πλημμυρική ς έκτασης. Στην παρούσα ανάλυση η πλημμυρική έκταση που χρησιμοποιήθηκε αποτελείται από την πλημμυρική έκταση που εκτιμήθηκε σύμφωνα με τα ιστορικά δεδομένα πλημμύρας του 2006. Η πιστοποίηση των αποτελεσμάτων για την εκτίμηση της αβεβαιότητας έγινε με την χρήση του προτεινόμενου ποσοτικού κριτηρίου αξιολόγησης αποτελεσμάτων Median Absolute Percentage Error (MdAPE) , όπου σε κάθε προσομοίωση συγκρινόταν η προσομοιωμένη πλημμυρική έκταση με την παρατηρούμενη έκταση πλημμύρας (πλημμυρική έκταση σύμφωνα με τα ιστορικά δεδομένα πλημμύρας του 2006). Έτσι, η διεξαγωγή των αποδεκτών λύσεων στηρίχθηκε στην παραπάνω διαδικασία πιστοποίησης για την δημιουργία των πιθανοτικών χαρτών πλημμύρας.

Επιπρόσθετα, διενεργήθηκαν διάφορες αναλύσεις ευαισθησίας συστήματος και ανάλυση ευστάθειας συστήματος για την ενδυνάμωση της ευστάθειας και της αξιοπιστίας του προτεινόμενου πλαισίου και της βέλτιστης δομής του. Οι παράμετροι που εμπλέκονται στην στοχαστική προσομοίωση πλημμύρας και εξετάστηκαν στο προτεινόμενο σύστημα είναι: 1) η απόσταση μεταξύ των διατομών της γεωμετρίας ποταμού, 2) ο αριθμός των αποδεκτών λύσεων, 3) το προτεινόμενο όριο τιμών (threshold level) κατά την διαδικασία αξιολόγησης των αποτελεσμάτων, και 4) η χρήση διαφορετικών ερωτητικών κατανομών στην διαδικασία παραγωγής των τιμών του συντελεστή τραχύτητας. Η ανάλυση της ευστάθειας του συστήματος περιλαμβάνει την δημιουργία πέντε όμοιων διαρθρώσεων συστήματος όπου χρησιμοποιήθηκαν ίδιες τεχνικές σύμφωνα με την βέλτιστη δομή του πλαισίου. Τέλος, έγινε σύγκριση και αξιολόγηση των αποτελεσμάτων που προέκυψαν από ντετερμινιστικές και στοχαστικές διαδικασίες για την χαρτογράφηση πλημμυρών σε περιοχές με ελλιπή δεδομένα. Το προτεινόμενο σύστημα εφαρμόστηκε σε συγκεκριμένο τμήμα του χειμάρρου Ξηριά, Βόλος, Ελλάδα.

Από τα αποτελέσματα της παρούσας έρευνας προκύπτει ότι η χρήση στοχαστικών διαδικασιών και η παραγωγή πιθανοτικών χαρτών πλημμύρας παρέχουν καλύτερες πληροφορίες σε σχέση με την πλημμυρίζουσα ζώνη και σε σύγκριση με την εφαρμογή ντετερμινιστικών μεθόδων. Επομένως, με την χρήση πιθανοτικών χαρτών πλημμύρας αυξάνεται η εγκυρότητα των αποτελεσμάτων και γι’ αυτό το λόγο είναι ένας ελκυστικός και πιο κατανοητός τρόπος απεικόνισης της πιθανότητας πλημμύρας. Τέλος, το κύριο συμπέρασμα της παρούσας έρευνας είναι ότι η χρήση στοχαστικών διαδικασιών στην εκτίμηση και χαρτογράφηση πλημμυράς μπορεί να αποτελέσει ένα πολύτιμο εργαλείο για τους ιθύνοντες αποφάσεων όσον αφορά στην καλύτερη ανάπτυξη σχεδίων διαχείρισης πλημμυρικής επικινδυνότητας και ελαχιστοποίησης των κοινωνικών και οικονομικών επιπτώσεων της πλημμύρας.

Εν κατακλείδι, στην παρούσα διδακτορική διατριβή παρουσιάζεται μια ολιστική προσέγγιση για την εκτίμηση και χαρτογράφηση των πλημμυρών σε λεκάνες απορροής και χειμάρρους με ελλιπή ή ανύπαρκτα μετεωρολογικά και υδρομετρικά δεδομένα. Η παρούσα έρευνα αποδεικνύει ότι η χρήση κλασσικών τεχνικών και μεθόδων για την διερεύνηση του φαινομένου της πλημμύρας μπορεί να συντελέσει στην δημιουργία ενός έγκυρου και αποτελεσματικού πλαισίου προσομοίωσης για την εκτίμηση πλημμυρικού κινδύνου και επικινδυνότητας σε χειμαρρικά υδατορρεύματα και υδρολογικές λεκάνες με ελλιπή δεδομένα. Τα τρία συστήματα που πλαισιώνουν το ενιαίο μεθοδολογικό πλαίσιο έχουν ως στόχο την 1) εκτίμηση και την χαρτογράφηση πιθανών περιοχών πλημμυρικής κατάκλισης, 2) εκτίμηση και ποσοτικοποίηση της ευαισθησίας και της αβεβαιότητας συγκεκριμένων παραμέτρων στην διαδικασία της μοντελοποίησης πλημμύρας. Επομένως, το προτεινόμενο μεθοδολογικό πλαίσιο ή ξεχωριστά τα επιμέρους συστήματα μπορούν να αποτελέσουν πολύτιμα εργαλεία για τους ιθύνοντες αποφάσεων με στόχο την παραγωγή έγκυρων και υψηλής ακρίβειας σχεδίων διαχείρισης πλημμυρικού κινδύνου και επικινδυνότητας σε λεκάνες απορροής και χειμάρρους με ελλιπή δεδομένα.

CHAPTER 1ο
INTRODUCTION

1 Introduction

1.1 Floods and Flash floods in Europe and Greece

In the last decades, natural and artificial environments have repeatedly experienced severe damages by natural hazards. One of the most destructive water-related natural hazards that directly affects human society is floods. Extreme flood events pose a severe threat to human society from ancient times. Last decades Europe has frequently been afflicted by numerous and disastrous flood events. Many studies suggest that the occurrence of flood events is increasing both in numbers and intensity and, the scientific community sees a strong correlation between this trend and the rise in human activities, such as land occupancy and changes in land use (Hall et al., 2014; Tsakiris et al., 2009). Floods are substantial hazards commonly associated with high percentage of mortality, social and economic damages worldwide. Between 1998-2009, Europe suffered from more than 200 flood events with approximately 1126 fatalities. Furthermore, in the last two decades, the annual mean flood damage in Europe is estimated approximately to € 4 billion per year (EEA, 2010; AghaKouchak et al., 2013).

A typical type of flooding in the Mediterranean region is flash floods (Aronica et al., 2012) that often have devastating and hazardous effects concerning infrastructure and, more importantly, such floods are associated with high rates of fatalities (Gruntfest and Handmer, 2001; Younis et al., 2008). Some significant extreme flash floods events that are mentioned below, took place in several European Mediterranean territories causing serious damages, economic and/or human losses: in France (Gaume et al., 2004; Delrieu et al., 2005), Greece (Papagiannaki et al., 2013; Kourgialas and Karatzas, 2014), Spain (Llasat et al., 2013) and in Italy (Molinari et al., 2014; Faccini et al., 2015).

Despite the worldwide recognition of flash floods, there is a lack of a uniform terminology. The following paragraphs present the most used and accepted terms for flash floods.

Based on the European Environment Agency report (2012) a flash flood:

> "Occurs as a result of the rapid accumulation and release of run-off waters from upstream mountainous areas, which can be caused by extreme rainfall, cloud bursts, landslides, the sudden break-up of a dike or failure of a flood control works. Over natural watersheds they typically occur in the instance of more than 200 mm of rain during less than six hours, while in built-up areas even rainfall of 50 mm

> within one hour can produce a local flash flood. They are characterized by a sharp rise followed by a relatively rapid decline causing high flow velocities. Discharges quickly reach a maximum level and diminish almost as rapidly".

Moreover, based on the Inter-Active Terminology for Europe (2017) a flash flood is:

> "A sudden flood of short duration and abrupt rise with a relatively high peak discharge (rate of flow), usually resulting from a very high intensity of rainfall over a small area"

Finally, according to the American Meteorological Society (AMS) Glossary (2017) it is presented a revised definition of a flash flood that is based on advances in understanding and their societal impacts warrant:

> "Flooding caused by rapidly rising water level in streams, creeks, rivers or other waterways, normally dry stream beds, or in urban areas, usually as a result of intense rainfall over a relatively small area or for moderate to intense rainfall over highly saturated or impervious land surfaces, and generally occurring within minutes to several hours of the rainfall event. Steep terrain tends to concentrate runoff into streams very quickly and is often a contributing factor. Changes in soil properties (e.g., burn areas from wildfires), hydrophobic or impervious soils, removal of surface vegetation, and excess runoff from warm rainfall on significant snowpack can also be important contributors. Additional causes of flash floods include ice jams, and levee and dam failures."

The majority of the presented studies of extreme flash flood events have a high percentage of mortalities. All the events were characterized by intense precipitation during a very short time over a relatively small area, rapid accumulation, fast rising of water level and a relatively high peak discharge. These extreme flash flood events have caused severe economic losses, damages to several public infrastructures (e. g. roads, railways) and building and vehicle damages. According to several studies presented by Parry and his associates (Parry et al., 2007), the probability of flash floods occurrence is going to rise throughout Europe in the following years. The uptrend of flash floods is directly related to the changes in land use (influence of human activities) and the expected pluviometric regime changes due to climate progression.

The observed escalation in magnitude, frequency and intensity of the flood events worldwide have driven to a rise of global awareness for flood damage mitigation measurements (Hall et al., 2014). Thus, European Union established the Flood Directive 2007/60/EC. The main goal of Flood Directive 2007/60/EC is the establishment of a generic framework for flood risk management and mapping within the European Union. The ultimate purpose of the framework is to reduce the consequences of floods to human health, the environment, sites of cultural heritage interest and the general economic activity. Nowadays, almost all EU countries have managed to fulfill their obligations

derived from the Flood Directive 2007/60/EC. Moreover, it is mandatory for all countries to update the flood management plans every six years. Hence, the implementation of the Flood Directive is an ongoing process where flood mapping is a necessary tool for all EU member states.

As far as the Greek territory is concerned, the entire country is experiencing severe flood events ever since the ancient times. In Greece, regular recording of flood events by civil protection agencies started relatively recently, limiting the systematic official records to the last two decades (Diakakis et al., 2012). In recent studies (SSW-MEECC, 2012; Diakakis et al., 2012), an extensive catalogue of flooding phenomena during the last 130 years in Greece has been compiled based on numerous sources. Specifically, in the last 130 years, 540 flood events have been identified and caused 686 human losses (Diakakis et al., 2012). Figure 1.1a illustrates the temporal distribution of flooding during the period of 1881-2010, while Figure 1.1b illustrates the flood casualties for the same period. From the histograms presented in Figure 1.1 one can observe an increasing trend in reported flood event numbers during the last decades, even though the number of human casualties remains relatively stable during the same period (Diakakis et al., 2012).

Moreover, Figure 1.2 presents the distribution of floods across Greece expressed as the number of events and as the number of casualties per administrational unit for the period 1880–2010, respectively (Diakakis et al., 2012). As shown in Figure 1.2a, the prefecture of Thessaly and especially the regional unit of Magnesia experiences an increased flood occurrence. Furthermore, Figure 1.2b demonstrates that the flood casualties are following approximately the same pattern with the flood occurrence. Based on the distribution of events expressed as the number of events per 100 km^2 in each of these units (Figure 1.2a) and the distribution of fatalities expressed as the number of casualties per 100. 000 individuals (Figure 1.2b), the regional unit of Magnesia is once more in the top of the list of the most vulnerable to flood territories.

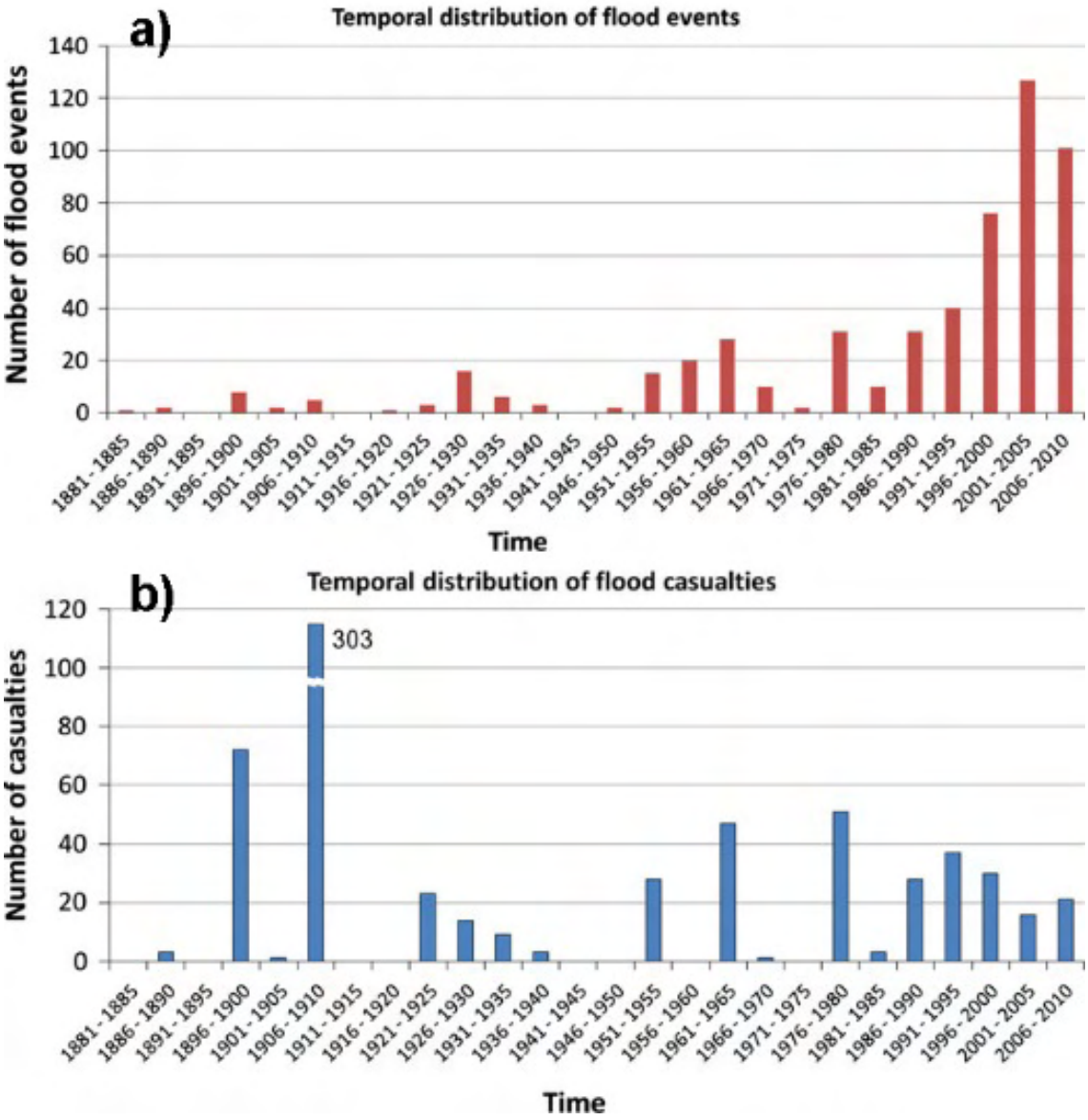

Figure 1.1. a) Temporal distribution of flood events and b) flood casualties between 1881 and 2010 (Source: Diakakis et al., 2012)

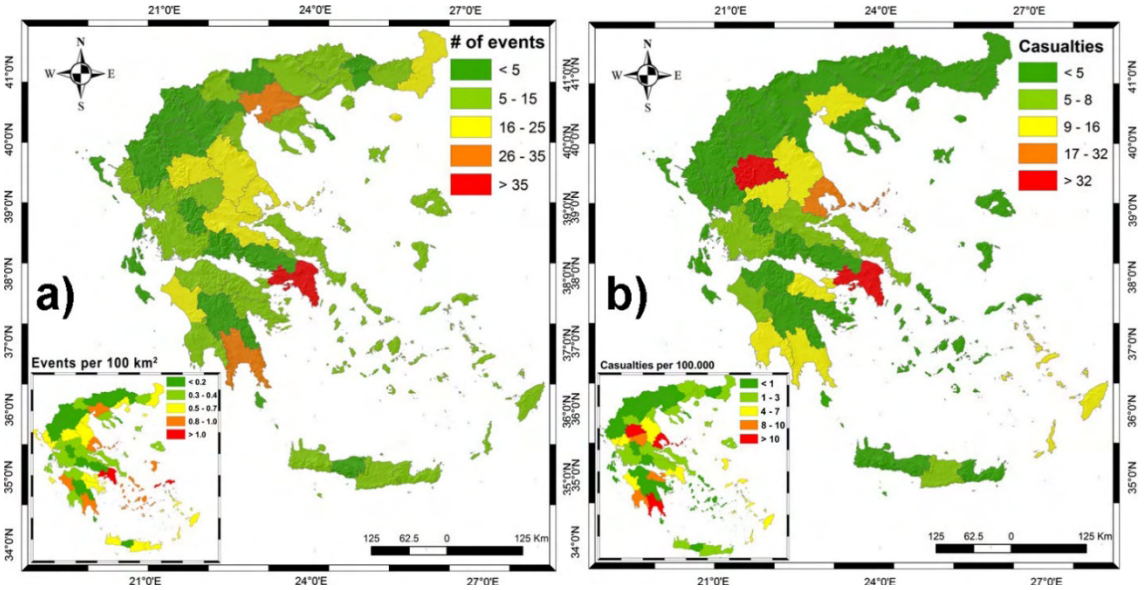

Figure 1.2. Distribution of floods across Greece expressed: a) as the number of events per administrational unit for the period 1880–2010. In the lower left corner distribution of events is expressed as the number of events per 100 km^2 in each of these units. b) as the number of casualties per administrational unit for the period 1880–2010. In the lower left corner distribution of fatalities is expressed as the number of casualties per 100. 000 individuals based on the 2001 population census (ELSTAT 2001) (Source: Diakakis et al., 2012).

In the study of Special Secretariat for Water, Ministry of Environment, Energy and Climate Change (2012), 1627 flood episodes were identified in 1076 locations and 297 flood episodes observed in 261 locations were considered to be important floods (Figure 1.3). This data, concerns flood events that occurred from 1896 to 2011 and presented in Figure 1.3 (SSW-MEECC, 2012). In Figure 1.3a,b there can be seen the spatial distribution of 1627 flood events pinpointed in 1076 locations and the flood events categories of the historical flood locations. Furthermore, Figure 1.3c,d present the spatial distribution of flooded areas in stremmas and the spatial distribution of flood damages in € respectively (visualized with graduated symbol). From the total amount of the recorded (1627) flood events only the 1097 events have records of flood damage with the damage cost ranging from 2573 to 5,869,406 €. According to Figure 1.3, spatial patterns were identified that highlight the prefecture of Thessaly and especially the regional unit of Magnesia having higher flood recurrence rates, great economic losses and big flooded areas (SSW-MEECC, 2012).

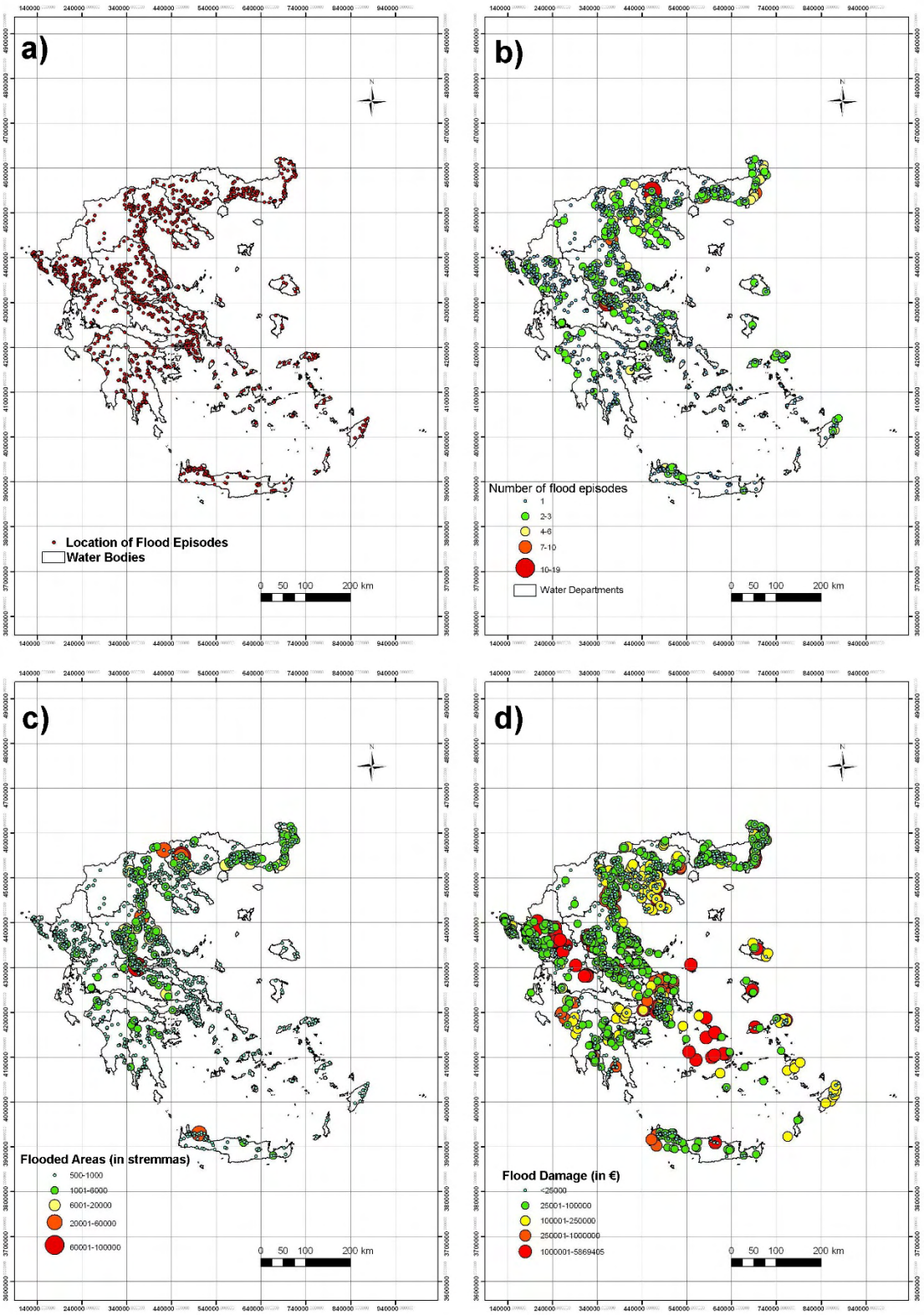

Figure 1.3. a) Locations of the historical flood events; b) Flood event categories of the historical flood locations; c) Flooded areas in stremmas and d) Flood damage in Euros of the historical flood events (Source: SSW-MEECC, 2012).

In general, both studies showed seasonality patterns with more events clustering in November and also showed that urban environments tend to present a higher flood recurrence rates than mountainous and rural areas. Therefore, the regional unit of Magnesia is categorized as an extremely vulnerable area to floods with the city of Volos to be an indicative study area, as an urban environment, for investigation of flood hazard and risk modelling and mapping.

1.2 Flood prone areas mapping at ungauged catchments

Nowadays, flood management is considered a spatial problem because of the impact of the terrain variations to the flood type and intensity (Foudi et al., 2015; Ahmadisharaf et al., 2016). The combination of GIS and Multiple Criteria Decision Making (MCDM) methods is a common procedure followed in the last decades because of the availability to choose multiple criteria from different origins (Chen et al., 2011). Typical approaches of flood management decision making neglect the spatial variability of the evaluation criteria (Qi et al., 2013). A basic process in the preliminary analysis of flood mapping is the detection of flood prone areas. A standard tool in the recognition process of flood-prone areas is the Digital Elevation Models (DEMs) and the DEM-derived geomorphological and hydrological attributes (i. e. slope, flow accumulation, flow direction, stream network, and catchment areas) (Noman et al., 2001,2003). Flood hazard assessment should affect the flood risk management mitigation strategies and planning, thus including the estimation of frequency, consequences, magnitude, as well as the intensity of the studied flood event. A standard process in flood hazard and risk analysis is the use of hydraulic-hydrodynamic and hydrologic models to estimate flood peaks and volumes, and the propagation in time and space of the flood wave into the river banks and over the floodplains. Also, the above-mentioned engineering practices are usually implemented at the river and riverine area scale where the assessment of flood risk mapping is crucial for the potential damages to infrastructure. The use of such methods in watershed scale is not easily applicable due to data availability restrictions. Thus, flood risk mapping at watershed scale continues to be a challenging task, even in developed countries (de Moel et al., 2009). Usually for operational implementations of recognizing Areas of Potential Significant Flood Risk (APSFR), the estimation is based on the intersection of the following elements: 1) potential flooded areas (estimated using a simple argument in slope and the alluvial deposition); 2) Important areas (estimated using buffers of one kilometer to important elements such as Protected Habitats, River network, Cities, Villages, Railway, Road network, Historical flood points, etc.); 3) Historical flood positions and the records from the local authorities (estimated using points of

historical flood positions) (e.g. SSW-MEECC, 2012). With the use of such simple combinations of indexes the outcomes tend to lead to erroneous flood hazard maps that have severe problems of flood prone areas overestimation. Therefore, it is obvious that the overestimation in flood hazard mapping can adversely affect the entire process of flood risk management mitigation strategies and planning.

In this study, a methodology has been proposed based on the use of DEM, DEM-derived attributes, hydrologic and climatic indices in combination with multi-criteria analysis methods to estimate flood-prone areas. The analysis of complex decision problems can be performed using a framework that integrates Multi Criteria Analysis (MCA) methods and GIS. By incorporating GIS with MCA methods, the selected elements/criteria can be organized into a hierarchical structure. The ultimate aim of the framework is to help the decision makers choose the optimum decision for the investigated primary goal by examining the relationships among the components of the problem (Boroushaki et al., 2010; Chen et al., 2011). Recently, the use of GIS-based Multi Criteria Decision Analysis (GIS–MCDA) techniques has become a trend in many scientific fields (Malczewski, 2006). One of the most applicable multi-criteria analysis (MCA) method that uses structuring of the factors into a hierarchical framework is the Analytical Hierarchy Process (AHP). The relative importance of various elements can be evaluated by the Decision Makers (DM) with the use of pairwise comparison tables. The score of each alternative can be estimated, in AHP method, by transforming the DM evaluations to numerical values (weights or priorities) (Saaty, 1980).

AHP is gaining popularity over the last decades and several variations of the original version have been developed such us fuzzy AHP that uses various fuzzy logic membership functions (e. g. triangular, trapezoidal) (Van Laarhoven, 1983; Buckley, 1985; Chang, 1996; Mikhailov, 2003). Despite the extended range of AHP applicability, many researchers support the Fuzzy AHP (FAHP) approach because the use of fuzzy logic approach in decision making problems resembles better the human way of thinking. FAHP requires monotonous computation, but in cases where decision problems are complex, the implementation of FAHP method realistically captures human judgment uncertainty (Erensal et al., 2006). Several applications of AHP integration into GIS have been applied in different scientific fields for: a) land use suitability, assessment, classification and planning, b) urban development, suitability and renewal (Chandio et al., 2013 and references therein), c) eco-environmental quality (Huang et al., 2010), d) landslides mapping (Yalcin and Bulut, 2007; Feizizadeh and Blaschke, 2013) e) earthquakes (Pal et al., 2008), f) health (Jeefoo and Tripathi, 2011), g) droughts (Babaei et al., 2013) h) floods (Pawattana and Tripathi, 2008; Khosravi et al., 2016) i) water resources management (Machiwal et al., 2011; Anane et al., 2012; Chowdary et al., 2013) and j) pollution (Negi and Jain, 2008).

Various researchers have applied AHP, FAHP and GIS modelling techniques for the estimation of flood-prone areas, flood hazard , flood risk and other natural disasters (Chen et al., 2011; Kourgialas and Karatzas, 2011; Park et al., 2013; Zou et al., 2013; Manfreda et al., 2011; Meyer et al., 2009; Stefanidis and Stathis, 2013; Tehrany et al., 2013; Radmehr and Araghinejad, 2015; Papaioannou et al., 2015; Khosravi et al., 2016; Tang et al., 2017; Kourgialas and Karatzas, 2017). A standard classification method, used in the majority of studies mentioned above, is the Jenks Natural Breaks classification method (Jenks, 1967). Moreover, in many studies, the classification of the selected criteria (spatial distributed criteria maps such as DEM-derived geomorphological and hydrological attributes) is achieved by using predefined subjective tables. For example, in the study of Radmehr and Araghinejad (2015), the selected criteria were classified with the use of fixed classes before the implementation of the MCA method. However, the selection of a different criteria classification technique could have resulted to a different spatial distributed flood hazard mosaic. To this direction, Chen et al., (2011) managed to overcome the limitations of predefined subjective tables by classifying the selected criteria with the use of specific rules in order to increase the subjectivity of the MCA framework for generalized applications.

Finally, even though the GIS-MCDM methodologies applied in flood management are valuable tools for preliminary analysis, they should be integrated with the use of a hydraulic-hydrodynamic model in order to estimate the characteristics of flood hazard (e.g. flood extent, flow velocity, water depth and duration) and flood risk. Hydraulic-hydrodynamic models are required for detailed representation of flow dynamics and to investigate the impact of a flood event (Teng et al., 2017).

1.3 Flood inundation modelling and mapping at ungauged streams

Detailed information about the flood extent, flood water depth, flood flow velocity, flood duration and how the flow affects several structures are some of the main flood characteristics which are necessary in flood risk management and mapping. Floodplain modelling, mapping, and risk management are often determined using several one-dimensional (1D) and two-dimensional (2D) hydraulic models (e. g.; Aronica et al., 2002; Horritt et al., 2007; Costabile and Macchione, 2015; Papaioannou et al., 2016). The capabilities of these models, for river flood modelling and accurate estimation of several flood characteristics, have been illustrated in many studies (e. g. Horritt et al., 2007; Di Baldassarre et al., 2010; Sarhadi et al., 2012; Domeneghetti et al., 2013; Dottori et al., 2013; Dimitriadis et al., 2016). The majority of these studies have been implemented at gauged watersheds with sufficient amount of data (e.g. discharge data, stage/discharge

relationships, accurate rainfall data, etc.). The availability of data has limited the applicability of these models to urban and suburban areas where the precise estimation of floodplain extent is feasible (Bates et al., 2006; Aggett and Wilson, 2009). Flood inundation modelling involves several sources of uncertainty such as: 1) input data (boundary and initial condition data, digital elevation models and channel bathymetry, hydraulic structures, roughness parameterization), 2) model structure (1D, 2D, quasi 2D, 1D/2D), 3) internal model parameters. Moreover, each type of uncertainty can have a significant or minor impact on the flood modelling and mapping process that influences the overall uncertainty.

A major factor of uncertainty is the Digital Elevation Model accuracy. Its estimation cannot be achieved without errors, especially in complex terrains and depends on the topographical technique that is used (Tsubaki and Fujita, 2010; Papaioannou et al., 2016). The most common techniques that are implemented for river geometry data collection and by extension the DEM creation are the regular ground surveying topographic approaches and photogrammetric techniques. However, the use of such techniques in flood inundation modelling, especially in compound river and riverine terrains, may work as a constraint in the spatial extent of the study area, thus affecting negatively the correctness of the produced DEM (Md Ali et al., 2015; Teng et al., 2015). These limiting factors can be surpassed with the use of new spatial tools that produce high-resolution digital elevation models leading to better hydraulic model configurations and accurate floodplain inundation mapping. The technological advancement of the last decade has driven the topographical survey sector to the development and use of new methods, tools and techniques such as the Airborne Light Detection and Ranging (LIDAR) and the Terrestrial Laser Scanners (TLS) or, and/or the Synthetic Aperture Radar (SAR). The use of these new tools and methods allows the production of high-resolution DEMs. A major advantage of TLS, in comparison to common topographical methods, is that it can provide detailed information on the river and riverine geometry and can improve the flood inundation modelling and mapping, especially in urban and suburban areas with complex terrain (Sampson et al., 2012).

Another essential factor in river flood modelling and mapping is the structure of the hydraulic-hydrodynamic model (1D, 2D, 1D/2D). The most typical hydraulic approach used in river flood modelling and mapping is the one-dimensional (1D). The frequent application of one-dimensional (1D) hydraulic models is based on their simplicity, the low data requirements, the small computing demands and the limited computational time (e.g. Pappenberger et al., 2005; Kourgialas and Karatzas, 2014; Teng et al., 2017). However, recent studies have been conducted using two-dimensional (2D) hydrodynamic models. The applicability of the two-dimensional (2D) hydrodynamic models have risen due to several improvements on the structure of the models and the development of new

parameter estimation techniques (Cook and Merwade, 2009; Tsakiris and Bellos, 2014; Costabile and Macchione, 2015; Shen et al., 2015; Teng et al., 2017). Finally, a modelling approach that gained high acceptance in river flood modelling is the 1D/2D approach because it combines the capabilities of 1D and 2D models (Werner et al., 2004; Apel et al., 2009; Liu et al., 2015; Teng et al., 2017).

Finally, except the use of the deterministic flood modelling, many recent studies have highlighted the use of probabilistic approaches mainly due to the following reasons (Pappenberger and Beven, 2006; Di Baldassarre et al., 2010; Domeneghetti et al., 2013; Dottori, et al., 2013; Romanowicz and Kiczko, 2016; Alfonso et al., 2016): (1) the different sources of uncertainty cannot be neglected in hydrologic/hydraulic modelling; (2) evaluation and estimation of the uncertainty should be a mandatory process in a hypothetically comprehensive analysis; (3) The use of probabilistic flood inundation maps can be a valuable tool in the hands of water resources managers in order to improve the design process of flood mitigation strategies. Hence, especially at an ungauged stream reach, a probabilistic flood modelling approach should be implemented for the provision of accurate results and to address the uncertainty.

1.4 Probabilistic flood inundation modelling and mapping at ungauged streams

The assessment of the flooded areas is achieved using probabilistic and/or deterministic hydraulic approaches (Teng et al., 2017). The use of a deterministic hydraulic approach is based on the calibration of the model using observed data from a historical flood event. Then, the calibrated model is applied for several observed flood events or for common designed floods (return period of 10, 25, 50, 100-years) for engineering purposes. The use of a deterministic approach in flood inundation modelling involves some basic assumptions and these are: 1) the selected hydraulic model has the ability to provide satisfactory representation of the river dynamics and accurate approximation of the inundated areas (usually flood extent and water depth); (2) the use of the model is based on the model parameter stability or time stationarity of model parameters. In other words, the estimated parameter values from the calibration process is used in all examined flood events where different conditions may exist; (3) all the parameters used in hydraulic-hydrodynamic simulations (e. g. stage-discharge relationships, input flood hydrographs, runoff measurements, validation areas) are assumed as “perfect” values (error-free) (Domeneghetti et al., 2013). Thus, to limit or avoid the abovementioned sources of uncertainty, a probabilistic approach is proposed for flood inundation modelling and mapping.

Many recent studies (Pappenberger and Beven, 2006; Di Baldassarre et al., 2010; Domeneghetti et al., 2013; Dottori, et al., 2013; Romanowicz and Kiczko, 2016; Alfonso et al., 2016; Papaioannou et al., 2017) highlight the use of probabilistic approaches as a substitute of the deterministic approach mainly due to the following reasons: (1) the different sources of uncertainty cannot be neglected in hydrologic/hydraulic modelling; (2) evaluation and estimation of the uncertainty should be a mandatory process in a hypothetically comprehensive analysis; (3) The use of probabilistic flood inundation maps can be a valuable tool in the hands of water resources managers in order to improve the design process of flood mitigation strategies. Hence, the use of a deterministic approach for flood inundation modelling and mapping could lead to inaccurate results which can negatively affect the flood mitigation strategic plans.

Uncertainty in flood modelling can be classified in two major types: (1) Natural or random uncertainty. This type of uncertainty is associated with the randomness of the natural processes (natural variability of floods); (2) Epistemic uncertainty. This type of uncertainty is associated with the model uncertainty (structure of the model/ the inability of the model to represent precise the physical phenomenon of flood), the model parameter uncertainty (the weakness for accurate quantification of the model parameters), the input data uncertainty (measurement errors, initial and boundary condition data accuracy, digital elevation models and channel bathymetry resolution, hydraulic structures, roughness parameterization), and the operational uncertainty (human factors that can affect the river and riverine area) (Tung and Yen, 1993; Apel et al., 2004; Merz and Thieken, 2005). Many studies have used probabilistic approaches in order to estimate the river flood modelling uncertainty due to roughness coefficient (e. g. Aronica et al., 2002; Werner et al., 2005; Pappenberger et al., 2005). The probabilistic process of floodplain mapping is based on hydraulic model setup and ensemble simulation for other observed or design flood hydrographs (e. g. Bates et al., 2004, Di Baldassarre et al., 2010).

When the probabilistic approach is used for engineering purposes it is not necessarily based on the structure of the hydraulic model (i. e. physically-based 2D model). Also, there is a hypothetical argument that a complex hydraulic model is likely to represent more realistically the physical process of the river and floodplain flow and with higher accuracy. In previous work of Papaioannou and his associates (Papaioannou et al., 2016) at the same study area of Xerias Stream (Volos, Greece), several 1D, 2D and coupled (1D/2D) hydraulic-hydrodynamic models have been examined and evaluated for flood inundation and mapping. Based on the results of that study, 1D hydraulic models may provide good approximations of the inundated area when high quality data (derived from TLS-LiDAR DEM) is used for the hydraulic model setup (model construction) (Papaioannou et al., 2016). Moreover the selection of 1D hydraulic-hydrodynamic model is a very

common choice in applications such as Monte Carlo analysis and probabilistic mapping of outputs. These applications are computationally intensive and the simulation time is an important factor of the processes (Di Baldassarre et al., 2010; Alfonso et al., 2016; Teng et al., 2017). Thus, all of the abovementioned factors should be taken into account in order to select the optimum model for probabilistic flood mapping.

1.5 Aim of Dissertation-Key Questions-Research Objectives

The aim of this dissertation is to investigate, produce and propose new methodologies in order to improve flood prone area recognition and flood modelling and mapping under uncertainty at ungauged catchments. The selected study area of Xerias watershed, Magnesia, Greece, is characterized by lack of data and measurements. A framework for flood prone areas recognition has been developed, examined and validated in the study region. Moreover, extensive sensitivity analysis on flood modelling and mapping has been implemented in the study region based on the selected topography, the modelling approach and the modelling configuration. Finally, a probabilistic flood inundation mapping framework has been developed for ungauged streams to estimate the uncertainty introduced by the roughness coefficient in hydraulic modelling.

To meet the scope of the dissertation, a number of key questions should be answered:

1. Is it possible to recognize/identify flood prone area in study areas with limited data (or no data) using Multi-Criteria Analysis (MCA) techniques and Geographic Information Systems (GIS) and to what extent?
    - Which criteria should be used and why?
    - Which is the optimum MCA technique that should be selected?
    - Which is the optimum clustering technique that should be implemented?
    - How does the configuration of the framework affect the outcomes?
    - Which is the best framework configuration for the identification of flood prone areas?

2. Can hydraulic-hydrodynamic modelling, typical post flood analysis combined with standard flood hydrograph estimation techniques, be used for accurate determination of the flood extent?
    - How does the DEM resolution affect the accuracy of the flood extent?
    - How does the terrain configuration affect the accuracy of the flood extent and the overall operation of the model?

- How does the modelling approach affect the accuracy of the flood extent and the overall operation of the model?
- How does the roughness coefficient affect the accuracy of the flood extent?
- How do the inline structures affect the accuracy of the flood extent and the overall operation of the model?
- Which is the optimum choice of hydraulic-hydrodynamic model for probabilistic floodplain mapping at ungauged areas?

3. Is it possible to use a hydraulic-hydrodynamic model for probabilistic flood inundation mapping when the only estimated information about the flood is the flood extent?
    - How can a researcher estimate the uncertainty in river flood modelling due to the roughness coefficient?
    - Which theoretical probability distribution can be used for the generation of roughness coefficient values and why?
    - Which evaluation metric can be applied for probabilistic flood inundation mapping when the validation data is based on the flood extent?
    - How many iterations should be implemented?
    - Which is the optimum cross sections distance?
    - How do the threshold changes affect the statistical criterion?
    - How can HEC-RAS hydraulic-hydrodynamic model be used for Monte Carlos simulations?
    - How GIS tools can be implemented for the visualization and the presentation of the results?
    - How can integration of HEC-RAS and GIS be achieved to a HEC-RAS Monte Carlo framework?

The detailed research objectives of the dissertation are:

1. Identification of potential flood prone areas-potential flood hazard areas by developing a Multi-Criteria analysis component for potential flood prone areas mapping. The main objectives of the proposed component are:
    - to evaluate the ability of using multi-criteria analysis and GIS to identify potential flood prone areas
    - to use geomorphological, topographical and land use indices for potential flood inundation areas identification and mapping

- to develop an objective GIS-based spatial multi-criteria evaluation framework for identification and mapping of potential flood prone areas.
- to examine how sensitive are some factors used in flood prone areas mapping such as: a) clustering technique; b) multicriteria approach; c) different configuration of the data.
- to select the most appropriate techniques and methods used in the identification of potential flood prone areas,
- to develop a component that can be applied in flood hazard estimation at areas with limited available information, and/or in areas where preliminary flood hazard evaluation is required for flood mapping purposes using hydrologic and hydraulic modelling.
- to apply and demonstrate the proposed component in Xerias Watershed, Volos, Greece

2. Identification of sources of uncertainty – sensitivity analysis of riverine spatial resolution and accuracy and modelling approach. The main objectives of the sensitivity analysis in flood modelling are:
   - to investigate the effect of riverine terrain spatial resolution on flood modelling and mapping.
   - to investigate the effect of the hydraulic-hydrodynamic schemes on flood modelling and mapping
   - to use DEMs of varying degree of accuracy created by Terrestrial Laser Scanning (TLS) point cloud data, classic land surveying and digitization of elevation contours from 1:5000 scale topographic maps.
   - to use several hydraulic models of different level of complexity.
   - to use common techniques for the estimation of the flood hydrograph for ungauged catchments.
   - to use standard post flood analysis techniques for the validation of the flood hydrograph and the calibration of the roughness coefficient.
   - to examine the sensitivity analysis on flood modelling and mapping using different hydraulic-hydrodynamic models, different DEM approaches and different river topography configurations for application at ungauged watersheds
   - to demonstrate the methodology at an ungauged stream reach of Xerias stream, Volos, Greece.
   - to investigate the ability of various models to be used for probabilistic flood modelling.

- to propose a methodology that could be applied in ungauged watersheds with limited available information, and/or in areas with compound geomorphology using typical hydrologic and post-flood analysis techniques for flood modelling and mapping purposes.

3. Development of a probabilistic flood inundation component for ungauged streams due to roughness coefficient uncertainty in hydraulic modelling. The main objectives of the proposed component are:
   - to evaluate the ability of using a 1D hydraulic-hydrodynamic model and GIS to produce probability maps of flood plain areas for ungauged catchments and flash flood events.
   - to use typical processes to determine the size distribution of river/stream bed material, empirical formulas, several probability distributions and the Latin Hypercube Sampling algorithm to generate different sets of Manning roughness coefficients.
   - to develop a Monte Carlo component (for ungauged streams) for uncertainty analysis of floodplain mapping due to roughness coefficient.
   - to demonstrate the component at the ungauged Xerias stream, Volos, Greece.
   - to produce a valuable tool that can provide useful information for planning and implementing flood risk mitigation strategies.

1.6 Dissertation Structure

Chapter 1 of the dissertation is essentially a bibliographic review of the existing methodologies and models. It is deducted from the review the necessity to investigate flood events and how to deal with them, especially at ungauged catchments. Specifically, a detailed scientific review is presented for: a) Floods and Flash floods in Europe and Greece; b) Flood prone areas mapping at ungauged catchments; c) Flood inundation modelling and mapping at ungauged streams; d) Probabilistic flood inundation modelling and mapping at ungauged streams.

Chapter 2 presents a detailed description of the study area (geography, climate, and geomorphology) together with information on the study flood event occurred at October 9th, 2006 and the available data. Also, the estimation of the flood hydrograph used in the study is presented, as well as the data collected from several sources concerning this specific flood event.

Chapter 3 presents the development of an objective GIS-based spatial multi-criteria evaluation component at catchment scale for the identification of potential flood prone areas at ungauged watersheds. Potential flood prone areas are identified using GIS data and techniques such as clustering/classification procedures and two MCDA methods the AHP and the FAHP. Two different approaches have been implemented and compared in order to investigate the sensitivity of the proposed component in the identification of the flood prone areas at ungauged watersheds. The first approach is a process where all the criteria (DEM-derived geomorphological and hydrological attributes which are related to the flood generation process) are normalized before the application of the MCA method and then, several clustering and classification techniques are applied to derive the final potential flood-prone areas. The second approach is a method where all the criteria are clustered before and after the MCA process for the production of the potential flooded area maps, without normalization. The derived flood prone maps in the two approaches have been classified with five different clustering techniques. The methodology is demonstrated to Xerias stream watershed, Volos, Greece. Historical flood inundation data (flash flood event of 2006 that flooded sub-urban and urban areas of Volos city) and simulated flooded area derived from hydrologic - hydraulic modelling of the flood event have been used to validate the methodology.

Chapter 4 is a detailed description of the field measurements performed. Specifically, this chapter describes the following: 1) LIDAR field survey with TLS instrument and processed LIDAR DEM creation; 2) Post flood analysis based on field surveying data measured using typical topographical techniques; 3) Wolman Pebble Count field survey for the estimation of stream bed roughness.

Chapter 5 presents several sensitivity analyses of different hydraulic-hydrodynamic modelling approaches in combination with several types of river and riparian areas spatial resolutions for floodplain mapping and flood inundation modelling at ungauged watersheds. The first part of the analysis (First level of sensitivity analysis) examines four different types of riverine geomorphology: a) Digital Terrain Model (DTM) created from TLS data, b) Digital Surface Model (DSM) created from TLS data, c) topographic land survey data and d) typical digitized contours from 1:5000 scale topographic maps. Modelling of the stream has been approached by the implementation of the following models: HEC-RAS 1D, MIKE11 (interpolated cross sections, DEM compilation), MIKE21 HD (Grid-based), MIKE21 HD FM (Flexible mesh), MIKE11/MIKE21 HD (Grid-based) and MIKE11/MIKE21 HD FM (Flexible mesh) through MIKE FLOOD platform. The second part of the analysis (Second level of sensitivity analysis) examines the sensitivity derived only by the modelling approaches using the riverine geomorphology created by TLS data

(DTM). The models used in this analysis are: a) One dimension (1D) hydraulic models: HECRAS, LISFLOOD (kinematic and diffusive wave approximation), MIKE11 (interpolated cross sections and DEM compilation approach), XPSTORM; b) Two dimension hydraulic models: HECRAS, LISFLOOD, MIKE21 (Grid-based and Flexible mesh), XPSTORM, FLO2D; c) Coupled (1D/2D) hydraulic models: HECRAS, MIKEFLOOD (Grid-based and Flexible mesh), XPSTORM. In both parts, standard hydrological methods for ungauged watersheds have been used for both the hydrograph and the flood peak estimation. The validation process consisted of 2x2 contingency tables that compare the simulated flooded area and the observed flooded area based on the historical extreme flash flood event of the year 2006. The simulated flooded area was derived from combinations of the study hydrodynamic models at several riverine configurations and different DEMs. Finally, the hydrodynamic-hydraulic model was selected using the results of the analysis and used further in this study.

Chapter 6 presents the development of a generic procedure for uncertainty analysis of floodplain mapping due to roughness coefficient that have been implemented at the ungauged Xerias stream, Volos, Greece. The HEC-RAS 1D hydraulic-hydrodynamic model is used to assess the uncertainty introduced by the roughness coefficient using Monte-Carlo simulations. Manning's *n* roughness coefficient initial ranges are estimated using several empirical formulas employing pebble count and field survey data, and various theoretical probability distributions are fitted and evaluated using several goodness-of-fit criteria. Latin Hypercube sampling has been used for the generation of different sets of Manning roughness coefficients and several realizations of flood inundation maps are created. The uncertainty is estimated based on a calibration process which is based only on the flood extent derived from historical flood records for an observed extreme flash flood event. Moreover, an extensive sensitivity analysis has been conducted in many factors of Monte Carlo procedure in order to extract the best setup options (different distance between the cross sections, use of several realizations sets, use of different acceptable threshold level, and use of different distribution for roughness coefficient generation). Finally, the component has been tested for stability.

Chapter 7 outlines the conclusions of the dissertation, the scientific and technical innovative elements of this dissertation and the future extension and use of the methods and models developed and used. At the end, the scientific publications produced during the development of this dissertation are presented and the financial support is acknowledged.

The scientific publications used and cited in the development of this research are listed at the end of the dissertation.

CHAPTER 2^{o}

STUDY AREA AND HYDROMETEOROLOGICAL ANALYSIS OF AN EXTREME FLASH FLOOD EVENT

2 Study area and hydrometeorological analysis of an extreme flash flood event

This Chapter presents the study area and the hydrometeorological analysis of the study extreme flash flood event. The study area is separated in the following three regions: 1) Xerias Watershed, 2) Upper Xerias Watershed, 3) Xerias stream reach. Moreover, information about the extreme flash flood event of October 9th, 2006 and the flood data collection process are presented in detail. Finally, the last part of this chapter presents the estimation process of the study event flood hydrograph.

2.1 Xerias watershed and the selected stream reach

Xerias Watershed

Xerias watershed is located in the south-eastern part of Thessaly region, Magnesia prefecture, Greece (Figure 2.1) and lies between latitude 39°20'0" to 39°28'41" N and longitude 22°49'22" to 23°03'15" E. Xerias watershed area is approximately 120 km^2. The altitude is ranges from 0 to 1600 m. The average and median elevation of the watershed are 458 m and 320 m respectively (Figure 2.2). Xerias stream drains through the City of Volos and has experienced frequent flood episodes due to intense storms. The climatological description is based on data retrieved from the Meteorological Station of Volos (operation period from 02/2007 to 07/2017) that is included in the Network of the National Observatory of Athens (NOA). The climate is typical Mediterranean with an average temperature of 17.8°C and a variation from 8.4 to 28.4°C (Figure 2.3). Summers are usually hot and dry, and temperatures sometimes reach up to 40°C. The average annual precipitation varies from 400–770 mm and occurs mainly in autumn, winter and spring (Figure 2.4). In this dissertation CORINE LAND COVER 2000 data, known as CLC2000, has been used for the determination of the land cover. The largest part of the study watershed is covered mainly by forest and semi natural areas (57.04 %), by agricultural areas (35.82 %) and artificial surfaces (7.14 %) (Figure 2.5a). The geology of the watershed has been estimated by digitizing the Institute of Geology and Mineral Exploration (IGME) maps (scale 1:50,000). Therefore, Schist geological structures cover a 48.96 % of the total area, karstic structures cover a 34.87 % and alluvial deposits cover a 16.18 % (Figure 2.5b).

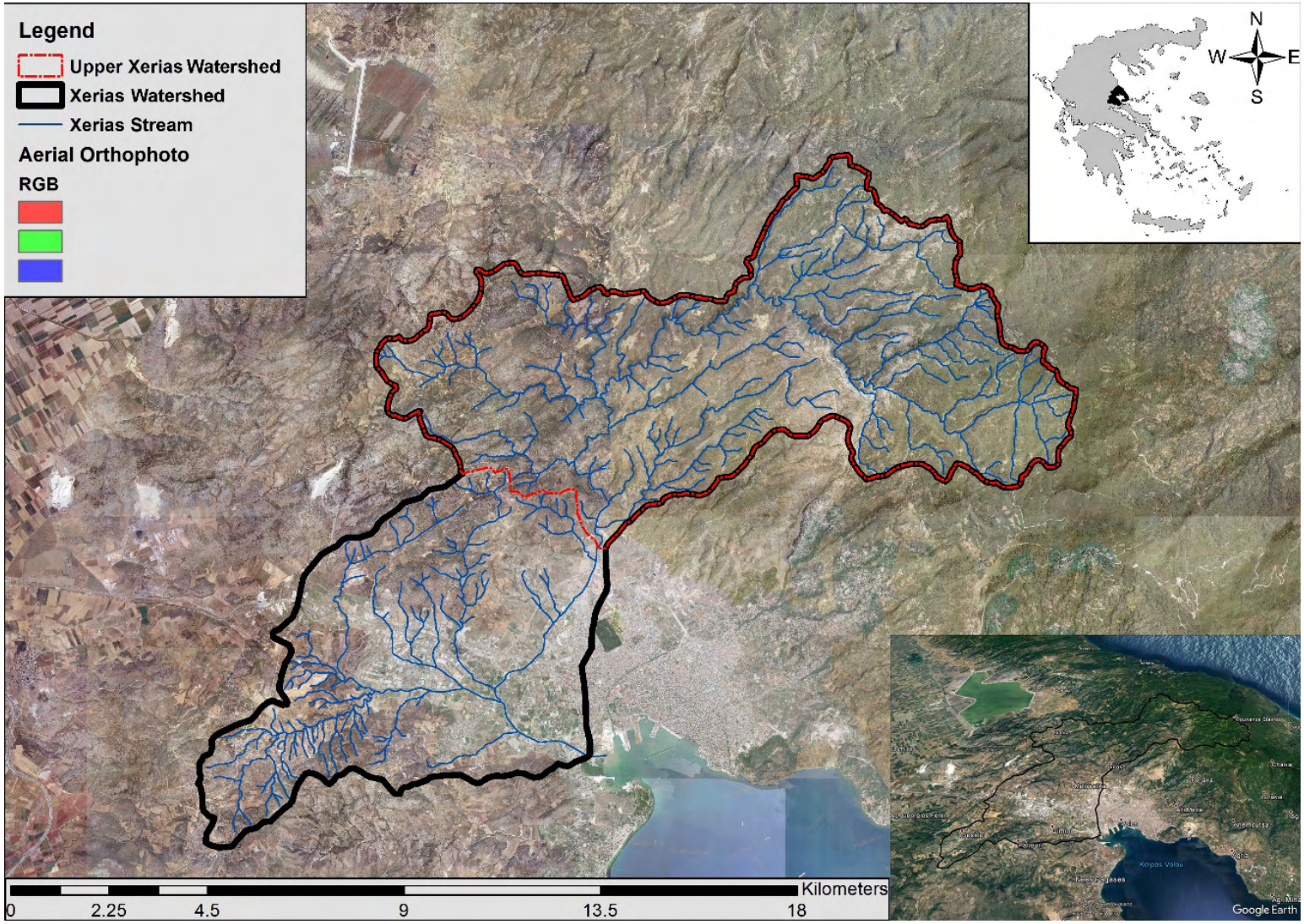

Figure 2.1. Xerias Watershed and Upper Xerias Watershed.

Upper Xerias Watershed

The area of the Upper Xerias Watershed is approximately 71 km^2 (Figure 2.1, Figure 2.6). The altitude is ranges from 52 to 1600 m (Figure 2.2, Figure 2.6) and the mean slope of the area is 28 %. The average and median elevation of the subwatershed are 672 m and 576 m respectively. The largest part of this subwatershed is covered mainly by forest and semi natural areas (80.47 %) and agricultural areas (19.54 %) (Figure 2.5a). Concerning the geology of the subwatershed, schist and gneiss impervious areas cover the 50.9 % of the total area, karstic limestone areas cover 42.3 % and alluvial deposits cover only the 6.8 % (Figure 2.5b).

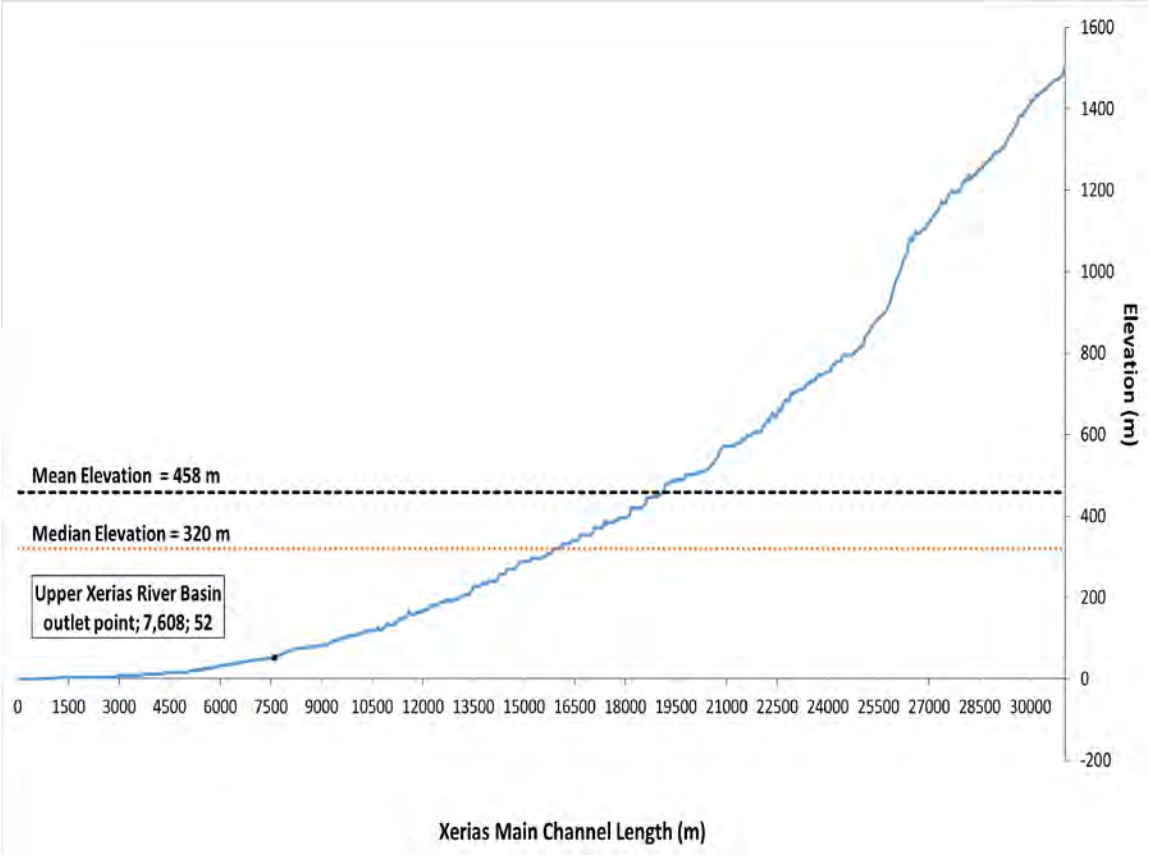

Figure 2.2. Xerias Watershed altitude profile.

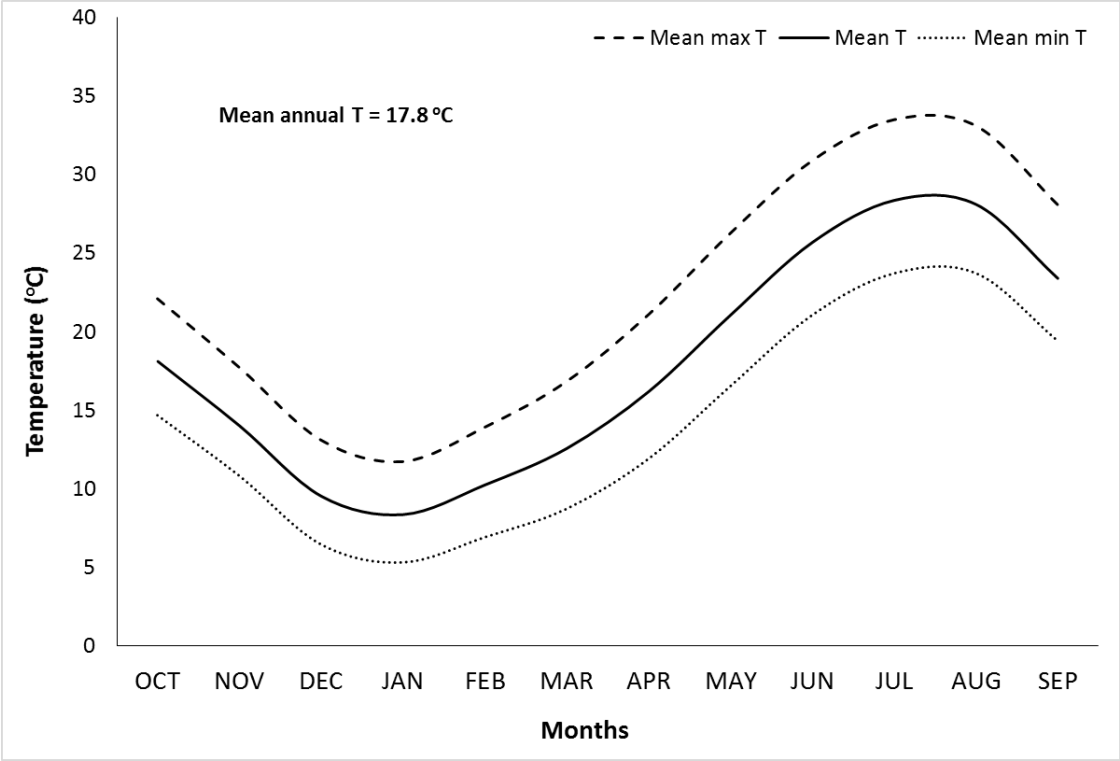

Figure 2.3.Mean monthly temperature in the City of Volos.

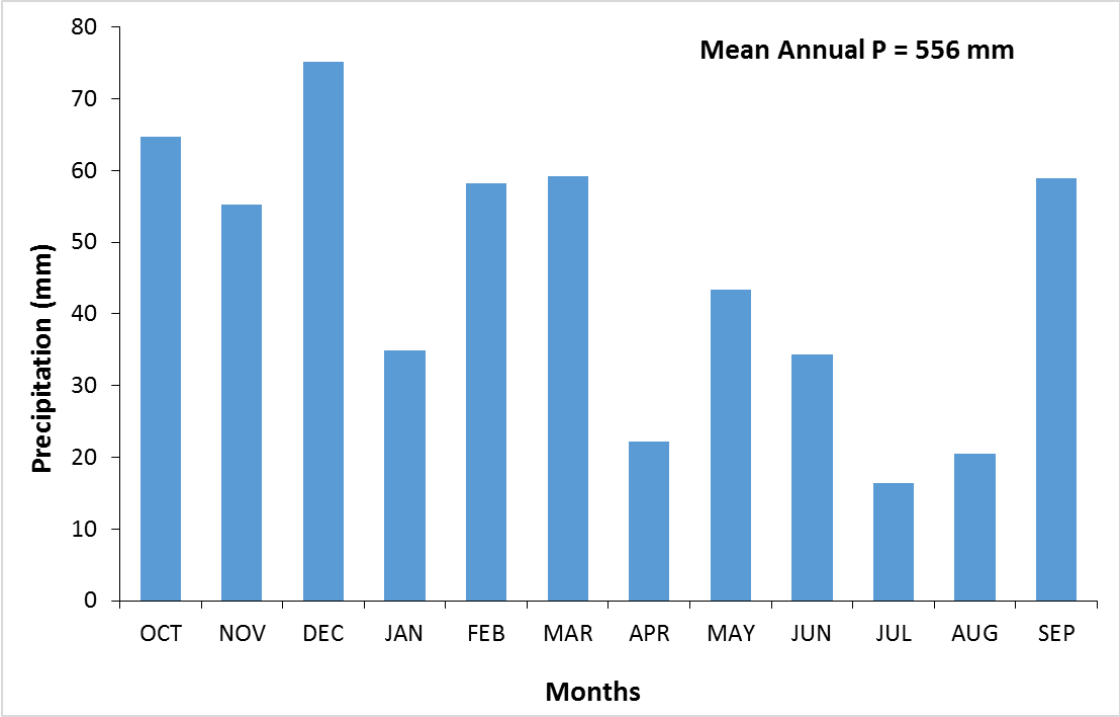

Figure 2.4. Mean monthly precipitation for the City of Volos.

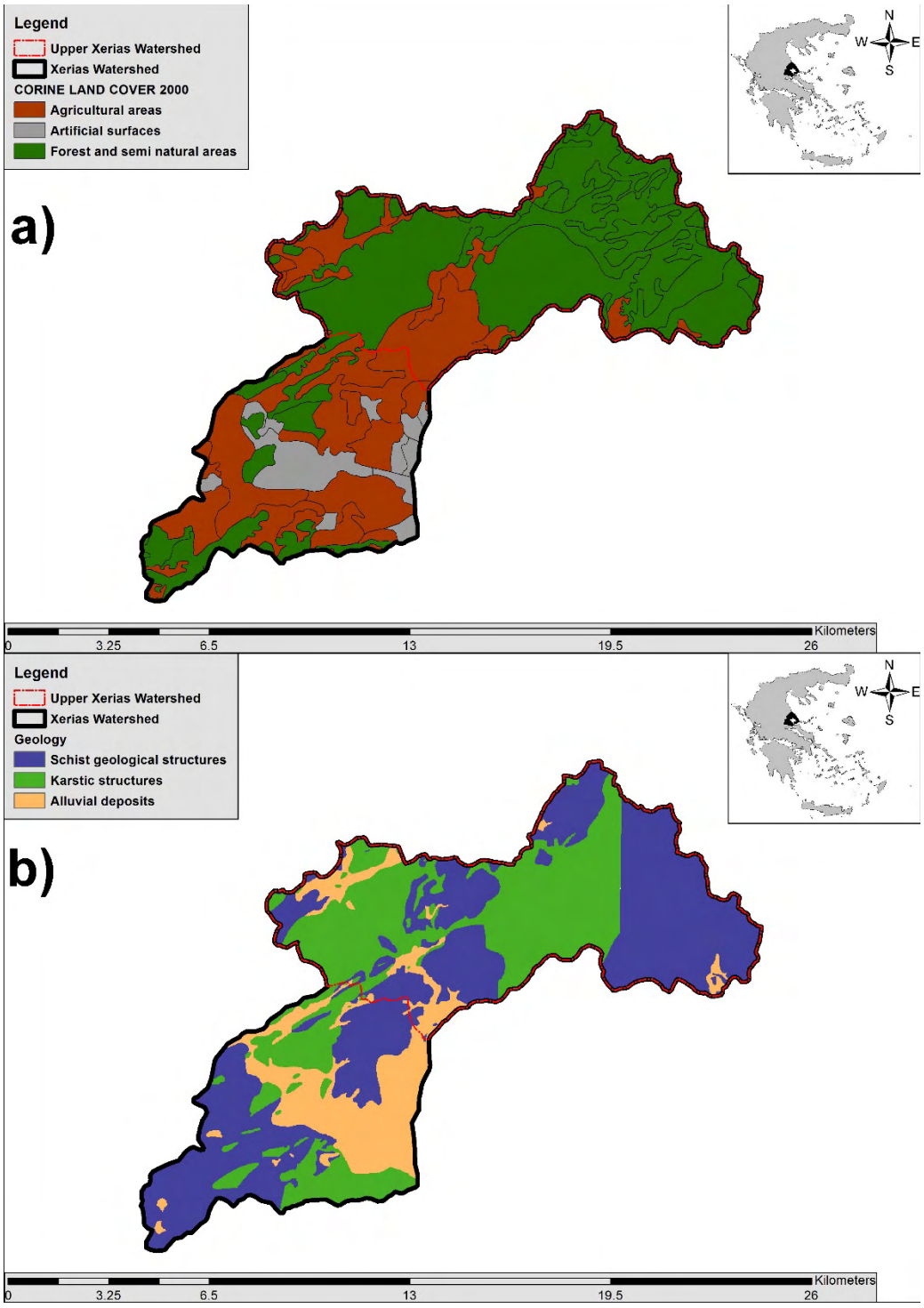

Figure 2.5. a) Xerias Watershed and Upper Xerias Watershed land cover, b) Xerias Watershed and Upper Xerias Watershed geology.

Xerias Stream Reach

The selected Xerias stream reach is located in a sub-urban area of Volos city (Figure 2.6). The examined stream length is approximately 2.2 km and the altitude is ranging from 22 to 52 m. More than the two-thirds (2/3) of the reach is surrounded by cultivating areas while the other part is surrounded by partially urbanized area. The gradient of the stream reach is 0.014 m which means that the altitude is rising approximately 14m/km. (Figure 2.7). In the selected stream reach exists there are three (3) bridges in a raw with variable lengths and widths (Figure 2.6, Figure 2.7). The bridges length (from the upstream to downstream) and width (left to right span) vary approximately from 5 to 56 m and 32 to 40m respectively (Figure 2.7). The distance between the bridges is 223 and 670m (Figure 2.6, Figure 2.7). The selection of the stream reach was based on the severe damages of the railway network during the extreme flash flood event of 2006. During this event the railway bridge was collapsed. Furthermore, the study stream reach selection was based on the ungauged nature of the watershed, the existence of typical bed material that usually observed in mountainous and semi-mountainous streams, and the complexity of the river topography. All the above-mentioned factors meet the research needs of the dissertation and justify the selection of the specific stream reach.

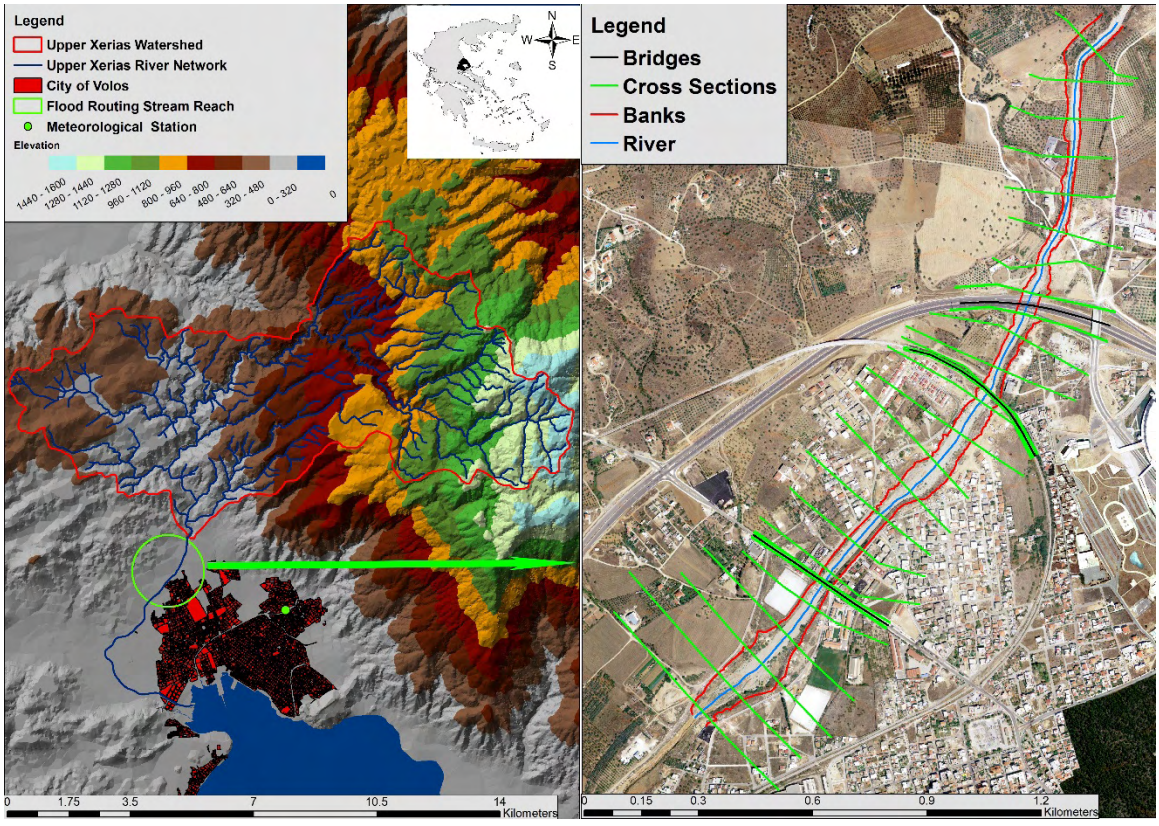

Figure 2.6. LEFT: Xerias stream study watershed. RIGHT: Flood routing stream reach.

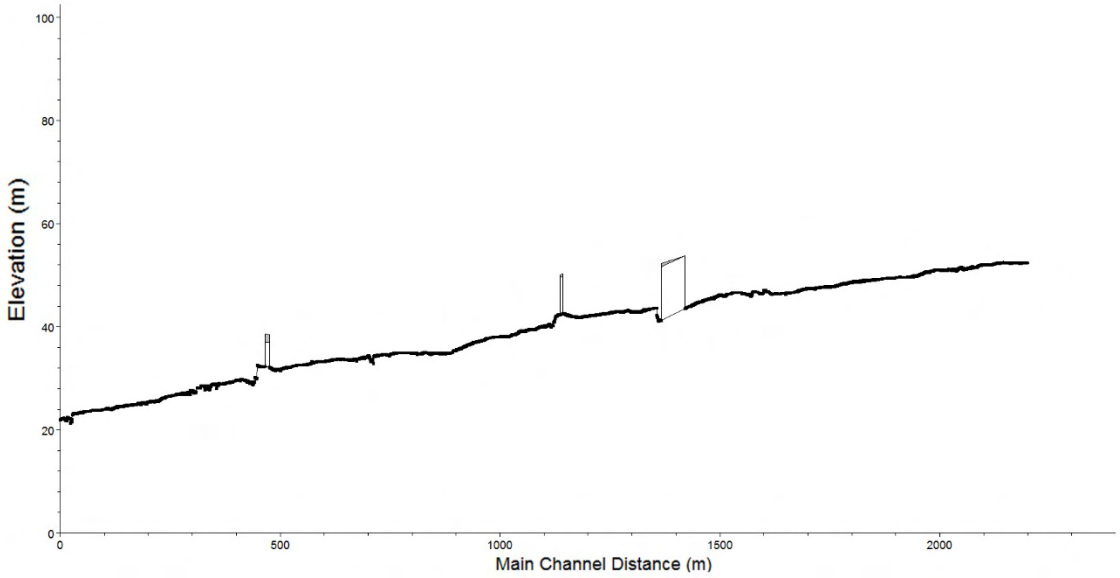

Figure 2.7. Xerias stream reach elevation profile

2.2 Flood event of 2006

2.2.1 Extreme flash flood event

In general, Greece is a country that can experience a variety of potential flooding threats produced by the diversity in the meteorology, topography, and hydrology. Given the meteorological and hydrological characteristics for many regions of Greece, flash floods associated with intense precipitation during a very short time over a relatively small area, rapid accumulation (steep slopes), fast rising of water level and a relatively high peak discharge are often a more pressing concern than riverine flooding from an expansive storm and/or large snowmelt runoff. Orographically enhanced storm events are common due to the rugged mountainous topography found throughout much of the country, especially at coastal areas. Thus, the majority of the watersheds that generate flash floods have the above mentioned characteristics. Usually, this kind of watersheds flow into the sea and their main channel is passing through built-up areas (village, city, etc.) of variable population of great economic and social importance. Flood frequency, intensities and type of precipitation show great variability with a complex topographical structure in watersheds as a consequence of changing climate nowadays. In this dissertation, Xerias watershed has been selected due to typical climatologic and geomorphologic conditions that generate flash floods. Therefore, the study watershed is a typical Mediterranean catchment with flash flood events. It should be mentioned that the methodologies

developed and applied in this study watershed can be applied in other watersheds with similar geophysical and hydrometeorological conditions. Several, historical flash flood episodes have been observed on the selected watershed (SSW-MEECC, 2012; Diakakis et al., 2012).

Particularly, on 9 October 2006, Magnesia region has been experienced heavy rainfalls in short time that resulted to severe pluvial and fluvial flooding of the city of Volos. The extreme flash flood episode has been recorded as one of the worst floods events of the Magnesia area. The evolution of the rainfall activity is presented in Figure 2.9e-h. In Figure 2.8a, the satellite image of Greece during the 9th October 2006 flood event is shown. Most of Greece, especially the central and eastern Greece, is covered by the clouds of the weather system. Moreover, in Figure 2.8b can be seen the infrared satellite image during the 9th October 2006 flood event, wherein with red coloured are highlighted the areas that experienced severe rainfall events, one of which is the Magnesia area and the Volos greater area. On that day, the study watershed has been affected by a low pressure system of 1,008 hPa that centered over the Aegean Sea and associated with a cold front (Yair et al., 2010). From the 500 hPa geopotential height (Figure 2.9a-d) can be seen the evolution of the weather system that is moving very slowly southeastward without further deepening. Therefore, this convective storm produced high intensity and continuous rainfall to the study watershed and caused flooding in city of Volos. Based on the study of Harats and his associates (Harats et al., 2010) the recorded total rainfall was 232 mm and lasted from 06:00 UTC to 18:00 UTC, 9 October 2006.

In this study, the rainfall data retrieved from the meteorological station of the Institute of Industrial Plants and Livestock – Department of Plant Protection, Volos has been taken into account. This meteorological station is installed in the area of Fytoko (Figure 2.6) and the total recorded rainfall was 211 mm (Table 2.1). The return period of the study event is estimated approximately at 100 years, based on prior Intensity-Duration-Frequency analysis at the study area (Papaioannou and Loukas, 2010) and the analysis of Koutsogiannis and Mahairas (2010). The extreme flash flood event mainly affected agricultural areas, the transportation networks and other technical infrastructures at the study watershed (Papaioannou et al., 2011). More than one fifth of Volos city area encountered heavy mudslides due to severe debris flow and the railroad bridge that connect Volos and Larissa cities collapsed (Figure 2.10).

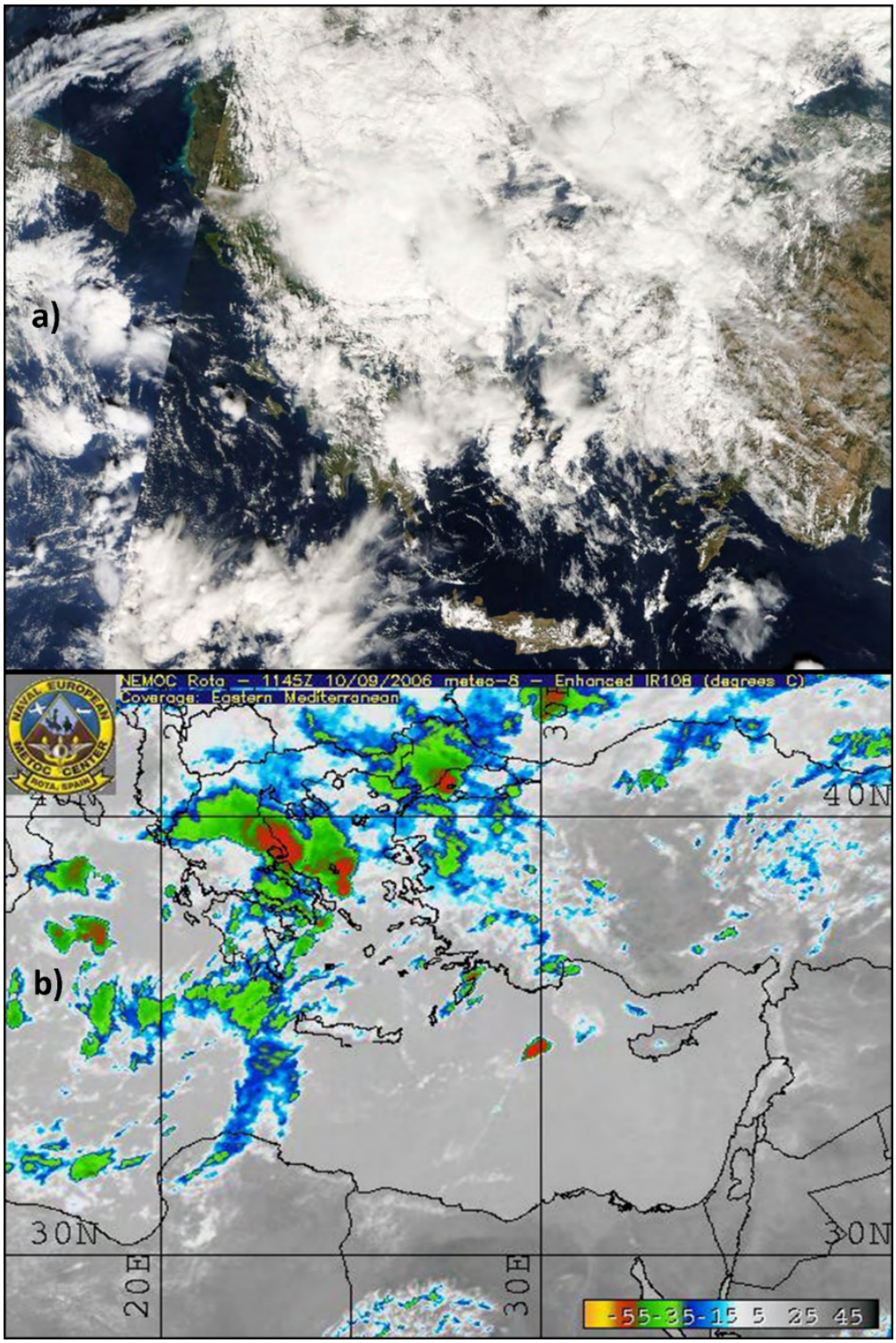

Figure 2.8. UP: Satellite image of Greece during the 9th October 2006 flood event (MODIS-Aqua/Terra). DOWN: Infrared satellite image during the 9th October 2006 flood event (METEOSAT from EUMETSAT) (Source: UP: http://lance-odis.eosdis.nasa.gov/imagery /subsets/?area=eu; DOWN: www.nemoc.navy.mil or https://www.eumetsat.int/).

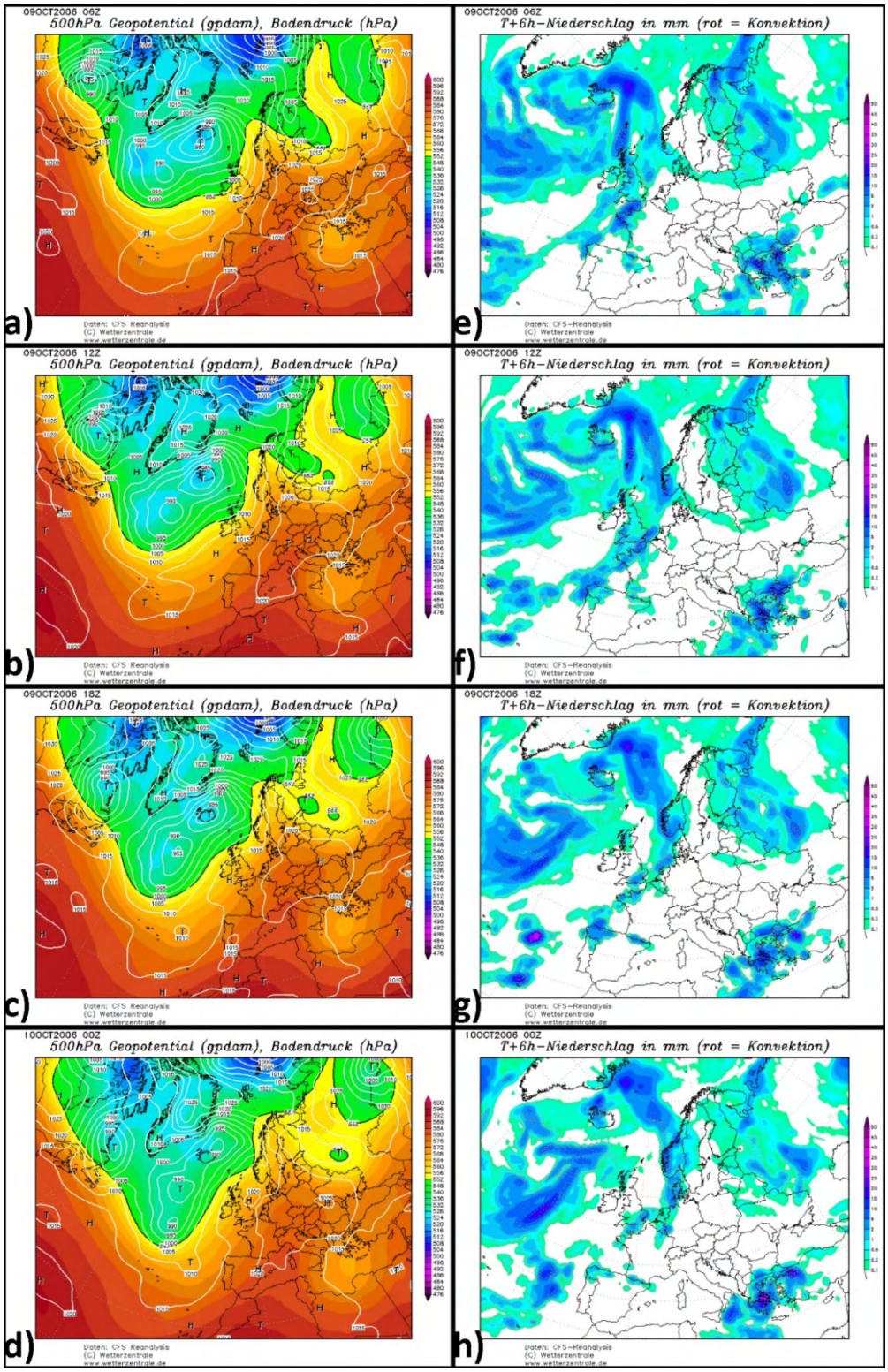

Figure 2.9. Climatological conditions during the 9th October 2006 event from 6Z to 0Z (Greece is located in the southeast part of the maps): a-d) Geopotential height (gph) at 500 hPa, e-h) Rainfall (Source: www.wetterzentrale.de).

Table 2.1. Rainfall data from Volos-Fytoko meteorological station (Source: Institute of Industrial Plants and Livestock – Department of Plant Protection, Volos)

Time (Eastern European Summer Time / UTC/GMT +3 hours)	Time interval	Total time	Total rainfall (mm)	Rainfall intensity (mm)
9:18:02	0	0	0.20	0.20
10:18:23	1:00:21	1:00:21	27.07	26.87
11:18:12	0:59:49	2:00:10	45.05	17.98
12:18:25	1:00:13	3:00:23	69.08	24.04
13:18:27	1:00:02	4:00:25	96.15	27.07
14:19:28	1:01:01	5:01:26	118.98	22.83
15:18:43	0:59:15	6:00:41	150.49	31.51
16:19:03	1:00:20	7:01:00	174.73	24.24
17:18:52	0:59:49	8:00:50	186.85	12.12
18:28:30	1:09:39	9:10:28	191.90	5.05
19:25:33	0:57:03	10:07:31	193.11	1.21
20:19:04	0:53:31	11:01:02	200.59	7.47
21:20:08	1:01:04	12:02:06	210.08	9.49
21:42:05	0:21:57	12:24:03	211.29	1.21

Figure 2.10. Photographs taken during and after the extreme flash flood event of 2006: a) Railway bridge after the occurrence of the event; b) Flooded cars in sub-urban area of Volos city; c) Central road in Volos city during the flood event; d) Condition of Xerias stream some hours after the peak flow (Source: a,b photos provided by Stauros Ntafis and Solonas Tsakiris, c,d photos provided by newspaper Thessaly).

2.2.2 Flood data collection

The collection of data concerning the 9th October flood event has been a hard and time-consuming process due to the insufficient amount of data, the storage of data in several authorities' archives, the format of data, the human factor (e.g. evaluation of flood extent testimonies) and sometimes the bureaucracy that delayed the entire process. The entire process of the flood data collection lasted approximately four months.
The historical flood records have been collected by:

- Several authorities such as the Administration of Technical works (Decentralized Administration of Thessaly Region), the Welfare Department of Volos Municipality and the Fire Department of Volos city.
- The newspapers of Volos "Thessaly" and "Taxydromos".
- Records from local amateur meteorologists Mr. Solonas Tsakiris and Mr. Stavros Ntafis.
- Local interviews and testimonies of flood victims.

All the above mentioned data have been transformed to features that include the spatial information and digitized through GIS environment in order to visualize the extent of the flood event based on the spatial distribution of the data. The final dataset includes points, polygons and polylines digitized by the following records (Figure 2.11): 1) Houses that were refunded for electrical machines damages (depicted with yellow points), 2) Companies that were compensated for flood damage (depicted with red points), 3) Buildings that were refunded for structural damages (depicted with blue points), 4) Flooded streets recorded by the Fire Department of the City of Volos (depicted with green lines).
As can be seen from Figure 2.11, the majority of the flood data collected are distributed in the lower part of Xerias stream and mainly inside the area of Neapoli district. Thus, further investigation of flood data has been necessary for the selected flood routing stream reach. In Figure 2.12 the flood data collected for the selected flood routing stream reach is presented. This flood data consist of the estimated area by newspaper articles and human testimonies of flood victims. The flood data collected for the specific flood routing stream reach will be referred from now on as "observed flooded area" or "validation area" or "calibration area". Unfortunately, none of the flood victim testimonies reported the flood water depth. Some of the testimonies have been categorized as unreliable because the interviewee gave unreliable flood extent.

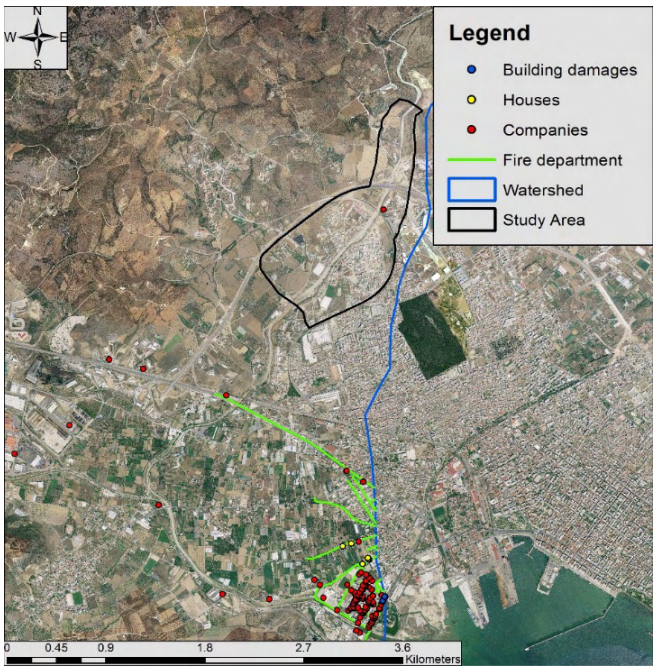

Figure 2.11. Spatial distribution of the flood data (event of 9th October 2006) collected by several authorities.

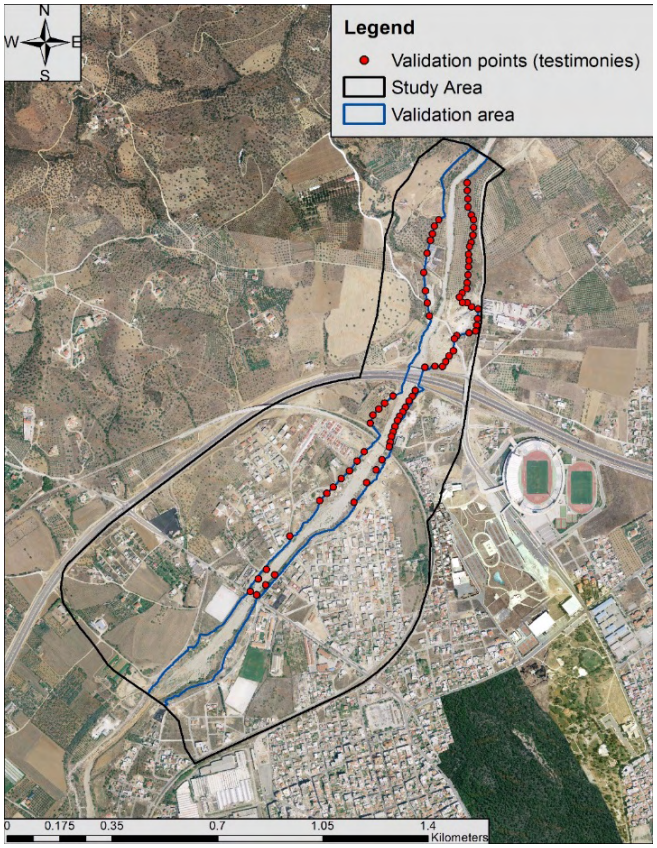

Figure 2.12. Flood routing stream reach reconstructed flood validation data.

2.3 Flood hydrograph estimation

A typical methodology followed for the determination of the instantaneous hydrograph for streams without flow records (ungauged catchments) is the Clark Instantaneous Unit Hydrograph (CIUH: Clark, 1945). Thus, a CIUH using Kinematic wave approximation has been used for the hydrograph generation of the 2006 extreme flash-flood event. The CIUH has been derived using a rainfall-runoff model based on Curve Number (CN) for the effective rainfall calculation, the estimation of time-area curves is based on Giandotti time of concentration formula and a linear convolution used for the runoff routing. The rainfall hyetograph used is based on the precipitation data presented in Table 2.1. The effective rainfall has been estimated using the Soil Conservation Service – Curve Number (SCS-CN) formulas (USDA-SCS, 1985):

$$CNI = \frac{CNII}{2.334 - 0.01334\,CNII} \tag{2.1}$$

$$CNIII = \frac{CNII}{0.4036 + 0.0059\,CNII} \tag{2.2}$$

$$Sk = \left(\frac{25400}{CN}\right) - 254 \tag{2.3}$$

$$P_e(t) = \begin{cases} \dfrac{(P_a - 0.2Sk)^2}{P_a + 0.8Sk}\,, for\ P_a > 0.2Sk \\ 0\,, for\ \ P_a =< 0.2Sk \end{cases} \tag{2.4}$$

$$I_e = \frac{P_e(t+1) - P_e(t)}{\Delta t} \tag{2.5}$$

where *CNI* is the curve number for dry soil moisture conditions; *CNII* is the curve number for average soil moisture conditions; *CNIII* is the curve number for wetter soil moisture conditions; *Sk* is the potential maximum retention; *CN* is the curve number; P_e is the accumulated precipitation excess at time *t*; P_a the accumulated rainfall depth at time *t*; I_e is the effective intensity; and Δt is the is the time interval.

SCS methodology has been applied successfully in several catchments of the Mediterranean area (e.g. Brocca et al., 2009; Tramblay et al., 2010). In this study, the estimation of CNII is based on the CLC2000 and the geological data of the study watershed (see Subsection 2.1). The value of CNII used in this analysis is the average value of seventeen (70) that derived from the estimated spatial distributed CN map. In Table 2.2 are presented the processed rainfall data.

Table 2.2. Processed rainfall data of the 2006 flood event

time t hr per 30 mins	P (mm)	P_e (mm)	I_e (mm)
0	0.00	0.00	0.00
0.5	13.46	0.31	0.62
1	26.91	4.70	8.78
1.5	35.98	9.52	9.64
2	45.00	15.24	11.43
2.5	56.96	23.78	17.10
3	68.93	33.11	18.65
3.5	82.44	44.26	22.30
4	95.96	55.91	23.29
4.5	107.22	65.86	19.91
5	118.44	75.98	20.23
5.5	134.17	90.40	28.84
6	150.13	105.25	29.70
6.5	162.27	116.67	22.84
7	174.32	128.08	22.83
7.5	180.60	134.06	11.96
8	186.68	139.86	11.60
8.5	188.97	142.05	4.37
9	191.14	144.13	4.16
9.5	192.31	145.25	2.25
10	192.95	145.86	1.22
10.5	196.25	149.03	6.33
11	200.44	153.05	8.04
11.5	205.09	157.51	8.94
12	209.75	162.00	8.98
12.5	211.29	163.49	2.97
13	211.29	163.49	0.00

Moreover, the runoff routing module used is essentially the convolution integral between the effective rainfall and the IUH (Instantaneous Unit hydrograph):

$$Q(t) = Aw \int_0^t I_e(\tau) IUH(t-\tau) d\tau \tag{2.6}$$

where $I_e(\tau)$ is the effective rainfall intensity over the block of rainfall at time τ; $IUH(t-\tau)$ is the ordinate of the Instantaneous Unit Hydrograph (IUH) at time $t-\tau$, and τ is the dummy time variable of integration.

Afterwards, the convolution integral is rewritten in the following discrete form due to the discrete quantities used:

$$Q_k = \sum_{j-1}^{k \le m} I_{e,j} UH_{k-j+1} Aw\, \Delta t \tag{2.7}$$

where m is the number of steps Unit Hydrograph (UH); n is the number of steps I_e, $k = w+m-1$; Δt is the is the time interval; Aw is the area of the watershed; $t = k*\Delta t$; and the Instantaneous Unit hydrograph is substituted with the Unit Hydrograph (UH).

The Time area-curve characteristics has been estimated using several DEM derived factors with the use of GIS and the Giandotti time of concentration formula (Table 2.3, Figure 2.13). The Giandotti formula is (Giandotti, 1937):

$$t_c = \frac{4\sqrt{Aw} + 1.5Lmax}{0.8\sqrt{H_{mref} - H_{ref}}} \tag{2.8}$$

Where t_c is the concentration time; Aw is the watershed area; H_{mref} is the mean elevation of the watershed; H_{ref} is the minimum elevation of the watershed; and $Lmax$ is the maximum main channel length.

The estimated Giandotti time of concentration is approximately 3.5 hr. According to the study of Efstratiadis et al., (2014), only the Giandotti time of concentration formula managed to give satisfactory results against 32 large flood events in Cyprus. Furthermore, the kinematic wave approximation has been based on the following UH formula:

$$UH_t = \frac{1}{Aw} \frac{A(t+1) - A(t)}{\Delta t} \tag{2.9}$$

Where $A(t)$ is the time-area curve; Aw is the area of the watershed; and Δt is the is the time interval.

MATLAB *conv* routine has been used for the calculations of the convolution. Finally, the estimated CIUH is presented in Figure 2.14.

Table 2.3. Time area-curve characteristics and the derived Unit Hydrograph

Giandotti time of concentration (3.5 hr) per 30 mins	Cells of grid per Area	Area (km^2)	Cumulative Area (km^2)	Normalized Area	UH (h-1)
0	0	0	0	0	0
0.5	13813	5.53	5.53	0.08	0.16
1	33867	13.55	19.07	0.27	0.38
1.5	40351	16.14	35.21	0.50	0.45
2	18022	7.21	42.42	0.60	0.20
2.5	25440	10.18	52.60	0.74	0.29
3	27566	11.03	63.62	0.90	0.31
3.5	18644	7.46	71.08	1	0.21

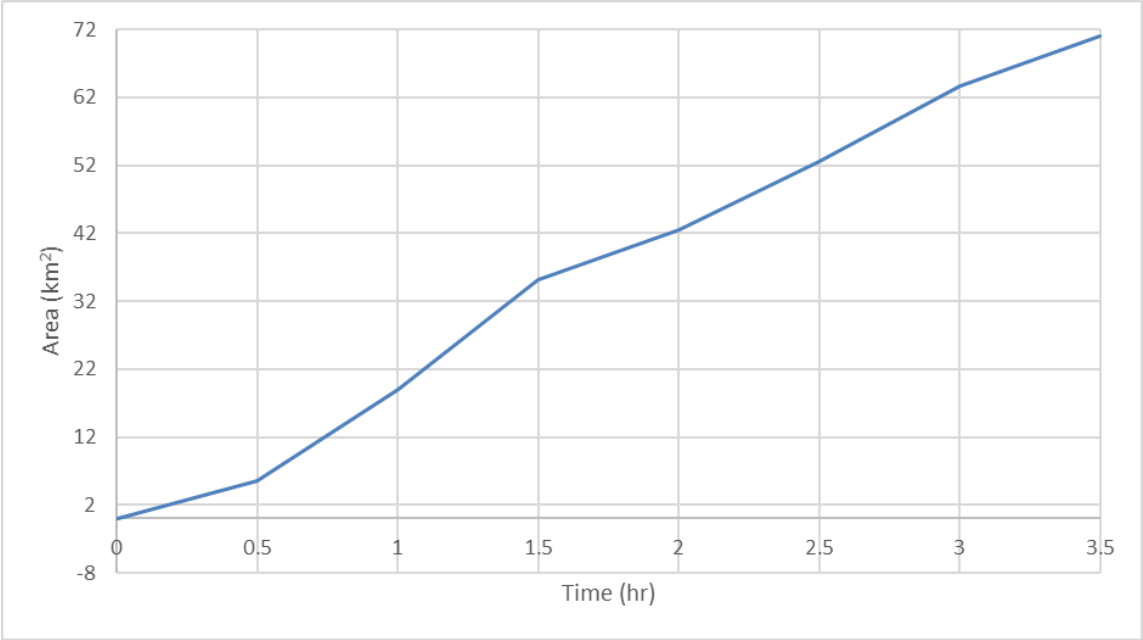

Figure 2.13. Time of travel versus cumulative area based on Giandotti formula.

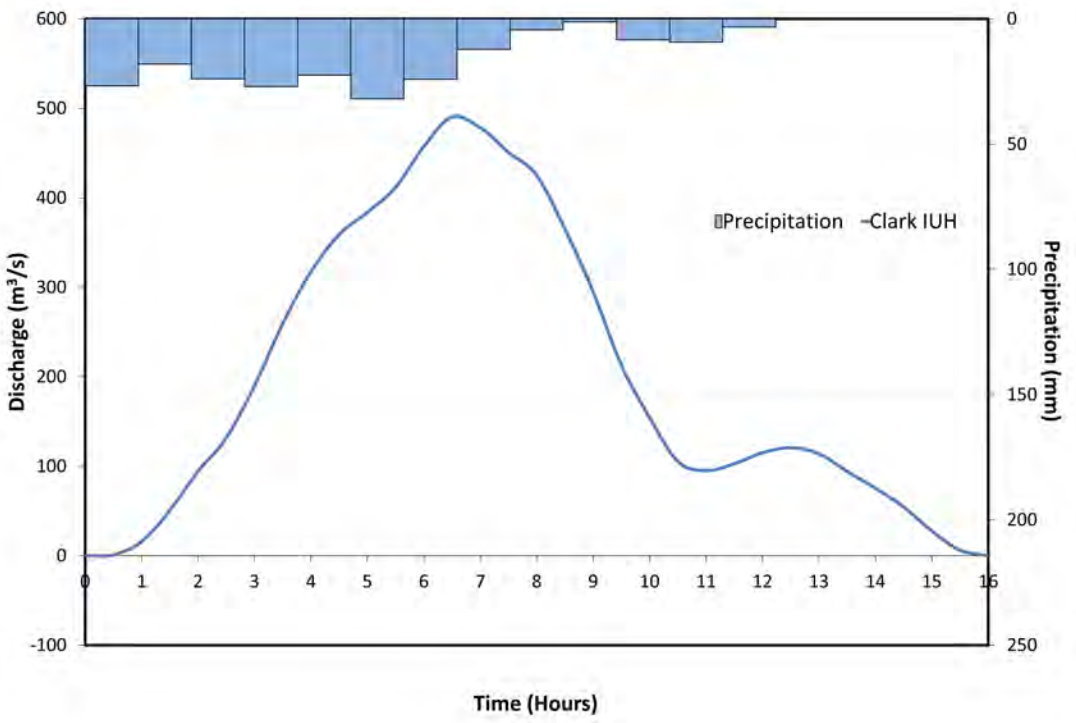

Figure 2.14. Hydrologic Response of Upper Xerias Watershed for the 09 October 2006 extreme storm event.

Finally, the relation of hydrological characteristics of a watershed with the geomorphologic parameters, especially at ungauged watersheds, can illustrate the hydrologic behavior with a simpler and more accurate way (Bhaskar et al., 1997; Kumar, 2015). Thus, the concept of a geomorphologic instantaneous unit hydrograph (GIUH) is proposed for illustration, especially at ungauged watersheds, by many authors (Rodriguez-Iturbe and Valdes, 1979; Gupta et al., 1980; Loukas et al., 1996; Hall et al., 2001; Kumar et al., 2007; Khaleghi et al., 2011; Hallema and Moussa, 2014; Hosseini et al., 2016). However it should be mentioned that other methodologies could be applied in the estimation of the flood hydrograph.

CHAPTER 3ο
FIELD SURVEY

3 Field survey

In order to determine quantitatively the important elements in the process of flood inundation modelling and mapping demands a variety of data and the estimation of several parameters. In this chapter, several field measurements performed for data collection and parameter estimation are presented. Specifically, this chapter describes the following: 1) LIDAR field survey; 2) Post flood analysis; 3) Wolman Pebble Count field survey. The LIDAR field survey has been conducted in order to create and use a high resolution bare earth DEM in the process of flood inundation modelling and mapping for sensitivity and uncertainty analysis. Moreover, the post flood analysis has been conducted in order to determine the primary value of roughness coefficient of the study flood routing stream reach and to validate the produced flood hydrograph using indirect measurements. Finally, the Wolman Pebble Count Field survey has been applied for indirect estimation of the roughness coefficient using several empirical equations.

3.1 LIDAR field survey

3.1.1 LiDAR data collection

Traditionally, the collection of topographic data sets has been based on photogrammetric or ground surveying methods. Despite the fact that these techniques are well established, when they are applied for flood inundation modelling, they are subject to certain limitations such as the time required for the measurements, the coverage of the study area and the accuracy of the derived data sets. The technological developments in recent years have provided the scientific community with new instruments and techniques, such as Terrestrial Laser Scanners (TLS) or Airborne Light Detection and Ranging (LIDAR). Airborne LIDAR data resolution range usually depends on the application needs. Their spatial resolution in horizontal axis can vary from 5–10 cm and provide vertical accuracy up to 25 cm (Baltsavias, 1999; Liu, 2008; Sampson et al., 2012). Despite the advantages of Airborne LIDAR, for small scale projects, their use is restricted by the high cost of data acquisition.

On the other hand, the use of TLS have gained popularity among the small scale projects due to their general applicability (e.g. for urban modelling, archeology, manufacturing, etc.) and because TLS can provide data of higher resolution compared to the Airborne

LIDAR. Nevertheless, LIDAR data sets become difficult to handle as the resolution and the study area increase. Moreover, the management of such huge data sets is a very demanding task and requires increased computational resources. Another difficulty in LiDAR data handling is the existence of non-surface objects such as vegetation cover, buildings, etc. The use of raw LIDAR data can provide the Digital Surface Model in which the natural and built features are depicted. The development of "bare earth" Digital Elevation Model (DEM) from LiDAR data is a very demanding and time-consuming process and involves the exclusion of non-surface objects (Sharma et al., 2010).

The rising applicability of Airborne LIDAR in the last decades has resulted in the development of several filtering methods that have been applied to aerial laser scanner point cloud data (Vosselman and Maas, 2014). As it is expected the filtering methods have been based on different approaches such as the mathematical examination of the morphology, the progressive densification of a triangle mesh, the linear prediction and robust hierarchic interpolation, etc. (Vosselman and Maas, 2014).

TLS data are mostly 3D as opposed to digital elevation models or airborne LiDAR data which can be considered 2.5D. This means that traditional data analysis methods based on raster formats (in particular the separation of vegetation from the ground, e.g. Sithole and Vosselman, 2004) or 2D vector data processing cannot, in general, be applied to ground based LiDAR data. Also, in TLS data, obstacles that derive by the perspective geometry of single terrestrial scans can be observed (Brodu and Lague, 2012). Although the airborne data filtering approaches are very helpful, fail to be applied effectively in processing ground-based scans at small scales. Hence, the use an efficient method or approach to remove natural and built features from TLS data is a challenging process (Sharma et al., 2010).

Geomorphologic filters, GIS operations and expert knowledge have been used in this study in order to create the "bare earth" DEM from high-resolution TLS point cloud datasets using last returns. Optech ILRIS 3D laser scanner has been used in this study for the collection of high accuracy topographic data. The TLS used in this analysis produces unregistered point cloud data. The "dry" state of the river and riverine area and the topography of the selected case study was suitable for the usage of a laser scanner. The main equipment used for the scanning process are: 1) ILRIS 3D TLS; 2) Power generator; 3) Robotic; 4) Tripod; 5) Cones; 6) Laptop; 7) wires; 8) Wooden sticks; 9) Hammer; 10) Paint spray (Figure 3.1c). The mounting of ILRIS 3D laser scanner on the robotic system allowed for a 360^{o} field view and freedom for tilting vertically. Moreover, the selection of the scanning resolution in specific areas is adjusted by the user. Thus, the scanning resolution varied from a few centimeters (short-distance objects) to thirty-five centimeters (long-distance objects). A zig-zag pattern has been followed in order to cover

the entire study area (Figure 3.1a). The total number of 86 scan stops has been applied to both sides of the river banks (Figure 3.1a).

The entire scanning process involves the following basic steps that have been repeated in each scan stop:

1. Preparation of the surface (vegetation removal, etc.) in the specified scan stop for the installment of the LIDAR and placement of the entire equipment (Figure 3.1c).
2. Marking with spray and installment the wooden sticks to the position of the cones inside the dry river and placement of ten (10) cones. The placement of the cones is based on the fact that the merging process relies on their visibility and the overlay between two point cloud data-sets. Hence, the placement of the cones has been established in areas of high visibility and with good spatial distribution inside the river allowing an overlapping area with five cones (Figure 3.1b).
3. Define the vertical tilt of the LIDAR and apply the preliminary photo shooting in 360^{o}. If the LIDAR calibration is accepted the user defines the scanning resolution for specific areas (e.g. Figure 3.2a), else the calibration process is repeated until acceptable installment is achieved.
4. When the scanning process finishes, the user should inspect the generated point cloud data (e.g. Figure 3.2b,c). To inspect the point cloud data, the user transform them into PIF format, in order to be processed by Polyworks software (Polyworks, 2007). Using the IMInspect tool (Polyworks v.10 software), the user can easily insect if the point cloud data are acceptable in order to procced to the scan stop, otherwise the process of scanning is repeated.

The time spent in each scan varies from 1.5 to 2.3 hours. The variation of the time spent per scan depends on the classification of the chosen resolution. Four different scans per inline structure (e.g. for the bridges) has been performed, for more accurate representation of the river inline structures (the pattern is depicted in Figure 3.1a). Approximately, a total area length of 2.4 km has been scanned with a maximum width of 750 m. Each scanned area, except the initial scan, has an overlapping area with the previous and the forward scan. The overlapping area between two scans covers a minimum length of fifteen (15) meters. Finally, the entire process of the LiDAR data measurements lasted from 16 June – 7 July 2010 and from 26 September – 11 October 2010.

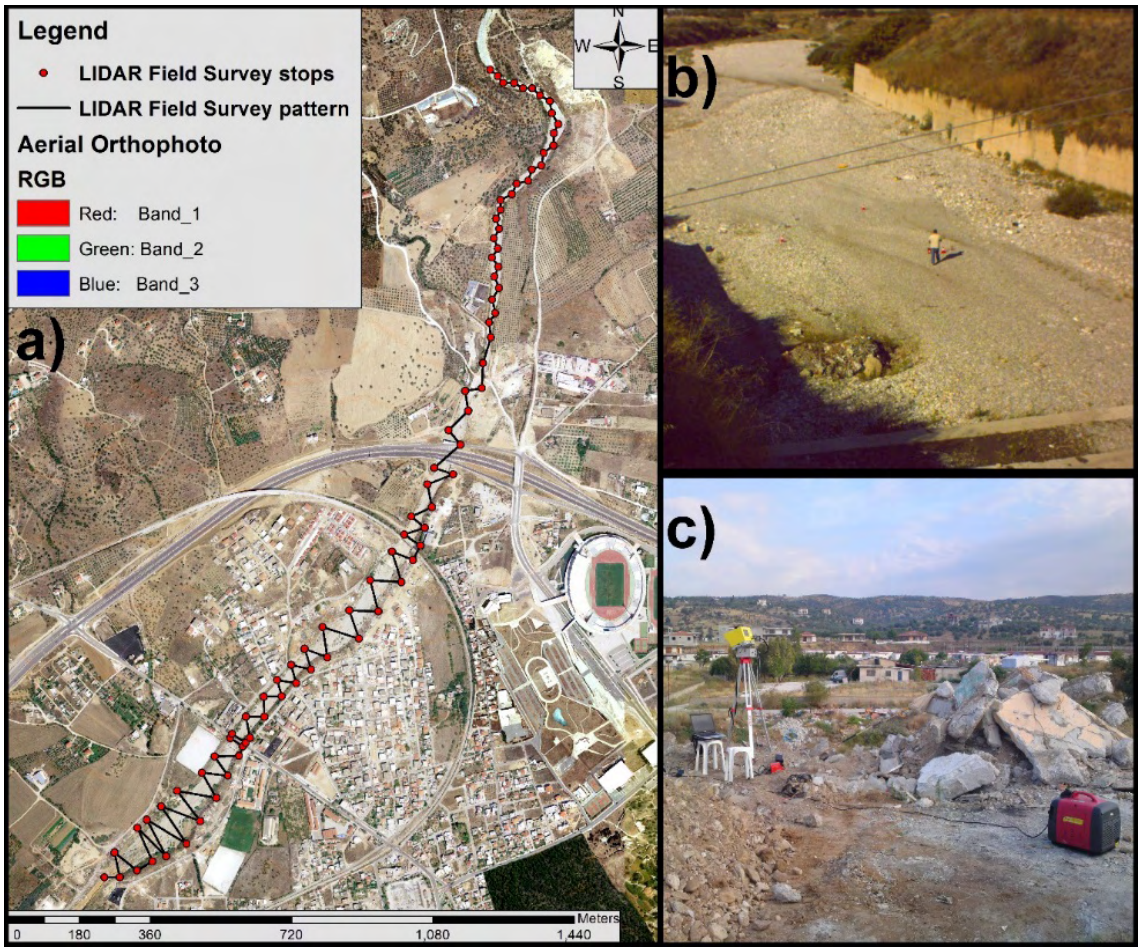

Figure 3.1. LIDAR field survey: a) Spatial distribution pattern; b) The process of cone placement; c) The entire equipment used during the process of scanning.

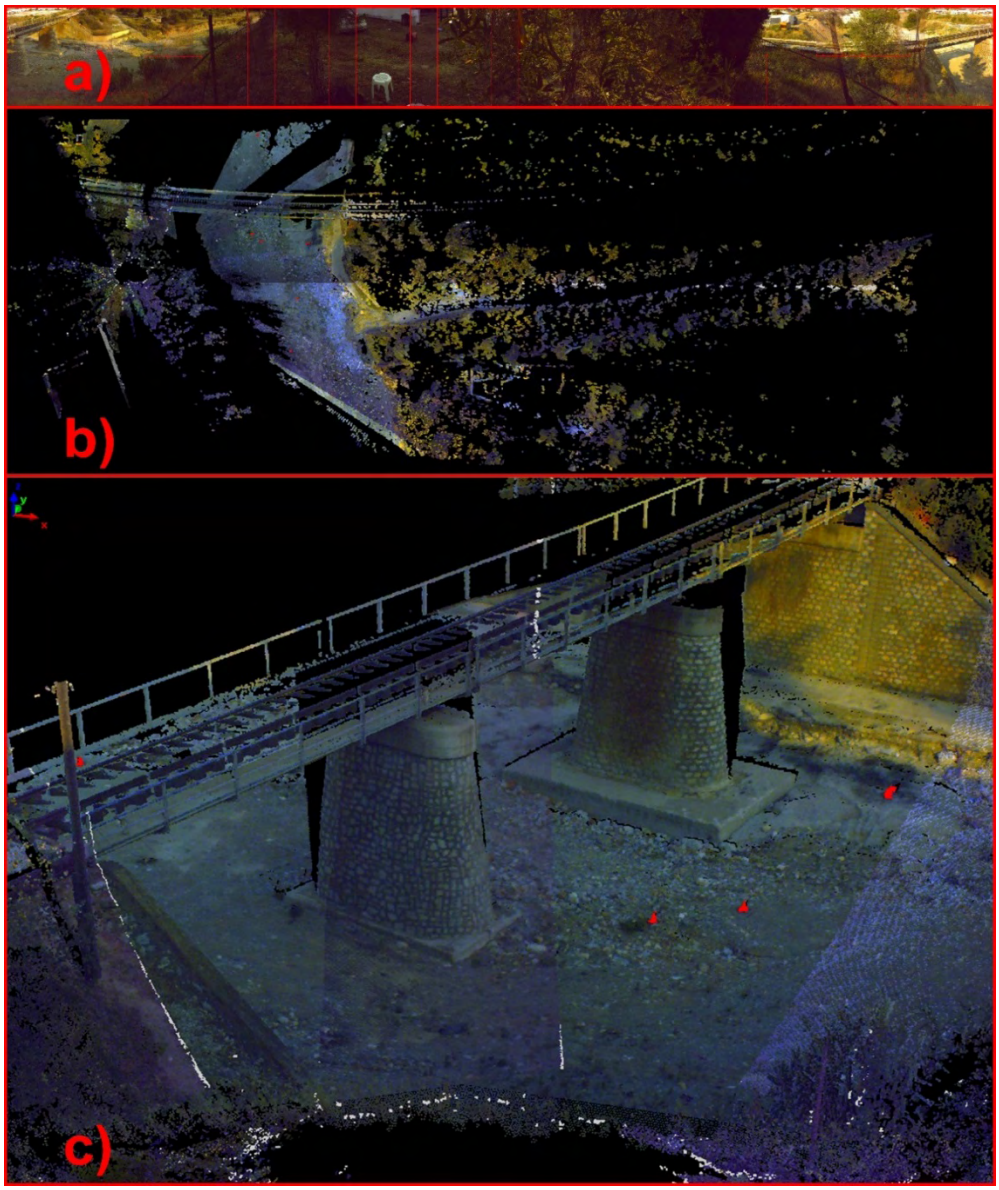

Figure 3.2. Example of LIDAR field survey: a) 360^{o} photographs taken during the scanning process; b) Panoramic view of the scanned data through Polyworks software; c) Specific part of the scan that presents the railway bridge through Polyworks software.

During the LiDAR data measurements, several problems have been encountered such as:

- The transportation of the entire heavy equipment to the field was a difficult process, especially when the weather was really hot. In some cases, the entire equipment had to be transferred by hands for more than 500 meters (Figure 3.3a).
- The scanning process needed more than one person (Figure 3.3b).
- Extended surface preparation (vegetation removal, settle down the equipment, etc.) was necessary for the installation of the LIDAR equipment in a scan stop

(Figure 3.3b).

- The scanning process, for finer resolution point cloud data, was very time consuming (Figure 3.3b).
- ILRIS 3D laser scanner was very sensitive to high and low temperatures (Figure 3.3c,d). In many cases, the LIDAR stopped the scanning process because of overheating or freezing, and the entire scan had to be repeated from the beginning because of severe distortion in the point cloud data.
- During a very light rainfall, the laser scanner was unable to produce normal point cloud data.
- Despite the fact that LIDAR can work in the darkness, the entire scanning process had to be done during the daylight in order to have the photographs of the area.
- Damage in the power generator due to high temperatures paused the scanning process for approximately one month.
- The entire process of scanning lasted 38 days.

Figure 3.3. Difficulties encountered during the scanning procedure: a) Carrying heavy equipment; b) Settle down the equipment and wait for the scanning procedure; c) Protect the equipment from high temperatures; d) Protect the equipment from low temperatures.

3.1.2 LiDAR point cloud processing and Processed LIDAR DEM generation

Despite the recent technological developments in the field of TLS data processing, the elimination of natural and built features from the DSM in order to create the "bare earth" DEM remains a difficult process. In this study, several softwares have been used for the processing of the scan data in order to create the georeferenced DSM and to remove the natural and built features (DEM generation process). The entire process of the LIDAR scan data processing in order to create the georeferenced DSM and the final "bare earth" DEM is presented in Figure 3.4. First and foremost all the collected point cloud data, produced by TLS, has been transformed into PIF format in order to be available for processing by Polyworks v10.0 software (Figure 3.2b,c). Then, each scan data has been pre-processed with the use of PIF-Edit tool. This pre-processing step involves the manual removal of the rough erroneous points. Afterwards, all point cloud data, derived from the 86 scans, were merged using IMAlign tool (Polyworks software).

The merging process has been achieved with a best fit analysis process using the Iterative Closest Point (ICP) algorithm. The best fit analysis between two point cloud data-sets involves the following steps:

1. Cautiously selection of the five (5) benchmark points (cones), which exist in the overlay area between the two point clouds, in order to bring closer the two point clouds.
2. Identification and selection of recognized common points within the overlapping area of the two point clouds in order to apply a better approaching of the two areas.
3. Step 2 is repeated until the two point clouds were close enough.
4. Implementation of the best-fit analysis process that uses the ICP algorithm.
5. Steps 2, 3 and 4 are repeated until the acceptable fitting is achieved.

The ICP algorithm is iteratively converging the selected points and registering them in a common coordinate system. The registration of the points is iteratively calculated by the ICP algorithm (Besl and McKay, 1992). In each iteration, the algorithm selects the closest points as correspondences and calculates the transformation (R, t) for minimizing the following equation (1):

$$E(R,t) = \sum_{i=1}^{N_m} \sum_{j=1}^{N_d} w_{i,j} \left\| m_i - \left(Rd_j + t\right) \right\|^2 \quad (3.1)$$

Where N_m and N_d are the numbers of points in the model, set M and data set D, respectively, and $w_{i,j}$ are the weights for a point match. The weights are assigned as

follows: $w_{i,j}$ = 1, if m_i is the closest point to d_j within a close limit, $w_{i,j}$ = 0 otherwise (Magnusson et al., 2009).

Subsequently, using the above-mentioned procedure, all point cloud data-sets are merged progressively. Then, the entire merged point cloud has been spatially referenced to the Greek Grid datum (EGSA87). The spatial distributed referencing has been based on approximately 3000 spatial referenced points retrieved from topographical survey data and the ICP algorithm using best-fit analysis (Figure 3.4). After the spatial referencing of the entire point cloud, the data has been separated into 86 parts similar to the initial areas. The separation of the point cloud has been applied due to data handling purposes, software limitations and computational limitations issues. With the use of the merged raw point cloud data, the Raw LIDAR DEM (Figure 3.5a) has been created.

In order to remove the natural and human features from each separate referenced point cloud data-set, all the data-sets have been transformed into LAS format and imported in Quick Terrain Modeler Version 7.0 (QTM) software. In this analysis, QTM has been used with a free temporary trial license. A powerful tool that is provided within QTM is the Above Ground Level (AGL) analysis. Using the AGL analysis, the elevation values of a point cloud is transformed to elevation values relative to the ground surface (lower elevation values of the point cloud). Hence, the recognition and elimination of the above ground points became feasible. The estimation of the ground level has been based on an auto-calculate command and by selecting different grid sampling values. This procedure was performed iteratively until the elimination of the non-ground points. All point cloud parts have been processed with the proposed iteratively procedure (Figure 3.4). Finally, an initial “bare earth” model has been produced by separating the ground and non-ground points using AGL analysis (QTM tool), as well as by manually removal of the unnecessary points.

Eventually, all the QTM-processed point cloud data were transformed to shapefile format (point) and inserted in ArcGIS (ArcMap v. 9.3/10.1, ESRI) for further processing. For computational and software limitations purposes all data has been transformed within ArcGIS into terrain datasets elements. The method applied for the construction of the terrain datasets elements is the z minimum point selection with a z-tolerance of 22 cm. The majority of the terrain datasets has been updated numerous times by manually removing erroneous points (Figure 3.4). Then, the final Processed LIDAR DEM has been created using 4,387,224 nodes (Figure 3.5b). In Figure 3.5 is highlighted the difference between the DSM (Raw LIDAR data) and DEM (processed LIDAR data) for a specific part of the study area. The entire process of the LIDAR point cloud processing and the processed LIDAR DEM generation lasted approximately six (6) months. The author spent for the merging and georeferenced process more than a month to the Laboratory of

Photogrammetry and Remote Sensing, School of Rural and Surveying Engineering, Aristotle University of Thessaloniki.

During the LiDAR data processing, several problems have been encountered such as:

a) The point cloud data handling was very difficult due to the extremely high number of the scanned points and the huge file size (e.g. the entire spatially referenced point cloud was 11GB in txt format).

b) Several file format conversions have been applied in order to have the data in the proper format for each software used.

c) The demands on computing power were really high, and due to computational limitations (graphic card, RAM, computer processor and hard disk demands were really high) the processing of the data has been achieved by decomposing the data into parts and composing them into one element many times.

d) The merging and georeferenced process were only applicable to a specific computer that was prepared only for this kind of analysis into the Laboratory of Photogrammetry and Remote Sensing, School of Rural and Surveying Engineering, Aristotle University of Thessaloniki.

e) The software limitations issues resulted to the decomposition of the data into parts and their composition into one element many times. Moreover, due to software limitations, the author used many times manual applications.

f) The entire process of the LIDAR point cloud processing and the generation of the processed LIDAR DEM lasted longer than the expected time.

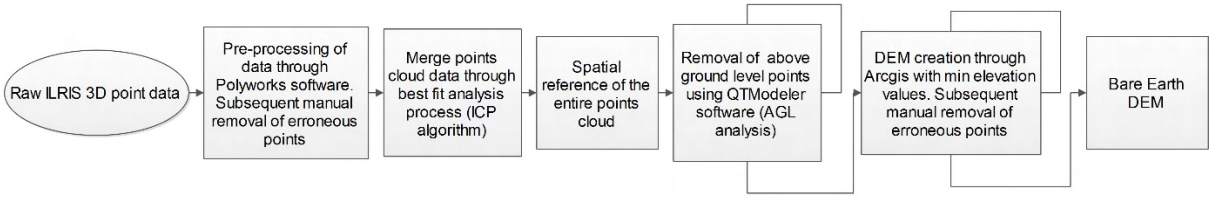

Figure 3.4. Flowchart of the LIDAR point cloud processing and the Processed LIDAR DEM generation.

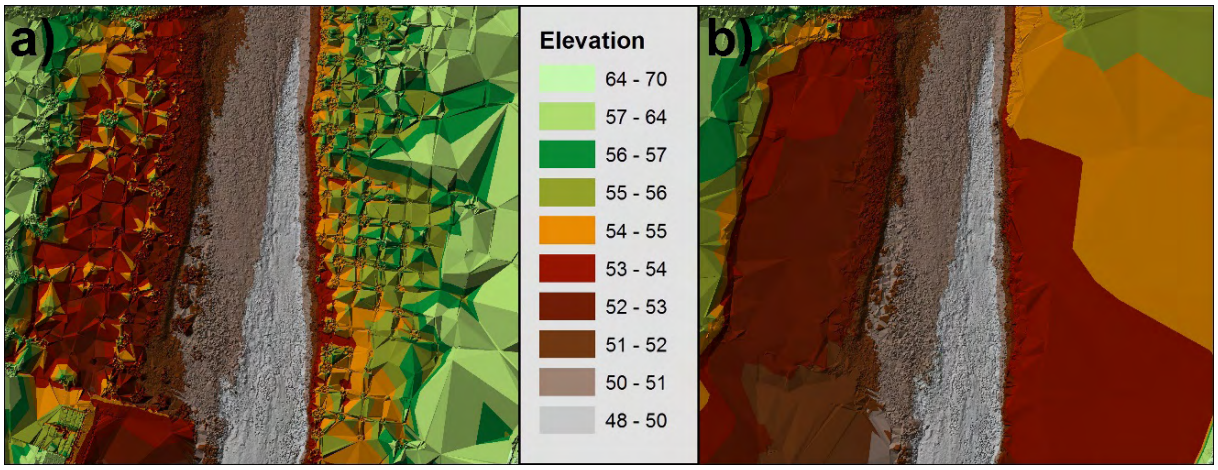

Figure 3.5. a) Digital Surface Model (Raw LIDAR data); b) Digital Elevation Model (processed LIDAR data).

3.2 Post flood analysis

The estimation of flood-peak in ungauged watersheds and streams is usually determined by indirect measurements. The majority of the indirect measurements were based on the open-channel hydraulic principles and the peak-stage profiles along specified cross sections of the stream. Usually, the indirect methods are applied in open channels where stage data is available or at several constructions such as bridges, culverts, and dams using stream stage instruments placed at those locations. Some of the traditional flood peak detection methods are the slope-area, the step-backwater, the contracted openings and the slope-conveyance technique. The traditional flood peak detection methods are usually based on high-water marks, precipitation records and specific open-channel hydraulic characteristics for at least two cross sections. These techniques are common practices in flow determination at ungauged watersheds.

In this analysis, the typical Manning formula, the slope-area method, and the hydraulic-hydrodynamic model HEC-RAS have been used for the validation of the estimated discharge and the roughness coefficient. For the implementation of the above-mentioned parameters (i.e. the open channel hydraulic parameters), a topographical survey was conducted in specific cross sections of the river. The selected parts of the river were selected based on a photograph taken at approximately 9.5 hours after the beginning of the extreme rainfall event of 09/10/2006. Unfortunately, the peak of the flood had passed by the time the picture was taken but as it can be seen in the photograph (Figure 3.6b) the water depth is satisfactory in order to implement a post flood analysis. The heights of the watermarks and the hydraulic parameters have been estimated, for specific river cross sections, based on data retrieved from a topographical survey.

Figure 3.6 shows the photograph with the watermarks, the river topography for the post flood analysis and a photograph of the river channel in dry conditions. Some of the necessary hydraulic parameters that were estimated using the watermark height value are the hydraulic radius and the cross sectional area. The evaluation of the roughness coefficient selection and the flood hydrograph has been achieved using the techniques of the post flood analysis. The first comparison involves the calculation of the discharge value using the estimated watermarks height and Manning formula (King, 1918):

$$\mathrm{Q} = \frac{1}{\mathrm{n}} \mathrm{A} \mathrm{R}^{\frac{2}{3}} \mathrm{S}_{\mathrm{f}}^{\frac{1}{2}} \tag{3.2}$$

where *A* = cross sectional area; *R* = hydraulic radius; S_f = slope of the channel; and *n* = Manning roughness coefficient.

The Manning formula was implemented in all three cross sections independently (Figure 3.6a), the discharge value was estimated approximately to 200 m^3/s and the Manning's roughness coefficient value was approximately found to be 0.035 in all cross sections. Thus, the Manning formula approximation of the discharge value was almost the same as the discharge value of CIUH (Figure 3.7). In the discharge value comparison process the captured time of the photograph (and the watermarks height) have been taken into account. The second methodology used for the evaluation of the roughness coefficient and the flood hydrograph was accomplished with the use of the flow measurements slope-area method (Herschy, 2009):

$$\mathrm{K} = \frac{\mathrm{A} \mathrm{R}^{\frac{2}{3}}}{\mathrm{n}} \tag{3.3}$$

$$\mathrm{Q} = \sqrt{\mathrm{S} \mathrm{K}_1 \mathrm{K}_2} \tag{3.4}$$

where, *A* = cross-sectional area; *R* = hydraulic radius ; conveyance *K* = a measure of the carrying capacity of the channel; *n* = Manning roughness coefficient; *S* = slope or energy gradient; and *Q* = discharge. The S parameter is computed with the assumption that

$$\mathrm{S} = \frac{(\mathrm{Z}_1 - \mathrm{Z}_2)}{\mathrm{L}} \tag{3.5}$$

and in the later stage, *S* is computed as follows:

$$\mathrm{S} = \frac{(\mathrm{Z}_1 - \mathrm{Z}_2) + 0.5 \left(\frac{\bar{\mathrm{v}}_1^2}{2\mathrm{g}} - \frac{\bar{\mathrm{v}}_2^2}{2\mathrm{g}} \right)}{\mathrm{L}} \tag{3.6}$$

where *L* = length of channel reach; Z_1 = elevation of water surface at section 1 above a common datum; Z_2 = elevation of water surface at section 2 above a common datum; $\bar{v}_1$

= mean velocity at section 1; $\bar{v}_2$ = mean velocity at section 2; g = acceleration due to gravity = 9.81.

The slope-area technique was implemented in the two pairs of the cross sections. The first pair consisted of the cross sections CR1 and CR2 and the second pair consisted of the cross sections CR2 and CR3 (Figure 3.6a). Both comparisons gave a discharge value of approximately 205 m^3/s and a roughness coefficient value of approximately 0.035. Thus, the estimated slope-area discharge was approximately the same as the discharge value of CIUH (Figure 3.7). Also, the last methodology was applied in the post flood analysis process using the HEC-RAS hydraulic-hydrodynamic model.

A trial and error optimization technique has been used in the wider area of the watermarks for a better approximation and testing of the roughness coefficient value (Figure 3.7). HEC-RAS trial and error optimization technique gave a discharge value of 210 m^3/s using 0.035 roughness coefficient value. The results of the validation techniques gave a good agreement of the discharge value with the flood hydrograph (Figure 3.7) and similar results for the roughness coefficient. Finally, the Manning roughness coefficient was set to 0.035 for the First level of sensitivity analysis (preliminary sensitivity analysis).

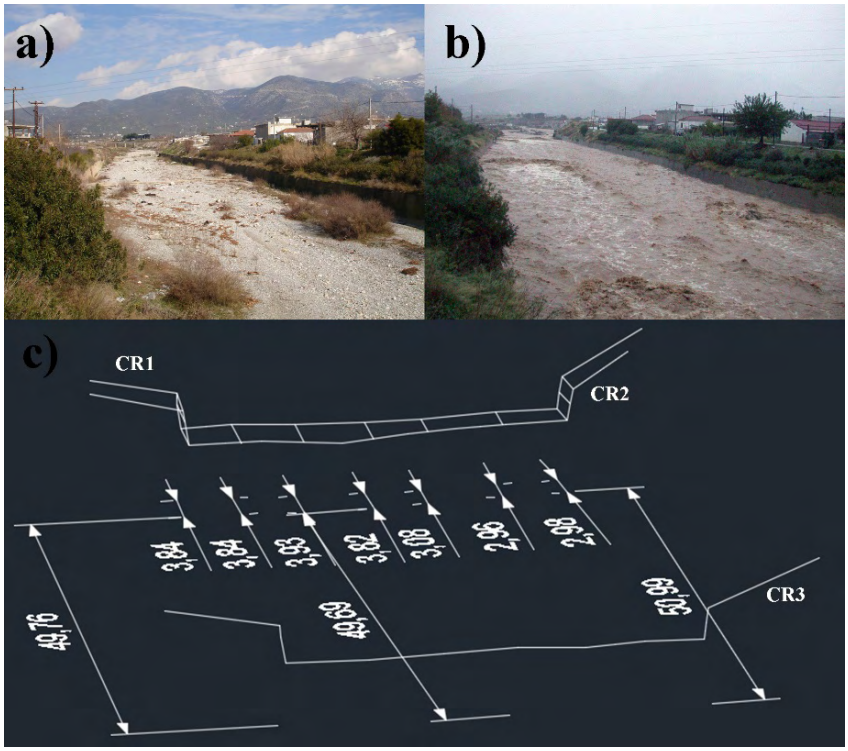

Figure 3.6. Post flood analysis river topography with watermarks (captured photograph). a) Photograph of the river in dry period, b) Photograph of the river from the 2006 flood event, c) Topographical survey cross sections.

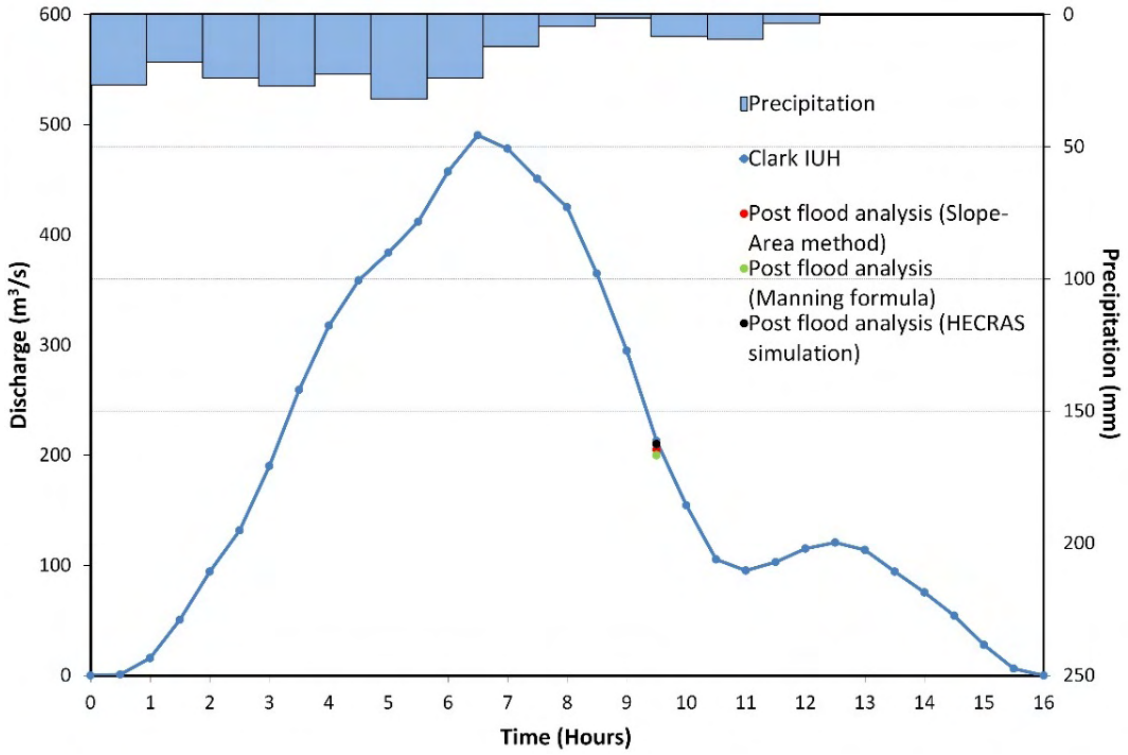

Figure 3.7. Validation of the flood hydrograph through post flood analysis

3.3 Wolman Pebble Count

A typical process used for the indirect estimation of the roughness coefficient at ungauged catchments is the evaluation of the size and type of the bed, banks and over-bank material of the channel (Coon, 1998). The estimation of the roughness coefficient is usually based on empirical formulas where the particle size is a keypoint parameter. However, the evaluation of the particle size based on the experience of the researcher can lead to an erroneous roughness coefficient value. Thus, for accurate estimation of the bed material size and roughness coefficient estimation, several sample techniques have been developed. The bed materials can be sampled either by Surface sampling methods or with Volumetric sampling methods. Surface sampling methods are accurate and fast methods and are typically used for predefined particle diameters.

The surface sampling methods are separated in pebble count, grid count and aerial sample method. Pebble count method is a typical technique for the estimation of the particle size in gravel and cobble-bed streams (Bunte et al., 2009; Ward et al., 2016). Also, pebble count method is appropriate for large sampling area coverage and in cases of dry streams (i.e. dry conditions) the field time can be minimized. In order to minimize the high

uncertainty related to the roughness coefficient values, the pebble count method and several empirical formulas have been used to estimate the final Manning's *n* roughness coefficient values.

During the Wolman pebble count process, the researcher has to measure the distance of the three major axis of a particle as shown in Figure 3.8. The three major axis are a) Long Axis; b) Intermediate Axis; c) Short Axis (Harrelson et al., 1994). In order to estimate the predefined diameters, all data should be classified based on standard particle size tables. The classification of the particles in standard classes is based on the pebble diameter. The pebble diameter is equal to the Intermediate Axis value when the value of Intermediate Axis is larger than the value of the Short Axis, else the value of the Short Axis is taken into account (Harrelson et al., 1994).

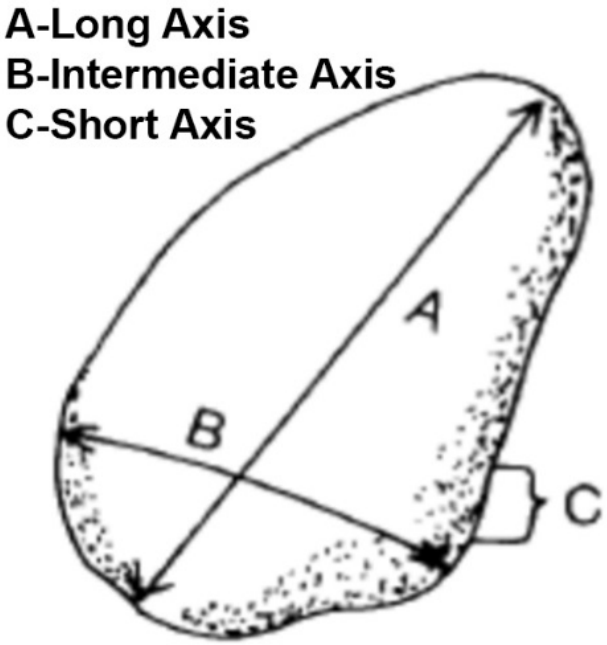

Figure 3.8. Particle axis taken into account during Wolman pebble count process: a) Long Axis-A; b) Intermediate Axis-B; c) Short Axis-C.

In Xerias stream reach, the Wolman pebble count method was conducted by using a zig-zag pattern and by selecting 958 particles with a step-toe procedure (Figure 3.9a). Typical examined stream bed materials are presented in Figure 3.9b,c. As expected, the size of the stream bed particles decreased while moving towards the lower part of the river. The data collected, covers approximately 70% of the entire area (Figure 3.9a) and has been used for the statistical analysis of the particle size (Table 3.1, Figure 3.10, Figure 3.11) and the computation of predefined diameters of d_{50}, d_{65}, d_{75}, d_{84}, and d_{94} (Table 3.3). In Table 3.1 is presented the detailed classification of all Pebble count samples. Figure 3.10

presents the percentage cumulative frequency distribution of pebble count sample sizes and the pebble count sample size frequency graph can be seen in Figure 4.11. As shown in Table 3.1 and Figure 3.11 the river bed is covered mainly by cobbles (46.1 %) followed by gravel (36.1 %) and boulder (17.8 %). Moreover, as illistrated in Figure 3.10, the median diameter of the collected data is approximatelly 90 mm.

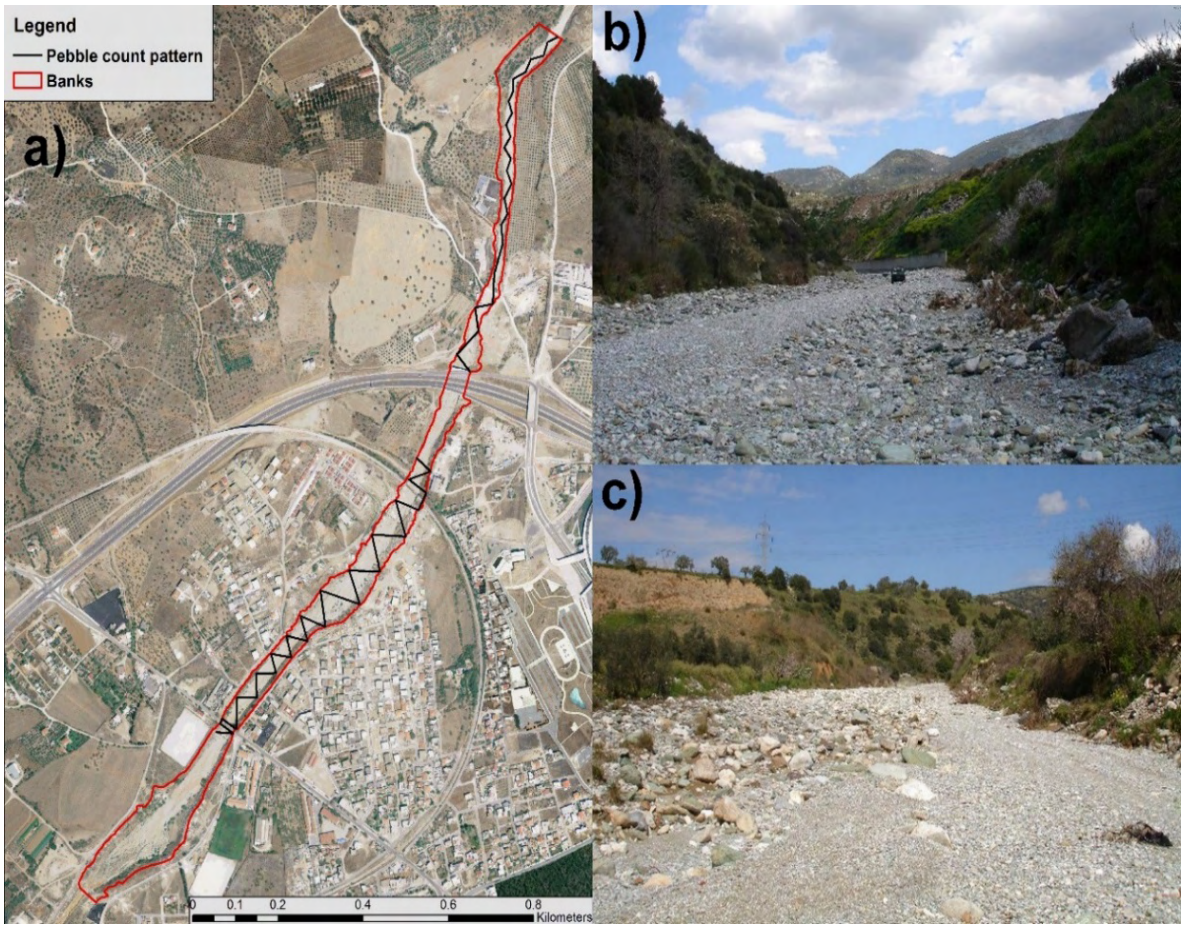

Figure 3.9. Pebble count field survey: a) Wolman pebble count method and typical examined river bed materials b) upstream section and c) downstream section.

Table 3.1. Pebble count data classification based on Wentworth scale (Bunte and Abt, 2001).

Particle Descriptions			Pebble Count Data		
Particle Sub-Category	**Particle Category**	**Particle size (mm)**	**Number of samples**	**Frequency (%)**	**Cumulative Frequency (%)**
Silt/Clay	SILT/CLAY	<0.062	0	0.0%	0.0%
Very Fine	SAND	0.062 - 0.125	0	0.0%	0.0%
Fine	SAND	0.125 - 0.25	0	0.0%	0.0%
Medium	SAND	0.25 - 0.50	0	0.0%	0.0%
Coarse	SAND	0.50 - 1.0	0	0.0%	0.0%
Very Course	SAND	1.0 - 2	0	0.0%	0.0%
Very Fine	GRAVEL	2 - 2.8	0	0.0%	0.0%
Very Fine	GRAVEL	2.8-4.0	0	0.0%	0.0%
Fine	GRAVEL	4 - 5.7	0	0.0%	0.0%
Fine	GRAVEL	5.7 - 8	0	0.0%	0.0%
Medium	GRAVEL	8 - 11.3	5	0.5%	0.5%
Medium	GRAVEL	11.3 - 16	9	0.9%	1.5%
Coarse	GRAVEL	16 - 22.6	18	1.9%	3.3%
Coarse	GRAVEL	22.6 - 32	49	5.1%	8.5%
Very Course	GRAVEL	32 - 45.0	137	14.3%	22.8%
Very Course	GRAVEL	45.0 - 64	128	13.4%	36.1%
Small	COBBLE	64 - 90.0	166	17.3%	53.4%
Small	COBBLE	90.0 - 128	108	11.3%	64.7%
Large	COBBLE	128 - 180	90	9.4%	74.1%
Large	COBBLE	180 - 256	77	8.0%	82.2%
Small	BOULDER	256 - 362	63	6.6%	88.7%
Small	BOULDER	362 - 512	48	5.0%	93.7%
Medium	BOULDER	512 - 724	24	2.5%	96.2%
Medium	BOULDER	724 - 1024	23	2.4%	98.6%
Large	BOULDER	1024 - 1450	13	1.4%	100.0%
Large	BOULDER	1450 - 2048	0	0.0%	100.0%
Very Large	BOULDER	2048 - 2900	0	0.0%	100.0%
Very Large	BOULDER	2900 - 4096	0	0.0%	100.0%
Bedrock	BEDROCK	> 4096	0	0.0%	100.0%
			958	**100.0%**	**100.0%**

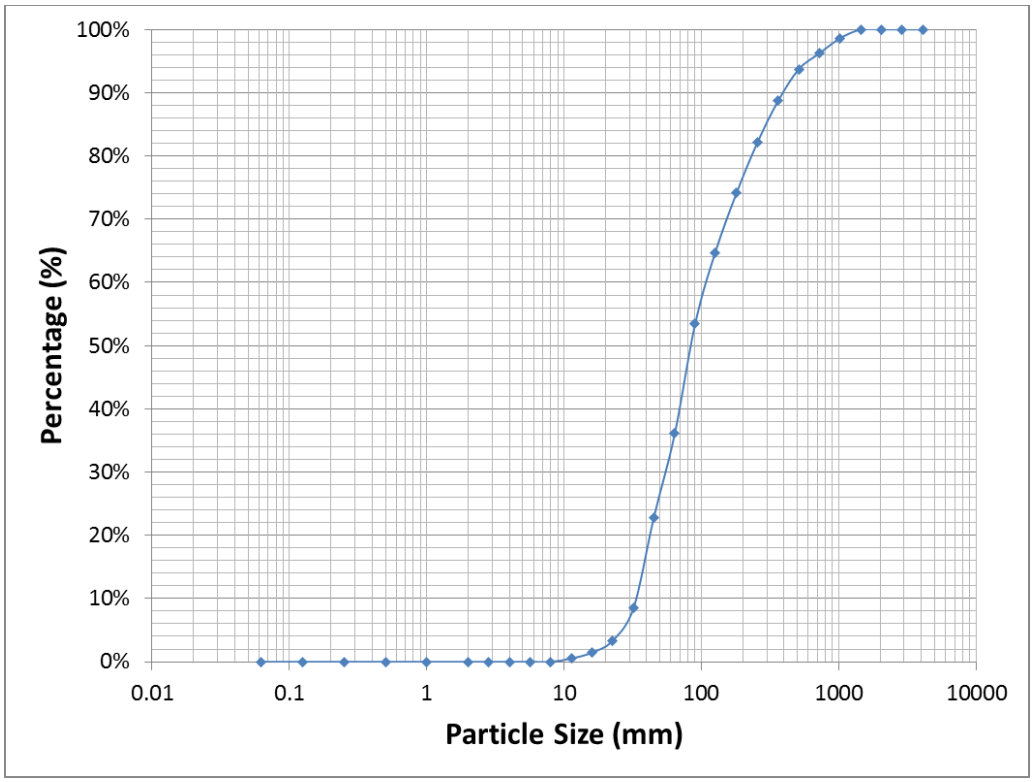

Figure 3.10. Percentage cumulative frequency distribution of the river bed particle size (log-scale)

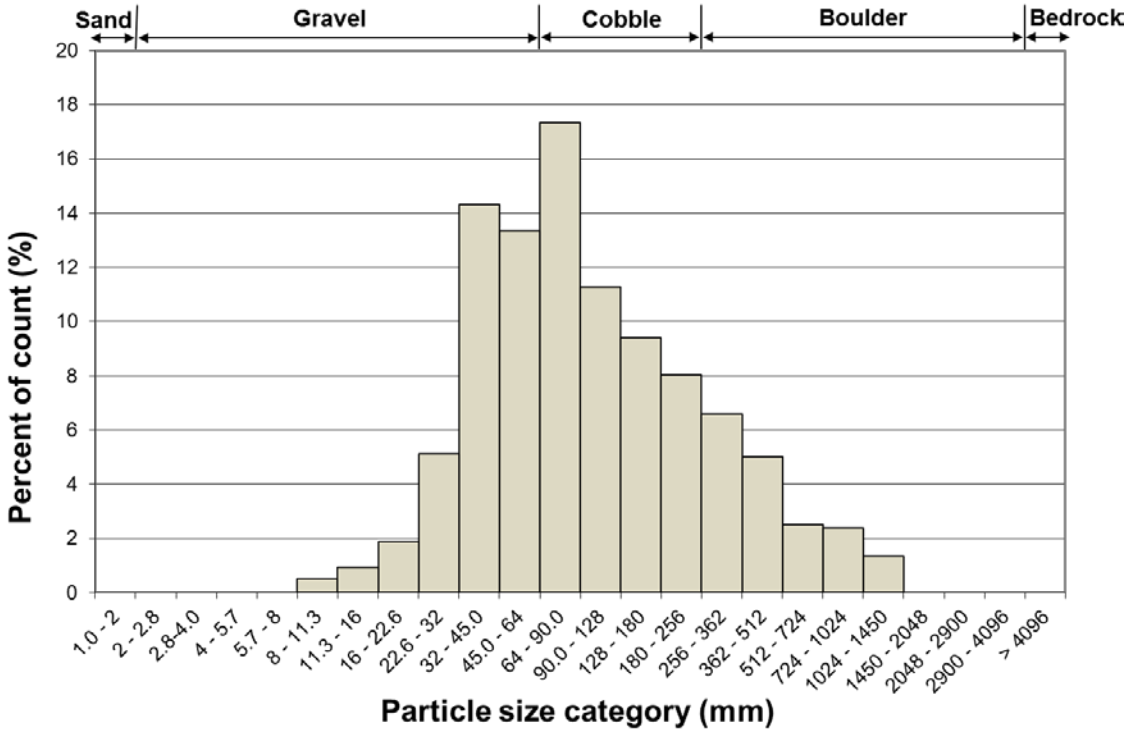

Figure 3.11. Pebble count sample size frequency graph.

Several empirical formulas recommended in the international literature for the estimation of Manning's roughness coefficient (*n*) values, mainly for gravel and cobble-bed streams, (Table 3.2), have defined the choice of the predefined size diameters (Table 3.3).

Table 3.2. Empirical relationships in the international literature for assessing Manning's roughness coefficient (n/ values).

A/A	Equation	Roughness (*n*) Coefficient Value	Source
1	$n = \frac{1}{(2.1 + 2.3x + 6\ln(10.8vR))}$	0.035	Gwinn and Ree, 1980
2	$n = \frac{0.1129R^{1/6}}{1.16 + 2\log\left(R/D_{84}\right)}$	0.043	Marcus et al., 1992
3	$n = 0.0326 + 1.3041S_W$	0.052	Loukas and Quick, 1996
4	$n = 0.322S_{fr}^{0.38}R^{-0.16}$	0.074	Romero et al., 2010
5	$n = \left[0.183 + \ln\left(\frac{1.762S_{fr}^{0.1581}}{Fr^{0.2631}}\right)\right]\left(\frac{D_{84}^{0.167}}{\sqrt{g}}\right)$	0.074	Romero et al., 2010
6	$n = (n_0 + n_1 + n_2 + n_3 + n_4)m$	0.103	Jarret, 1985
7	$n = (n_0 + n_1 + n_2 + n_3 + n_4)m$	0.074	Jarret, 1985
8	$n = 0.121(S_W)^{0.38}(R)^{0.08}$	0.061	Chang, 2012
9	Base scenario estimated using guidelines of Chow (1959) Extreme case scenario using guidelines of Chow (1959)	0.106 0.12	Chow, 1959
10	$n = 0.104(S_W)^{0.177}$	0.049	Chang, 2012
11	$n = \frac{D_{90}^{1/6}}{15.29}$	0.056	Ho and Huang, 1992
12	$n = \frac{D_{90}^{1/6}}{16}$	0.054	Ho and Huang, 1992
13	$n = 0.0593D_{50}^{0.179}$	0.038	Javan et al., 1992
14	$n = 0.0561D_{65}^{0.179}$	0.039	Javan et al., 1992
15	$n = 0.0495D_{90}^{0.16}$	0.043	Javan et al., 1992
16	$n = 0.0431D_{90}^{1/6}$	0.037	McKay and Fischenich, 2011
17	$n = 0.0439D_{90}^{1/6}$	0.038	McKay and Fischenich, 2011
18	$n = \left[0.183 + \ln\left(\frac{1.7462S_{fr}^{0.1581}}{Fr^{0.2631}}\right)\right]\frac{(D_{84})^{1/6}}{\sqrt{g}}$	0.072	Ugarte and Madrid-Aris, 1994
19	$n = \left[0.183 + \ln\left(\frac{1.3014S_{fr}^{0.0785}\left(\frac{R}{D_{84}}\right)^{0.0211}}{Fr^{0.1705}}\right)\right]\frac{(D_{84})^{1/6}}{\sqrt{g}}$	0.076	Ugarte and Madrid-Aris, 1994
20	$n = \left[0.219 + \ln\left(\frac{1.3259S_{fr}^{0.0932}\left(\frac{R}{D_{50}}\right)^{0.026}}{Fr^{0.2054}}\right)\right]\frac{(D_{50})^{1/6}}{\sqrt{g}}$	0.075	Ugarte and Madrid-Aris, 1994
21	Optimum value according to calibration process	0.09	

n = Manning's n roughness coefficient (m^3/s), x = retardance class, v= velocity (m/s), R = hydraulic radius (m), D_i = characteristic size of bed material which is larger than i% of particles (m), Sw = water surface slope (m/m), S_{fr} = energy slope (m/m), Fr = Froude number, g = acceleration due to gravity (m/s^2).

Table 3.3. Estimated predefined diameters

Predefined diameters	d_s, (mm)
d_{16}	38.86
d_{35}	62.41
d_{50}	84.83
d_{75}	188.39
d_{84}	285.81
d_{90}	400.13
d_{95}	618.88

The estimation of the roughness coefficient values has been based on the empirical formulas shown in Table 3.2, in which the following assumptions apply:

1. The energy gradient friction slope is assumed similar to the stream bed slope. Thus, the normal depth determination has been estimated using the stream bed slope.
2. All necessary hydraulic parameters (e.g. flow velocity, hydraulic radius, Froude number) have been determined based on their estimation using HEC-RAS hydraulic-hydrodynamic model and the optimum roughness value derived from the deterministic optimization analysis using Critical Success Index scores (Figure 3.12). Thus, the median of the total estimated hydraulic parameters has been used in the associated empirical formulas. Further details on the deterministic optimization analysis using CSI scores can be found in Chapter 5 and Chapter 6.

Finally, the results derived from the application of Table 3.2 empirical formulas have been used for the determination of the empirical distribution of roughness coefficient.

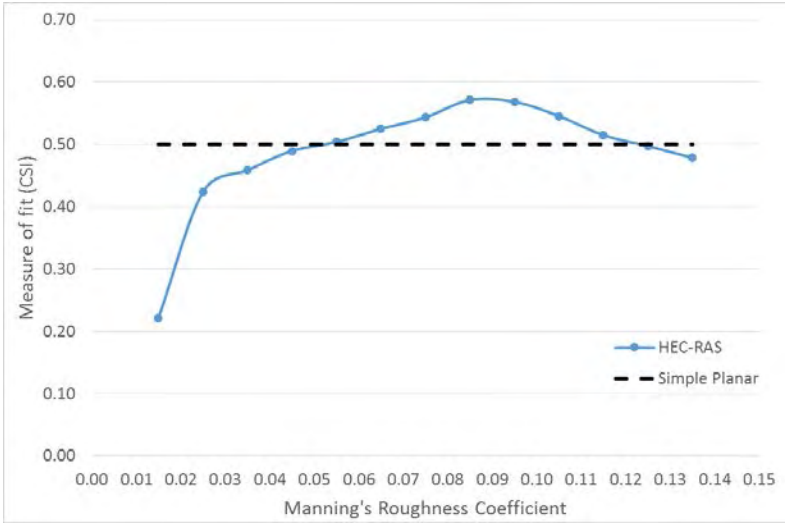

Figure 3.12. HEC-RAS model responses to changes in roughness coefficient values (Manning's n), regarding CSI and selected threshold for acceptable behavioral models.

In summary, this chapter presents several field measurements used for data collection, and related methodologies used for data processing and parameters estimation. The outcomes of the LIDAR field survey process are the Processed (bare earth) and the Raw (including natural and built environment) LIDAR DEM. The post flood analysis process has been used for the validation of the produced flood hydrograph and the primary estimation of the Manning's *n* roughness coefficient. The generated LIDAR DEMs and the outcomes of the post flood analysis are major parameters needed for sensitivity and uncertainty analysis of floodplain modelling and mapping process (Chapter 5,6). Finally, with the use of Wolman Pebble Count Field survey several typical particle size diameters have been estimated. Thus, several empirical formulas have been used for the estimation of Manning's *n* roughness coefficient and the generation of the empirical probability distribution. The derived empirical probability distribution has a key role in the sensitivity analysis of the "Uncertainty analysis component" which is presented in Chapter 6.

CHAPTER 4ο
IDENTIFICATION AND MAPPING OF FLOOD PRONE AREAS COMPONENT

4 Identification and mapping of flood prone areas component

4.1 Introduction

Over the last 15 years many combined Geographical Information Systems with Multi-Criteria Analysis techniques have been used for the estimation of flood-prone areas, flood hazard and/or risk mapping and flood vulnerability analysis (Rahmati et al., 2016; Radmehr and Araghinejad, 2015; Sowmya et al., 2015; Khosravi et al., 2016; Nandi et al., 2106; Tang et al., 2017; Gigovic et al., 2017; Kourgialas and Karatzas, 2017; Xiao et al., 2017). The rise in these studies is justified due to the complex nature of the decision problems, the evolution in GIS applications and the need for spatially distributed answers-solutions and in many cases the severe lack of data. Some of the already mentioned indicative studies use criteria based on previous studies without further investigation (e.g., Xiao et al., 2017), or the criteria are clustered based on predefined subjective tables (e.g., Rahmati et al., 2016) and common GIS clustering techniques (e.g., Gigovic et al., 2017). In other cases, the use of classified criteria to identify flood prone areas and/or produce the flood hazard maps (e.g. Radmehr and Araghinejad, 2015) is done in the beginning of the analysis and sometimes the structure of the proposed frameworks is assumed perfect without further investigation (luck of sensitivity analysis for the selected methodologies) (e.g., Sowmya et al., 2015). A typical methodology followed in the recognition of Areas of Potential Significant Flood Risk (APSFR), is based on the intersection of flood related elements such as the potential flooded area, important areas and historical flood positions (collected by many sources). Each of this elements is estimated using simple indexes such as slope (<2%) and the alluvial deposition; buffers of Protected Habitats and/or River network, etc.; and points of historical flood locations) (e.g. SSW-MEECC, 2012). With the use of such simplistic indexes the results tend to lead to flood prone areas overestimation and erroneous flood hazard maps. Therefore, it is obvious that the overestimation of flood prone areas can adversely affect the entire process of flood risk management mitigation strategies and planning.

This study develops an objective GIS-based spatial multi-criteria evaluation component at catchment scale for the identification and mapping of potential flood prone areas at ungauged watersheds. Potential flood prone areas are identified using GIS data and

techniques such as clustering/classification procedures and two MCDA methods the AHP and the FAHP. Two different approaches have been implemented and compared in order to investigate the sensitivity of the proposed component in the identification of the flood prone areas at ungauged watersheds. The first approach is a process where all the criteria (DEM-derived geomorphological and hydrological attributes which are related to the flood generation process) are normalized before the MCA method and then, several clustering and classification techniques are applied to derive the final potential flood-prone areas. The second approach is a method where all the criteria are clustered before and after the MCA process for the production of the potential flooded area maps. The derived flood prone maps in the two approaches have been classified with five different clustering techniques. The methodology is demonstrated to Xerias watershed, Thessaly region, Greece. Historical flood inundation data (flash flood event of 2006 that flooded sub-urban and urban areas of Volos city) and simulated flooded area derived from hydrologic - hydraulic modelling of the flood event have been used to validate the methodology. The proposed component is developed for decision makers to identify potential flood prone areas caused from flash and fluvial floods with minimum subjectivity in order to be applied at larger spatial scales for gauged and ungauged catchments. The employed component could be applied in flood hazard estimation and mapping at areas with limited information available, and/or in areas where preliminary flood hazard evaluation is required for flood mapping purposes using typical hydrologic and hydraulic methods at ungauged watersheds.

4.2 Study Area

The study area is the watershed of Xerias stream located in the region of Thessaly and in the prefecture of Mangesia, Greece (Figure 4.1.a). The selection of Xerias stream based on the fact that the city of Volos has been repeatedly experienced severe flood events due to the location of the river (Xerias stream drains through the City of Volos) and intense storm phenomena. This study investigates the flood episode on 9th October 2006 which is one of the most hazardous flood events that the city of Volos experienced. The impacts of this flood event were mainly on agricultural areas, transportation networks and other technical infrastructures at the study watershed (Papaioannou et al., 2013). Validation of the methodology based on the analysis of the flood episode occurred in October 9th, 2006, the historical flood inundation data and flooded area derived from hydrologic and hydraulic modelling were used (Papaioannou et al., 2011). The historical flood records filed by several authorities, newspapers, local interviews and testimonies of flood victims have been collected and digitized within a GIS (Figure 4.1.b). The final dataset includes points, polygons and polylines digitized by the following records (Figure

4.2): 1) Houses that were refunded for electrical machines damages, 2) Companies that were compensated for flood damage, 3) Buildings that were refunded for structural damages, 4) Flooded streets recorded by the Fire Department of the City of Volos, 5) Estimated area by newspaper articles and 6) Testimonies of flood victims.

Hydraulic modelling has been used to estimate the flood extent (validation are referred as "modelled flooded area") (Figure 4.2, Figure 4.3). The data used in hydraulic modelling consist of high resolution DEM (Terrestrial laser scanner DEM with vertical accuracy of 25 cm) and the derived Clark's instantaneous unit hydrograph (see Chapter 2). A first attempt for the calibration of roughness coefficient value and the validation of the Clark Instantaneous Unit Hydrograph, as presented in Chapter 2, has been achieved with the use of different post flood analysis methods, as presented in Chapter 3. The results of the post flood analysis showed that the optimized value of Manning's roughness coefficient is 0.035. Thus, this value of roughness coefficient and the CIUH have been used in one-dimensional hydraulic model HEC-RAS for the estimation of the "modelled flooded area" presented in Chapter 5 (Figure 4.3). Finally the total percentage of the validation area is divided to 91% validation area that consist of the historical data and the 9% which is based on the hydraulic analysis. Further details about the study area can be found in Chapter 2.

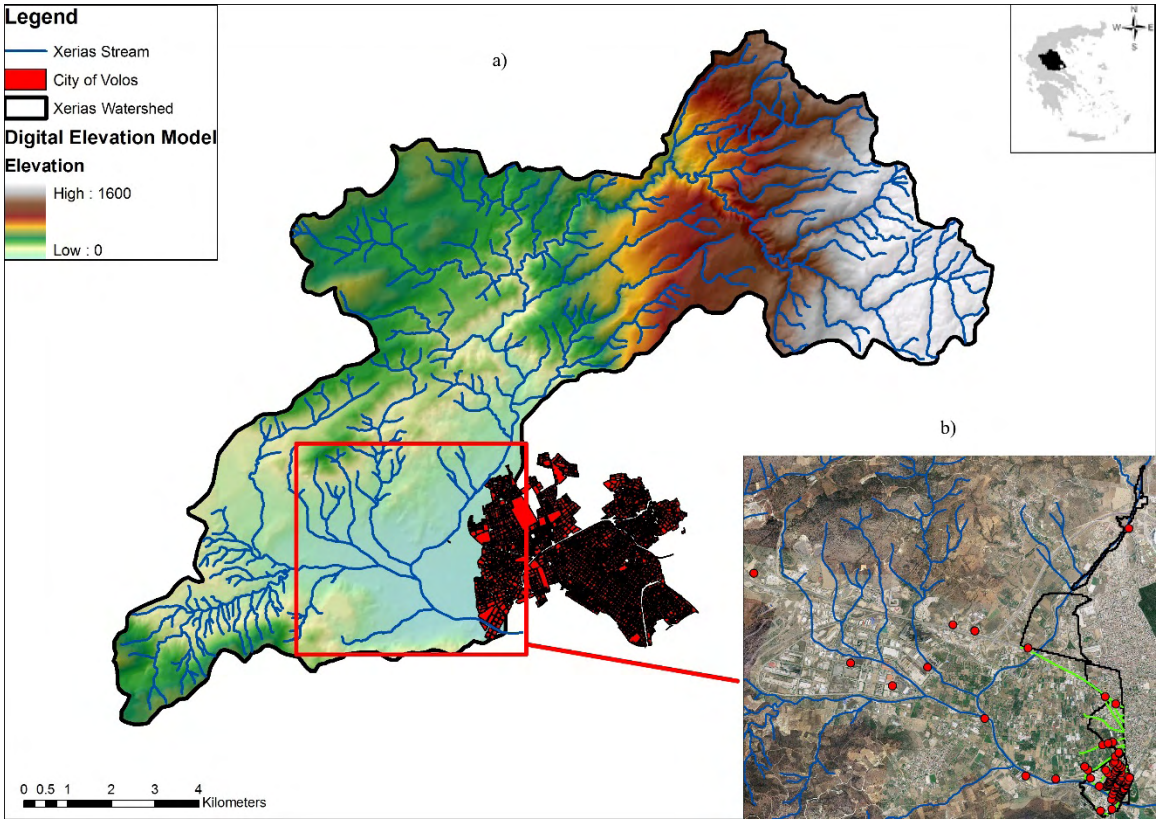

Figure 4.1. The study watershed a) Xerias Watershed and b) historical flood inundation areas used for validation of the component.

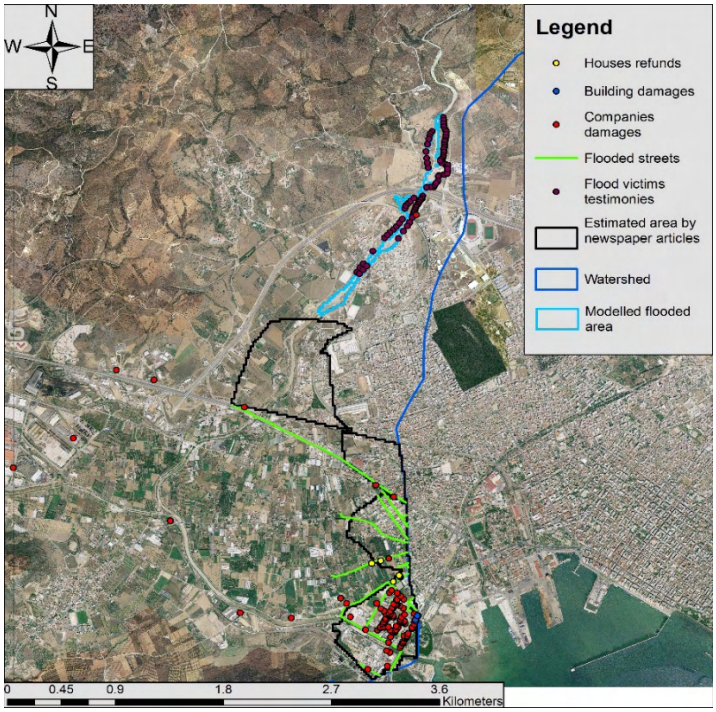

Figure 4.2. Detailed representation of all data used for the validation of the component.

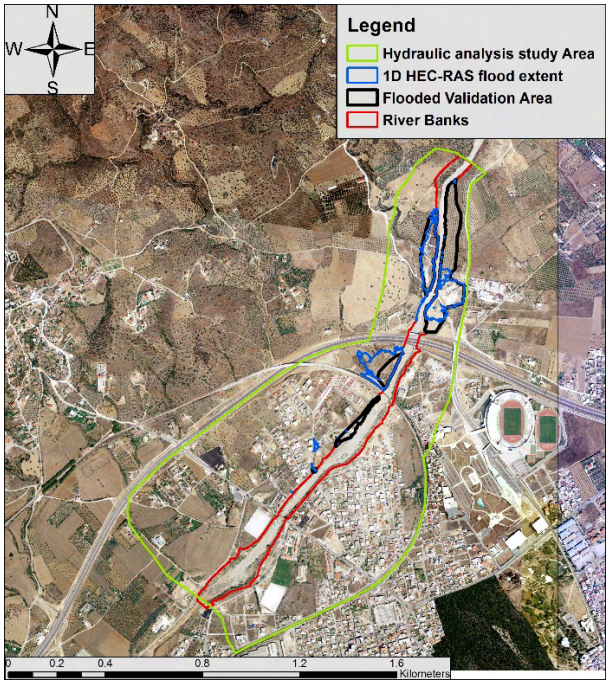

Figure 4.3. Study area for the hydraulic simulation and the estimated flood extent using 1D HEC-RAS hydraulic model ("modelled flooded area").

4.3 Methodology

The developed flood prone areas identification and mapping component composed by a GIS-based spatial multi-criteria analysis and the evaluation structure. The component is implemented in catchment scale and, its primary objective is to identify potential flood prone areas. Figure 4.4 presents in detail the flowchart of AHP, FAHP and GIS processes of the applied method. The methodology is separated in two different approaches, but both approaches have some common steps in the analysis and these are: a) Criteria selection procedure, b) Development of AHP and FAHP methods and their evaluation process, c) Use of Boolean Algebra and the weights estimated from AHP and FAHP for the union of the criteria in a single flood-prone area map, d) Validation of the final flood-prone area maps with historical flood data and hydraulic simulation data. The difference in both approaches is that, in the first approach, all criteria are normalized, with min-max methodology, in order to perform Boolean algebra through GIS analysis, while in the second approach, the criteria are classified at the start of the process using all used clustering techniques and then, they are applied for flood-prone areas mapping using Boolean algebra through GIS.

All methodologies that applied in the proposed component, have been examined thoroughly and combined in order to minimize the subjectivity of the entire system. Minimization of the subjectivity is an essential constraint in the application of multi-criteria evaluation methods. The proposed component, described in this chapter (Chapter 4), is developed for the identification of potential flood prone areas using mainly geomorphological data and minimum subjectivity. The component can be a valuable tool for decision makers and the flood management authorities.

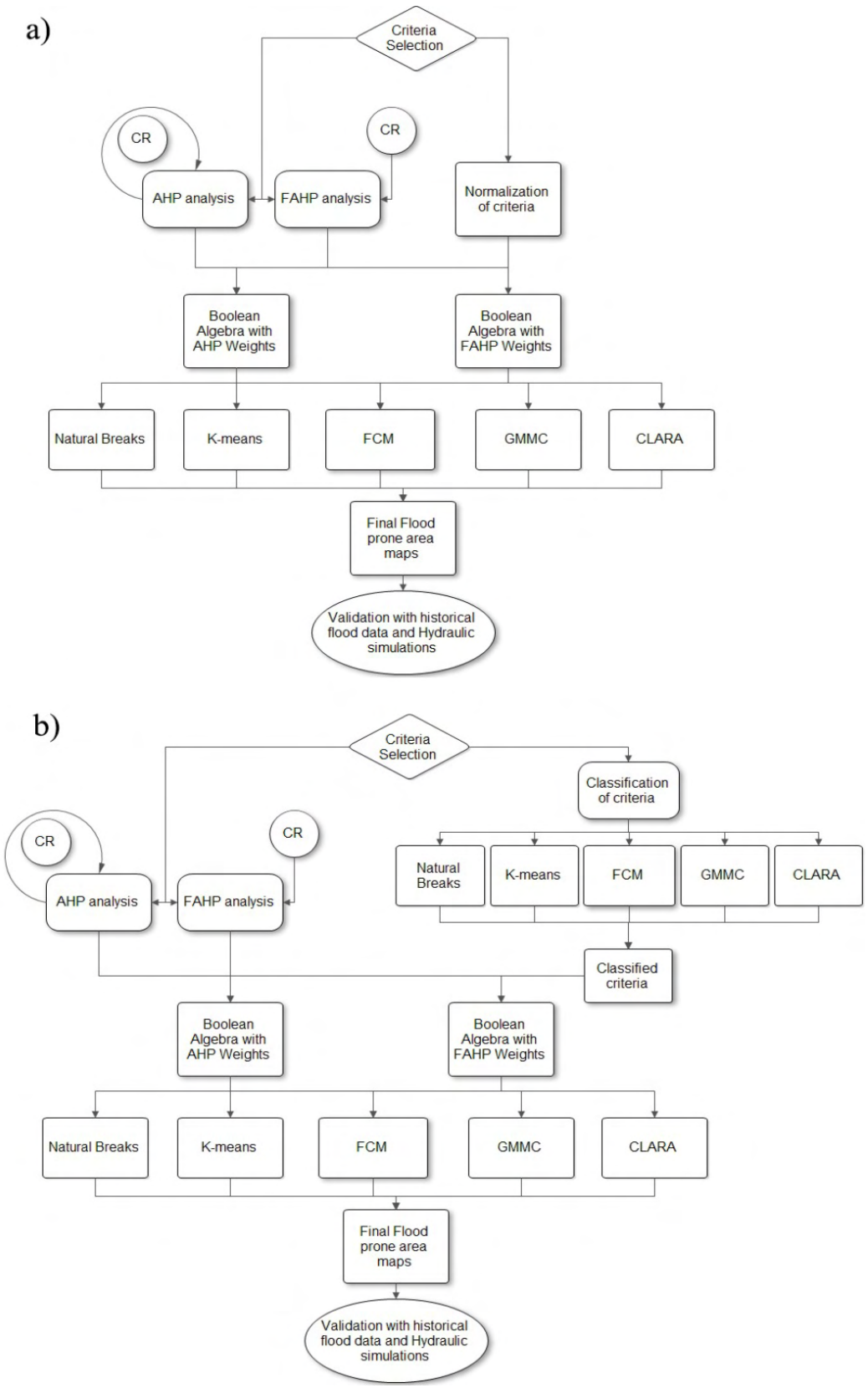

Figure 4.4. Flowchart of the applied methodology: a) 1st Approach b) 2nd Approach

4.3.1 Multi-Criteria Analysis Methods

Multiple criteria analysis (MCA) is a framework of methodologies aiming to help decision making for complex problems. With the use of MCA techniques the decision makers can improve the transparency and the subjectivity of their choice (Dunning et al., 2000; Romero and Rehman, 1987). Multi-Criteria Analysis (MCA) is used to analyse a series of alternatives or objectives intending to rank them from the most preferable to the least preferable using a structured approach. The results of MCA consist of a series of weights connected to the objectives.

Hajkowicz and Collins, (2007) defined MCA as a decision model which contains:

- The decision options (policy makers ought to rank or assign score to them)
- The criteria (typically in different units) and
- The performance measures (decision option scores against each criterion).

An evaluation matrix *X* of *n* decision options of the problem and *m* criteria is the structural element of a MCA model. $x_{i,j}$ is the evaluation given to decision option *i*th counting on the criterion *j*th, w_j is the weight of criteria *j*. A limitation of the MCA model is that it should have a minimum number of two criteria and two decision options ($n \geq 2$ and $m \geq 2$). The composition of *X* and *W* can be either qualitative and/or quantitative data. For ranking or score evaluation of the decisions, options can be used a variety of MCA algorithms.

The following, one or both, functions can be defined by the MCA algorithms:

$$r_i = f_1(X, W) \tag{4.1}$$

$$u_i = f_2(X, W) \tag{4.2}$$

Where the rank position of decision option *i* is expressed as the number r_i and the overall performance score of option *i* is expressed with u_i. A wider MCA decision-making process includes the solution of r_i and u_i.

MCA process described by many authors (RAC, 1992; Howard, 1991; Hajkowicz and Collins, 2007) and contain the following main steps: 1) Define the decision options (objectives), 2) Define evaluation criteria, 3) Construct the evaluation matrix *(xi,j)*, 4) Normalization of the datasets, 5) Weight estimation of the criteria, 6) Evaluation of the options (rank or score the options), 7) Sensitivity analysis process, 8) Decision making stage. This step-by-step procedure includes many iterations and re-evaluation of each step as the analysis occurs. Two MCA methods have been applied and compared for the

estimation of the relative weight importance. These methods are the Analytical Hierarchy Process (AHP) and the Fuzzy Analytical Hierarchy Process (FAHP).

Analytical Hierarchy Process

Analytical Hierarchy Process (AHP) belongs to Multi-criteria analysis (MCA) methodologies, and its employment is based on the factors structuring into a hierarchical framework. The structure of this framework describes the problem. Afterward, several priorities for alternatives are constructed according to the user judgment. Moreover, with the use of pairwise comparison table the decision-makers can examine the relative importance of various elements. In AHP, the estimation of the scores of each alternative can be accomplished with the transformation of the evaluations to numerical values (weights or priorities) (Saaty, 1980). In this study, the regular Saaty (1980) extent analysis method of AHP has been applied. A lower than 10% Consistency Ratio is used to have an acceptable consistency in the pairwise comparison table.

Four axioms govern the theoretical basis of AHP (Golden et al., 1989). A short description of the axioms is presented in the next paragraph for a better understanding of the methodology (a thorough description of the axioms can be found in Saaty, T.L. 1986; Saaty 1987; Harker and Vargas, 1987).

Axiom 1. The reciprocal condition. With the assumption that i and j are two sub-criteria (or alternatives) out of the set of sub-criteria A, a pairwise comparison table a_{ij} of this sub-criteria can be created, by the decision maker, under any criterion $c \in C$ on a reciprocal ratio scale; i.e.

$$a_{ji} = 1/a_{ij} \text{ for all } i,j \in A.$$

Axiom 2. p-homogeneity. The infinite advantage of one sub-criterion against another one, by the decision maker, is not allowed when comparing any two sub-criteria (or alternatives) $i,j \in A$, under any criterion $c \in C$; i. e.,

$$a_{ij} \neq \infty \text{ for all } i,j \in A.$$

Axiom 3. Dependence. The decision problem can be formulated as hierarchy

Axiom 4. Expectations. All alternatives and criteria that influence the specified decision problem are formulated in the hierarchy. According to the intuition of the decision maker, all decisions must be represented as alternatives and criteria in the hierarchical structure.

Moreover, compatible priorities should be assigned according to the intuitions (Golden et al., 1989).

AHP involves the following six essential steps (Lee et al., 2008; Bhushan and Ray, 2004):
Step 1: Definition of the unstructured problem and absolute declaration of the objectives. A major phase in AHP is the decomposition of the decision problem into the goal, criteria, sub-criteria and alternatives and its appropriate hierarchical structure. The structure of hierarchy is based on the direct connection between the elements of stage one with those of the below stage. This type of connection of the lowest stages of hierarchy, every element is directly or indirectly associated with every other. A hierarchy is comparable to upturned tree design and similar to a neat network. According to Saaty (1980), a convenient way to structure the hierarchy is to work Top-down from the goal and bottom-up from the alternatives until the levels are connected and comparisons can be made possible. A generic hierarchic structure can be seen in Figure 4.5. At the top level of the hierarchy is the objective or goal of the problem and at the bottom level of the structure are the alternatives. The levels of criteria and sub-criteria are positioned between the levels of goal and the alternatives. An important tip in the comparison of the elements is that the decision maker should count the contribution of the levels with a bottom-up logic.

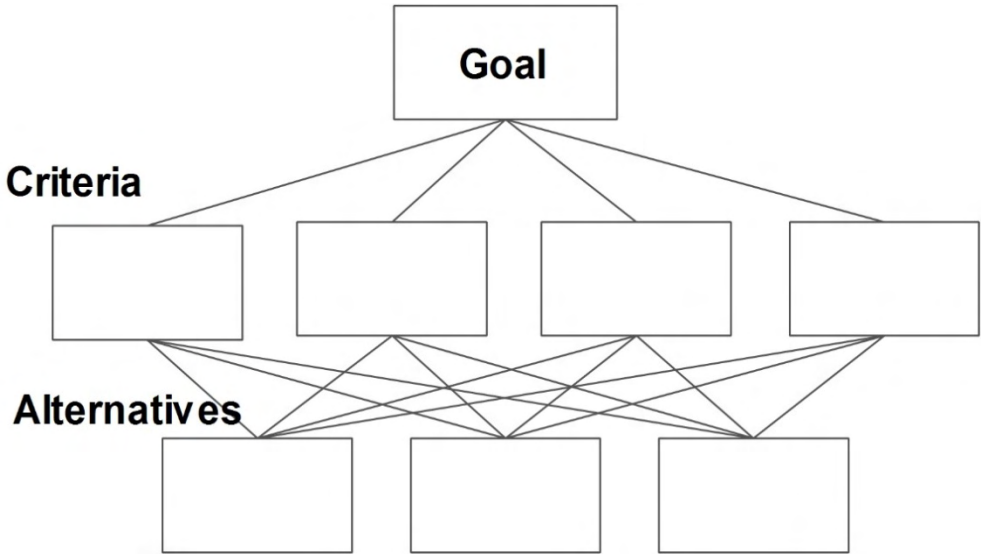

Figure 4.5. Generic hierarchic structure

Step 2: Development of the AHP hierarchy. Decision-makers and/or experts are expected to correspond to the hierarchic structure to collect the data. The collection of the data is achieved with the use of a qualitative scale pairwise comparison. Decision-makers and/or experts rate the compared elements according to Table 4.1 format. In the example of

Table 4.1, the comparison shows that two factors (A, B) have equal significance. After the evaluation of each criterion, the data is converted into qualitative numbers. Table 4.2 presents the linguistic scale for importance, the intensity of importance and the values for reciprocal scale.

Table 4.1. Format of pairwise comparisons

A					**X**					**B**
	Extremely strong	**Very strong**	**strong**	**Marginally strong**	**Equal**	**Marginally strong**	**Strong**	**Very strong**	**Extremely strong**	

Table 4.2. AHP and FAHP linguistic scales for relative importance (Adapted from Saaty, 1980 and Zhou, 2012)

	AHP		**FAHP**	
Linguistic scale for importance	**Intensity of imprortance**	**Values for reciprocal scale**	**Triangular fuzzy scale**	**Triangular fuzzy reciprocal scale**
Equally important	1	1	(1, 1, 1)	(1, 1, 1)
Intermediate 1	2	1/2	(1, 2, 3)	(1/3, 1/2, 1)
Moderately important	3	1/3	(2, 3, 4)	(1/4, 1/3, 1/2)
Intermediate2	4	1/4	(3, 4, 5)	(1/5, 1/4, 1/3)
Important	5	1/5	(4, 5, 6)	(1/6, 1/5, 1/4)
Intermediate 3	6	1/6	(5, 6, 7)	(1/7, 1/6, 1/5)
Very important	7	1/7	(6, 7, 8)	(1/8, 1/7, 1/6)
Intermediate 4	8	1/8	(7, 8, 9)	(1/9, 1/8, 1/7)
Absolutely important	9	1/9	(9, 9, 9)	(1/9, 1/9, 1/9)

Step 3: Creation of the pairwise comparison table. The qualitative numbers (Table 4.2) derived from the second step (criteria evaluation) are concentrated and structured to a matrix that is well known as pairwise comparison table. The matrix is separated in the upper right part, and the lower left part from the diagonal elements of the matrix equal to 1. One of the two parts of the matrix (e.g. (*j, i*) values) consists of the reciprocal values of the other part (e.g. (*i,j*) values). If the value in the *i*th row is more than 1, then the criterion the *i*th row is assumed of better importance than the criterion in the *j*th column and vice versa. An example of a pairwise comparison table can be seen in Table 4.3.

Table 4.3. Example of AHP pairwise comparison table

	DEM	Slope	Aspect	Flow Ac.	HOFD	VOFD	TPI	WI	CN	MFI
DEM	1	1/6	2	1/7	1/3	1/5	1/3	1/9	1/6	1
Slope	6	1	4	1/5	2	1/5	1/2	1/7	1/2	4
Aspect	1/2	1/4	1	1/7	1/2	1/6	1/5	1/8	1/5	1/3
Flow Ac.	7	5	7	1	4	2	3	1/2	2	5
HOFD	3	1/2	2	1/4	1	1/3	1/3	1/7	1/5	2
VOFD	5	5	6	1/2	3	1	2	1/4	2	4
TPI	3	2	5	1/3	3	1/2	1	1/3	3	5
WI	9	7	8	2	7	4	3	1	5	9
CN	6	2	5	1/2	5	1/2	1/3	1/5	1	3
MFI	1	1/4	3	1/5	1/2	1/4	1/5	1/9	1/3	1

Step 4: Estimation of the relative weights. The first stage of the relative weights estimation consists of the multiplication of all values in each row (for the same criterion) together. Then the calculation of the *n*th root of all criteria or sub-criteria or alternatives. In the first stage, the process calculates the eigenvector. In the second stage, the decision-maker should normalize the aforementioned *n*th root to get the final normalized eigenvector that is termed as "weight" for each criterion. In the process of step 4, the eigenvalue of each criterion is calculated and is going to be used in the next step.

Step 5: Consistency evaluation. The comparison table consistency is evaluated with the Consistency Ration (CR) estimation process. This, is a crucial step (of AHP method) because the decision maker's choice in the comparison table introduces the subjectivity. If the CR fail to achieve an acceptable level, the comparison table should be re-examined. Details about Consistency Ratio (CR) are presenting in the Sub-Section 4.4.2.

Step 6: Overall rating of the method. For the final estimation of the ratings, the priorities are categorized to local and global. The transformation from local to global priorities goes with a bottom-up process where the ratings are multiplied by the weights and aggregated first to local and then with the same process to the global rating.

Fuzzy Analytical Hierarchy Process

With the establishment of the AHP in the family of MCA techniques several variations of AHP have been created. One that is used frequently, in the last decade, is the Fuzzy Analytical Hierarchy Process (FAHP). FAHP combine several fuzzy logic methods or

theories with AHP (van Laarhoven and Pedrycz, 1983; Buckley, 1985; Chang, 1996; Mikhailov, 2003). According to Erensal and his associates (Erensal et al., 2006) the standard process of AHP cannot totally present the human way of thinking, despite the varied range of its applications. Regardless of the fact that FAHP may require tedious computations, it can be a skilfil/helpful method that captures human judgment of uncertainty (Erensal et al., 2006). In this study, the basic concept of FAHP by Chang (1996) has been applied. The steps of this process are similar to the AHP steps that were described in the previous paragraphs. FAHP is using triangular fuzzy numbers (TFN) *M* (Figure 4.6) in the pairwise comparison process and is denoted as (*l,m,u*) where *l*≤ *m*≤*u*. *l* denotes the lower possible value, *m* denote a possible value, and *u* denote the biggest possible value of the described fuzzy event. The TFN can be defined as:

$$u_M(x) = \begin{cases} (x-l)/(m-l) & l \le x \le m \\ (u-x)/(u-m) & m \le x \le u \\ 0 & otherwise \end{cases} \quad (4.3)$$

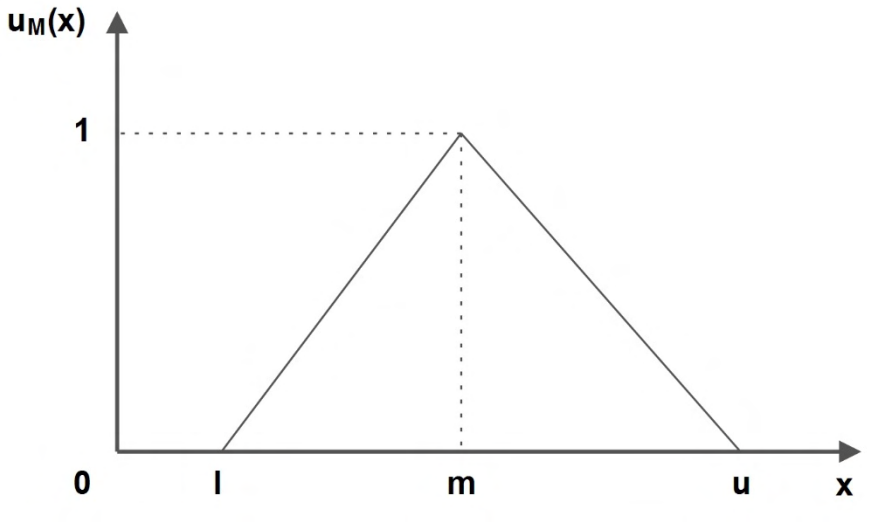

Figure 4.6. Triangular fuzzy number M

Different sets of linguistic scales to fuzzy numbers transformations have been tested (Bulut et al., 2012; Lee, 2010). The defuzzification method used in this analysis is the centroid method:

$$\tilde{A} = \frac{\int \mu_{\tilde{A}}(x) x dx}{\int \mu_{\tilde{A}}(x) dx} \quad (4.4)$$

where the TFN is indicated as $\tilde{A}$=(*l,m,u*). For TFN as in equation 3.3, the centroid is equal to (*l*+*m*+*u*)/3.

According to Basaran (2012), many researchers do not take into account the CR process when using FAHP process. In this analysis, the CR process is taken into account and all of the comparison tables and the transformed linguistic scales of importance to fuzzy triangular scale numbers with the lowest consistency ratio (lower than 10 %) finally are used, as proposed by Zhou (2012) (Table 4.2).

4.3.2 Clustering-Classification Techniques

Cluster analysis (clustering) is used to group a set of objects according to their similarity. Cluster analysis is extensively used in a variety of applications e.g. data analysis, image processing, etc. In some applications, the cluster analysis can also be called as data segmentation (Han et al., 2009). World widely, a variety of clustering algorithms and models is used in many scientific fields. The categorization of the clustering algorithms is based on their cluster model. Maimon and Rokach, (2005) suggest dividing the clustering algorithms to the following categories: 1) Partitioning Method 2) Hierarchical Method 3) Density-Based Method 4) Grid-Based Method 5) Model-Based Method 6) Constraint-Based Method.

The methods that have been selected in this analysis belong to the category of partitioning methods because they construct k partitions of the data and were applied with k equal to five in order to create five vulnerability classes of flood prone areas. Therefore in this study, the clustering methods have been used are : 1) Natural Breaks classification method (Jenks), 2) K-mean clustering method, 3) Fuzzy c-mean (centroid-based clustering methods), 4) Gaussian Mixture Model Clustering (distribution-based clustering methods), 5) Clustering Large Applications method (CLARA).

The discretization of the spatial distribution of hazard areas was set to five (5) hazard classes. This setup was set a priori due to the variety of the different selected criteria, the different spatial distribution of the values in each criterion and to minimize the computational time of the classification-clustering techniques. This assumption is also followed in similar studies for the identification of flood-prone areas, flood hazard mapping and flood risk mapping (eg. Diakakis, 2011; Kourgialas and Karatzas, 2011; Stefanidis and Stathis, 2013; Zou et al., 2013; Asare-Kyei et al., 2015; Chen et al., 2015; Kourgialas and Karatzas, 2016).

As mentioned previously, two approaches have been applied: in the first approach, all clustering techniques were applied only at the end of the component in order to classify the final potential flooded areas and, in the second approach, the clustering techniques were applied directly to the criteria (at the beginning of the component) and after the MCA application for the creation of flood-prone areas and their associated flood hazard

degree. The abovementioned clustering-classification techniques are described in the next paragraphs.

Natural Breaks: Jenks' Natural Breaks is the most widely used clustering method that exists in the majority of the GIS softwares. Natural breaks is a data classification method for the determination of the optimum arrangement of values into separate classes so that they can be displayed on a choropleth map (Jenks, 1967). The method is based on the identification of class breaks where the data that has similar values are grouped. With this approach, the difference between the classes is maximized. The method can locate grouping and patterns inherited in the data, reducing the differences within a class and accentuates the differences between the created classes. In short, Jenks Optimization method is trying to lessen the variance within classes and to maximize the variance between classes. The most applied and well known (in GIS packages) algorithm is a follow-up of Fisher, (1958) work and can be found in Jenks and Caspall, (1971). Natural breaks classifiction technique is one of the most common classification methods that is used in GIS and especially for flood risk areas classification. Jenks' Natural Break clustering technique involves the following four essential steps (de Smith et al., 2015):

- Step1: The number of classes, *k*, of the chosen attribute *x*, depends on the user selection.
- Step2: As initial class, boundaries are used a pair of *k-1* uniform or random values that created with a [min(*x*), max(*x*)] range.
- Step3: Calculate the mean of all initial classes and the sum of squared deviations of class members from the mean values. Furthermore, it is estimated the Total Sum of Squared Deviations (TSSD).
- Step4: Symmetrically assigns the individual values of each class to the adjacent classes. This is achieved with the adjustment of the class boundaries and the observation of the TSSD if it can be reduced. This procedure works iteratively and ends when the TSSD values are under the threshold level. A true optimization is not guaranteed and it should optionally be repeated the steps to achieve more TSSD values for their comparison.

K-mean: K-mean clustering method uses an iterative algorithm that minimizes the sum of distances from each object to its cluster centroid, over all clusters. The algorithm moves objects between clusters until the optimization of sum. Lloyd's algorithm (k-means clustering) allocate any *n* observations to precisely one of *k* clusters defined by centroids (the number of *k* clusters is specified at the beginning of the process). The algorithm involves the following five steps (Lloyd, 1982):

1. Selection of initial *k* cluster centers (centroid).

2. Computation of the distances (point-to-cluster-centroid). The distances calculated for all observations to each centroid.
3. The observations are assigned to the cluster with the shortest centroid distance or are assigned to a different centroid if the realignment minimizes the sum-of-squares point-to-cluster-centroid distances.
4. Obtain new k centroids by computing the mean of the observations per cluster.
5. Steps two (2) and four (4) are repeated until a maximum number of iteration is achieved or the clusters assignments stabilized.

The k-mean clustering method that is implemented in this analysis is using the k-means++ algorithm for cluster center initialization. The k-means++ algorithm uses a heuristic process to find centroid seeds for k-means clustering. By using the k-means++ algorithm can be improved the running time and the quality of Lloyd's algorithm results (Arthur and Vassilvitskii, 2007). With the assumption that the number of clusters is *k,* the k-means++ algorithm select the seeds as (Mathworks, 2013):

1. Uniformly at random select, from data set *X,* an observation value. The chosen value c_1 is declared as the first centroid.
2. Estimate the distances between observations and c_1. Where the distance between the centroid *j* (c_j) and the observation *m is designated as* $d(x_m, c_j)$.
3. For the selection of the following centroid, c_2 at random from *X* with probability is used the following equation:

$$\frac{d^2(x_m, c_1)}{\sum_{j=1}^{n} d^2\left(x_j, c_1\right)} \tag{4.5}$$

4. For the selection of the *j* center the following stages should be implemented:
    a. Calculation of the distances between observations and centroids and assignment of observations to the centroid with the shortest distance
    b. Selection of centroid *j* at random from *X* (for $m = 1,\ldots,n$ and $p = 1,\ldots,j-1$) with probability

$$\frac{d^2\left(x_m, c_p\right)}{\sum_{\{h_i x_h \in C_p\}} d^2\left(x_j, c_1\right)} \tag{4.6}$$

Where C_p is the set of all observations closest to centroid c_p and x_m belongs to C_p.

With abovementioned stage, each subsequent center is selected with a probability comparative to the distance from its center to the closest center that has already been chosen.

5. Step four (4) is repeated till k centroids are chosen.

The default and mostly used distance method in k-mean function is the 'sqEuclidean' (i.e. the Squared Euclidean distance) method where each centroid is the mean of the points in that cluster. The alternate distance method is the 'cityblock' (i.e. the Sum of absolute differences) where each centroid is the component-wise median of the points in that cluster (Mathworks, 2013). The formulas of 'sqEuclidean' and the 'cityblock' distance are:

'sqEuclidean' $$d(x,c) = (x-c)(x-c)' \quad (4.7)$$

'cityblock' $$d(x,c) = \sum_{j=1}^{p} \left| x_j - c_j \right| \quad (4.8)$$

Where, *x* is an observation (eg. a row of *X* numerical matrix), *c* is a centroid (a row vector), and *p* is the dimensional space.

These two variances of K-means cluster method were employed and examined. In order to avoid local minima the method has been applied iteratively 1,000 times, for both distance methods, with a new set of initial cluster centroid positions each time.

Fuzzy C-mean: In 1981, Bezdek established the Fuzzy C-Means (FCM) clustering technique (Bezdek, 1981) which is an evolution of previous clustering techniques. In FCM clustering approach the components of the analysis may belong to two or more clusters with different membership value. FCM is a typical method used in pattern recognition. The algorithm works iteratively until the production of an optimal C partition by minimizing the weighted within group sum of squared error objective function:

$$J_m = \sum_{i=1}^{D} \sum_{j=1}^{N} \mu_{ij}^{m} \left\| x_i - c_j \right\|^2 \quad (4.9)$$

where *m* is any real number greater than 1, and it is set to 2.00 by Bezdek; μ_{ij} is the degree of membership of x_i in the cluster *j*; x_i is the ith of d-dimensional measured data; c_j is the dimension center of the cluster; ||*|| is an equation that defines the similarity between any measured data and the center; *D* is the number of data points, and *N* is the number of clusters (Alata et al., 2008).

The Fuzzy C-mean algorithm involves the following five steps (Mathworks, 2013):

1. Arbitrarily initialize the cluster membership values, μ_{ij}
2. For the calculation of the cluster centers is used the algorithm:

$$c_j = \frac{\sum_{i=1}^{D} \mu_{ij}^{m} x_i}{\sum_{i=1}^{D} \mu_{ij}^{m}} \tag{4.10}$$

3. μ_{ij} is updated with the following equation:

$$\mu_{ij} = \frac{1}{\sum_{k=1}^{N} \left(\frac{\|x_i - c_j\|}{\|x_i - c_k\|} \right)^{\frac{2}{m-1}}} \tag{4.11}$$

4. Estimate J_m (objective function)

Steps two (2) and four (4) are repeated till the improvement of J_m. Objective function J_m assumed as improved when it is above the minimum threshold or until it reaches the maximum number of iterations.

In order to achieve crisp values from the FCM clustering technique, a defuzzification process should be applied. In this study, the maximum membership procedure was applied for the transformation of the fuzzy partition matrix *U* to a crisp partition. The procedure assigns object *k* to the class *C* with the highest membership (Yang and Huang, 2007):

$$C_k = arg_i\{max(u_{ik})\}, i = 1,2,..c. \tag{4.12}$$

With this procedure, the fuzzy values were converted to crisp values and made possible the visualization of the results.

Gaussian Mixture Model: Gaussian Mixture Model Clustering (GMMC) is an important and widely used clustering technique that is based on probability density estimation using Gaussian mixture models and the procedure Expectation-Maximization algorithm to fit the model parameters (Bishop, 2008; Dempster et al., 1977; Nock and Nielsen, 2006). The algorithm assigns posterior probabilities to each component density on each observation. Then, the clusters are allocated by selecting the component that maximizes the posterior probability. In Gaussian Mixture Models (GMM) the clusters are modeled as Gaussian distributions and the algorithm works iteratively in order to converge to a local optimum. The GMMC method implemented in this analysis uses the main principle of k-means++ algorithm (use of heuristic to find centroid seeds for the clustering technique) to initialize the EM algorithm (i.e. the initial parameter values for a fitted Gaussian mixture model

were selected by k-means++ algorithm). With the assumption that the number of clusters is *k* the k-means++ algorithm choose the initial parameter values as follows (Mathworks, 2013):

1. The component mixture probability is selected to be the uniform probability $p_i=1/k$, where $i = 1, ..., k$.
2. The covariance matrices is selected to be diagonal and identical, where $\sigma_i=diag(a_1,a_2,...,a_k)$ and $a_j=var(X_j)$.
3. The first initial component center μ_1 is selected uniformly from the entire dataset of *X*.
4. The selection of the center *j* is achieved by:
    a. Computing the Mahalanobis distances from each observation to each centroid
    b. Assign each observation to its closest centroid
    c. Select centroid *j* at random from *X* (for $m = 1,...,n$ and $p = 1,...,j - 1$) with probability

$$\frac{d^2(x_m, \mu_p)}{\sum_{h;x_h \in M_p} d^2(x_h, \mu_p)} \quad (4.13)$$

    Where M_p is the series of all observations closest to centroid μ_p and x_m belongs to M_p and $d(x_m,\mu_p)$ is the distance among observation *m* and μ_p.
    With abovementioned stage, each subsequent center is selected with a probability comparative to the distance from its center to the closest center that has already been chosen.
5. Step four (4) is repeated till the *k* centroids are chosen.

Most of the studies categorize the GMMC as a soft clustering method where the posterior probabilities for each point indicate that each data point has some probability of belonging to each cluster (Mathworks, 2013). In this study, the method was applied iteratively 1,000 times.

CLARA: Clustering LARge Applications (CLARA) is a k-medoid partitioning clustering technique created to deal with large data sets (Kaufman and Rousseeuw, 1986). The obstacle of the large datasets has been overcome with the transformation of the time and storage requirements to linear rather than quadratic. This was achieved with the use of sampling process. Accordingly, rather than finding similar objects from the complete data set, CLARA selects a sub-dataset (sample) and partition it into k clusters with the use of Partitioning Around Medoids (PAM) clustering technique (Kaufman and Rousseeuw, 1990). After the selection of the k representative objects from the sub-dataset, each

observation (of the complete dataset) is approximated to the closest medoid (Ng and Han, 1994). The k representative objects are selected to minimize dissimilarity (Kaufman and Rousseeuw, 1986):

$$\frac{1}{n}\sum_{i=1}^{n}(i, m_i) \tag{4.14}$$

where n = objects of the dataset, d = dissimilarity measure, m_i = representative object closest to object i.

The process is functioning iteratively and, each time, is trying to select a better set of clusters till the k representative objects to be located closer the medoid.

In each iteration, the evaluation of the clustering is conducted with the estimation of the average (equivalent to the sum) of the dissimilarities of the observations against their closest medoid. Then, the sub-dataset with the minimum value is retained. On the last partition, additional analysis is accomplished. In each iteration, the observations are added randomly to the set. Finally, the medoids acquired from the best sub-dataset are stored in each data set until a better update prevails and/or till the sample size is reached (Maechler et al., 2016). The method is applied iteratively 1,000 times with one percent sample size (3,000 points) of the total dataset size.

4.4 Estimation of Flood-Prone Areas in the Xerias Watershed

The proposed flood prone areas identification and mapping component have been applied at Xerias Watershed, Greece (Figure 4.1 **,** see Chapter 2). The criteria used in this analysis mainly consist of quantitative geomorphological and hydrometeorological indices that can be produced quickly with the utilization of the digital elevation models. The combination of the multi-criteria analysis methods and clustering-classification techniques derived several relationships among the selected criteria. Then, based on several combinations, different flood-prone area maps have been produced and incorporated to the final flood prone areas maps.

4.4.1 Criteria Identification

A critical step in flood prone areas recognition procedure using geomorphologic indices is the choice of the criteria. An effective flood hazard mapping framework that detects flood prone areas and flood hazard degree is a framework where the selected criteria are well associated with the physical process of the flood generation mechanism. Another

important factor in the criteria selection is the time consumption for their analysis and their availability; the selected features should have a quick and straightforward estimation procedure for the entire study area. In order to investigate the use of flood-related possible criteria, a preliminary analysis has been conducted using linear correlation analysis. In this analysis, 32 flood-related geomorphological attributes setups were examined (Table 4.4) (Papaioannou et al., 2011). For the estimation of the correlation coefficient have been used the equation:

$$Correl(X,Y) = \frac{\sum(x-\bar{x})(y-\bar{y})}{\sqrt{\sum(x-\bar{x})^2(y-\bar{y})^2}} \quad (4.15)$$

where $\bar{x}$ and $\bar{y}$ are the sample means of array *X* and array *Y*.

The preliminary analysis involved the following criteria: 1) DEM= Elevation, 2) Slope 3) Aspect = Modified aspect according to the direction of storms, 4) Flow Ac = Flow Accumulation , 5) Flow Dir = Flow Direction, 6) Fill = depressionless DEM, 7) Hillshade = surface representation, 8) HOFD = Horizontal Overland Flow Distance, 9) VOFD = Vertical Overland Flow Distance, 10) OFD = Overland Flow Distance, 11) VDCN = Vertical Distance to Channel Network, 12) SPI = Stream Power Index, 13) TPI = Topographic Position Index (implemented with different pixel sampling perimeter of 3,5,10,20,30,40,50,75,100), 14) WI = Wetness Index (modified wetness index from SAGA GIS software), 15) TWI = Topographic Wetness Index, 16) CN = Curve Number (SCS method), 17) WE = Wind Effect (implemented with different grid directions of 0,360,45,90,135,180,225,270,315), 18) MFI = Modified Fournier Index.

The resulting criteria setup consists of 10 criteria (Table 4.5) that prevailed among the others according to the Pearson correlation analysis and the personal engineering judgment according to the flood generation mechanisms and the knowledge of the study area. The selected criteria are: 1) DEM, 2) Slope, 3) Aspect, 4) Flow Ac., 5) HOFD, 6) VOFD, 7) TPI, 8) WI, 9) CN, 10) MFI. The spatial resolution used in this analysis is 20m cell size. Furthermore, all the chosen features have been transformed as normalized indices to improve the objectivity and strengthen the general applicability of the proposed component in other watersheds. Figure 4.7 shows the ten selected geomorphologic indices and their normalized spatial distribution used for the detection of potential flood-prone areas. An extensive analysis of each selected criterion is presented in the following paragraphs.

DEM: The DEM of the study area was created with the use of 20m contour lines. The DEM was scaled conversely because lowlands are more vulnerable to flooding (Burrough et al., 2015).

Slope: Slope is one of the main byproducts of the DEM. The slope created with the use of the DEM and the standard slope estimation formula (percent of slope = (rise/run)*100).

Flow Ac.: Flow accumulation is somehow a byproduct of the DEM and is frequently used for the definition of channel networks. Its implementation is based on flow direction (single flow D8 algorithm). The accumulated flow is estimated by the accumulated weight of the total cells amount that is flowing into each lower cell in the output raster. A cell with high flow accumulation value defines concentrated flow and can be interpreted as stream channel cell (Jenson and Domingue, 1988).

HOFD: Horizontal Overland Flow Distance index is estimated using the movement of the water from cell to cell and not as Euclidean distances. The main input data of HOFD index is the DEM and the river network of the area. In this study, the Multiple Flow Direction algorithm has been used (Quinn et al., 1991). The metric system of the distance is in the same units as the heights and cells size values from the DEM.

VOFD: Vertical Overland Flow is estimated using the vertical distance among the cell elevations and the elevations calculated for the channel network in that cell. The main input data of VOFD index are the DEM and the river network of the area. The process is separated into two steps (Olaya, 2004):

1) In the first step, the channel elevation is assigned from the DEM elevation for each channel network cell. For the oddment cells, interpolated elevation values of the channel cells are assigned. With this process, an elevation level based channel network is estimated.
2) In the second step, the new estimated channel network is subtracted from the DEM in order to create a new feature where the channel cells have zero value, and the rest cells have a different one.

Non-channel cells will be assigned with a value which represents the elevation difference between these cells and the channel that flows through them, where applicable. The metric system of the distance is in the same units as the heights and cells size value from the DEM (Olaya, 2004).

Table 4.4. Pearson correlation coefficient matrix of the preliminary criteria analysis.

	DEM	Slope	Aspect	Flow Ac.	Flow Dir.	Fill	Hillshade	HOFD	VOFD	OFD	VDCN	SPI	TPI (3)	TPI (5)	TPI (10)	TPI (20)	TPI (30)	TPI (40)	TPI (50)	TPI (75)	TPI (100)	WI	TWI	CN	WE (0°, 360°)	WE (45o)	WE (90o)	WE (135o)	WE (180o)	WE (225o)	WE (270o)	WE (315o)	MFI
DEM	**1.00**	0.37	0.08	0.05	-0.02	-1.00	-0.15	-0.23	0.29	0.23	-0.28	0.01	-0.04	0.05	-0.07	-0.11	-0.14	-0.17	-0.20	-0.28	-0.34	0.44	0.28	-0.03	-0.06	-0.49	-0.60	-0.49	-0.33	-0.25	0.08	0.09	-1.00
Slope	0.37	**1.00**	0.00	0.05	-0.08	-0.37	0.03	-0.25	0.26	0.24	-0.28	-0.02	0.00	-0.03	0.08	0.12	0.12	0.12	0.11	0.08	0.06	0.69	0.64	-0.08	0.11	-0.20	-0.20	-0.13	-0.04	-0.04	0.16	0.21	-0.37
Aspect	0.08	0.00	**1.00**	-0.01	-0.53	-0.08	-0.55	-0.14	0.05	0.14	-0.12	0.01	0.00	0.01	-0.02	-0.03	-0.03	-0.04	-0.04	-0.06	-0.07	0.01	-0.10	0.07	0.06	0.01	-0.09	-0.17	-0.20	-0.14	-0.03	0.06	-0.08
Flow Ac.	0.05	0.05	-0.01	**1.00**	-0.03	-0.05	0.00	0.05	0.06	-0.05	-0.06	0.37	-0.09	0.10	-0.09	-0.09	-0.09	-0.09	-0.09	-0.09	-0.09	0.14	0.28	-0.05	-0.07	-0.08	-0.08	-0.08	-0.08	-0.08	-0.07	-0.07	-0.05
Flow Dir.	-0.02	-0.08	-0.53	-0.03	**1.00**	0.02	0.30	0.07	-0.03	-0.07	0.09	-0.01	0.03	-0.03	0.02	0.01	0.01	0.01	0.02	0.02	0.03	-0.07	-0.06	-0.02	-0.07	-0.06	0.04	0.09	0.11	0.08	0.05	-0.03	0.02
Fill	-1.00	-0.37	-0.08	-0.05	0.02	**1.00**	0.15	0.23	-0.30	-0.22	0.29	-0.02	0.04	-0.06	0.08	0.11	0.14	0.17	0.20	0.28	0.34	-0.45	-0.29	0.04	0.06	0.49	0.60	0.50	0.33	0.26	-0.08	-0.08	1.00
Hillshade	-0.15	0.03	-0.55	0.00	0.30	0.15	**1.00**	0.02	-0.08	-0.02	0.04	-0.01	0.00	-0.01	0.03	0.05	0.06	0.07	0.07	0.08	0.09	0.02	0.04	-0.04	-0.08	0.06	0.17	0.19	0.18	0.07	-0.05	-0.11	0.15
HOFD	-0.23	-0.25	-0.14	0.05	0.07	0.23	0.02	**1.00**	0.35	-1.00	-0.10	0.04	-0.08	0.11	-0.15	-0.19	-0.20	-0.19	-0.18	-0.15	-0.11	-0.19	-0.08	-0.13	-0.12	0.01	-0.01	-0.02	-0.02	-0.04	-0.23	-0.22	0.23
VOFD	0.29	0.26	0.05	0.06	-0.03	-0.30	-0.08	0.35	**1.00**	-0.36	-0.73	0.05	-0.31	0.39	-0.50	-0.55	-0.53	-0.50	-0.46	-0.40	-0.36	0.46	0.35	-0.13	-0.38	-0.51	-0.47	-0.49	-0.49	-0.46	-0.24	-0.28	-0.29
OFD	0.23	0.24	0.14	-0.05	-0.07	-0.22	-0.02	-1.00	-0.36	**1.00**	0.11	-0.04	0.09	-0.12	0.16	0.20	0.21	0.20	0.19	0.15	0.11	0.18	0.08	0.13	0.12	-0.01	0.02	0.03	0.02	0.05	0.23	0.22	-0.23
VDCN	-0.28	-0.28	-0.12	-0.06	0.09	0.29	0.04	-0.10	-0.73	0.11	**1.00**	-0.05	0.40	-0.50	0.63	0.69	0.66	0.61	0.56	0.47	0.41	-0.51	-0.40	0.06	0.46	0.58	0.54	0.61	0.59	0.58	0.32	0.38	0.28
SPI	0.01	-0.02	0.01	0.37	-0.01	-0.02	-0.01	0.04	0.05	-0.04	-0.05	**1.00**	-0.21	0.19	-0.17	-0.16	-0.15	-0.14	-0.14	-0.13	-0.12	0.08	0.17	-0.03	-0.09	-0.07	-0.08	-0.08	-0.09	-0.08	-0.10	-0.09	-0.01
TPI (3)	-0.04	0.00	0.00	-0.09	0.03	0.04	0.00	-0.08	-0.31	0.09	0.40	-0.21	**1.00**	-0.94	0.76	0.55	0.45	0.39	0.35	0.29	0.25	-0.25	-0.34	0.02	0.41	0.40	0.39	0.42	0.43	0.44	0.41	0.41	0.04
TPI (5)	0.05	-0.03	0.01	0.10	-0.03	-0.06	-0.01	0.11	0.39	-0.12	-0.50	0.19	-0.94	**1.00**	-0.90	-0.70	-0.58	-0.51	-0.46	-0.38	-0.32	0.28	0.35	-0.03	-0.49	-0.45	-0.45	-0.49	-0.50	-0.51	-0.46	-0.48	-0.05
TPI (10)	-0.07	0.08	-0.02	-0.09	0.02	0.08	0.03	-0.15	-0.50	0.16	0.63	-0.17	0.76	-0.90	**1.00**	0.89	0.77	0.69	0.62	0.52	0.44	-0.29	-0.32	0.05	0.57	0.51	0.51	0.57	0.60	0.58	0.51	0.55	0.07
TPI (20)	-0.11	0.12	-0.03	-0.09	0.01	0.11	0.05	-0.19	-0.55	0.20	0.69	-0.16	0.55	-0.70	0.89	**1.00**	0.96	0.89	0.83	0.71	0.61	-0.28	-0.27	0.09	0.64	0.55	0.54	0.63	0.68	0.63	0.54	0.60	0.11
TPI (30)	-0.14	0.12	-0.03	-0.09	0.01	0.14	0.06	-0.20	-0.53	0.21	0.66	-0.15	0.45	-0.58	0.77	0.96	**1.00**	0.98	0.93	0.82	0.72	-0.29	-0.24	0.11	0.66	0.55	0.55	0.64	0.71	0.64	0.54	0.61	0.14
TPI (40)	-0.17	0.12	-0.04	-0.09	0.01	0.17	0.07	-0.19	-0.50	0.20	0.61	-0.14	0.39	-0.51	0.69	0.89	0.98	**1.00**	0.99	0.90	0.81	-0.30	-0.23	0.12	0.67	0.55	0.55	0.65	0.72	0.65	0.54	0.61	0.17
TPI (50)	-0.20	0.11	-0.04	-0.09	0.02	0.20	0.07	-0.18	-0.46	0.19	0.56	-0.14	0.35	-0.46	0.62	0.83	0.93	0.99	**1.00**	0.95	0.87	-0.30	-0.22	0.12	0.66	0.55	0.56	0.66	0.72	0.65	0.53	0.60	0.20
TPI (75)	-0.28	0.08	-0.06	-0.09	0.02	0.28	0.08	-0.15	-0.40	0.15	0.47	-0.13	0.29	-0.38	0.52	0.71	0.82	0.90	0.95	**1.00**	0.97	-0.32	-0.22	0.12	0.63	0.53	0.56	0.65	0.71	0.64	0.51	0.57	0.28
TPI (100)	-0.34	0.06	-0.07	-0.09	0.03	0.34	0.09	-0.11	-0.36	0.11	0.41	-0.12	0.25	-0.32	0.44	0.61	0.72	0.81	0.87	0.97	**1.00**	-0.33	-0.21	0.11	0.58	0.52	0.55	0.63	0.67	0.62	0.48	0.53	0.34
WI	0.44	0.69	0.01	0.14	-0.07	-0.45	0.02	-0.19	0.46	0.18	-0.51	0.08	-0.25	0.28	-0.29	-0.28	-0.29	-0.30	-0.30	-0.32	-0.33	**1.00**	0.76	-0.22	-0.33	-0.52	-0.48	-0.48	-0.44	-0.44	-0.16	-0.21	-0.45
TWI	0.28	0.64	-0.10	0.28	-0.06	-0.29	0.04	-0.08	0.35	0.08	-0.40	0.17	-0.34	0.35	-0.32	-0.27	-0.24	-0.23	-0.22	-0.22	-0.21	0.76	**1.00**	-0.16	-0.24	-0.38	-0.37	-0.36	-0.32	-0.32	-0.17	-0.17	-0.28
CN	-0.03	-0.08	0.07	-0.05	-0.02	0.04	-0.04	-0.13	-0.13	0.13	0.06	-0.03	0.02	-0.03	0.05	0.09	0.11	0.12	0.12	0.12	0.11	-0.22	-0.16	**1.00**	0.19	0.13	0.08	0.07	0.10	0.08	0.07	0.13	0.03
WE (0°, 360°)	-0.06	0.11	0.06	-0.07	-0.07	0.06	-0.08	-0.12	-0.38	0.12	0.46	-0.09	0.41	-0.49	0.57	0.64	0.66	0.67	0.66	0.63	0.58	-0.33	-0.24	0.19	**1.00**	0.56	0.30	0.55	0.77	0.59	0.27	0.72	0.06
WE (45o)	-0.49	-0.20	0.01	-0.08	-0.06	0.49	0.06	0.01	-0.51	-0.01	0.58	-0.07	0.40	-0.45	0.51	0.55	0.55	0.55	0.55	0.53	0.52	-0.52	-0.38	0.13	0.56	**1.00**	0.64	0.55	0.62	0.83	0.21	0.29	0.49
WE (90o)	-0.60	-0.20	-0.09	-0.08	0.04	0.60	0.17	-0.01	-0.47	0.02	0.54	-0.08	0.39	-0.45	0.51	0.54	0.55	0.55	0.56	0.56	0.55	-0.48	-0.37	0.08	0.30	0.64	**1.00**	0.78	0.55	0.54	0.60	0.37	0.60
WE (135o)	-0.49	-0.13	-0.17	-0.08	0.09	0.50	0.19	-0.02	-0.49	0.03	0.61	-0.08	0.42	-0.49	0.57	0.63	0.64	0.65	0.66	0.65	0.63	-0.48	-0.36	0.07	0.55	0.55	0.78	**1.00**	0.78	0.55	0.44	0.64	0.49
WE (180o)	-0.33	-0.04	-0.20	-0.08	0.11	0.33	0.18	-0.02	-0.49	0.02	0.59	-0.09	0.43	-0.50	0.60	0.68	0.71	0.72	0.72	0.71	0.67	-0.44	-0.32	0.10	0.77	0.62	0.55	0.78	**1.00**	0.70	0.31	0.51	0.33
WE (225o)	-0.25	-0.04	-0.14	-0.08	0.08	0.26	0.07	-0.04	-0.46	0.05	0.58	-0.08	0.44	-0.51	0.58	0.63	0.64	0.65	0.65	0.64	0.62	-0.44	-0.32	0.08	0.59	0.83	0.54	0.55	0.70	**1.00**	0.40	0.43	0.26
WE (270o)	0.08	0.16	-0.03	-0.07	0.05	-0.08	-0.05	-0.23	-0.24	0.23	0.32	-0.10	0.41	-0.46	0.51	0.54	0.54	0.54	0.53	0.51	0.48	-0.16	-0.17	0.07	0.27	0.21	0.60	0.44	0.31	0.40	**1.00**	0.59	-0.09
WE (315o)	0.09	0.21	0.06	-0.07	-0.03	-0.08	-0.11	-0.22	-0.28	0.22	0.38	-0.09	0.41	-0.48	0.55	0.60	0.61	0.61	0.60	0.57	0.53	-0.21	-0.17	0.13	0.72	0.29	0.37	0.64	0.51	0.43	0.59	**1.00**	-0.08
MFI	-1.00	-0.37	-0.08	-0.05	0.02	1.00	0.15	0.23	-0.29	-0.23	0.28	-0.01	0.04	-0.05	0.07	0.11	0.14	0.17	0.20	0.28	0.34	-0.45	-0.28	0.03	0.06	0.49	0.60	0.49	0.33	0.26	-0.09	-0.08	**1.00**

* DEM= Elevation, Aspect = Modified aspect according to the direction of storms, Flow Ac = Flow Accumulation , Flow Dir = Flow Direction, Fill = depressionless DEM, Hillshade = surface representation, HOFD = Horizontal Overland Flow Distance, VOFD = Vertical Overland Flow Distance, OFD = Overland Flow Distance, VDCN = Vertical Distance to Channel Network, SPI = Stream Power Index, TPI = Topographic Position Index, WI = Wetness Index, TWI = Topographic Wetness Index, CN = Curve Number, WE = Wind Effect

Table 4.5. Pearson correlation coefficient matrix of the ten (10) sellected criteria.

	DEM	Slope	Aspect	Flow Ac.	HOFD	VOFD	TPI	WI	CN	MFI
DEM	1.00									
Slope	0.37	1.00								
Aspect	0.08	0.00	1.00							
Flow Ac.	0.05	0.05	-0.01	1.00						
HOFD	-0.23	-0.25	-0.14	0.05	1.00					
VOFD	0.29	0.26	0.05	0.06	0.35	1.00				
TPI	0.05	-0.03	0.01	0.10	0.11	0.39	1.00			
WI	0.44	0.69	0.01	0.14	-0.19	0.46	0.28	1.00		
CN	-0.03	-0.08	0.07	-0.05	-0.13	-0.13	-0.03	-0.22	1.00	
MFI	-1.00	-0.37	-0.08	-0.05	0.23	-0.29	-0.05	-0.45	0.03	1.00

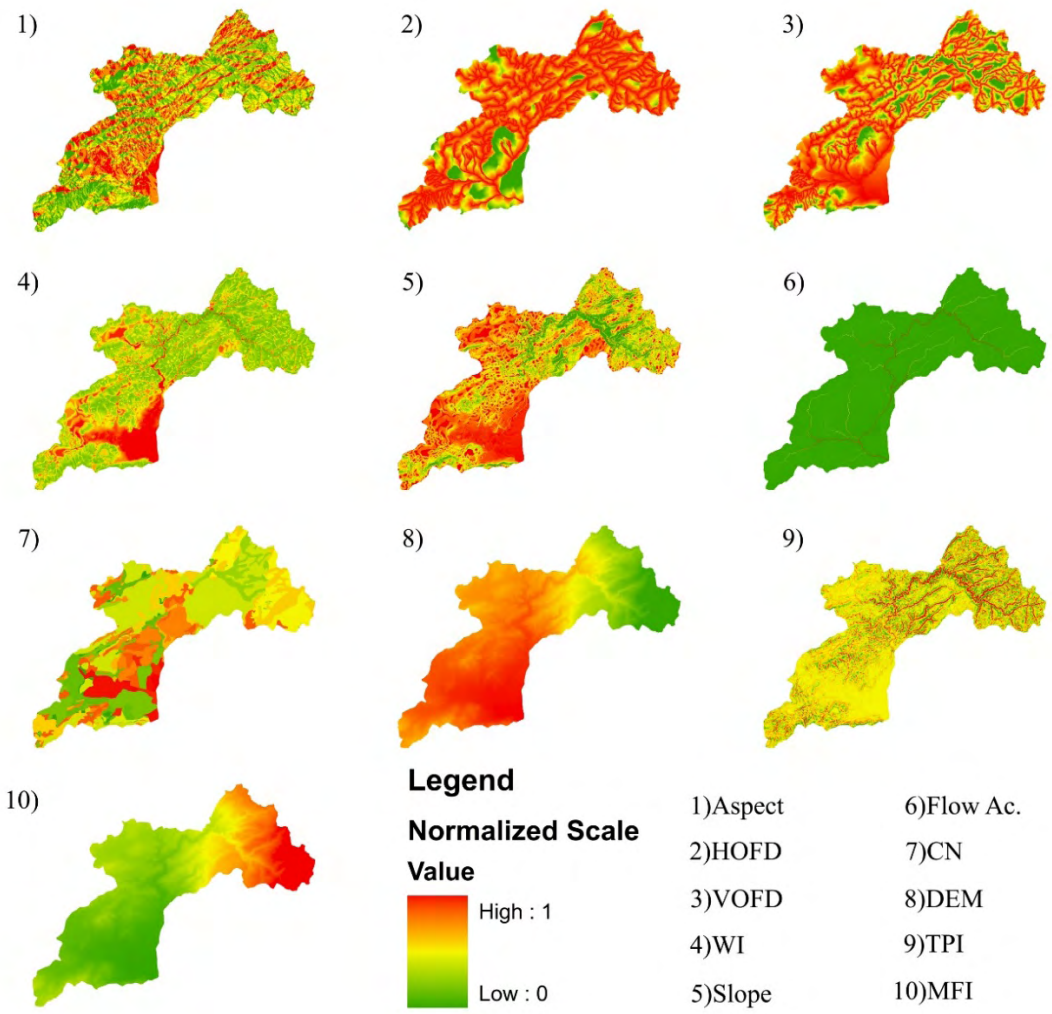

Figure 4.7. Selected criteria and their normalized spatial distribution

Aspect: Another byproduct of the DEM is the consideration of the slope direction. This is termed as "Aspect" and determines the maximum change rate of the downslope direction from each cell to its neighbors. The reference point of aspect is the actual north of zero degrees (0º, 360o). The Aspect feature is calculated with the technique of 3 x 3 moving window (Burrough et al., 2015). In this study, the feature of aspect has been modified by implementing different weights in the aspect. The additional weighting was made according to the direction of storms based on extreme weather conditions at the study area. A case of extreme weather conditions is presented in Chapter 2. The South aspect has been selected as the most critical aspect of flood generation due to the main direction of the extreme weather conditions in the study area. The final modified aspect criterion was separated to the following flood-prone area classes (Figure 4.8): 1) Very Low—North, 2) Low—Northeast, Northwest, 3) Moderate—East, West 3, 4) High—Southeast and Southwest, 5) Very high—South.

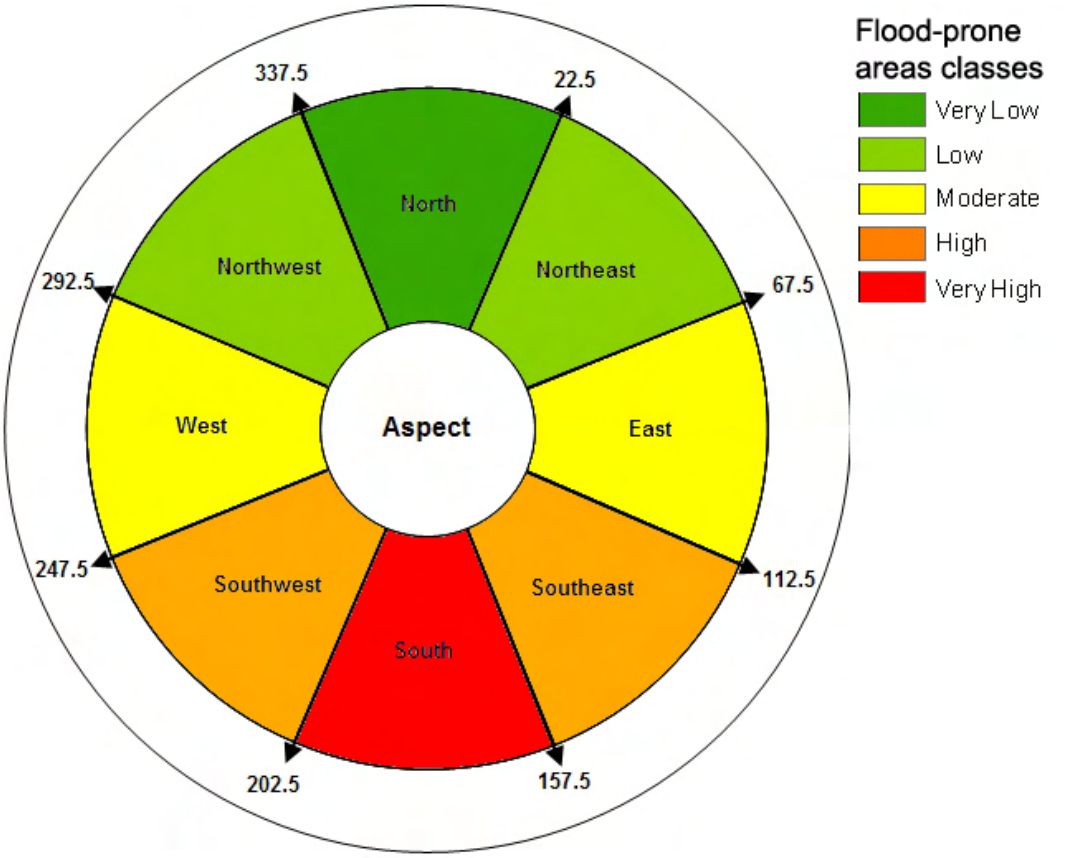

Figure 4.8. Variation of the Aspect criterion including its flood-prone area classes that emphasizes southbound storm systems

TPI: Topographic Position Index is an index that displays the landscape locations into different morphological classes (eg. valleys, canyons, flat areas, mid-slope areas, ridgetops, hilltops etc) The TPI used in this study is a generalization of Fels and Zobel, (1995) Landscape Position Index (LPI) that was presented thoroughly by Weiss (2001). The estimation of TPI is based on the difference between the elevation value of a cell and the mean elevation value of the neighboring cells. A small circular neighborhood should be used when screening refers to small streams or drainages (Tagil and Jenness, 2008). In our study, the TPI was estimated with the use of circle neighborhood option and a radius of 5 cells.

WI: Topographic Wetness Index (TWI) or Compound Topographic Index (CTI) is a common index that describes the soil water content and surface saturation zones (indicates the tendency of a cell to produce runoff). According to Kirkby (1975), a physical attribute of flood inundation areas is the Topographic Wetness Index (TWI). TPI can be estimated with the use of the slope gradient (β) and the upslope contributing area (or catchment area) (A_s) (Kringer, 2010):

$$TWI = ln\left(\frac{A_s}{tan\beta}\right) \tag{4.16}$$

The upslope contributing area (A_s) is calculated with the use of Freeman (1991) multiple flow direction method. In this study, an evolution of the TWI, the SAGA Wetness Index (WI) (Bohner et al., 2002) is used where, hydrologically homogeneous conditions are assumed. The WI is based on a modified version of upslope contributing area ($A_{s,m}$) that is estimated with the use of slope gradient (β) and the neighboring maximum values of the upslope contributing area ($A_{s,max}$). The modified upslope contributing area ($A_{s,m}$) algorithm functions iteratively till no further change is observed (Bohner and Selige, 2006):

$$A_{s,m} = A_{s,max}\left(\frac{1}{15}\right)^{\beta\exp(15^{\beta})} \quad for\ A_{s,m} < A_{s,max}\left(\frac{1}{15}\right)^{\beta\exp(15^{\beta})} \tag{4.17}$$

Then, the WI calculated as:

$$WI = ln\left(\frac{A_{s,max}}{tan\beta}\right) \tag{4.18}$$

WI does not consider the flow as a slim layer, in contrast with conventional algorythms, in the estimations of the upslope contributing area. Hence, WI predicts for cells situated in valley floors with a small vertical distance to a channel a more realistic, higher potential

soil moisture and iteratively modifies the upslope contributing area of each grid cell in dependence of neighboring maximum values using a slope-dependent equation unless the results remain unchanged by additional iterations (Bohner et al., 2002).

CN: An extensively used method in hydrologic practices is the Curve Number (CN), developed by the USDA Natural Resources Conservation Service (Natural Resources Conservation Service). CN is an empirical parameter used in hydrology for predicting the runoff volume in small ungauged catchments (typical application of rainfall-runoff models) or the infiltration from rainfall excess. CN is defined with the use of geomorphologic and physiographic properties such as the soil type and land use. Furthermore, CN is assumed to be constant in different parts of a catchment or even in the entire catchment (Rutkowska et al., 2015). CN value ranges from 0 to 100, is provided by tables given in the National Engineering Handbook, Section 4 (SCS, 1956). In this study, the CN values that have been used (Table 4.6) proposed by Miliani et al. (2011), where the CN value is based on the hydrologic soil group and the CORINE land cover classification.

MFI: One of the most widely used indices of rainfall erosivity is the R factor of USLE. Many studies have proven that R factor is highly correlated with soil loss (Renard and Freimund, 1994). In 1960, Fournier created the Fournier Index (*FI*) that is correlated with river sediment loads:

$$FI = \frac{p_{max}^2}{P} \tag{4.19}$$

Where p_{max} = average monthly rainfall of the wettest month of the year (mm), *P* =average annual rainfall amount (mm).

A paradox in the *FI* formula is that, if the denominator (*P*) increases and the nominator (pmax) remains constant, the *FI* decreases, thus concluding to erroneous results. Therefore, in 1980 Arnoldus evolved the MFI to the Modified Fournier Index and proved that *MFI* is linearly correlated to the *R* factor and is a better approximation of it. *MFI* takes into account the rainfall of all months in the year:

$$MFI = \sum_{1}^{12} \frac{p^2}{P} \tag{4.20}$$

Where *Σ*: the 12-month summation, *p*: the average monthly rainfall, and *P*: the average annual rainfall.

Table 4.6. Curve Number Value on Based on Hydrologic Soil Group and CORINE Land Cover

CORINE land cover class	Hydrologic soil group			
	A	B	C	D
1.1.1 Continuous urban fabric	89	92	94	95
1.1.2 Discontinuous urban fabric	77	85	90	92
1.2.1 Industrial or commercial units	81	88	91	93
1.2.2 Road and rail networks and associated land	98	98	98	98
1.2.3 Port areas	81	88	91	93
1.2.4 Airports	72	82	87	89
1.3.1 Mineral extraction sites	72	82	87	89
1.3.2 Dump sites	72	82	87	89
1.3.3 Construction sites	72	82	87	89
1.4.1 Green urban areas	68	79	86	89
1.4.2 Sport and leisure facilities	49	69	79	84
2.1.1 Non-irrigated arable land	49	69	79	84
2.1.2 Permanently irrigated land	49	69	79	84
2.1.3 Rice fields	59	70	78	81
2.2.1 Vineyards	67	77	83	87
2.2.2 Fruit trees and berry plantations	65	75	82	86
2.2.3 Olive groves	65	75	82	86
2.3.1 Pastures	49	69	79	84
2.4.1 Annual crops associated with permanent crops	62	71	78	81
2.4.2 Complex cultivation patterns	67	78	85	89
2.4.3 Land principally occupied by agriculture, with significant areas of natural vegetation.	67	78	85	89
2.4.4 Agroforestry areas	45	66	77	83
3.1.1 Broad-leaved forest	60	65	70	77
3.1.2 Coniferous forest	60	65	70	77
3.1.3 Mixed forest	60	65	70	77
3.2.1 Natural grassland	60	65	74	80
3.2.2 Moors and heathland	60	65	74	80
3.2.3 Sclerophyllous vegetation	60	65	74	80
3.2.4 Transitional woodland-scrub	60	65	74	80
3.3.1 Beaches, dunes, sands	25	55	70	77
3.3.2 Bare rocks	68	79	86	89
3.3.3 Sparsely vegetated areas	68	79	86	89
3.3.4 Burnt areas	68	79	86	89
3.3.5 Glaciers and perpetual snow	79	79	79	79
4.1.1 Inland marshes	98	98	98	98
5.1.1 Water courses	99	99	99	99
5.1.2 Water bodies	99	99	99	99
5.2.1 Coastal lagoons	99	99	99	99

Rainfall is a significant factor of flood generation process and has been used in this and other similar studies as MFI factor (extreme precipitation case scenario) (Kourgialas and Karatzas, 2011, Kazakis et al., 2015). Monthly and annual precipitation values, and rainfall intensity were estimated with the use of the data retrieved by four (4) meteorological stations that located close to Xerias watershed. The period selected for this analysis is from 1960 to 2002. The data used for MFI estimation are presented in Table 4.7.

Table 4.7. Meteorological stations data and MFI values

Meteorological Stations	X (longitude in m)	Y (latitude in m)	Z (elevation in m)	MFI
Volos	409346	4357591	3	45.65
Makrinitsa	412380.4	4361533	690	85.53
Ali Meria	412644.41	4358127	120	49.46
Anghialos	396252	4344804	15	48.69

The creation of MFI based on a regression analysis with the elevation and MFI values of the stations plus the interpolated residuals created with the Spline method. Table 4.5 shows that only MFI is correlated to the DEM as expected, since MFI is calculated based on DEM using a linear precipitation gradient.

4.4.2 Pairwise Comparison Tables—Expert Survey

In 1860, Fechner initially proposed the pairwise comparison method which was evolved into its current state by Thurstone 1927. Saaty, developed the analytic hierarchy process based on pairwise comparison. As mentioned before in Sub-section 4.3.1, an essential step in the AHP application is the pairwise comparison analysis where the criteria and alternatives are evaluated by the decision makers. Table 4.1, Table 4.2 and Table 4.3 show the format of pairwise comparison, the linguistic scales of importance and an example of a pairwise comparison table respectively. Furthermore, a significant step of pairwise comparison analysis in AHP is the estimation of the reliability of the decision maker's answers regarding CR. CR is used to estimate the consistency of judgments in comparison to random judgments taken from large samples. Saaty (1987) defined the CR as:

$$CR = \frac{CI}{RI} \tag{4.21}$$

$$CI = \frac{\lambda_{max} - n}{n - 1} \tag{4.22}$$

where *CR* = consistency ratio ; *CI* = consistency index ; *RI* = Random consistency index (Table 4.8) ; λ_{max} = principal eigenvalue (largest eigenvalue) ; *n* = size of the comparison matrix.

Table 4.8. Average random consistency index of sample size 500 matrices

n	1	2	3	4	5	6	7	8	9	10
RI	0	0	0.58	0.9	1.12	1.24	1.32	1.41	1.45	1.49

According to Saaty, if the CR is smaller or equal to 10%, the inconsistency is acceptable otherwise a revision of the judgments is obligatory (Alonso and Lamata, 2006). The use of pairwise comparison tables decreases the complexity of a problem because it uses only two components (a pair) each time. In this study, nine (9) experts in the field of hydrology filled the pairwise comparison tables. All the results were normalized and examined with the CR indicator. In FAHP case, CR has been estimated with the use of the simple centroid method (Chang and Wang, 2009). The acceptable CR has been assigned to 10% according to the number of the selected indices and the methodology used. In AHP when the CR was bigger than the threshold used, the experts modified their pairwise comparison tables until an approved CR was achieved. Similarly, in FAHP, CR has been used with acceptable results (equal or less than 10%). Finally, two different configurations have been used where the term “Expert Knowledge” refers to a scientist that his research field is focused on flood modelling and mapping and the “Group of Experts” refers to the answers of all nine (9) experts in the field of hydrology. Thus, the weights extracted from the comparison tables categorized in two cases where the weights of “Expert Knowledge” and the median of all expert weights are presented as “Group of Experts” have been taken into account for the analysis.

4.4.3 Criteria Classification

The clustering/classification techniques used in this study are presented thoroughly in Sub-Section 4.3.2 and are: 1) Natural Breaks, 2) K-mean with Euclidean distance method, 3) K-mean with Cityblock distance method, 4) FCM, 5) GMMC and 6) CLARA with Euclidean distance calculation. The entire methodology has been applied using two

different approaches according to the clustering choice. In the first approach, all criteria are normalized at the beginning of the process, then, Boolean algebra has been applied through GIS analysis, and, finally, the results have been classified (or clustered) into five (5) flood prone categories. In the second approach, all criteria classified (or clustered) into five (5) classes at the onset of the process, then Boolean algebra has been performed through GIS analysis, and, finally, the results have been classified (or clustered) into five (5) flood prone categories to produce the final results. In both approaches, Boolean algebra and the summation of the criteria multiplied by the respective relative weights (AHP, FAHP) have been used to create the potential flood-prone areas criteria. Finally, these criteria were classified according to the presented clustering methods. In the second approach, the clustering techniques were applied only with the respective clustering technique for the production of the final classified results (i.e. the criteria that have been classified with FCM technique at the beginning are connected only with the same clustering technique, FCM, at the end of the analysis to produce the final map of 5 flood prone categories, see Figure 4.4). The combination of AHP-FAHP and GIS is very popular among a wide variety of studies, and most of these studies do not examine the clustering-classification technique effect. Usually, the classification technique used in these cases is a simple technique provided by the GIS software. With the use of several classification techniques a sensitivity analysis has been conducted to 1) discover the dependency of the output on input parameters, 2) identify the most sensitive criteria in clustering techniques, 3) reveal the effect of using different clustering methods on the mapping results. After the application of the AHP and FAHP, the final flood-prone areas (criteria) were classified with the above six clustering techniques. The five potential flood prone classes are 1) Very Low—value 1, 2) Low—value 2, 3) Moderate—value 3, 4) High—value 4, 5) Very high—value 5.

4.5 Results – Discussion

Pairwise comparison application and analysis produced the relative weights of the study factors. Table 4.9 presents these weights for both MCA methods (AHP and FAHP, respectively) and shows that the most important factors are the Wetness Index followed by the Curve Number (CN). Hence flood prone areas identification depends mainly on these two factors. An important finding revealed from Table 4.9 is that in AHP all criteria contribute in the estimation process whereas in FAHP some criteria with minor weights are eliminated from the process. Consistency ratio of the pairwise comparison is 4.3 and 6.8 % for AHP and FAHP, respectively. An example of the spatial distribution of the applied clustering methods in MCA is presented in Figure 4.9. This figure shows the final maps of

AHP Group of Experts (1st approach), whereas Figure 4.10 shows the same approach for FAHP application.

The majority of the clustering techniques demonstrates a similar spatially-distributed pattern in the classes of potential flooded areas with an exception at lowlands for the first approach and with differences in GMMC method for the second approach. The choice of experts (group of experts or expert knowledge) seems to be insensitive to the MCA methods in both approaches. The distribution of the classes of the derived flood prone maps is presented in Table 4.10 for the two approaches and MCA methods using Expert knowledge. The classes for all classification methods in the first approach are ranging between 3.13 and 18.16 % and in the second are ranging from 5.17 to 24.53 % (Table 4.10).

Table 4.9. AHP and FAHP relative weights of the criteria and their consistency ratios.

Criteria and consistency ratios	Relative weights			
	AHP Expert Knowledge	**AHP Group of experts (median value)**	**FAHP Expert Knowledge**	**FAHP Group of experts (median value)**
DEM	0.03	0.03	0	0
Slope	0.09	0.11	0.09	0.13
Aspect	0.02	0.02	0	0
Flow Ac.	0.14	0.15	0.18	0.19
HOFD	0.13	0.08	0.14	0.05
VOFD	0.05	0.07	0	0.03
TPI	0.07	0.08	0.02	0.06
WI	0.25	0.26	0.31	0.32
CN	0.2	0.17	0.26	0.22
MFI	0.02	0.03	0	0
CR	4.30%	4.30%	6.70%	6.80%

Table 4.10. Percentage of flood prone areas classes of AHP and FAHP "Expert Knowledge" for both approaches.

1st approach						
Flood prone areas classes	**Natural Breaks**	**K-means euc.**	**K-means cit.**	**FCM**	**GMMC**	**CLARA**
AHP Expert Knowledge						
Very Low	17.31	17.29	20.53	17.10	8.22	20.26
Low	33.25	32.24	27.48	31.88	25.18	27.43
Moderate	25.99	25.93	24.13	26.05	36.11	24.30
High	16.86	17.41	17.19	17.66	20.13	17.32
Very High	6.60	7.13	10.66	7.30	10.35	10.69
FAHP Expert Knowledge						
Very Low	20.76	20.45	22.44	19.80	19.31	22.21
Low	34.05	32.19	27.47	32.07	15.89	27.19
Moderate	24.02	24.70	24.05	25.18	37.72	24.44
High	15.63	16.67	16.47	16.94	20.92	16.58
Very High	5.54	5.99	9.56	6.01	6.16	9.57
2nd approach						
Flood prone areas classes	**Natural Breaks - Natural Breaks**	**K-means euc. - K-means euc.**	**K-means cit. - K-means cit.**	**FCM - FCM**	**GMMC - GMMC**	**CLARA - CLARA**
AHP Expert Knowledge						
Very Low	19.54	18.60	19.87	16.36	14.70	18.81
Low	28.28	27.45	24.94	25.69	15.31	23.00
Moderate	23.62	23.79	22.42	25.98	46.27	21.74
High	20.76	22.18	21.34	22.07	0.00	21.16
Very High	7.80	7.99	11.44	9.90	23.73	15.29
FAHP Expert Knowledge						
Very Low	21.09	23.08	21.77	21.10	14.53	29.46
Low	30.75	30.78	27.18	27.70	25.06	28.14
Moderate	25.93	25.23	24.23	25.59	36.63	22.54
High	15.18	14.27	18.19	16.15	9.79	12.33
Very High	7.05	6.64	8.64	9.46	13.99	7.53

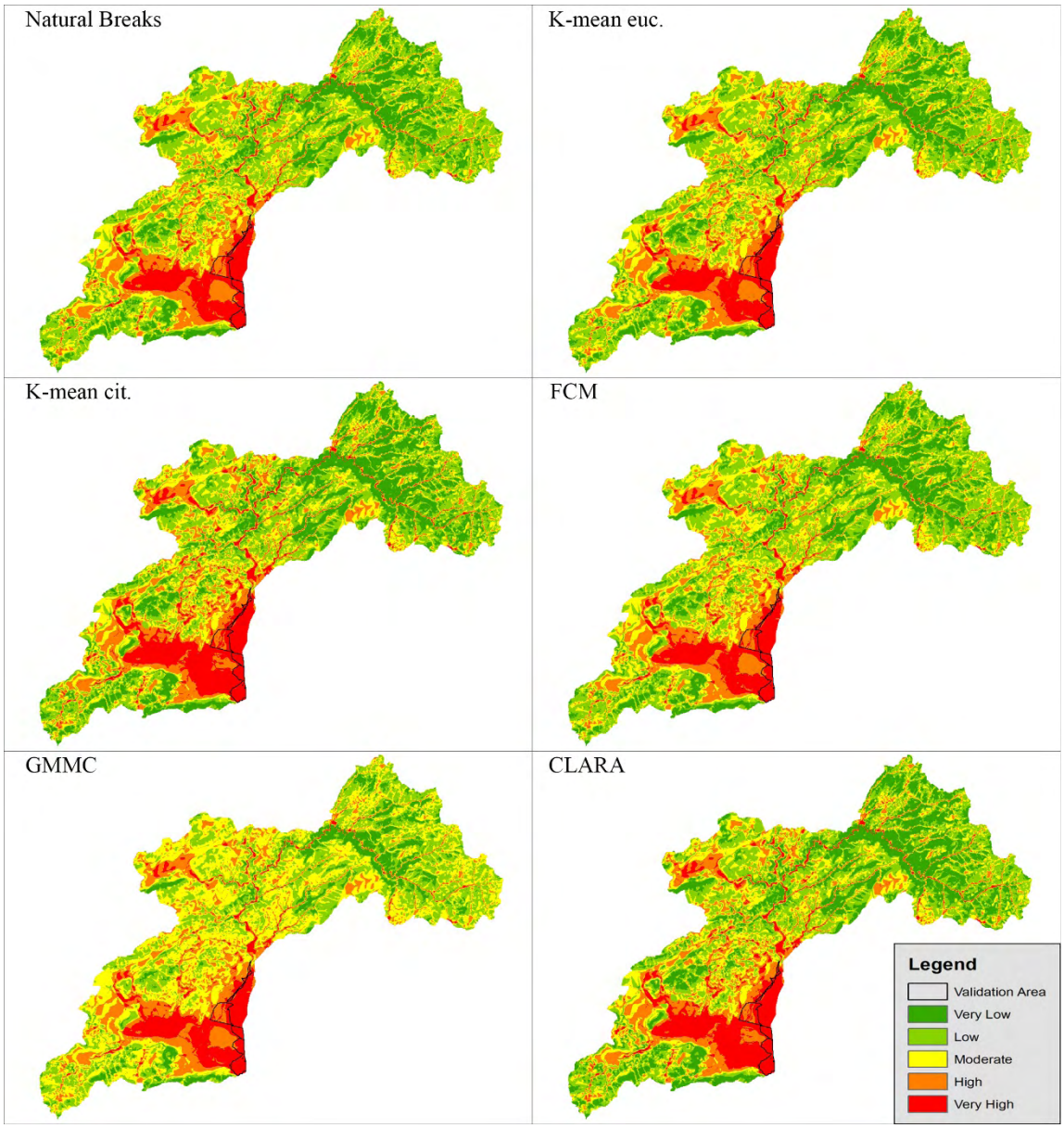

Figure 4.9. Final maps of AHP Group of Experts, 1st approach

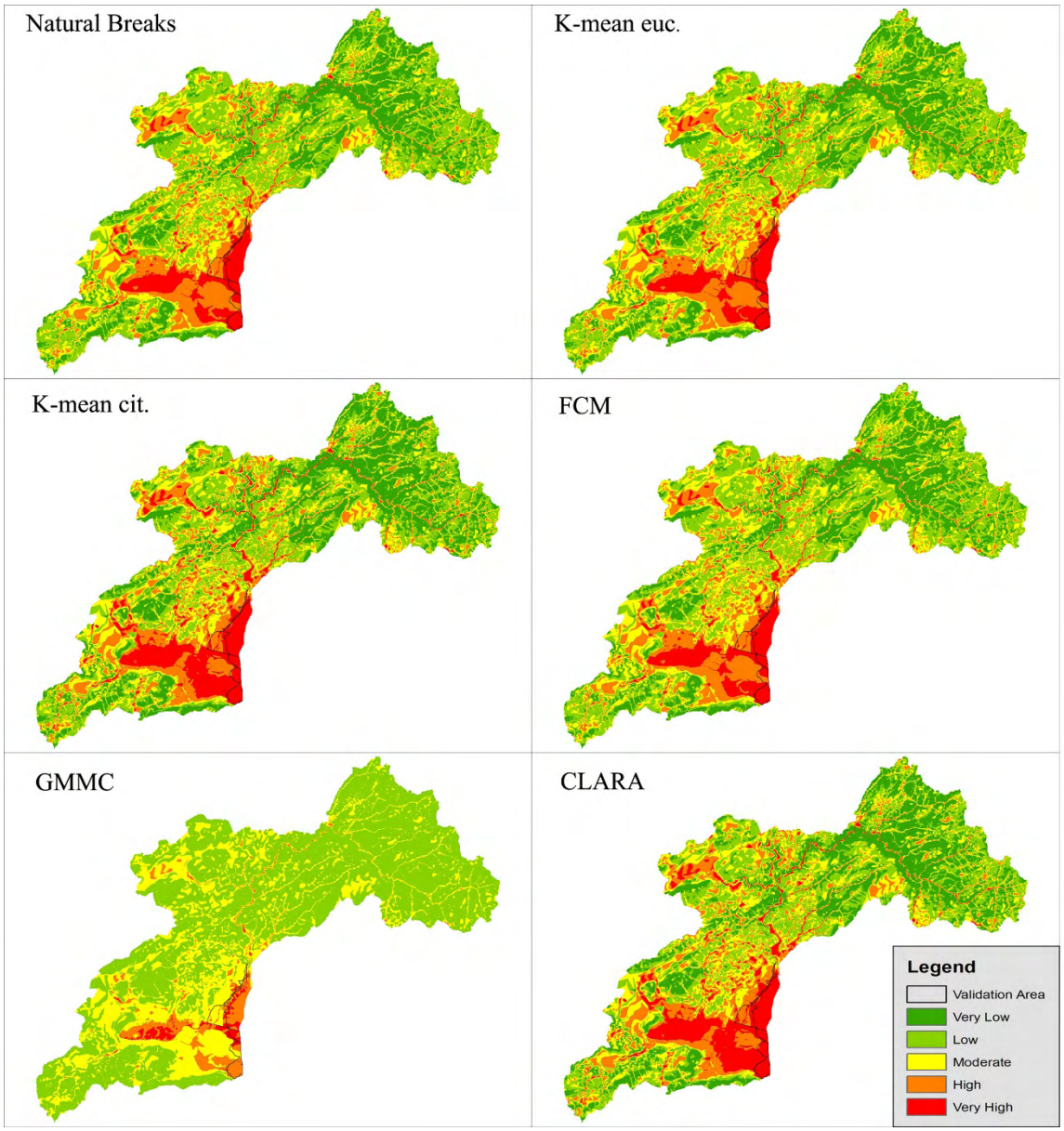

Figure 4.10. Final maps of FAHP Group of Experts, 1st approach

For validation of the produced flood prone area, based on the analysis of the flood episode occurred in October 9th, 2006, the historical flood inundation data and flooded area derived from hydrologic and hydraulic modelling were used (Papaioannou et al., 2011) (Figure 4.2, Figure 4.3) (details for the hydraulic modelling are presented in Chapter 5). Figure 4.11 presents the comparison of all clustering methods for both approaches and shows the contribution of each class on the validation flooded areas only. Flood hazard degree based on the derived flood prone areas mapping shows that only three hazard classes are participates in the validation area.

Furthermore, it is observed that K-means cit. and CLARA techniques have the largest contribution in the Very High class, in the first approach (Figure 4.11). In the 2nd approach none of the methods consistently outperformed the other study methods. A general remark is that AHP has larger agreements than FAHP in Very High hazard class (Figure 4.11) and the choice of the selected pairwise comparison tables (Expert knowledge or Group of experts) is insensitive on the MCA methods. This finding demonstrates the general application of the procedure and the minimization of subjectivity of MCA methods. In the first approach all classification methods show similar patterns in the estimation of flood prone areas. However, K-means cit. and CLARA have the highest contribution percentage in Very High class (i.e. for AHP Expert knowledge 77.9 % and 78 %, respectively).

Finally, it is observed that in one case (first approach), the GMMC technique for FAHP group of experts has larger differences in the classes' distribution. This is probably due to the convergence algorithm of GMMC method which gave different distribution patterns. In general GMMC technique was the most unstable method for this case study and in some cases even failed to create the desired number of classes. The comparisons between the two different approaches showed that, using normalized data (criteria) before the MCA application have better response to the component than the clustering application. In general, at watershed scale, the two approaches present approximately 25 % discordant classes. In validation, flooded area was better represented using the first approach. Finally, in the majority of the cases, Natural Breaks (Jenks) method had the smallest contribution percentage in Very High class. Hence, caution and comparison with other clustering techniques is recommended when only Jenks method is applied in mapping purposes.

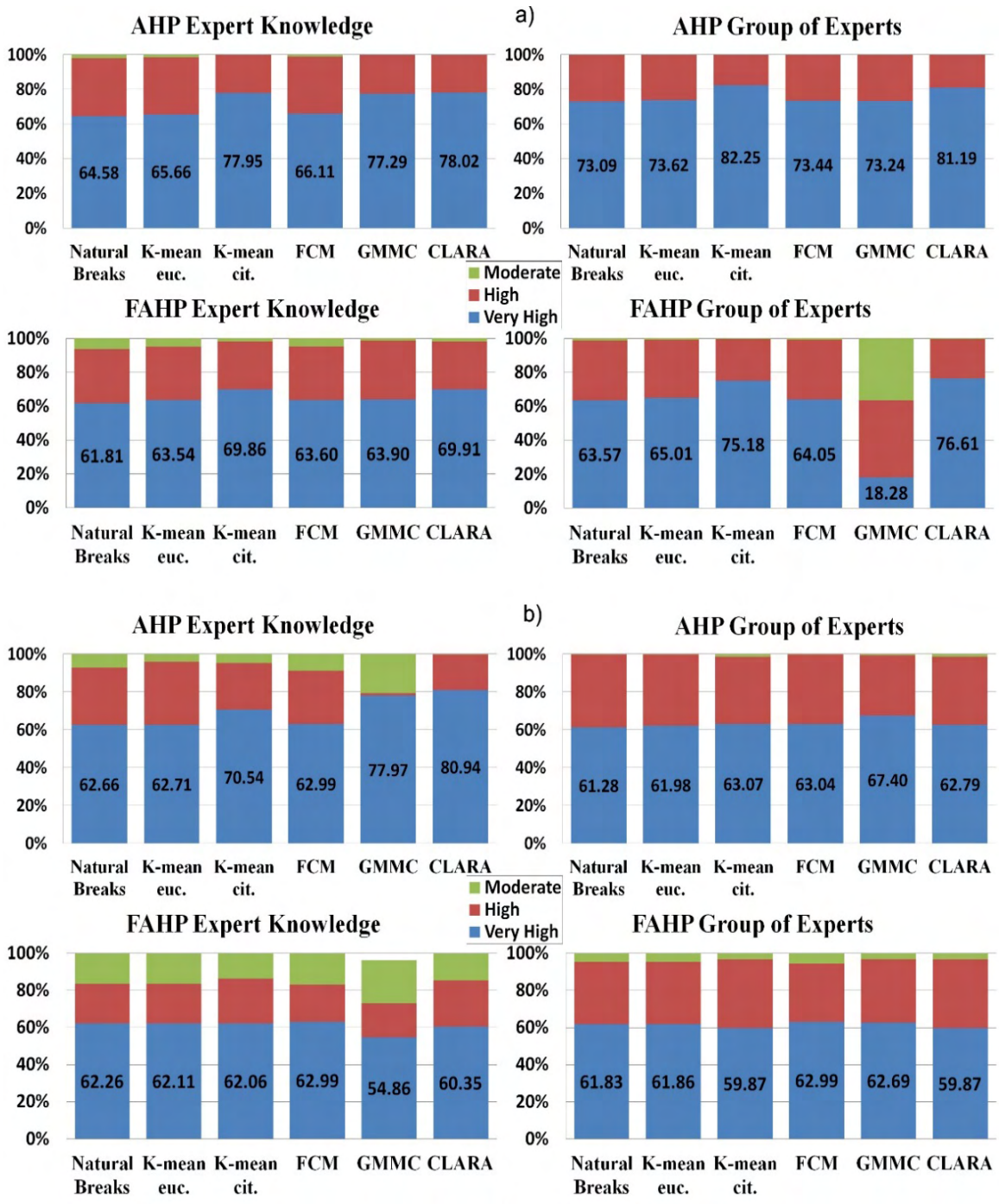

Figure 4.11. Classes participation percentage on validation areas for all the examined cases. a) 1st approach, b) 2nd approach

4.6 Concluding Remarks

Last decades, many researchers have examined the use of AHP, FAHP or GIS modelling techniques for the estimation of flood-prone areas, flood hazard, flood risk and other natural disasters (e.g. Meyer et al., 2009; Chen et al., 2011; Kourgialas et al., 2011; Manfreda et al., 2011; Zou et al., 2013; Stefanidis and Stathis, 2013; Tehrany et al., 2013; Chen et al., 2015; Hazarika et al., 2016). All of the above mentioned studies are using AHP or FAHP or other techniques. An important remark from the selected studies is that the selection of the criteria is based usually on literature review and/or on the authors' choice according to the respective study area. The majority of this studies specify the flood hazard of each criterion using fixed classes for each criterion (e.g. DEM flood hazard classes: Very High "0m-50m" , High "50-100", Medium "100-150", Low "150-200", Very Low "200-250"). The separation of these classes depends on the knowledge of the specific study area and/or literature reviews and/or specific classification approach. Another notable remark is that many of the selected studies have classified the criteria in a specified number of flood hazard classes at the beginning and before the application of merging (Boolean algebra) were the final flood prone area map is produced. Moreover, some of the selected studies have used specified weights, according to literature review, for each criterion.

In this study an objective GIS-based spatial multi-criteria evaluation component has been applied at catchment scale and could be used in decision making for flood prone area assessment. The methodology is based on limited data and information with minimum subjectivity in multicriteria analysis. The selection of the criteria is based on literature review and on preliminary criteria analysis using Pearson correlation coefficient. Furthermore, it incorporates expert opinion and knowledge on the criteria and their weights, and provides a component for helping the decision maker through multi-criteria combination problems. Several sensitivity analysis test has been conducted in order to highlight the optimum component configuration. The main results obtained from the methodology against historical flood events and flood inundation modelling verified the credibility of the method. In the two study approaches, AHP has a better response than FAHP, is independent on the choice of the selected pairwise comparison tables (Expert knowledge or Group of experts) and is insensitive to the MCA methods. All previous studies have used only one MCA method either AHP or FAHP and thus, no comparison could be made with the results of the present study. The first approach, in which all criteria have been normalized at the beginning of the process and the flood hazards classes estimated after the criteria merging process using Boolean algebra, gave better results than the second approach, in which the criteria classified in classes at the beginning and after the Boolean algebra merging classified into flood hazard classes. This

result shows that the estimation of the flood prone areas can be optimized by using the same range value for all criteria and make feasible the general applicability of the component. In addition, the majority of clustering techniques is giving a similar spatial pattern in the classes of potential flooded areas with an exception at lowlands where two clustering techniques have better response (K-means cit. and CLARA) (Figure 4.9, Figure 4.10 and Figure 4.11). Most of the previous studies are using the Jenks' Natural Breaks method because it is the typical approach provided in the majority of the GIS packages or the classification is achieved using standard tables of flood hazard classification. In this study the Jenks' Natural Breaks method provided the smallest contribution percentage in Very High Flood Hazard class among the other tested clustering techniques. Moreover, the use of K-means cit. and CLARA clustering approaches provided better estimations of the flood hazard classes at lowlands where the flood prone areas are likely to exist. The sensitivity analysis using different clustering techniques proved that the selection of a clustering technique may provide an important improvement to the results. This results indicate the general application of the procedure and the minimization of subjectivity of MCA methods.

Application of the proposed component in Xerias Watershed showed that multiple MCA techniques should be taken into account in initial low-cost detection surveys of flood-prone areas. Furthermore, the use of multiple clustering techniques is necessary in preliminary analysis of flood risk mapping where observed flood inundation areas have been estimated in order to not only simulate the flood-prone areas but also to evaluate their associated flood hazard degree. The integration of spatial data and application of GIS-based multi-criteria evaluation procedures could provide a superior database and guide map for decision makers in order to produce potential flood prone areas maps. The employed component could be applied in flood hazard estimation at areas with limited available information, and/or in areas where preliminary flood hazard evaluation is required for flood mapping purposes using hydrologic and hydraulic modelling.

The proposed component in its current form can be used only for flood hazard estimation. The simulation using a hydraulic-hydrodynamic model is mandatory for accurate investigation of the flood extent.

Finally, the optimum combination of the tested methodologies that is proposed for flood prone areas recognition is the use of the fist approach with the following configurations:

- Production of the following criteria according to the proposed guides: 1) DEM, 2) Slope, 3) Aspect, 4) Flow Ac., 5) HOFD, 6) VOFD, 7) TPI, 8) WI, 9) CN, 10) MFI.
- Normalization of all criteria with min-max methodology at the beginning of the entire process.
- Implementation of AHP technique using CR evaluation metric.

- Application of Boolean algebra in GIS environment using the AHP derived weights from the previous step.
- Classification of the produced maps from the previous step using the K-mean clustering technique with “cityblock” distance configuration. Five hazards classes should be selected in the clustering procedure.
- Generate the final flood prone areas maps

The proposed component could be further investigated. Possible areas of investigation are:

- Application/verification of the proposed component to other river watersheds.
- Application/verification of the proposed component in a study area were the flood extent can be produced with the use of remote sensing techniques.
- Investigation of other MCA techniques (e.g. rough number theory in MCA analysis).

Perform an uncertainty analysis on final results of the methodology due to the ariability of the results of AHP for the Group of Experts. This analysis could be achieved by fitting probability distributions on the responses of the experts for each criterion and performing Monte Carlo simulations by checking the sum of weights (it should be equal to 1).

CHAPTER 5ο
SENSITIVITY ANALYSIS COMPONENT

5 Sensitivity analysis component

5.1 Introduction

The hazardous effect of the extreme flood events occurred in the last decades motivated several researchers for further investigation of the floodplain dynamics, as well as their feedbacks, and the role of hydrological/hydraulic variables (e.g., flood hydrograph, roughness coefficient, river and riverine terrain spatial resolution, DEM accuracy, etc.) in flood risk management and mapping (e.g. Bates and De Roo, 2000; Horritt and Bates, 2002; Pappenberger et al., 2005; Dutta et al., 2007; Apel et al., 2009; Neal et al., 2010; Grimaldi et al., 2013; Kourgialas and Karatzas, 2014; Dimitriadis et al., 2016; Bellos and Tsakiris, 2016; Teng et al., 2017; Altenau et al., 2017). Despite the increasing studies in the field, rapid and accurate flood modelling and mapping remains a substantial challenge in hydraulic and hydrologic researches. This is due to the nature of the flooding process that is chaotic and complex.

Another important fact that supports the ongoing investigation on flood inundation modelling is the uncertainty introduced by the high number of input parameters (e.g., DEM spatial resolution and accuracy, roughness coefficient etc.), the severe lack of data in some cases (ungauged catchments), the hydraulic-hydrodynamic modelling approach selection and the parameterization process used in flood inundation modelling (Merz and Thieken, 2005; Neelz and Pender, 2009, 2010, 2013; Freer et al., 2013). However, most of the studies mentioned above pay attention at a certain type of models or specific modelling types such as 2D hydraulic-hydrodynamic models, or at shock capturing schemes or study areas with sufficient amount of data. Furthermore, with the new technological advances in computer sciences and informatics the evolution of several hydraulic-hydrodynamic modelling packages has resulted in great improvements in them, while other modelling packages have been surpassed or even discontinued.

One of the main purposes of this study is to address the sensitivity of different hydraulic-hydrodynamic modelling approaches in combination with several types of river and riparian areas spatial resolutions on floodplain mapping and flood inundation modelling at ungauged watersheds. The first part of the analysis (preliminary analysis) examines four different types of riverine geomorphology: a) Digital Terrain Model (DTM) created from TLS data, b) Digital Surface Model (DSM) created from TLS data, c) topographic land

survey data and d) typical digitized contours from 1:5000 scale topographic maps. Modelling of the stream flow has been approached by the implementation of the following models: HEC-RAS 1D, MIKE11 (interpolated cross sections, DEM compilation), MIKE21 HD (Grid-based), MIKE21 HD FM (Flexible mesh), MIKE11/MIKE21 HD (Grid-based) and MIKE11/MIKE21 HD FM (Flexible mesh) through MIKE FLOOD platform. The second part of the analysis examines the sensitivity derived only by the modelling approaches using the riverine geomorphology created by TLS data (DTM). The models used in this analysis are: a) One dimension (1D) hydraulic models: HEC-RAS 1D, LISFLOOD (kinematic and diffusive wave approximation), MIKE11 (interpolated cross sections and DEM compilation approach), XPSTORM; b) Two dimension hydraulic models: HEC-RAS 2D, LISFLOOD, MIKE21 (Grid-based and Flexible mesh), XPSTORM, FLO2D; c) Coupled (1D/2D) hydraulic models: HEC-RAS, MIKEFLOOD (Grid-based and Flexible mesh), XPSTORM. In the analysis, standard hydrological methods for ungauged watersheds have been used for both the hydrograph and the flood peak estimation. The validation process consisted of 2x2 contingency tables that compare the simulated flooded area and the observed flooded area based on the historical extreme flash flood event of October 9th, 2006. The simulated flooded area was derived from combinations of the study hydrodynamic models at several riverine configurations and DEMs derived by various methods/measurements.

5.2 Study Event and Area

In October 09/10/2006, the city of Volos in Magnesia, Greece, was severely affected by an extreme flash flood event. That day, several types of the local infrastructure, transportation networks, and agricultural areas were damaged by the destructive power of the flood. The return period of the specific flood event is estimated to approximately 100 years according to previous analysis of Intensity-Duration-Frequency curves in the wider region. Xerias watershed is characterized by a lack of data (ungauged watershed). Thus, Clark Instantaneous Unit Hydrograph (CIUH) was used for the estimation of the 2006 extreme flash flood event hydrograph. In the preliminary part, calibration of the model parameters (roughness coefficient) and validation of the CIUH were based on post-flood analysis using watermarks. In the second part of the analysis, a deterministic parameter calibration has been performed to obtain the optimized values of model parameters (e.g. roughness coefficient). Finally, the flood extent of the specific event (Figure 5.1), was estimated with the use of historical data and records, such as a) flood records from newspapers, b) records collected from several authorities, c) local interviews and testimonies of flood victims. Further details on the study event and area can be found in Chapter 2.

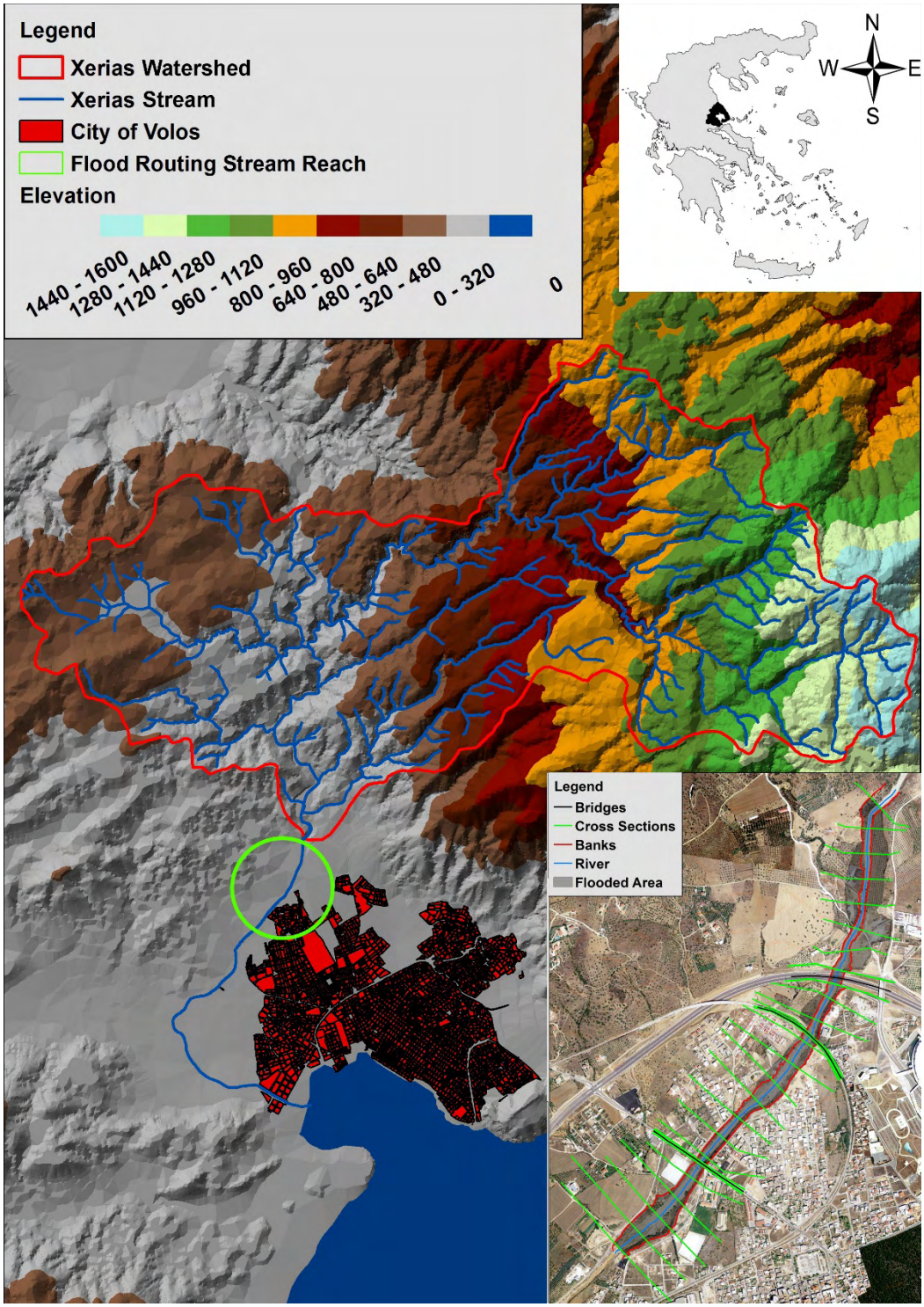

Figure 5.1. The study watershed of Xerias and the flood routing stream reach with the historical flood inundation area used for validation of the component.

5.3 Modelling approaches

All EU member states are obligated by the EU Directive on floods (2007/60) to produce and update their flood maps using the most efficient and suitable tools for floodplain modelling and mapping. A typical choice when it comes to the selection of hydraulic modelling approach is the 1D-models for reasons of simplicity, efficiency, availability (i.e. existence of open source and freeware software) and the small computational time (Tsakiris, 2014).

Nonetheless, the effectiveness of the 1D-modelling approach may be decreased creating inaccurate flood maps when complex river topography is examined. Therefore, the investigation and selection of the most appropriate modelling approach are mandatory in flood modelling and mapping of areas with complex river and riverine terrain.

<u>One dimension (1D) hydraulic models</u>

- **HEC-RAS model.**

HEC-RAS hydraulic hydrodynamic model is one of the most acknowledged and applied one-dimensional (1D) models worldwidely. HEC-RAS was developed by the Hydrologic Engineering Center (HEC) of United States Army Corps of Engineers (USACE) (Brunner, 2016a). HEC-RAS model is associated with numerous studies on floodplain modelling and mapping (e.g. Pappenberger et al., 2005; Kunzler et al., 2012; Gain et al., 2015). In many of these studies, the choice of HEC-RAS was mainly based on the fact that the model can simulate the flow over a plethora of hydraulic structures with standard or irregular shape (culverts, weirs, road overtopping, etc). A significant advantage of HEC-RAS is the ease is assessing both steady and unsteady flow conditions in the river channel, floodplain, and riparian areas.

Below follows a presentation of both steady and unsteady flow conditions equations.

a) <u>1D Steady Flow</u>

The one-dimensional (1D) steady flow water surface solver is founded on the one-dimensional energy equation (Figure 5.2):

$$Z_2 + Y_2 + \frac{a_2 V_2^2}{2g} = Z_1 + Y_1 + \frac{a_1 V_1^2}{2g} + h_e \quad (5.1)$$

Where Z_1, Z_2 are the elevation of the main channel inverts; Y_1,Y_2 are the water depth at cross sections; V_1,V_2 are mean velocities (total discharge/ total flow area); a_1,a_2 are the velocity weighting coefficients; g is the gravitational acceleration and; h_e is energy head loss (Brunner, 2016a).

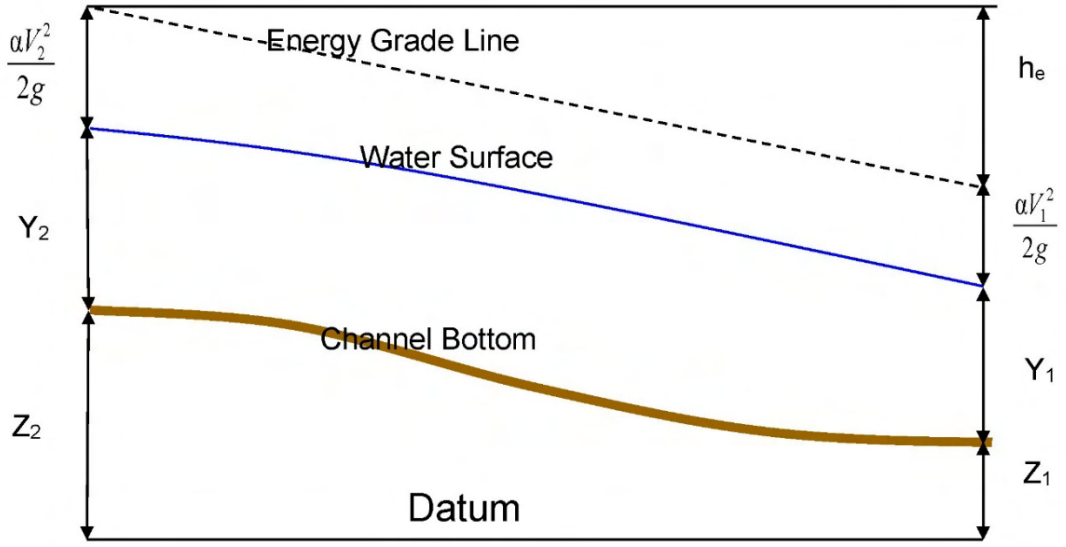

Figure 5.2. Energy equation parameters representation (Source: Brunner, 2016a)

The equation of the energy head loss (h_e) takes into account the friction losses and comparison or expansion losses that occur between two cross sections and is expressed as:

$$h_e = L_{dl}\bar{S}_f + C\left|\frac{a_2 V_2^2}{2g} - \frac{a_1 V_1^2}{2g}\right| \quad (5.2)$$

where L_{dl} is the discharge-weighted reach length; S_f is the representative friction slope between two sections and; C is the expansion or contraction loss coefficient (by default the contranction value is 0.3 and the expansion value is 0.1).

According to the discharge, the average weighted distance between two successive cross-sections L is calculated according to the following equation:

$$L_{dl} = \frac{L_{lob}\bar{Q}_{lob} + L_{ch}\bar{Q}_{ch} + L_{rob}\bar{Q}_{rob}}{\bar{Q}_{lob} + \bar{Q}_{ch} + \bar{Q}_{rob}} \quad (5.3)$$

where L_{lob}, L_{ch}, L_{rob} are the cross section reach lengths specified for flow in the left overbank, main channel, and right overbank, respectively.

In order to determine the cross section velocity and total conveyance, HEC-RAS uses a subdivision technique to split the flow into units where the velocity has a uniform distribution. Thus, the process of subdivision technique includes the flow separation in the overbank areas with the use of the n-value breakpoints that are defined by the user for each cross section (points where the n-value change) (Figure 5.3).

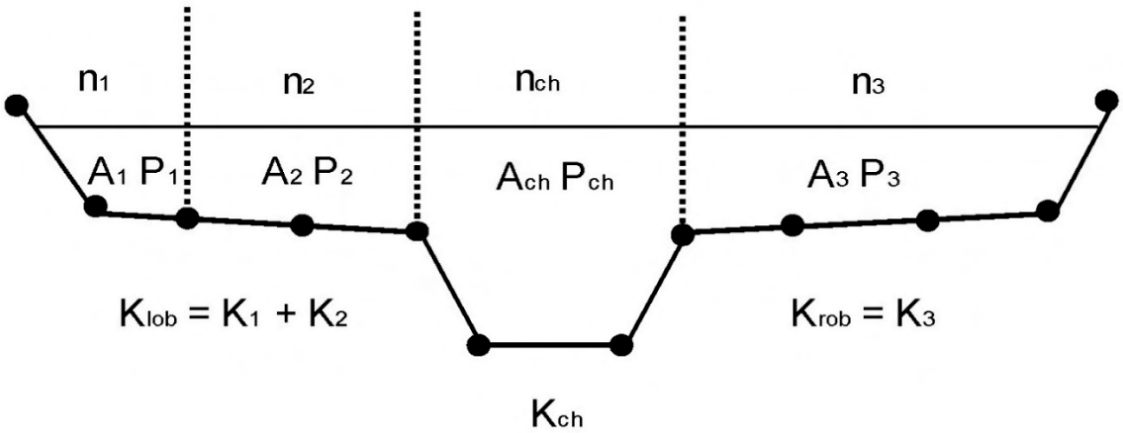

Figure 5.3. Default Conveyance Subdivision method, HEC-RAS (Source: Brunner, 2016a)

The conveyance is estimated for each subdivision using the Manning's equation (English units):

$$Q = KS_{fr}^{1/2} \tag{5.4}$$

$$K = \frac{1.486}{n} AR^{2/3} \tag{5.5}$$

where *K* is the conveyance for subdivision; *n* is the Manning's roughness coefficient for subdivision; *A* is the flow area for subdivision; *R* is the hydraulic radius for subdivision (area / wetted perimeter) and; S_{fr} is the slope of the energy gradeline.

Finally, all the incremental conveyances in the overbanks are summed in order to obtain a conveyance for the left and the right overbank. The conveyance of the main channel is estimated as a single conveyance element. The summation of the three conveyances (right, channel, left) gives the total conveyance for each cross section.

b) <u>1D Unsteady Flow</u>

The solver of the unsteady state conditions is based on the full, dynamic, 1-D Saint Venant Equation (Brunner, 2016a). Figure 5.4 shows the interaction between the floodplain and the channel flows by illustrating the two-dimensional characteristics of the flow. With the rise of the water depth, the flow is transferred aside from the main channel resulting in the inundation of the floodplain and the filling of the setup storage areas. With the rise of the water depth, the floodplain starts to transfer the water downstream. This flow usually follows a shorter path in comparison to the main channel. As soon as the stream stage starts to decrease, the supplement water starts to move from the overbank to the main channel (Brunner, 2016a).

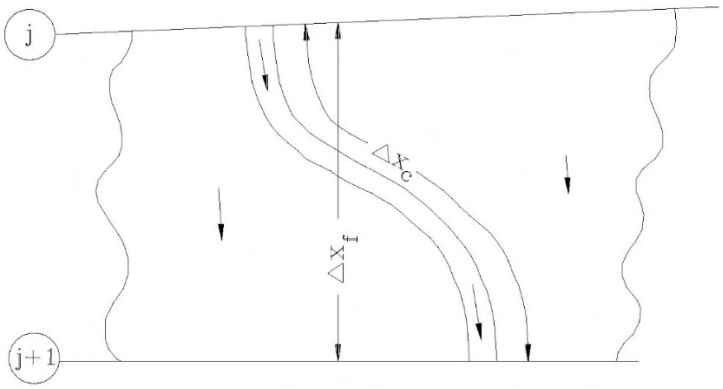

Figure 5.4. Floodplain and main channel flows (Source: Brunner, 2016a)

The fact that the main flow direction is aligned along the channel has a result of an accurate approximation of the two-dimensional flow field by a one-dimensional representation. The ponding areas observed outside of the main channel can be simulated as storage areas where the channel and the storage area interact (water is moving from the channel to the storage area and back forward). The overbank flow can be estimated as flow from a different river network (Brunner, 2016a).

The presented floodplain/channel complication has been met with a plethora of solutions. A typical approach is to totally neglect the overbank conveyance by assuming that the overbank operates as storage. In cases where the channel is restrained by levees and the floodplain operates as a storage area or is covered with dense vegetation, the proposed assumption can be suitable, especially for large rivers (e.g.,. Mississippi River). In the late 70s, Fread (1976) and Smith (1978) solved the problem with the division of the entire system in two different channels. They assessed the momentum and continuity equations for each channel. The problem was simplified using the assumption that at each cross section the horizontal water surface is regular to the flow direction; such that the momentum exchange among the floodplain and the channel was insignificant and the distribution of the discharge follows the conveyance, i.e. (Brunner, 2016a):

$$Q_c = \varphi Q \tag{5.6}$$

where Q_c is the channel flow; Q is the total flow; $\varphi = K_c/(K_c + K_f)$; K_c is the channel conveyance and; K_f is the floodplain conveyance.

With the use of the above-mentioned assumptions, the one-dimensional equations of motion are merged into the following single set (Brunner, 2016a):

$$\frac{\partial A}{\partial t} + \frac{\partial(\Phi Q)}{\partial x_c} + \frac{\partial[(1-\Phi)Q]}{\partial x_f} = 0 \quad (5.7)$$

$$\frac{\partial Q}{\partial t} + \frac{\partial(\Phi^2 Q^2/A_c)}{\partial x_c} + \frac{\partial\left[(1-\Phi)^2 Q^2/A_f\right]}{\partial x_f} + gA_c\left[\frac{\partial Z}{\partial x_c} + S_{fc}\right] + gA_f\left[\frac{\partial z}{\partial x_f} + S_{ff}\right] = 0 \quad (5.8)$$

In Equations (5.7) and (5.8), the full expression of the 1D Saint Venant equations has been taken into account (i.e. the estimation of the flood wave propagation is based on the dynamic wave solution). The differential equations (5.7) and (5.8) solution is achieved with the use of the indirect scheme of finite difference (Box Scheme). The graphical illustration of the Box Scheme is presented in Figure 5.5.

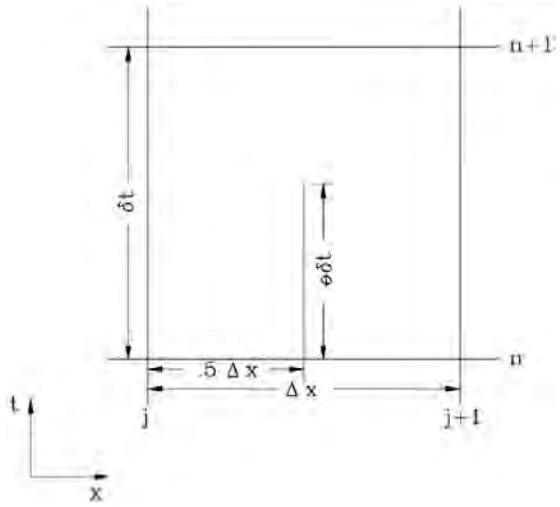

Figure 5.5. Common graph of finite difference cell (Source: Brunner, 2016a)

- **MIKE11 model**.

The MIKE 11 software that has been developed by the Danish Hydraulic Institute (DHI) is a one-dimensional hydraulic-hydrodynamic model. The unsteady flow simulation of streams and floodplains is accomplished with the use of an implicit, finite difference scheme. An essential feature of the model is the availability to use several hydraulic structures (culverts, weirs, road overtopping, etc.) in a flow routing analysis (DHI, 2014a). MIKE 11 is a worldwidely acknowledged 1D hydraulic-hydrodynamic model for floodplain modelling and mapping. In the literature, many studies indicate the extent of use of the MIKE 11 model. (e.g. Ahmed, 2010; Yazdi et al., 2012; Kourgialas and Karatzas, 2012; Jena et al., 2016; Papaioannou et. al, 2016; Gu et al., 2016; Duc Tran et al., 2017).

MIKE 11 uses the well-known “Saint Venant” equations where the vertically integrated equations of conservation of volume and momentum are solved with the fully dynamic

description (fully dynamic shallow water flow equations). For the solution of 'Saint Venant' equations, MIKE11 software assumes the following: (DHI, 2014a):

- the water conditions characterized by homogeneity and incompressibility, i.e. the variations of density are assumed insignificant.
- the gradient of the river bottom is small
- the water depth is small in comparison to the wave lengths. With this assumption is ensured the flow direction can be parallel to the river bottom, i.e. vertical acceleration may be ignored and can be assumed a hydrostatic pressure fluctuation along the vertical one.
- the flow is subcritical

The first transformation of "Saint Venant" Equations regarding the conservation of mass and the momentum conservation respectively are (DHI, 2014a):

$$\frac{\partial(Hb)}{\partial t} = -\frac{\partial(Hb\bar{u})}{\partial x} \tag{5.9}$$

$$\frac{\partial(Hb\bar{u})}{\partial t} = \frac{\partial(\acute{a}Hb\bar{u}^2)}{\partial x} - Hbg\frac{\partial h}{\partial x} \tag{5.10}$$

where *H is* the depth; *b is* the width; $\bar{u}$ is the average velocity along the vertical and; *α'* is the distribution coefficient of vertical velocity.

The integration of equations (5.9) and (5.10) aims to describe the flow through cross-sections of any shape (even irregular). This is achieved by the division of the entire cross section to multipart sets of rectangular cross sections (Figure 5.6).

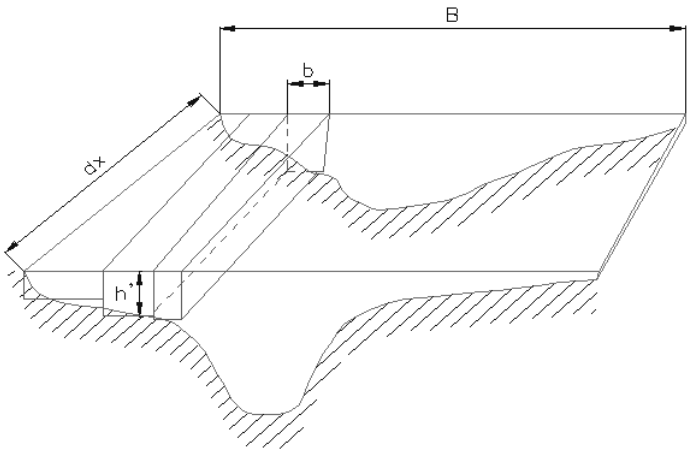

Figure 5.6. Cross-section divided into a series of rectangular channels (Source: DHI, 2014a)

The final transformed "Saint Venant" Equations for the conservation of momentum and mass that include the hydraulic resistance are respectively (DHI, 2014a):

$$\frac{\partial Q}{\partial x} + \frac{\partial A}{\partial t} = q \tag{5.11}$$

$$\frac{\partial Q}{\partial x} + \frac{\partial \left(\frac{Q^2}{A}\right)}{\partial x} + gA\frac{\partial h}{\partial x} + \frac{gQ|Q|}{C^2AR} = 0 \tag{5.12}$$

where Q is the discharge (m^3/s); A is the flow area (m^2); q is the lateral inflow (m^2/s); h is the stage above datum (m); n is Manning's coefficient ($m^{1/2}/s$); R is the hydraulic radius (m); γ is the momentum distribution coefficient; g is the acceleration due to gravity ($9.81 m^2/s$); x is the longitudinal distance in the direction of the flow (m) and; t is the elapsed time (s).

In the following text, there is an outline of the process of the equation solver at each time step. Each model level (kinematic, diffusive, dynamic) uses the same solution method. The transformation of Equations (5.11) and (5.12) to an implicit finite difference equations set is executed on a computational grid where *Q*- and *h*-points are altered, i.e. in Figure 5.7 can be seen the computation process for each time step where the discharge, *Q* and water level *h*, are calculated respectively. Based on the user demands, the model generates the computational grid automatically. The *Q*-points have a standard positioning in the midway among neighboring *h*-points, while *h*-points distance may vary (Abbott and Ionescu, 1967). Discharge is defined as positive in the positive *x*-direction (increasing chainage). The numerical scheme used in MIKE11 implementation consists of a 6-point Abbott-scheme and can be seen in Figure 5.8.

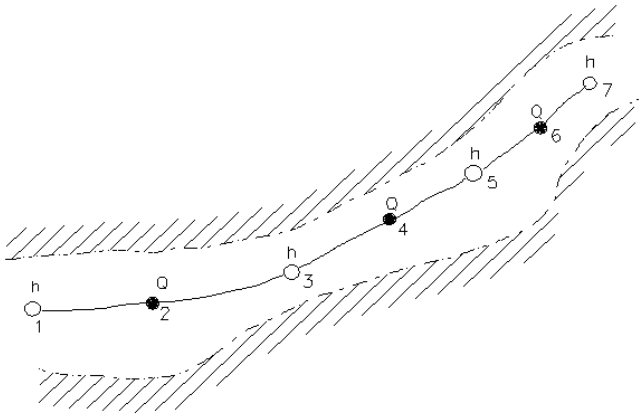

Figure 5.7. Channel section with computational grid (Source: DHI, 2014a)

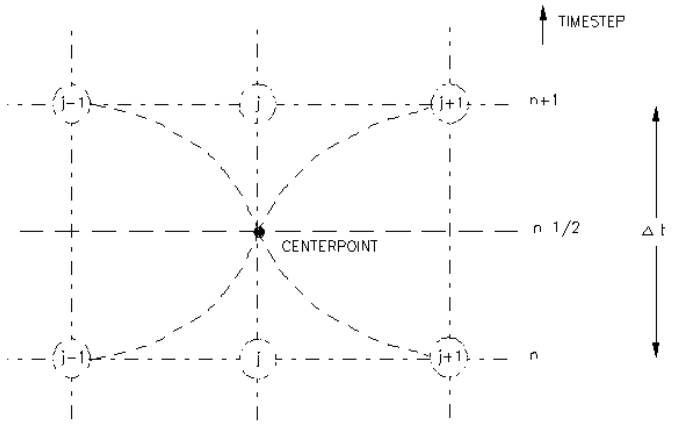

Figure 5.8. Centred 6-point Abbott scheme (Source: DHI, 2014a)

- **XPSTORM model.**

XPSTORM is another model that can be used for hydraulic-hydrodynamic simulations and has been applied for flood modelling and mapping. XPSTORM hydraulics engine also solves the well-known "Saint Venant" equations where the vertically integrated equations of conservation of volume and momentum are solved with the fully dynamic description (fully dynamic shallow water flow equations) (Akram et al., 2014; XPSTORM, 2017a). The fully dynamic shallow water equations are similar/the same as in HEC-RAS 1D and MIKE11. The model can simulate accurately backwater effects, flow reversal, surcharging, pressure flow, tidal outfalls, and interconnected ponds. The modelling of looped networks, multiple outfalls, and accounts for storage in conduits are also allowed. Finally, the 1D solver platform is based on the EPA SWMM engine, but various proprietary enhancements have been applied in its present form (XPSTORM, 2017b).

<u>Two-dimensional (2D) hydraulic models</u>

- **MIKE21 model**

MIKE 21 is a widely used two-dimensional hydrodynamic model with many applications in floodplain modelling and mapping (e.g. Karim et al., 2015; Teng et al., 2015; Ticehurst et al., 2015; Liu and Lim, 2017). MIKE 21 was also developed by Danish Hydraulic Institute. A favorable feature that the model provides is the selection of two diverse terrain setups: i) rectangular grid (MIKE21 HD), ii) flexible mesh elements (MIKE 21 HD FM). Furthermore, the model has the ability to use several hydraulic structures (culverts, weirs, road overtopping, etc) in the flow simulation process. Independent of the terrain setup selection, the main solver core of the MIKE 21 hydrodynamic module is based on the numerical solution of the two-dimensional shallow water equations (DHI, 2014b). Below, is a detailed presentation of the three-dimensional incompressible Reynolds-averaged

Navier-Stokes equations that the model uses, subject to the assumptions of Boussinesq on hydrostatic pressure. The basic equations of the solver are the local continuity equation and the two horizontal momentum equations for the x- and y-component, respectively (DHI, 2014c):

$$\frac{\partial u}{\partial x}+\frac{\partial v}{\partial y}+\frac{\partial w}{\partial z}=S \tag{5.13}$$

$$\begin{aligned}\frac{\partial u}{\partial t}+\frac{\partial u^2}{\partial x}+\frac{\partial vu}{\partial y}+\frac{\partial wu}{\partial z}=fv-g\frac{\partial \eta}{\partial x}-\frac{1}{\rho_0}\frac{\partial p_a}{\partial x}-\frac{g}{\rho_0}\int_z^{\eta}\frac{\partial \rho}{\partial x}dz\\ -\frac{1}{\rho_0 h}\left(\frac{\partial s_{xx}}{\partial x}+\frac{\partial s_{xy}}{\partial y}+\right)+F_u+\frac{\partial}{\partial z}\left(v_t\frac{\partial u}{\partial z}\right)+u_sS\end{aligned} \tag{5.14}$$

$$\begin{aligned}\frac{\partial v}{\partial t}+\frac{\partial v^2}{\partial y}+\frac{\partial uv}{\partial x}+\frac{\partial wv}{\partial z}=fu-g\frac{\partial \eta}{\partial y}-\frac{1}{\rho_0}\frac{\partial p_a}{\partial y}-\frac{g}{\rho_0}\int_z^{\eta}\frac{\partial \rho}{\partial y}dz\\ -\frac{1}{\rho_0 h}\left(\frac{\partial s_{yx}}{\partial x}+\frac{\partial s_{yy}}{\partial y}+\right)+F_v+\frac{\partial}{\partial z}\left(v_t\frac{\partial v}{\partial z}\right)+v_sS\end{aligned} \tag{5.15}$$

where t is the time; x, y and z are the Cartesian co-ordinates; η is the surface elevation; d is the still water depth; $h = \eta + d$; is the total water depth; u, v and w are the velocity components in the x, y and z direction; g is the gravitational acceleration; ρ is the density of water; $f = 2\Omega sin\varphi$ is the Coriolis parameter (Ω is the angular rate of revolution and φ the geographic latitude); s_{xx} ,s_{xy} ,s_{yx} ,and s_{yy} are components of the radiation stress tensor; v_t is the vertical turbulent (or eddy) viscosity; p_α is the atmospheric pressure; ρ_0 is the reference density of water; S is the magnitude of the discharge due to point sources and; u_s, v_s is the velocity by which the water is discharged into the ambient water; F_u and F_v are the horizontal stress terms described using a gradient-stress relation which is simplified to (DHI, 2014c):

$$F_u=\frac{\partial}{\partial x}\left(2A\frac{\partial u}{\partial x}\right)+\frac{\partial}{\partial y}\left(A\left(\frac{\partial u}{\partial y}+\frac{\partial v}{\partial x}\right)\right) \tag{5.16}$$

$$F_v=\frac{\partial}{\partial x}\left(A\left(\frac{\partial u}{\partial y}+\frac{\partial v}{\partial x}\right)\right)+\frac{\partial}{\partial y}\left(2A\frac{\partial v}{\partial y}\right) \tag{5.17}$$

where A is the horizontal eddy viscosity.

a) **MIKE 21 Hydrodynamic Module (Grid-based- Single grid)** (DHI 2014d,e)

The Hydrodynamic Module (HD) of MIKE 21 converts, in the space-time domain, the equations of mass and momentum (continuity) by integrating them with the Alternating Direction Implicit (ADI) methodology (DHI, 2014d). The Double Sweep (DS) algorithm is used to solve the equation matrices calculated for each direction and each individual grid line. Figure 5.9 shows the expression of different terms (basic equations of the solver) on a staggered grid in x, y-space (DHI, 2014e).

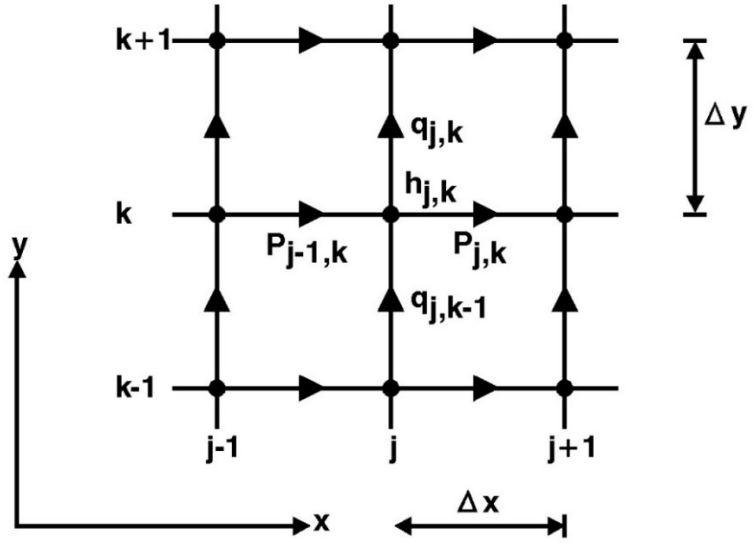

Figure 5.9. Difference Grid in x,y-space (source: DHI, 2014e)

An illustration of the time centering of the three top equations of MIKE 21 HD can be seen in Figure 5.10 (DHI, 2014e).

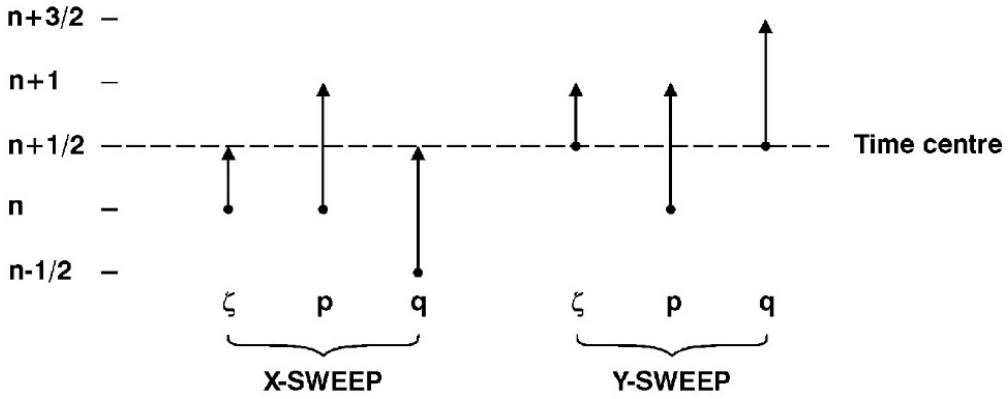

Figure 5.10. Time Centering (source: DHI, 2014e)

One-dimensional sweep is used during the process of solving the equation by alternating between x and y directions. The selection of the "side-feeding" technique (Figure 5.11) is the optimum estimation methodology that avoids further iterations (DHI, 2014e).

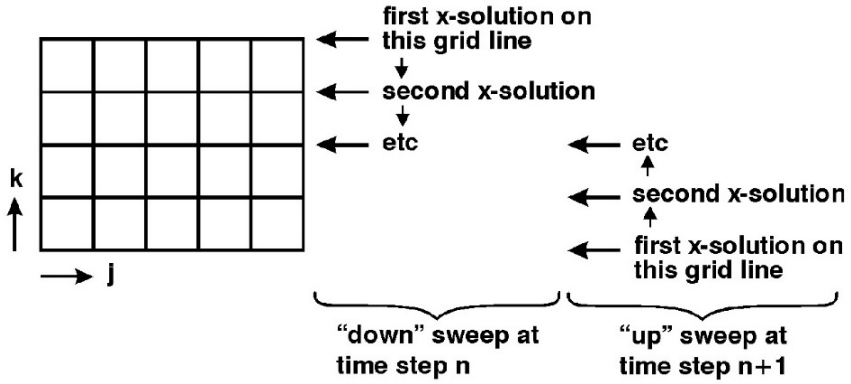

Figure 5.11. Side-feeding technique (source: DHI, 2014e)

b) **MIKE 21 Hydrodynamic Module FM (Flexible mesh)**

A cell-centered finite volume method is used for the spatial discretization of the original equations (DHI, 2014b). The discretization of the spatial domain is achieved with the subdivision of the continuum into non-overlapping cells/elements. The elements shape, in the horizontal plane of an unstructured grid, can be either triangular or quadrilateral. The model allows for two different approaches in spatial domain discretization: 1) Simple bathymetry adjustment approach (Figure 5.12) and, 2) Advanced bathymetry adjustment approach (Figure 5.13) (DHI, 2014c). The solver is based on Roe's scheme (Roe, 1981) that computes the convective fluxes. With the use of this approximation of Riemann solver, the discontinuous solutions are possible to be handled (DHI, 2014b).

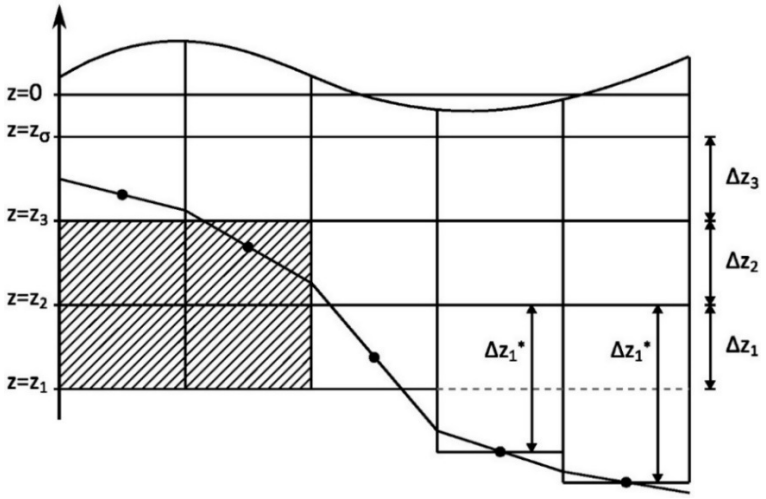

Figure 5.12. Simple bathymetry adjustment approach (source: DHI, 2014c)

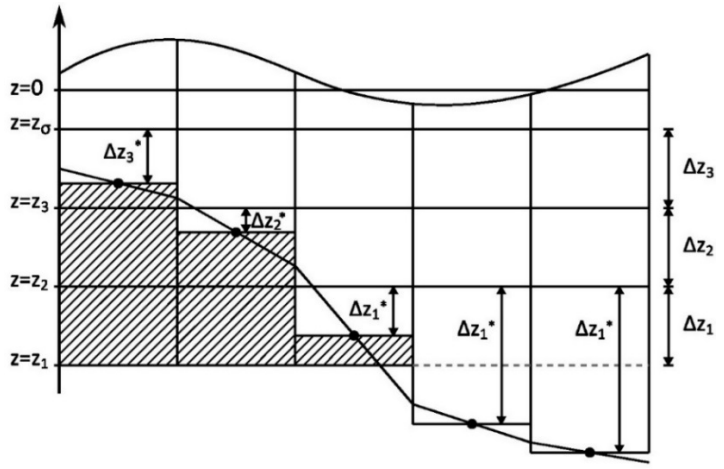

Figure 5.13. Advanced bathymetry adjustment approach (source: DHI, 2014c)

- **HECRAS model**

HEC-RAS 2D solves the full 2D Saint Venant equations or the 2D diffusive wave equations. A simplified version of Navier-Stokes equations is the Shallow Water equations. In order to approximate the turbulent motion using eddy's viscosity the following assumptions are: a) Reynolds averaged equation is used, b) the flow is incompressible, c) the density and the hydrostatic pressure are uniform and d) the horizontal length scale is bigger than the vertical length scale. Thus, the implementation of these assumptions to the Navier-Stokes equations results to small vertical velocity and hydrostatic pressure (Brunner, 2016a) and, also, to the differential form of Shallow Water equations.

In some shallow flows the main terms of momentum equations are the barotropic pressure gradient (gravity) term and the bottom friction terms. In these cases, the unsteady, advection, and viscous terms can be neglected resulting to the transformation of the momentum equation to a two dimensional form of the Diffusion Wave Approximation. The combination of mass conservation with the two dimensional form of the Diffusion Wave Approximation results to the Diffusive Wave Approximation of the Shallow Water (DSW) equations. In addition, the sub-grid bathymetry approach is used in HEC-RAS 2D modelling (Brunner, 2016a).

The discretization of the mass conservation equation is achieved with the use of a finite volume technique. Each grid cell includes information (e.g. hydraulic radius, volume and cross sectional area) and can be computed using the bathymetry in a pre-processing step (Casulli, 2009). In the mathematical equations below, the bottom surface elevation is given by *z(x,y)*; the water depth is *h(x,y,t)*; and the water surface elevation is (Brunner, 2016a):

$$H(x, y, t) = z(x, y) + h(x, y, t) \tag{5.18}$$

Using assumption b, the continuity equation is expressed as:

$$\frac{\partial H}{\partial t} + \frac{\partial (hu)}{\partial x} + \frac{\partial (hv)}{\partial y} + q = 0 \tag{5.19}$$

where *t* is time; *u* and *v* are the velocity components in the x- and y- direction respectively; and *q* is a source/sink flux term.

Combining the previously mentioned assumptions (assumptions a,b,c,d) results to small vertical velocity and to an almost hydrostatic pressure. A vertically-averaged version of the momentum equation is suitable if the baroclinic pressure gradients (variable density) are absent, strong wind forcing exists and the pressure is non-hydrostatic. Under these conditions, the terms of Vertical velocity and vertical derivative can be omitted and the shallow water equations can be obtained. Therefore, the momentum equations are expressed as follows (Brunner, 2016a):

$$\frac{\partial u}{\partial t} + u\frac{\partial u}{\partial x} + v\frac{\partial u}{\partial y} = -g\frac{\partial H}{\partial x} + v_t\left(\frac{\partial^2 u}{\partial x^2} + \frac{\partial^2 u}{\partial y^2}\right) - c_f u + f_v \tag{5.20}$$

$$\frac{\partial v}{\partial t} + u\frac{\partial v}{\partial x} + v\frac{\partial v}{\partial y} = -g\frac{\partial H}{\partial x} + v_t\left(\frac{\partial^2 v}{\partial x^2} + \frac{\partial^2 v}{\partial y^2}\right) - c_f v + f_u \tag{5.21}$$

Where *u* and *v* are the velocities in the Cartesian directions; *g* is the gravitational acceleration; v_t is the horizontal eddy viscosity coefficient; c_f is the bottom friction coefficient; and *f* is the Coriolis parameter.

Diffusion Wave Approximation of the Shallow Water Equations

With the use of extra constrains on the physics of the flow, the barotropic pressure gradient and bottom friction can be related using the diffusion wave form of the momentum equation. This leads to the Diffusion Wave Approximation of the Shallow Water Equations which is a very useful relation due to its simplicity (Brunner, 2016a). A

convenient denotation is that the hydraulic radius and the face cross section areas can be expressed as a function of the water surface elevation *H*, so *R= R(H)*, *A=A(H).*

Diffusion-Wave Form of the Momentum Equation.

The Shallow water momentum equation can be simplified, in cases where shallow frictional and gravity controlled flow conditions exist, by disregarding the terms of unsteady, advection, turbulence and Coriolis. Thus, the flow movement is driven by the barotropic pressure gradient balanced by bottom friction. The simplification of the momentum equation results to the typical Diffusion-Wave form of the Momentum Equation (Brunner, 2016a):

$$V = \frac{-\left(R(H)\right)^{2/3}}{n} \frac{\nabla H}{|\nabla H|^{1/2}} \tag{5.22}$$

where *V* is the velocity vector; *R* is the hydraulic radius; *H* is the surface elevation gradient; and *n* is the empirically derived Manning's n.

Diffusion-wave approximation of the Shallow Water Equations.

The determination of velocity by a balance between barotropic pressure gradient and bottom friction can lead to the use of the Diffusion Wave form of the Momentum equation (5.22) instead of the full momentum equation and the corresponding system of equations. Finally, the substitution of Diffusion Wave equation (5.22) in the mass conservation equation (vector form) generates the typical differential form of the Diffusion Wave Approximation of the Shallow Water (DSW) equation (Brunner, 2016a):

$$\frac{\partial H}{\partial t} - \nabla \cdot \beta \nabla H + q = 0 \tag{5.23}$$

where $\beta = \frac{\left(R(H)\right)^{5/3}}{n|\nabla H|^{1/2}}$

- **LISFLOOD model (quasi 2D approach).**

LISFLOOD-FP (bristol.ac.uk) developed by University of Bristol (LISFLOOD-FP, 2017) is a raster-based model (quasi-2d) that examines both steady and unsteady flow conditions (Dimitriadis et al., 2016). The two-dimensional base model uses the equation of continuity of mass in each cell and the equation of continuity of momentum between cells. Even though the two-dimensional base model is applied in two dimensions, the one-dimensional momentum equation is implemented across each face of each grid cell so that the fluxes through each cell face are separated from each other (Neal et al., 2012).

Thus, the two-dimensional base model represents 2-D dynamic flow fields on the floodplain. Figure 5.14a presents the conceptual diagram of the two-dimensional base model LISFLOOD-FP. The main assumption of this model is that the flow among two cells is a function of the free surface height difference among those cells (LISFLOOD-FP, 2017):

$$\frac{dh^{i,j}}{dt} = \frac{Q_x^{i-1,j} - Q_x^{i,j} + Q_y^{i,j-1} - Q_y^{i,j}}{\Delta x \Delta y} \tag{5.24}$$

$$Q_x^{i,j} = \frac{h_{flow}^{5/3}}{n}\left(\frac{h^{i-1,j} - h^{i,j}}{\Delta x}\right)^{1/2} \Delta y \tag{5.25}$$

where $h_{i,j}$ is the water free surface height at the node *(i,j)*; *Dx* and *Dy* are the cell dimensions; *n* is the effective grid scale Manning's friction coefficient for the floodplain; Q_x and Q_y describe the volumetric flow rates between floodplain cells (Q_y is defined analogously to Q_x); h_{flow} (flow depth) represents the depth through which water can flow between two cells. The parameter h_{flow} is estimated by subtracting the highest bed elevation from the highest water free surface among the two cells (LISFLOOD-FP, 2017).

A modification of the Two-Dimensional Model is the Subgrid Channel Two-Dimensional Model. The main changes adapted in the Subgrid Channel Two-Dimensional Model are: 1) the model can represent (or simulate) the river channel at any size lower than the represented grid resolution and 2) hydraulic geometry theory is used for the estimation of the unknown channel depth from observable variables (e.g. bank elevation and channel width) (Neal et al., 2012). Using the subgrid approach, the channel is represented as a feature within the 2D grid structure.
An approximation of one-dimensional St. Vernant equation is used (without advection). The Subgrid Channel Two-Dimensional Model can calculate the merged flow of water within each cell. This flow contains both the channel flow and the related across the adjacent floodplain flow. Figure 5.14b,c shows the subgrid channels model and an example of a subgrid section respectively.

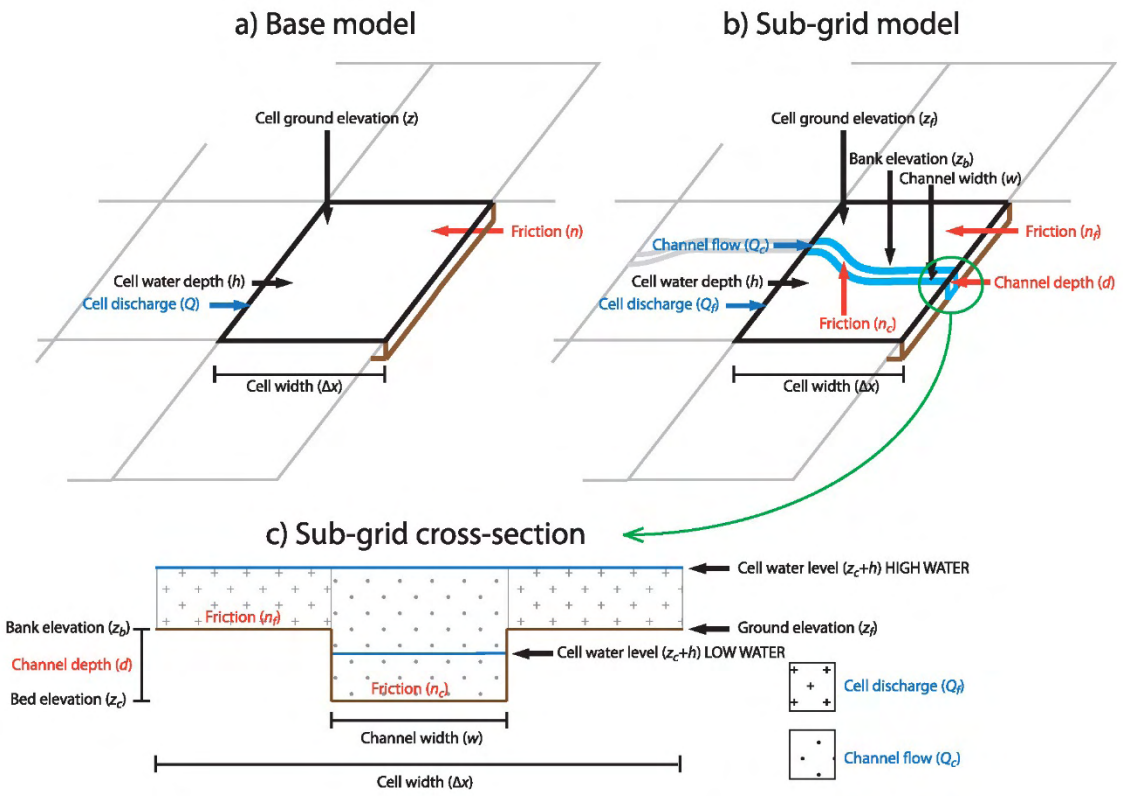

Figure 5.14. Conceptual diagram of (a) LISFLOOD-FP base model, (b) subgrid channels model, and (c) subgrid section (source: Neal et al., 2012).

- **XPSTORM model.** XPSTORM

XPSTORM is another model that is used for two dimensional hydraulic-hydrodynamic simulations and has been applied for flood modelling and mapping. The two dimensional XPSTORM hydraulics engine solves the depth averaged 2D shallow water equations (SWE). The computational solver is based on the alternating direction implicit (ADI) finite difference methodology (Stelling, 1983). The derivation of SWE is based on the assumptions that the vertical acceleration is insignificant and the horizontal velocity is vertically uniform. This hypothesis is valid when the value of wave length if much bigger than the water depth. In the 2D mass continuity differential equation, X momentum conservation and Y momentum conservation equations are presented respectively (XP2d, 2017):

$$\frac{\partial \zeta}{\partial t} + \frac{\partial (Hu)}{\partial x} + \frac{\partial (Hv)}{\partial y} = 0 \qquad (5.26)$$

$$\frac{\partial u}{\partial t} + u\frac{\partial u}{\partial x} + v\frac{\partial u}{\partial y} - c_f v + g\frac{\partial \zeta}{\partial x} + gu\left(\frac{n^2}{H^{4/3}} + \frac{f_l}{2g\partial x}\right)\sqrt{u^2+v^2} - \mu\left(\frac{\partial^2 u}{\partial x^2} + \frac{\partial^2 u}{\partial y^2}\right) + \frac{1}{\rho}\frac{\partial p}{\partial x} = F_x \quad (5.27)$$

$$\frac{\partial v}{\partial t} + u\frac{\partial v}{\partial x} + v\frac{\partial v}{\partial y} - c_f u + g\frac{\partial \zeta}{\partial y} + gv\left(\frac{n^2}{H^{4/3}} + \frac{f_l}{2g\partial y}\right)\sqrt{u^2+v^2} - \mu\left(\frac{\partial^2 v}{\partial x^2} + \frac{\partial^2 v}{\partial y^2}\right) + \frac{1}{\rho}\frac{\partial p}{\partial y} = F_y \quad (5.28)$$

where ζ is the water surface elevation; u and v are the depth average velocity components in X and Y directions; H is the water depth; t is time; x and y are the distances in X and Y directions respectively; c_f is the Coriolis force coefficient; n is the Manning's n roughness coefficient; f_l is the energy loss coefficient; μ is the horizontal diffusion of momentum coefficient; p is the atmospheric pressure; ρ is the water density and; F_x and F_y are the sum of components of external forces in X and Y directions respectively.

- **FLO2D model.** FLO2D

FLO2D is another raster-based model (quasi-2d) that, although the model is applied in two dimensions, the one-dimensional mass continuity and momentum conservation equations are implemented using an explicit central finite difference scheme (Dimitriadis et al., 2016). The mass continuity and momentum conservation equations that FLO2D uses are expressed respectively (Flo-2d, 2017):

$$\frac{\partial h}{\partial t} + \frac{\partial hV}{\partial x} = i \quad (5.29)$$

$$S_f = S_0 - \frac{\partial h}{\partial x} - \frac{V}{g}\frac{\partial V}{\partial x} - \frac{l}{g}\frac{\partial V_x}{g\partial t} \quad (5.30)$$

where h is the flow depth; V is the depth-averaged velocity in one of the eight flow directions x; i is the excess rainfall intensity; S_f is the friction slope component; S_0 is the bed slope.

Despite the fact that the FLO2D solver has the ability to simulate flow movement in multi-directions, for the floodplain flow simulation, it computes the average flow velocity at one direction at a time across the grid element boundary. The total possible flow directions are eight: north, east, south, west, northeast, southeast, southwest and northwest (Flo-

2d, 2017). The average flow velocity is computed independently across each one of eight potential flow directions (Dimitriadis et al., 2016).

Coupled one/two (1D/2D) dimensional hydraulic models

- **MIKE FLOOD (MIKE11/MIKE21).**

The coupling platform, developed by Danish Hydraulic Institute, which combines the two-dimensional model MIKE 21 and the one-dimensional model MIKE 11 in a single environment is MIKE FLOOD. The process of coupling between MIKE 21 and MIKE11 is accomplished using the following linkage options: 1) Standard Link, 2) Lateral Link, 3) Structure Link, 4) Side Structures Link and 5) Zero Flow links (XFlow=0 and YFlow=0) (DHI, 2014f). Many studies have demonstrated the MIKEFLOOD model applicability in flood modelling and mapping (e.g. Chen et al., 2012; Wen et al., 2013; Samantaray et al., 2015; Vozinaki et al., 2015). Details about Mike 21 and Mike 11 solvers can be found in the previous paragraphs of subchapter 5.3 (Chapter 5). MIKE 11 is generally used for the simulation of flow inside the river channel and MIKE 21 (Gird based or Triangular mesh based) is used for floodplain flow simulation.

- **HEC-RAS model.**

A typical combination of coupled 1D/2D flood modelling applications is the use of HECRAS 1D solver in the river channel and the HECRAS 2D solver in the floodplain. The linkage of the different solver schemes can be established with the use of 1) Lateral structures (weirs), 2) Directly connecting an upstream river reach to a downstream 2D flow area, 3) Directly connecting an upstream 2D flow area to a downstream river reach. Details about HECRAS 1D and HECRAS 2D solvers can be found in the previous paragraphs of subchapter 5.3 (Chapter 5).

- **XPSTORM model.**

XPSTORM 1D solver is applied in the river channel and XPSTORM 2D solver is applied in the floodplain. The linkage of the different solver schemes is established by carving a 1D network through a 2D domain (Syme, 1991). Details about XPSTORM 1D and XPSTORM 2D solvers can be found in the previous paragraphs of subchapter 5.3 (Chapter 5).

- **LISFLOOD model.**

The two-dimensional base model is used in the floodplain analysis while the hydraulic-hydrodynamic simulation of the main river is achieved with the use of either Diffusion or Kinematic wave solver. Details about LISFLOOD 2D solvers can be found in the previous paragraphs of subchapter 5.3 (Chapter 5). The linkage of the different solver schemes is

established using the diffusive wave scheme. Thus, the linking of the floodplain (2D) and the channel (1D) schemes is accomplished using the quasi, two-dimensional continuity equation (Trigg et al., 2009; Bates et al., 2013; Dimitriadis et al., 2016).

$$\frac{\partial A}{\partial t} + \frac{\partial Q}{\partial x} = q \tag{5.31}$$

$$S_0 - \frac{Q^2 n^2 Pw^{4/3}}{A^{10/3}} - \left[\frac{\partial h}{\partial x}\right] = 0 \tag{5.32}$$

where *Q* is flow of the channel; *A* the cross sectional wetted area; *q* the flow into the channel from other sources; *n* the Manning's roughness coefficient; and *Pw* the wetted perimeter of the flow; S_0 is the bed slope, *h* is the flow depth.

The term in brackets in equation (5.32) is the diffusion wave term. By switching off or on this term the model can use either kinematic or diffusion wave approximations (Bates and Roo, 2000). Finally, when the depth exceeds over the banks in a specified channel cell the water is transferring to the adjacent floodplain areas.

5.4 Dem accuracy

In a hydraulic-hydrodynamic model, the accuracy of the river and riverine geometry representation is a major factor that influences significantly the flood simulations and depends on the accuracy of the Digital Elevation Model that is used. In the First level of sensitivity analysis in sub-chapter (5.6), several DEMs have been used while in the Second level of sensitivity analysis, sub-chapter (5.7), the DEM with the best results from the preliminary analysis was selected. The preliminary analysis part includes the use of several packages as HEC-GeoRAS tool, MIKE GIS, MIKE ZERO to generate four different DEMs. These DEMs differ in vertical accuracy, bathymetry details and horizontal resolution. The DEMs used in the First level of sensitivity analysis (subchapter 5.6) are:

- Processed LIDAR DEM

Optech ILRIS 3D laser scanner has been used to produce point cloud data. The point cloud data collection process was feasible for unbiased sampling under several conditions such as sunny weather without clouds, satisfactory hydraulic conditions (dry river channel), etc. The pattern followed in the data collection was in zigzag in order to have overlay areas for the merging process. The total number of scans for both bank sides of the river is 86. After data was collected, all scanned areas were merged to a single one in the

Polyworks 3D environment. Then, in order to create the high-resolution Processed LIDAR (bare earth), several DEM editing processes have been used such as geomorphological filters, expert knowledge, and GIS operations. The pre and post processing methodology of the TLS Digital Terrain Model (Processed LIDAR DEM) is described in CHAPTER 4 and Papaioannou et al. (2013). The triangular irregular network that was produced has a vertical accuracy of 22 cm (due to software limitations).

- Raw LIDAR DEM

Raw LIDAR DEM created by raw point cloud LIDAR data. The produced triangular irregular network has a vertical accuracy of 22 cm (due to software limitations). Points from the vegetation and other physical or technical objects- obstructions were also included. This information led to several discrepancies in the DEM.

- Topographical surveying DEM

The Topographical surveying DEM has been created using typical topographical surveying processes. Although such a survey can give accurate topographical characteristics about the points, when this information is used for DEM creation, the gaps between the points are usually filled with linear interpolation. In this analysis, there have been used approximately 3000 points for the DEM creation. The final derived DEM is in triangular irregular network format using Delaunay triangulation. The vertical resolution ranges between millimeters and few centimeters. Independent of the accuracy of the points, the final DEM lacked of detailed geometry information in specific areas of the river. Several corrections have been applied especially in the bridges sections to make the DEM appropriate for hydraulic simulations.

- Digitized 1:5000 map DEM

Topographic maps of 1:5000 scale with contour lines at 4 meters interval have been used to create the Digitized 1:5000 map DEM. The initial contour lines have been digitized and included in the final DEM. The derived DEM is in triangular irregular network format using Delaunay triangulation. The vertical accuracy of the contour lines is low, since 4 meters is long for an interval and the final DEM was missing critical values in and outside the river.

All the DEMs created in this analysis have been tested for the creation of the following different river geometries: 1) Processed LIDAR River Geometry derived, 2) Raw LIDAR River Geometry derived 3) Topographical surveying River Geometry derived and 4) Digitized 1:5000 map River Geometry. In the Second level of sensitivity analysis (sub-chapter 5.7), only the Processed LIDAR DEM has been used and several packages as GIS, HEC-GeoRAS tool, MIKE GIS, MIKE ZERO, XPSTORM, FLO-2D in order to create the river and riverine area topography for each modelling configuration.

5.5 Validation process

The validity of the outcomes in hydraulic-hydrodynamic modelling is accomplished in many studies with the use of gauged data or with sufficient amount of watermarks with good spatial distribution upon the study area (eg. Aronica et al., 1998; Pappenberger et al., 2005; Kiczko et al., 2103). An alternate process to test the validity of the outcomes in floodplain mapping is to take into account the flood extent using accurate satellite images taken at the time of the flood event (eg. Horrit and Bates, 2001, 2002; Aronica et al., 2002; Alfieri et al., 2013).

In many cases, especially in the Mediterranean region, the watershed is ungauged, water level measurements data do not exist and satellite data is not available. For these cases, the most common techniques, for flood extent approximation, include field investigation, local people interviews, flood compensation documents, etc. Thus, the validation data is reproduced by many sources and usually it's a specified area of the flood extent. In this study because of the ungauged character of Xerias stream the above-mentioned techniques have been used for the flood extent approximation.

A common index that is used as a performance measurement between a simulated area comparative to a validation area is known as skill scores. A Standard Verification System for the skill scores estimation is provided by the World Meteorological Organization (WMO) (Jolliffe and Stephenson, 2011). The most common process in skill scores estimation is the establishment of 2x2 contingency table (Table 5.1). In both analysis conducted in this study, several skill scores have been analyzed such as CSI, POD (Hit Rate aka probability of detection), HSS (Heidke Skill Score), EDI (Extreme Dependency Index) etc. Among the tested skill scores, CSI was identified in a recent study as an effective validation measure in flood mapping when the focus is on the spatial distribution of the flood extent (Horrit and Bates, 2001; Aronica et al., 2002; Alfieri et al., 2014; Nguyen et al., 2015; Altenau et al., 2017). Thus, in validation of the simulated flooded areas against the historical flooded area (reference area), the well-established skill score entitled "Critical Success Index" (CSI) or "Threat Score" (TS) has been selected. This validation methodology was applied in both the First level of sensitivity analysis (Subsection 5.6) and the Second level of sensitivity analysis (Subsection 5.7).

Table 5.1. Typical example of 2x2 contingency table

Event simulated	**Event Observed**		
	Yes	No	Total
Yes	A_c (Hit)	B_c (False alarm)	$A_c + B_c$
No	C_c (Miss)	D_c (Correct rejections)	$C_c + D_c$
Total	$A_c + C_c$	$B_c + D_c$	$A_c+B_c+C_c+D_c$

The estimation of CSI is based on the 2x2 contingency table values and is expressed with the following equation:

$$CSI = \frac{A_c}{(A_c + B_c + C_c)} \tag{5.33}$$

where A_c = Hit - event simulated to occur, and did occur; B_c = False alarm - event simulated to occur, but did not occur and; C_c = Miss - event simulated not to occur, but did occur.

5.6 First level of sensitivity analysis

The aim of the First level of sensitivity analysis is to address the sensitivity of different hydraulic-hydrodynamic modelling configurations and several river and riparian areas spatial resolutions on floodplain mapping and flood inundation modelling at ungauged watersheds. Typical hydrological methodologies have been used for the generation of the hydrograph (details can be found in Chapter2: Study Area). A post flood analysis process with watermarks has been used for the validation of the Manning's *n* roughness coefficient and the generated hydrograph.

Three different configuration sets have been established for the analysis. The first configuration setting consists of the examination of one dimensional hydraulic-hydrodynamic models, HECRAS and MIKE 11. The second configuration setting consists of the examination of two dimensional hydraulic-hydrodynamic models, MIKE 21 HD and MIKE 21 HD FM. The third configuration setting consists of the examination of the coupled 1D/2D hydraulic-hydrodynamic models MIKE11/MIKE21 HD and MIKE11/MIKE21 HD FM through MIKE FLOOD platform.

All the different configurations sets have been applied using four different types of DEMs accuracies: a) Digital Terrain Model (DTM) created from TLS data, b) Digital Surface Model (DSM) created from TLS data, c) topographic land survey data and d) typical digitized contours from 1:5000 scale topographic maps. Figure 5.15 illustrates the flowchart of the First level of sensitivity analysis. The purpose of this analysis is to examine the sensitivity of the main factors involved in hydraulic modelling and, by extension, to examine the influence in the accuracy of the flood inundation mapping process at ungauged watersheds.

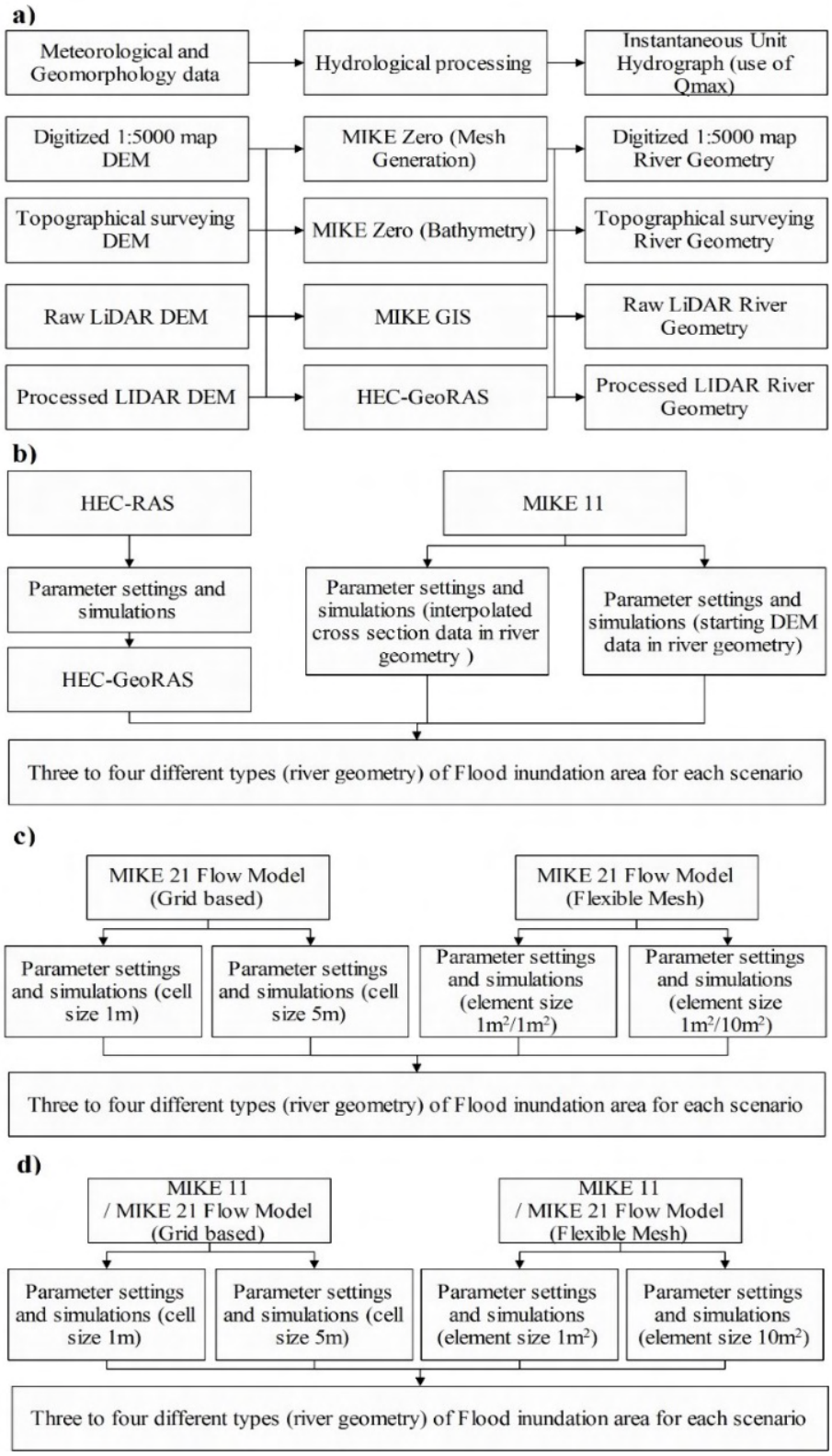

Figure 5.15. First level of sensitivity analysis Flowchart. a) Data preprocessing and input data, b) one dimension (1D) hydraulic model approach, c) two dimension (2D) hydraulic model approach, d) coupled 1D/2D dimensions hydraulic model approach.

5.6.1 Post flood analysis

In many studies, especially at ungauged watersheds, the flow determination is based on indirect measurements. These measurements take into account open-channel hydraulic principles in combination to peak-stage profiles along specified cross sections of the stream. In this analysis, the typical Manning formula, the slope-area method and the hydraulic-hydrodynamic model HEC-RAS has been used for the validation of the estimated discharge (CIUH) and the roughness coefficient.

The post flood analysis based on topographical survey data (Figure 3.6c) that has been collected for specific cross sections of the river. A photograph from the flood event has been used for the estimation of the high water marks among the selected cross sections (Figure 3.6a,b). Based on topographical survey data it was possible to estimate the hydraulic parameters and the height of the watermarks in the study cross sections. Further details about the post flood analysis can be found in CHAPTER 3 (Field measurements). The results of the validation techniques showed a good agreement of the discharge value with the flood hydrograph (Figure 3.7) and similar results for the roughness coefficient. Finally, the Manning's roughness coefficient was found to be equal to 0,035.

5.6.2 Estimation of flooded areas in the Xerias stream flood routing stream reach

The methodology of First level of sensitivity analysis on flood modelling and mapping using different hydraulic-hydrodynamic models associated with several DEM accuracies was applied at a selected 2.2 km river reach of the lower part of Xerias Watershed at Volos, Greece (Figure 5.1). Common hydrological methods and techniques for ungauged watersheds have been used for the estimation of flood hydrograph: 1) time area curves and 2) CIUH. The flood hydrograph estimation is presented in details in CHAPTER 2. Different modelling configurations have been used for the production of the flooded areas.

This configurations consisted of the combination of different modelling approaches (1D, 2D, 1D/2D) with several DEM with varying accuracy (Processed LIDAR DEM, Raw LIDAR DEM, Topographical surveying DEM, Digitized 1:5000 map DEM). The validation process was based on the comparison between simulated flooded areas and historical data of the flood event using the Critical Success Index (CSI). The sensitivity analysis is presented below.

5.6.3 River topography configurations

A basic factor in the First level of sensitivity analysis is the different river topography spatial resolutions derived from different DEM accuracies. The DEM accuracy that was used in the analysis of the 1D hydraulic-hydrodynamic models was 1m. HEC-RAS version 4.1 and MIKE 11 version 2012/2014 have been used in 1D flood modelling. The basic limitation of HEC-RAS model related to the topography is that the model cannot accept more than 500 points in a cross section. Thus, for the HEC-RAS cross sectional topography setup an internal automated point filter has been used in order to decrease the number of points to the acceptable threshold. Concerning MIKE 11 model, two different river topography setups have been used. The first uses the common setup where the interpolated cross section data is used in the production of the flood map. The second river topography setup uses the DEM information between the cross-sections to produce of the flood map. Both 1D models used equal number of cross sections and with the same interval distances of 100m. The only difference among the cross sections of the two models is that HECRAS can provide irregular scheme in cross sections compared to MIKE 11 that the shape of the cross sections can only be in straight lines (Figure 5.16a,b).
MIKE 21 HD and MIKE 21 HD FM version 2012/2014 were used in 2D flood modelling. In addition, MIKE 21 HD (rectangular grid) was configured with 1m and 5m cell size. MIKE 21 HD FM (flexible mesh) was configured with a mesh spatial resolution of $1m^2$ and $10m^2$ for the river and the floodplain, respectively. MIKE FLOOD platform version 2012/2014 has been used in coupled flood modelling. In this model platform, the river channel has been simulated with the use of MIKE 11 with the second river topography setup and the floodplain has been simulated with the use of MIKE 21 HD with 1m and 5m cell size. An additional combination in MIKE FLOOD platform, simulated the river channel using MIKE 11 with the second river topography setup and the floodplain was simulated with the use of MIKE 21 HD FM with elements $1m^2$ and $10m^2$ (Figure 5.15). Finally the number of linking points in MIKE FLOOD varies approximately from 230 to 2840 and depends on the resolution of the geometry.

5.6.4 Modelling configurations

For the implementation of the sensitivity analysis, the parameters of all modelling configurations were set as constants with exception to DEM accuracy and the spatial resolution. According to the post flood analysis the Manning's roughness coefficient value has been set to 0.035 for the entire flood routing stream reach. Recent studies propose the use of steady flow simulations for the performance evaluation in flood modelling (Horritt and Bates, 2002; Dimitriadis et al., 2016). Thus, for all the simulations a constant

inflow has been used in order to achieve steady state conditions. The utilized discharge value of 490m^3/s was derived from the CIUH. All modelling configurations take into account the three bridges that appear in the study area. Below, follows a presentation of some specific parameters settings according to the user manuals guidelines. The bridges setting has been achieved by using accurate data derived from both the topographical survey and the construction drawings of the bridges.

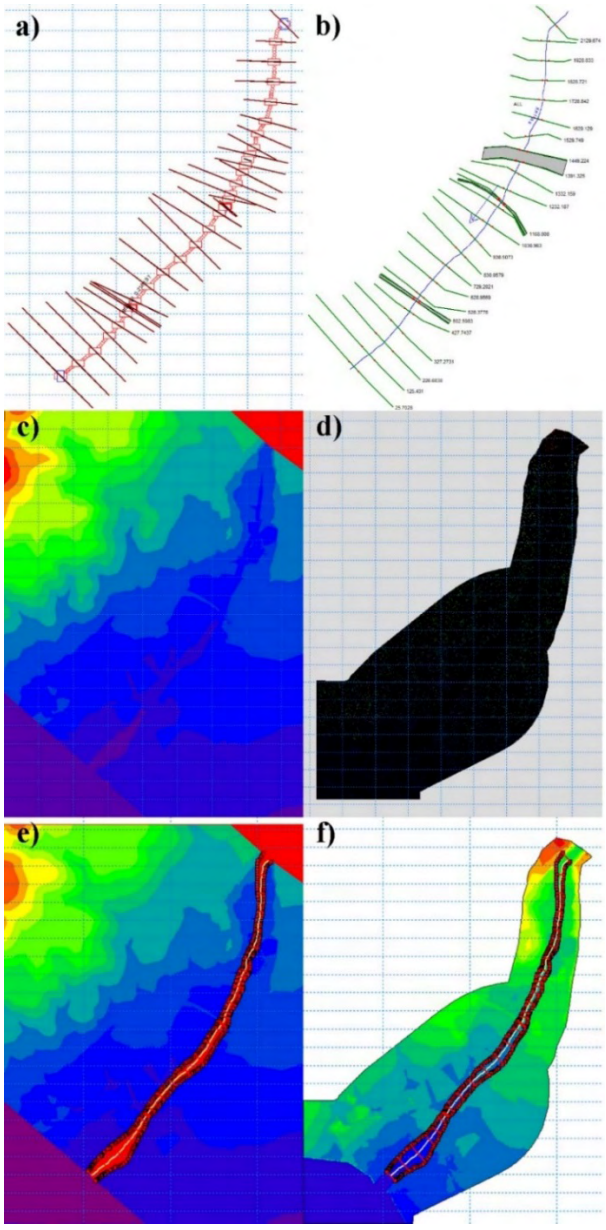

Figure 5.16. Example of the examined river topographies configurations: a) MIKE11, b) HEC-RAS, c) MIKE21 HD, d) MIKE21 HD FM, e) MIKE FLOOD (MIKE 11/ MIKE 21 HD) and f) MIKE FLOOD (MIKE 11/ MIKE 21 HD FM). The direction of flow is from North-East to South-West.

In HEC-RAS the contraction and expansion parameters have been set according HEC-RAS guides and the existence or not of hydraulic structures (three bridges exist in the study area) (Brunner, 2016a). In DHI models the initial flooding and drying depth conditions were adjusted to 0.003 and 0.002, respectively, according to the DHI standards. Moreover, the Coriolis forcing has been omitted and for the inland flooding the constant "flux based" eddy viscosity formulation has been selected based on DHI guidelines (DHI, 2014d). In all 2D modelling configurations the bridges have been imported as culverts and weirs due to software limitations. The width, height and the length of the culverts and weirs have been adjusted according to the measured opening areas of each bridge separately. Furthermore, in MIKE FLOOD, the linking process has been achieved with the use of lateral links among the 1D and 2D modelling configurations. All modelling configurations that were used in the First level of sensitivity analysis (Subsection 5.6), with different DEM configurations and several alternative modelling approaches have been examined and are presented in Figure 5.15.

5.6.5 Results-Discussion

A sensitivity analysis on floodplain mapping and modelling was applied for different hydraulic modelling and DEM spatial resolution configurations. Historical data and records of the extreme flash flood event that occurred in October 9th, 2006 were used for the evaluation of the sensitivity analysis. Based on the available data the observed flood extent polygon of the event was estimated and then used for the evaluation of the hydraulic-hydrodynamic simulations. The comparison of the simulated and the observed flooded area was examined in the validation procedure with the Critical Success Index.
Table 5.2 presents the CSI for several configurations and shows that from the two factors (input DEM accuracy and model structure) examined the most important one is the DEM accuracy (variation of the CSI values from 0.14 to 0.64). This finding proves the importance of the DEM accuracy in flood modelling and mapping efficiency. The visualization of the results is presented in Figure 5.17 as Box and Whisker plots according to CSI for (a) all DEM spatial resolution configurations and (b) all the modelling approach configurations. An important finding revealed from
Table 5.2 and Figure 5.17a is that the processed LIDAR DEM configurations give the highest CSI values and are in good agreement with the observed historical data (validation area). A general remark is that the distribution of the CSI in all modelling approaches is following approximately the same pattern where the processed LIDAR DEM have the largest CSI scores, following by the topographical surveying DEM and the Raw LIDAR DEM

(Figure 5.17a). The last position in the ranking belongs to the digitized 1:5000 map DEM that clearly failed to have a good agreement with the validation flooded area (Table 5.2, Figure 5.17a).

Specifically, the CSI values for all the examined scenarios of the processed LIDAR DEM ranged between 0.41 and 0.64, the Raw Lidar ranged from 0.27 to 0.47, the topographical surveying ranged from 0.31 to 0.44 and the digitized 1:5000 map ranged from 0.14 to 0.17. CSI range values for the DEM accuracy is larger in Raw and Processed LIDAR DEM, followed by the topographical surveying and the digitized 1:5000 map (Table 5.2, Figure 5.17a). Another significant outcome is the importance of the correct pre-processing of LIDAR data that affects significantly the outcomes of flood mapping. Finally it should be mentioned that the topographical surveying configurations gave remarkable results when compared with the raw lidar results.

The results for the model structure intercomparison are also presented in Table 5.2 and Figure 5.17b. Highest scores are achieved with the 2D, followed by the 1D/2D and the 1D modelling approach as expected. However, the range of CSI values is larger in 2D modelling, followed by the 1D/2D and the 1D modelling (Table 5.2, Figure 5.17b). Figure 5.18 presents in detail, the Box and Whisker plots of the CSI values of the DEM spatial resolution for each modelling approach separately, for (a) 1D modelling approach (b) for 2D modelling approach and (c) for 1D/2D modelling approach. An important outcome is that the distribution of the CSI values in Topographical surveying DEM give better results in the coupled modelling approach instead of the 2D modelling approach and approximately the same between 1D and 2D model type (topographical surveying in Table 5.2, Figure 5.18a,b,c).

Furthermore, regarding the digitized 1:5000 map accuracy, the 1D and the coupled (1D/2D) modelling approaches gave slightly better results than the 2D modelling approach. As far as the processed LIDAR DEM and Raw LIDAR DEM accuracy is concerned, the distribution of CSI is following a similar pattern as the general one that can be seen in Figure 5.17b and Table 5.2. Figure 5.19 presents the optimum simulated results of the flooded validation area (CSI score), where, all modelling approaches are produced with the LIDAR DEM configuration. From top to bottom, the modelling approaches are: 1D, 2D, 1D/2D. Finally, the best results in 1D modelling approach is achieved with the HEC-RAS model (0.46 CSI score). In 2D modelling approach the configuration of MIKE 21 HD - 1m cell size (0.64 CSI score) is the best and in the coupled modelling approach the best results are achieved with the combination of MIKE11 and MIKE 21 HD with 5m cell size (0.55 CSI score).

Table 5.2. Critical Success Index for all the modelling approaches configurations

1D			
	HEC-RAS	MIKE11 Interpolated cross section	MIKE 11 DEM
Processed Lidar	**0.46**	0.41	0.44
Raw LiDAR	**0.31**	0.27	0.28
Topographical surveying	0.33	0.31	**0.35**
Digitized 1:5000 map	**0.17**	0.16	0.15

2D				
	MIKE 21 Flow Model 1m cell size	MIKE 21 Flow Model 5m cell size	MIKE 21 Flow Model Flexible mesh $1m^2/1m^2$	MIKE 21 Flow Model Flexible mesh $1m^2/10m^2$
Processed Lidar	**0.64**	0.63	0.59	0.54
Raw LiDAR	-	0.45	0.46	**0.47**
Topographical surveying	0.35	**0.36**	0.31	0.35
Digitized 1:5000 map	0.15	0.15	0.15	0.15

1D/2D				
	MIKE11 / MIKE 21 Flow Model 1m cell size	MIKE11 / MIKE 21 Flow Model 5m cell size	MIKE11 / MIKE 21 Flow Model Flexible mesh $1m^2/1m^2$	MIKE11 / MIKE 21 Flow Model Flexible mesh $1m^2/10m^2$
Processed Lidar	0.54	**0.55**	0.48	0.48
Raw LiDAR	0.41	**0.42**	0.34	0.35
Topographical surveying	**0.44**	0.42	0.40	0.40
Digitized 1:5000 map	0.16	0.14	**0.17**	**0.17**

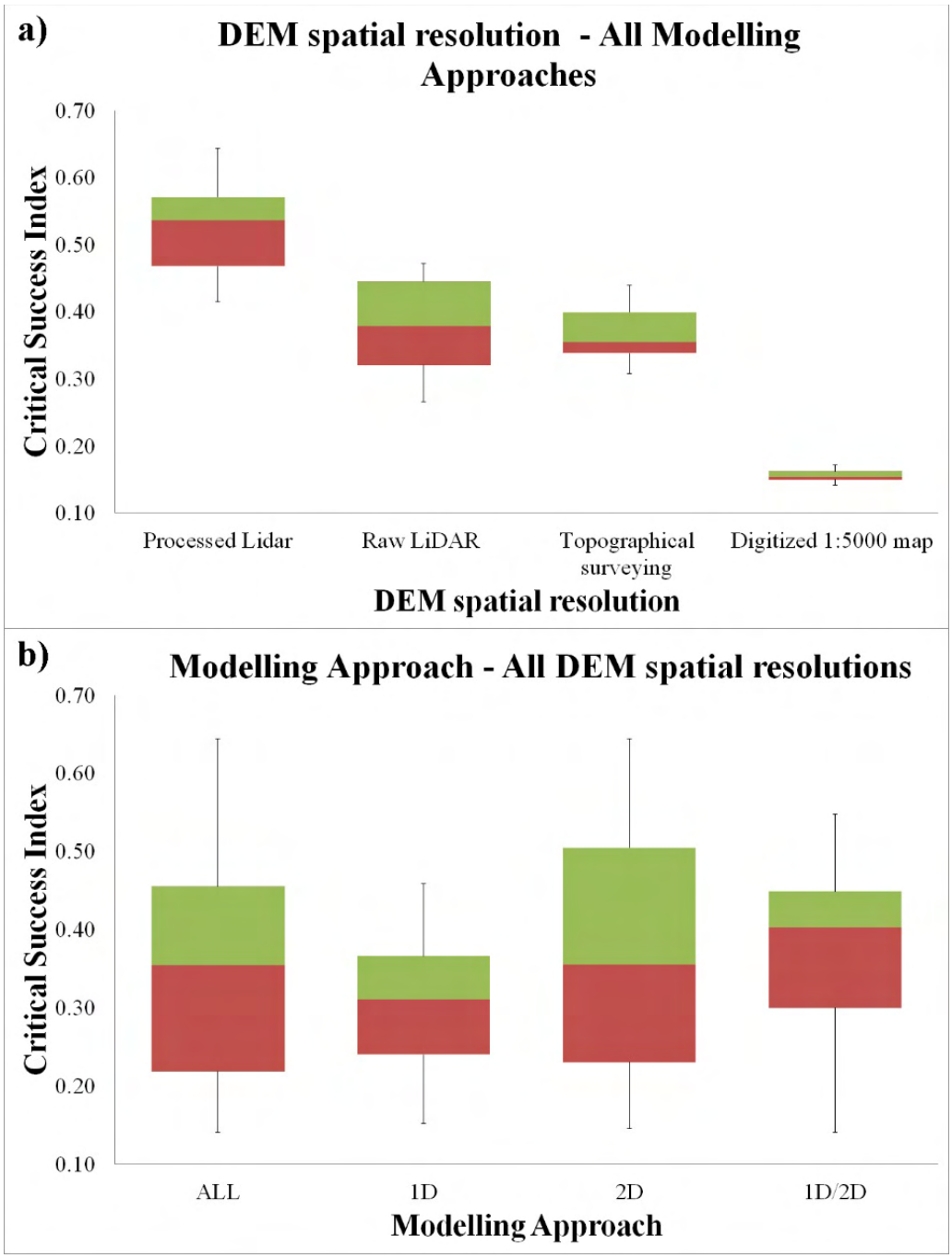

Figure 5.17. Box and Whisker plots according to CSI for (a) all the DEM spatial resolution configurations and (b) all the modelling approach configurations.

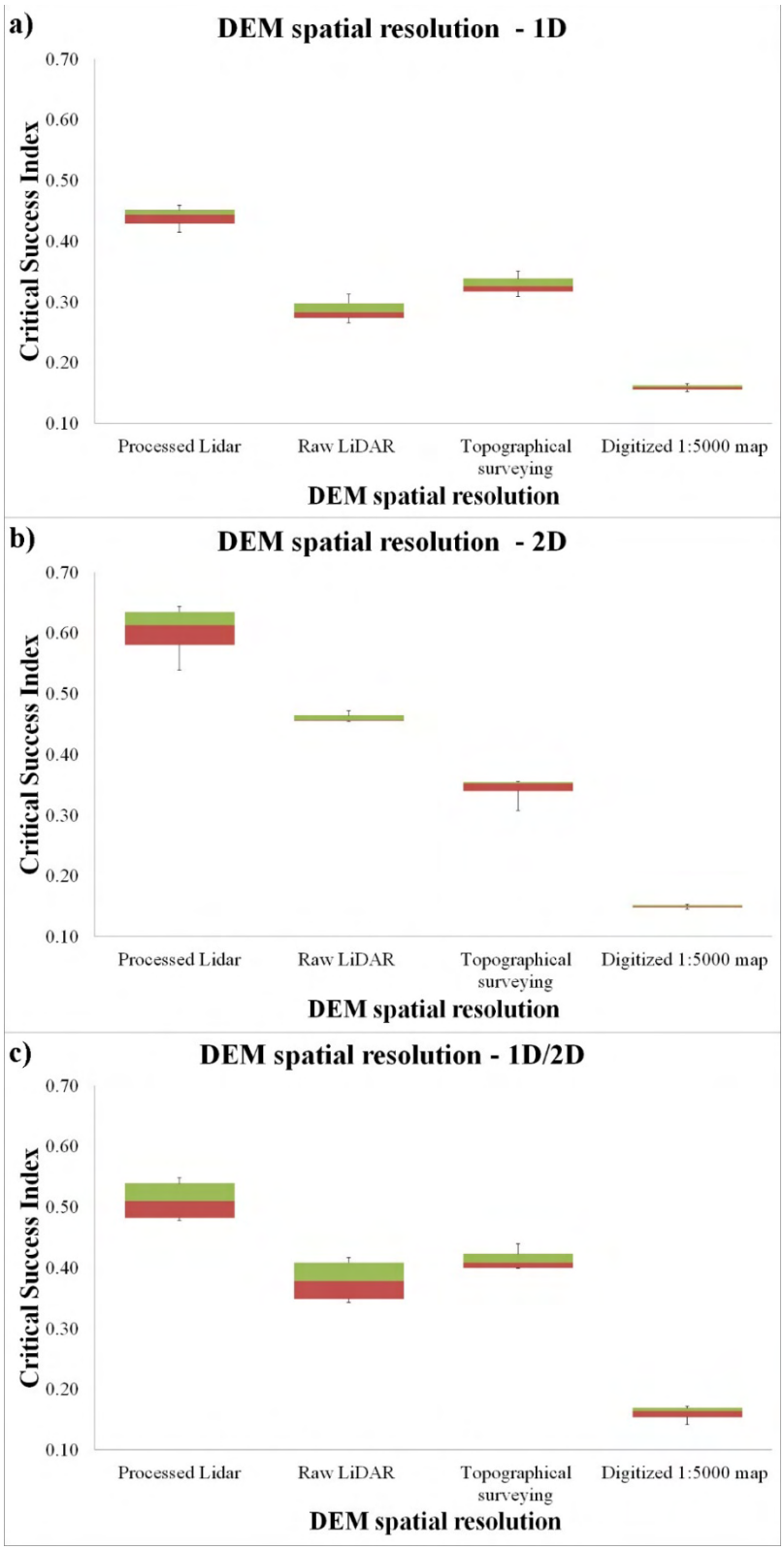

Figure 5.18. Box and Whisker plots of all the DEM spatial resolution configurations according to CSI (a) for 1D modelling approach (b) for 2D modelling approach and (c) for 1D/2D modelling approach.

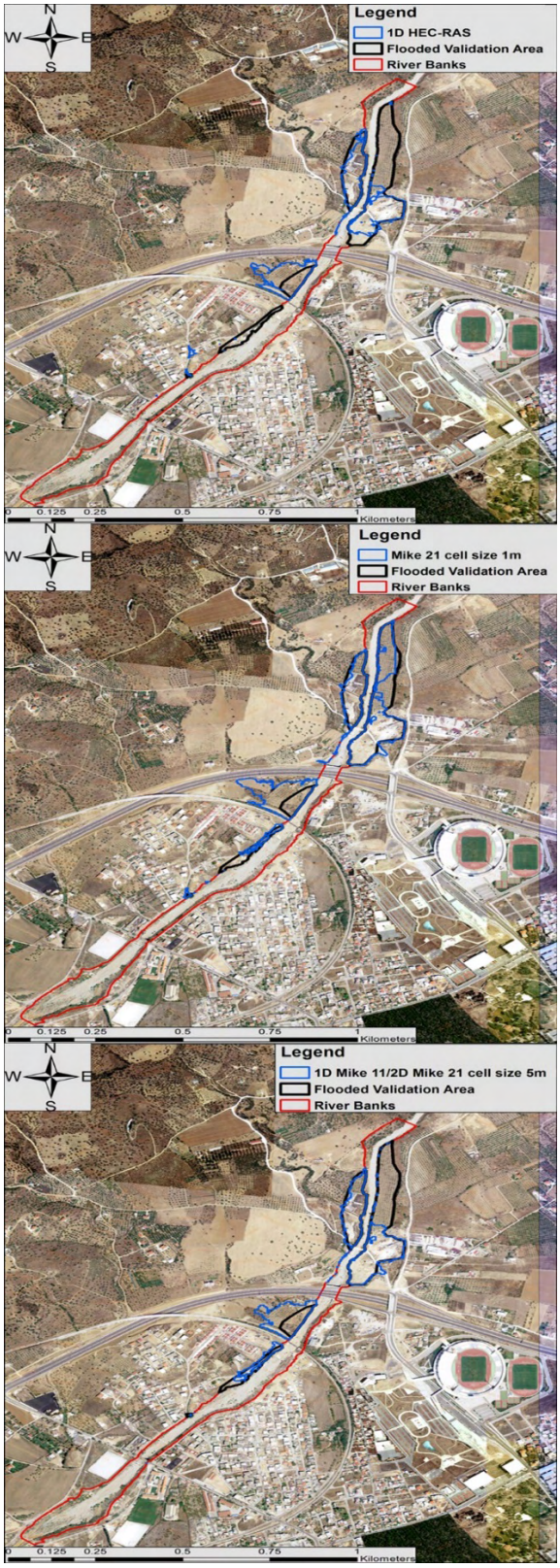

Figure 5.19. Best simulated results according to the CSI score. LIDAR DEM configuration is the selected one for all of the cases. From top to bottom the modelling approaches are: 1D, 2D, 1D/2D.

5.7 Second level of sensitivity analysis

The aim of the "Second level of sensitivity analysis" is to address the sensitivity of various hydraulic-hydrodynamic modelling configurations on floodplain mapping and flood inundation modelling at ungauged watersheds. Typical hydrological methodologies have been used for the generation of the hydrograph (details can be found in Chapter 2: Study Area). A deterministic optimization technique has been used for the optimization of the roughness coefficient value. The deterministic optimization has been implemented using HEC-RAS 1D hydraulic-hydrodynamic model. The final decision for the Manning's roughness coefficient determination was based on optimization analysis using CSI scores and personal judgment according to the 09/10/2006 flood event conditions, and the land uses of the floodplain area. The optimized value of Manning's roughness coefficient was necessary because the value of Manning's roughness coefficient (n=0,035) used in the First level of sensitivity analysis was based on the post flood analysis for a flow level much lower to the peak flow of the event.

Three different configurations sets of models have been established for the analysis and the estimation of the flooded areas. The first configuration setting consists of the one-dimensional hydraulic-hydrodynamic models HEC-RAS, MIKE 11 and XPSTORM. The second configuration setting includes the examination of the quasi-2D and two-dimensional hydraulic-hydrodynamic models MIKE 21 HD, MIKE 21 HD FM, XPSTORM, LISFLOOD-FP, HEC-RAS, and FLO2D. The third configuration setting consists of the coupled 1D/2D hydraulic-hydrodynamic models MIKE11/MIKE21 HD and MIKE11/MIKE21 HD FM through MIKE FLOOD platform, XPSTORM, HEC-RAS, and LISFLOOD-FP.

All the different configuration sets have been applied using the Digital Terrain Model (DTM) created from TLS data according to the previous "First level of sensitivity analysis". The validation process was based on the comparison of the simulated flooded areas with the historical data of the flood event using CSI. Figure 5.20 illustrates the flowchart of the "Second level of sensitivity analysis". The purpose of this analysis is to examine the sensitivity of the hydraulic modelling selection in combination with different configurations (i.e. to include or not the use of bridges and to experiment with different resolutions in the model structure) and, by extension, how this choice influence the accuracy of the flood inundation mapping process at ungauged watersheds. The implementation of the "Second level of sensitivity analysis" is presented below.

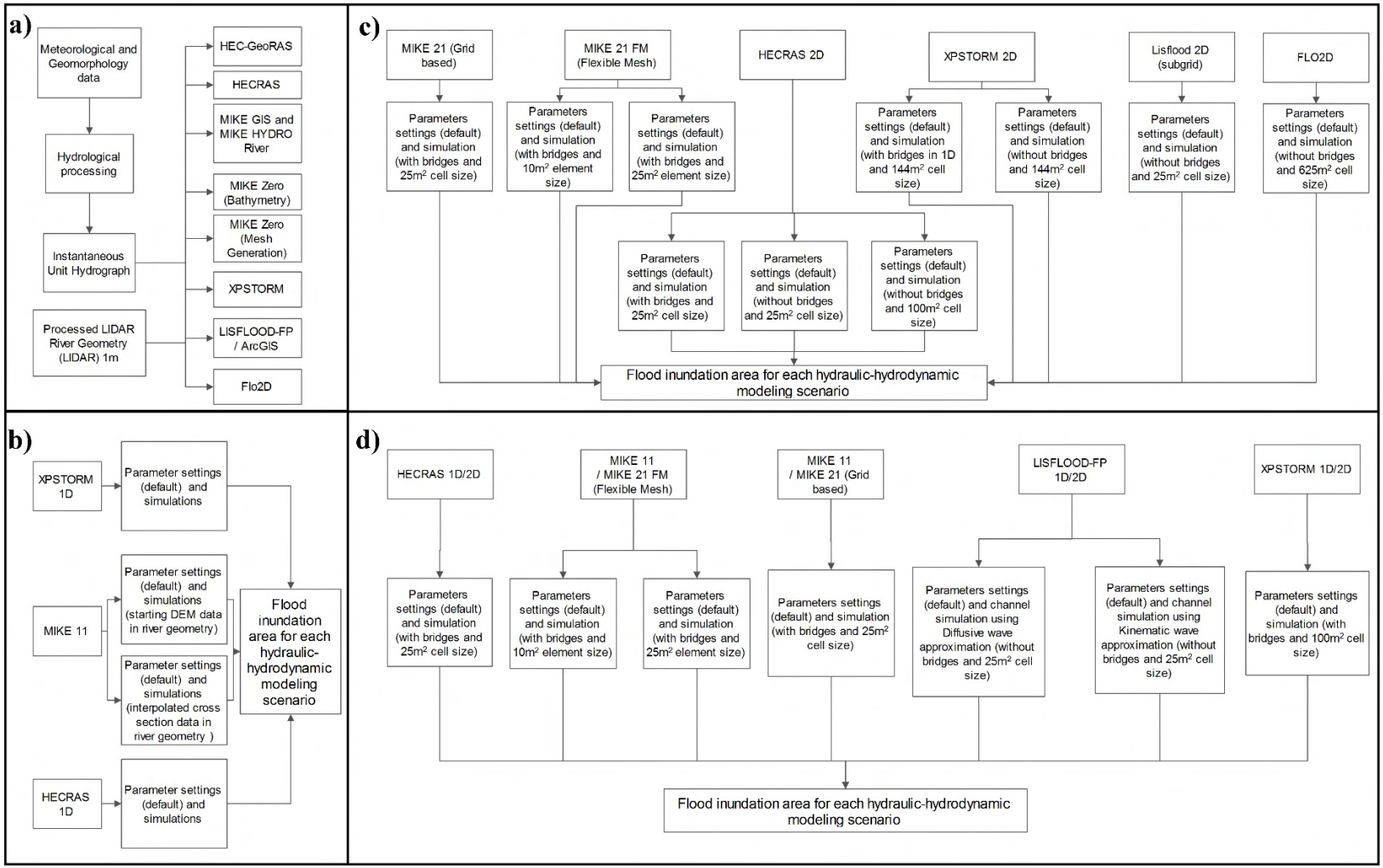

Figure 5.20. Second level of sensitivity analysis Flowchart. a) Data preprocessing and input data, b) one dimension (1D) hydraulic model approach, c) two dimension (2D) hydraulic model approach, d) coupled 1D/2D dimensions hydraulic model approach.

5.7.1 River topography configurations

A basic factor that has been taken into account in the "Second level of sensitivity analysis" is the selection of the modelling approach. The same DEM accuracy of the 1D hydraulic-hydrodynamic models has been set to 1m (same with the "First level of sensitivity analysis"). HEC-RAS version 5, MIKE 11 version 2014 and XPSTORM commercial version 2014 has been used in 1D flood modelling. HEC-RAS and MIKE 11 limitations and the topography settings are the same with the "First level of sensitivity analysis". XPSTORM has been used in evaluation mode for a 30 day trial with limitations to the nodes and the cross sections number. The maximum number of nodes and cross sections that were available and used in XPSTORM evaluation license is only twenty (20).

MIKE 21 HD and MIKE 21 HD FM version 2014, HEC-RAS version 5, XPSTORM commercial version 2014, LISFLOOD-FP version 5.9.6 and FLO2D GDS commercial version 2009 have been used in 2D flood modelling. The majority of the 2D hydraulic-hydrodynamic modelling configurations use a cell size of 5m ($25m^2$) with some exceptions due to modelling limitations or further investigation purposes (i.e. investigate how the modelling configuration affects the simulation time and the accuracy of the results). The models that use different cell size due to software limitations are: 1) XPSTORM evaluation mode that uses a 12m cell size, 2) FLO2D evaluation mode that uses a 25m ($625m^2$) cell size (Figure 5.20). XPSTORM model does not allow the user to apply a finer than 12m ($144m^2$) grid and FLO2D cell size set to 25m ($625m^2$) because of the following limitation of the program. In FLO2D the result of the division of Q_{peak} by the surface area of the grid element A_{surf} should be in the range of 0.03 cms/m^2 < Q_{peak}/A_{surf} < 0.3 cms/m^2. Thus, the model run faster when the result of the division is closer to 0.03 cms/m^2 and slower when the value is closer to 0.3 cms/m^2. In this case study, the Q_{peak} is 490.43 m^3/s which made the simulation with FLO2D extremely time-consuming with a finer grid resolution. The models that use different cell size due to further investigation purposes is HEC-RAS and MIKE21 FM. HEC-RAS has been tested with the lower grid resolution of 10m ($100m^2$), and MIKE21 FM has been tested with the finer mesh element resolution of approximately 3.3m ($10m^2$) (Figure 5.20).

MIKE FLOOD platform version 2014, HEC-RAS version 5, XPSTORM commercial version 2014 and LISFLOOD-FP version 5.9.6 has been used in the coupled 1D/2D flood modelling. All the coupled 1D/2D hydraulic-hydrodynamic modelling configurations used a cell size of 5m ($25m^2$) with some exceptions due to modelling limitations or further investigation purposes. The first exception refers to the coupled 1D/2D XPSTORM that has been applied using 10m cell size (Figure 5.20). The second exception refers to the MIKE FLOOD configuration that uses the combination of MIKE11 and MIKE21 FM with a finer mesh

element resolution of approximately 3.3m (10m^2) (Figure 5.20). In MIKE FLOOD platform, the river channel has been simulated with MIKE 11 configuration that uses the DEM information between the cross-sections and the floodplain has been modelled with the use of MIKE 21 HD or MIKE 21 HD FM. The number of linking points in MIKE FLOOD was approximately 230. LISFLOOD-FP coupled model has been implemented with the use of two different wave approximations for the river channel flow simulation. Thus, the river channel has been simulated using Diffusion or Kinematic solver and the adaptive solver was used for the floodplain flow simulation. Finally, XPSTORM evaluation mode has been applied using 10m cell size for floodplain due to software limitations (evaluation mode does not allow the user to apply a finer grid) (Figure 5.20).

5.7.2 Modelling configurations

For the implementation of the "Second level of sensitivity analysis", the parameters of all modelling configurations were set as constants with exception to the geometry configuration in some cases. The determination of Manning's roughness coefficient has been based on Jarret (1984) formula and a deterministic analysis conducted using several roughness coefficient values and the CSI score as evaluation metric (Figure 3.12). The Jarret's is based on data retrieved from high gradient natural channels with cobble and bolder bed materials. Thus, the use of the specific formula for the selected study area is appropriate. The Jarret's formula is expressed as:

$$n = 0.39 + S_{fr}^{0.38} R^{-0.16} \tag{5.34}$$

where n is the Manning's roughness coefficient; S_{fr} is the energy gradient friction slope; and R is the hydraulic radius.

The assumption that the energy gradient friction slope is the same with the river bed slope has been used for the estimation of the roughness coefficient. Furthermore, the hydraulic radius determination is based on the estimation of the hydraulic radius using the optimum roughness value derived from the deterministic optimization analysis using CSI scores (Figure 3.12). Thus, the median of the total estimated hydraulic radius have been used in the Jarret equation for the determination of the roughness value coefficient. Further details on the estimation of roughness coefficient values using empirical formulas is presented in Chapter 4. The estimated value of roughness coefficient by the Jarret formula is 0.074. Finally, according to the Manning's roughness coefficient analysis, the value have been set to 0.07 for the entire flood routing stream reach. All simulations have

been implemented using the CIUH because all models are using unsteady state flow conditions. The simulation time step has been set to 1 sec for all models.

The majority of the several modelling configurations (2/3 of the cases) take into account the three existing bridges (that included) of the study area. The geometry of the bridges was represented using accurate data retrieved from a topographical survey and the construction drawings (projects) of the bridges. The bridges were omitted in some cases due to model limitations and/or to investigate how the simulation time and the accuracy of the model is affected (Figure 5.20). The modelling configurations that omitted the bridges setup in the hydraulic-hydrodynamic simulation due to model limitations are the LISFLOOD-FP configurations (2D, 1D/2D). This is because the model considers a bridge as a structure only if the pixel size is the same as the bridge length and width. In this study, one of the bridges has a length (from the upstream to downstream) of approximately 56 m and width (left to right span) of approximately 40 m. In order to implement simulation with LISFLOOD-FP including the bridges, the configuration of the geometry should be at least 56 m (3136m^2). This pixel resolution is enormous for the study area in consideration. Below, there are presented some specific parameters settings according to the guides from user manuals.

HEC-RAS-1D and MIKE 11 configuration based on the preliminary analysis guides (Brunner, 2016a; DHI, 2014d). XPSTORM-1D modelling configuration based on the default values proposed by XPSOLUTIONS guides (XPSTORM, 2017a,b). Concerning the 2D modelling approaches, the bridges configuration is the same as the “First level of sensitivity analysis”. In the coupled 1D/2D approaches the linking is achieved using several approaches that depend on the model in use. In all coupled 1D/2D configurations the 1D model has been used for the channel simulation and the 2D model for the floodplain flow simulation. Specifically, in MIKE FLOOD, the linking process has been achieved with the use of lateral links among the 1D and 2D modelling configurations. HEC-RAS linking was achieved using a lateral structure that worked as a weir. XPSTORM linking is based on the advanced 2D/1D linking methodology presented in the works of Syme, 2001. Moreover, LISFLOOD-FP linking is based on the use of a Diffusive wave scheme (quasi-two-dimensional continuity equation). Finally, the “Second level of sensitivity analysis” was implemented using different modelling approaches that consist of different modelling configurations.

Some notable comments for the availability of the models and their capabilities/disabilities are:

- All models have user-friendly window environment except LISFLOOD-FP were all data preparations should be in specific format files (usually .txt).
- XPSTORM and FLO2D models have been used in free evaluation mode.

- All models are commercial software, except for LISFLOOD-FP (University of Bristol) and HEC-RAS (US Army Corps of Engineers).
- For the implementation of LISFLOOD-FP the main channel elevation should have positive gradient.
- XPSTORM model has been repeatedly crashed down and have limitations in the number of nodes, cross sections, and mesh elements in the evaluation mode.
- FLO2D limitation in the simulation process ($0.03 cms/m^2 < Q_{peak}/A_{surf} < 0.3\ cms/m^2$) caused problems in the setup of the model (the model was prepared for several DEM resolutions) and in simulation time.
- All models are capable of using bridges in the river channel. LISFLOOD-FP can use bridges with the limitation that the DEM pixel size should be the same with the geometry (width, length) and bridges calculations are available only in sub-grid mode. DHI models (i.e. MIKE models) and XPSTORM recognize bridges as culverts and weirs. HEC-RAS can simulate the bridges with detailed geometry in the 1D approach and in the 2D approach are represented as culverts and weirs.
- LISFLOOD-FP and FLO2D have been used without the bridges implementation due to the size of the bridges, the pixel limitation, and the models limitation.
- Almost a double size area accounted in the mesh construction of MIKE21 HD and MIKE21 HD FM (version 2012/2014) models due to a problem in the downstream boundary condition (flow was not eliminated in the boundary). Thus, the entire DEM has been recreated by interfering in the downstream area form. Specifically, the downstream area was reshaped in order to work as a reservoir that concentrates the flow in it, in order not to have back water effect in the river and the floodplain.
- For the conduction of unsteady state simulations, small fiddle of some parameters have been implemented in all models according to each model guides. The parameter fiddle affected only the stability of the simulation process and not the overall flood modelling setup.
- DHI models (e.g. MIKE models) have the ability to select and use a big amount of parameters (e.g. wind effect, Coriolis forcing, precipitation- evapotranspiration, wave radiation, etc.).
- All models utilized the original DEM except LISFLOOD-FP, MIKE21 HD and MIKE21 HD FM where the DEM have been edited for simulation purposes.

5.7.3 Results-Discussion

A sensitivity analysis on floodplain mapping and modelling was applied for different hydraulic modelling approaches and configurations at an ungauged catchment. LIDAR high-resolution DEM has been used in order to exclude one of the major factors afflicting the flood modelling results. The evaluation of the "Second level of sensitivity analysis" followed the same methodology as in the "First level of sensitivity analysis". Critical Success Index score has been used as a comparison measurement between the simulated and the observed flooded area.

Table 5.3 presents the CSI for all modelling approaches and configurations and shows that the CSI values vary from 0.49 to 0.7. This finding is significant because it proves that, independently on the modelling approach selection, almost all results achieved an acceptable value (acceptable solution can be assumed above 0.5 in CSI score). The visualization of the results is presented in Figure 5.22 as Box and Whisker plots according to CSI for all the modelling approach configurations. An important and expected finding revealed from Table 5.3 and Figure 5.22 is that the highest CSI scores are achieved with the 2D, following by the 1D/2D and the 1D modelling approach.

A general remark is that the variation of CSI is bigger in 2D modelling approach followed by the coupled 1D/2D and 1D modelling approaches (Figure 5.22). Specifically, the CSI values for the 1D examined scenarios range between 0.49 and 0.57, the 2D scenarios ranging from 0.53 to 0.7, the coupled 1D/2D scenarios ranging from 0.51 to 0.66 (Table 5.3, Figure 5.22). It should be mentioned as a significant outcome that the median CSI score of 1D modelling approach is included in the range of CSI scores of the other two modelling approaches. In Figure 5.23, the optimum simulated results of the flooded validation area (CSI score) are presented for all modelling approaches configurations. The modelling approaches are: a) 1D, b) 2D, c) 2D, d) 1D/2D. The best results in 1D modelling approach are achieved with the MIKE11 (DEM) modelling approach (0.57 CSI score). In 2D modelling approach the configuration of LISFLOOD-FP 2D subgrid ($25m^2$ - without bridges) and HEC-RAS 2D ($100m^2$ - without bridges) (0.7 CSI score) are the best, and in the coupled modelling approach the best results are achieved with the combination of MIKE11/MIKE21 HD FM ($25m^2$) (0.66 CSI score).

Another significant factor, in hydraulic-hydrodynamic modelling applications for engineering purposes is the simulation time. The results for the simulation time intercomparison are also presented in Table 5.4, Figure 5.24 and Figure 5.25. Lowest simulation times are achieved with the 1D, following by the 1D/2D and the 2D modelling approach as expected. However, an important factor affecting the simulation time is the resolution of the mesh geometry and the use of inline structures or not (bridges). Some simulations were implemented in order to investigate the difference in simulation time

for the same model when using an alternate mesh resolution or without the bridges (HEC-RAS 2D without bridges and resolution of 100m^2 and 25m^2, MIKE 21 HD FM with 10m^2 resolution).

XPSTORM model achieved low simulation times probably because of the big mesh geometry value (2D, 1D/2D modelling approaches) and the fact that less nodes and cross sections have been used in comparison to the other models (1D modelling approach). Specifically, XPSTORM models have a score of 0.42 min in 1D modelling approach and follow with approximately the same value 2.5 min in all other simulations (2D with bridges, 2D without bridges, 1D/2D). Regardless the fact that FLO2D has been used with a big mesh resolution of 625m^2, the simulation time is considerably high (2085 min) due to software limitations (the mesh resolution is connected to the flow value and the simulation time). LISHFLOOD-FP has achieved the best simulation times in 2D (5.18 min) and 1D/2D (2.9 and 3.9 min) among the modelling configurations with the same mesh resolution (25m^2) (Table 5.4, Figure 5.25). Despite that LISFLOOD-FP achieved excellent simulation times the implementation of the model using inline structures was not feasible due to model limitations (big inline structures distances and small pixel resolution). Both MIKE 11 configurations (1D modelling approach) attained the same simulation time of 1.6 min.

Furthermore, the simulation time of MIKE 21 HD (25m^2 with bridges) configuration, in 2D modelling attained a value of 340 min and the time decreased approximately 90 percent (30 min) in the coupled modelling approach. In addition, the simulation time of MIKE 21 HD FM (25m^2 with bridges) configuration, in 2D modelling attained a value of 533 min and the time decreased approximately 78 percent (116 min) in the coupled modelling approach (Table 5.4, Figure 5.25). In the configuration of MIKE 21 HD FM (10m^2 with bridges) where a better mesh resolution was used, the simulation time in 2D modelling approach doubled (1380 min) and almost tenfold in the coupled modelling approach (1017 min) (Table 5.4, Figure 5.25). The difference between the two MIKE 21 HD FM (10m^2 with bridges) configurations (2D, 1D/2D) decreased to 26 percent. The simulation time of HEC-RAS 1D achieved a value of 2 min.

Moreover, the simulation time of HEC-RAS (25m^2 with bridges) configuration, in 2D modelling attained a value of 152 min and the time decreased approximately 45 percent (82.47 min) in the coupled modelling approach (Table 5.4, Figure 5.25). The comparison of HEC-RAS 2D (25m^2) configuration with and without bridges showed that the simulation time decreased from 152 min to 39.37 min (74%). The use of HEC-RAS 2D without bridges and with a lower mesh resolution (100m^2) gave even lower simulation time (10.4 min) (Table 5.4, Figure 5.25). Figure 5.25 presents the Box and Whisker plots of the simulation time for the modelling approaches configuration with the same mesh resolution of 25m^2

(simulation time in minutes) (a) for 2D modelling approach and (b) for 1D/2D modelling approach.

An important outcome according to these results is that the existence of inline structures (bridges) can provide an impressive rise to the simulation time. Furthermore, the changes in mesh resolution suggested that the simulation time is totally connected with the resolution used and can be increased dramatically with a finer resolution (Table 5.4, Figure 5.25). Finally, the variation of the simulation time is smaller in 1D modelling approach followed by the coupled (1D/2D) and the 2D modelling approach.

Table 5.3. Critical Success Index for all the modelling approaches and configurations ("Second level of sensitivity analysis").

1D					
Hydraulic model	XPSTORM 1D	MIKE11 (Interpolated DEM)	MIKE11 (DEM)	HEC-RAS 1D	
CSI	0.49	0.54	**0.57**	0.53	
2D					
Hydraulic model	XPSTORM 2D (144m^2 - bridges)	XPSTORM 2D (144m^2 - without bridges)	MIKE21 HD (25m^2 - bridges)	MIKE 21 HD FM (25m^2 - bridges)	MIKE 21 HD FM (10m^2 - bridges)
CSI	0.58	0.53	0.60	0.60	0.56
Hydraulic model	LISFLOOD-FP 2D subgrid (25m^2 - without bridges) Quasi-2D	HEC-RAS 2D (100m^2 - without bridges)	HEC-RAS 2D (25m^2 - without bridges)	HEC-RAS 2D (25m^2 - bridges)	FLO2D (625m^2 - without bridges)
CSI	**0.70**	**0.70**	0.68	0.60	0.56
1D/2D					
Hydraulic model	XPSTORM 1D/2D (100m^2)	MIKE11/MIKE21 HD (25m^2)	MIKE11/MIKE21 HD FM (25m^2)	MIKE11/MIKE21 HD FM (10m^2)	HEC-RAS 1D/2D (25m^2)
CSI	0.51	0.64	**0.66**	0.63	0.64
Hydraulic model	LISFLOOD-FP (Diffusive wave-channel/ without bridges/ 25m^2 in floodplain)	LISFLOOD-FP (Kinematic wave-channel / without bridges/ 25m^2 in floodplain)			
CSI	0.63	0.54			

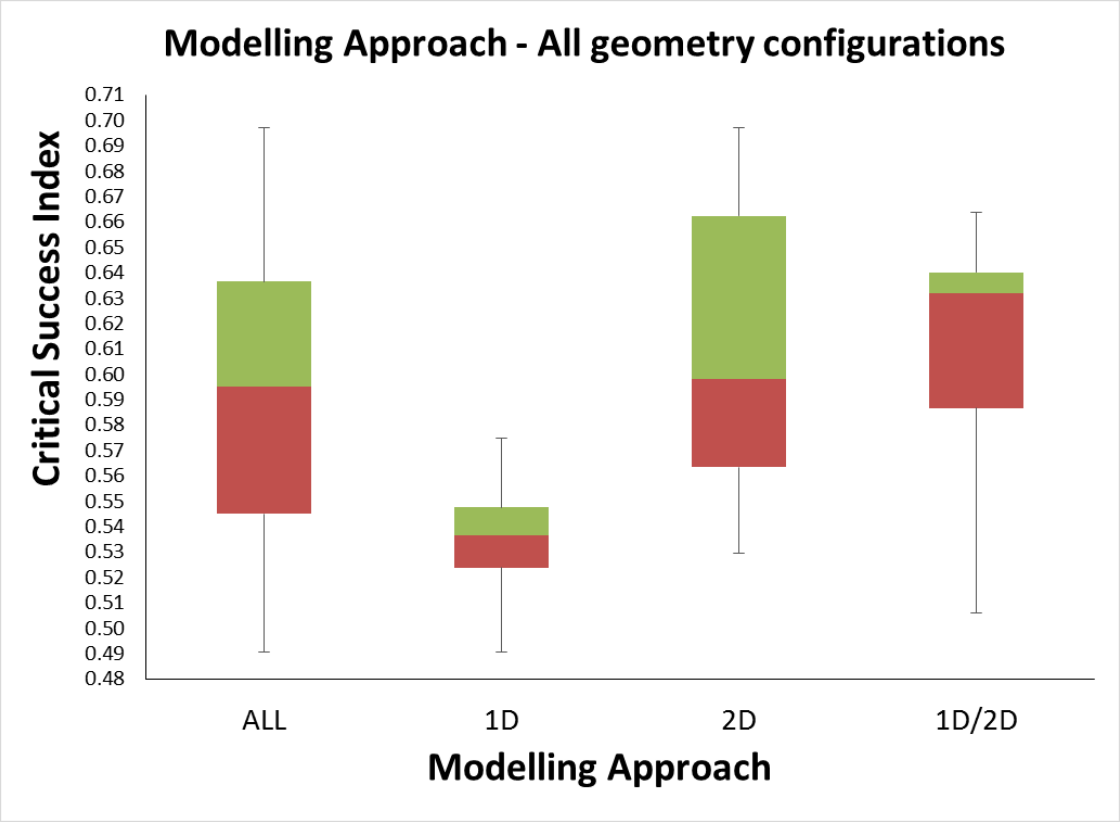

Figure 5.21. Box and Whisker plots according to CSI for all the modelling approach configurations ("Second level of sensitivity analysis").

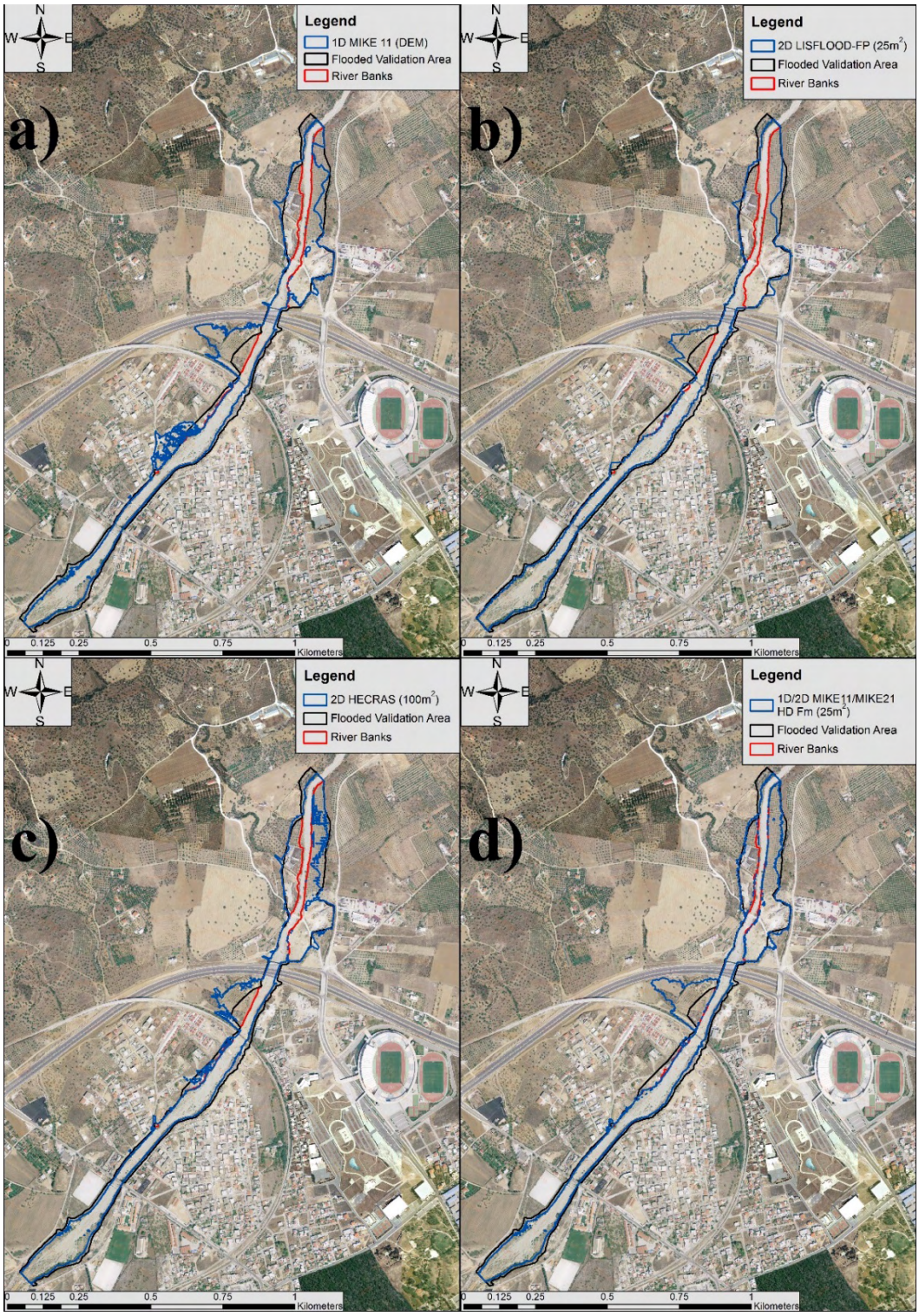

Figure 5.22. Best simulated results according to the CSI score. LIDAR DEM configuration is the selected one for all of the cases. The modelling approaches are: a) 1D, b) 2D, c) 2D, d) 1D/2D.

Table 5.4. Simulation time for all the modelling approaches and configurations ("Second level of sensitivity analysis").

1D					
Hydraulic model	XPSTORM 1D	MIKE11 (Interpolated DEM)	MIKE11 (DEM)	HEC-RAS 1D	
sim time (min)	**0.42**	1.60	1.60	2.00	
2D					
Hydraulic model	XPSTORM 2D (144m^2 - bridges)	XPSTORM 2D (144m^2 - without bridges)	MIKE21 HD (25m^2 - bridges)	MIKE 21 HD FM (25m^2 - bridges)	MIKE 21 HD FM (10m^2 - bridges)
sim time (min)	**2.50**	2.52	340.00	533.00	1380.00
Hydraulic model	LISFLOOD-FP 2D subgrid (25m^2 - without bridges) Quasi-2D	HEC-RAS 2D (100m^2 - without bridges)	HEC-RAS 2D (25m^2 - without bridges)	HEC-RAS 2D (25m^2 - bridges)	FLO2D (625m^2 - without bridges)
sim time (min)	**5.18**	10.40	39.37	152.00	2085.00
1D/2D					
Hydraulic model	XPSTORM 1D/2D (100m^2)	MIKE11/MIKE21 HD (25m^2)	MIKE11/MIKE21HD FM (25m^2)	MIKE11/ MIKE 21 HD FM (10m^2)	HEC-RAS 1D/2D (25m^2)
sim time (min)	**2.54**	30.00	116.00	1017.00	82.47
Hydraulic model	LISFLOOD-FP (Diffusive wave-channel/ without bridges/ 25m^2 in floodplain)	LISFLOOD-FP (Kinematic wave-channel / without bridges/ 25m^2 in floodplain)			
sim time (min)	3.90	**2.90**			

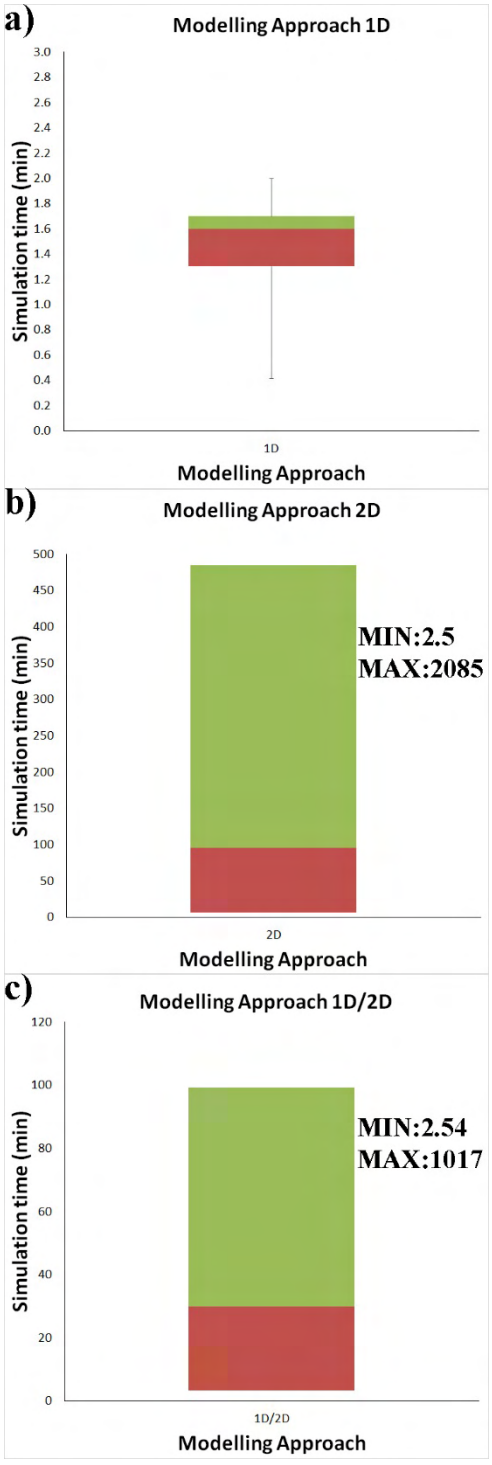

Figure 5.23. Box and Whisker plots of the simulation time for all the modelling approaches (simulation time in minutes) (a) for all configurations of 1D modelling approach (b) for all configurations of 2D modelling approach and (c) for all configurations of 1D/2D modelling approach.

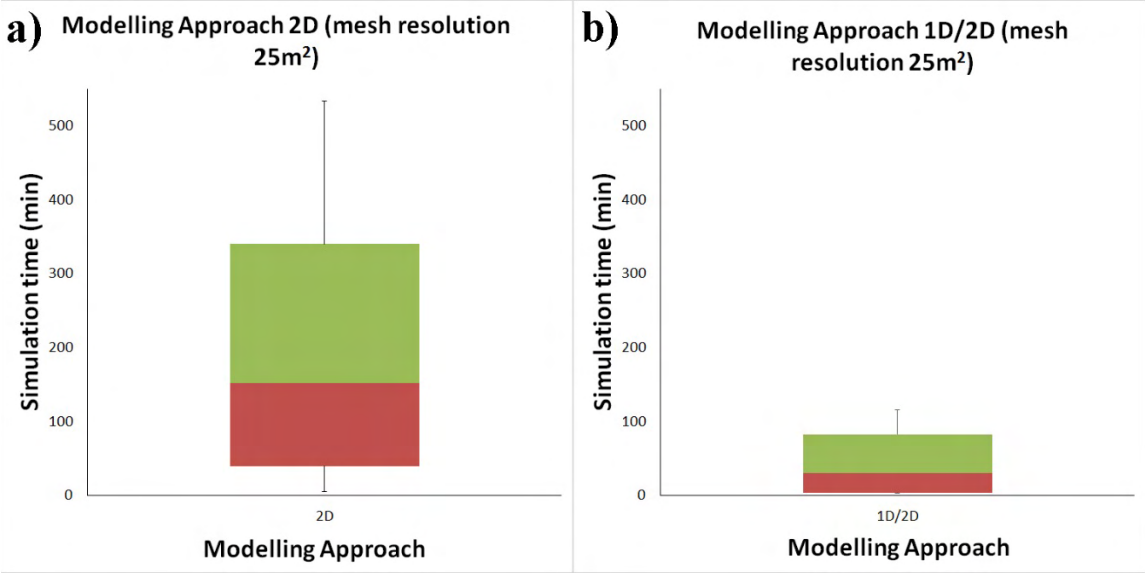

Figure 5.24. Box and Whisker plots of the simulation time for the modelling approaches configuration with the same mesh resolution of 25m^2 (simulation time in minutes) (a) for 2D modelling approach and (b) for 1D/2D modelling approach.

5.8 General remarks from the sensitivity analysis

First level of sensitivity analysis

In the First level of sensitivity analysis the use of different hydraulic-hydrodynamic models and several DEM with varying level of accuracy for flood analysis and mapping have been examined and compared. The sensitivity analysis methodology is based on limited data, typical hydrological and post flood analysis techniques for ungauged catchments. Furthermore, several flood data sources have been incorporated (e.g. data collected from several authorities, newspapers, local interviews and testimonies) for the estimation of the historical flood extent area (validation area). The overlay results attained from the methodology against historical flood extent data were validated through the objective qualitative criterion of CSI that takes into account the spatial distribution of the flooded area.

From the two study factors, according to the CSI score, the DEM accuracy dominated against the selection of the modelling approach. Hence input data uncertainty is more important than the model structure in this study area. DEM accuracy factor ranked first in the processed LIDAR, second in the Raw LIDAR DEM and the topographical surveying DEM and last place was for the digitized 1:5000 map which also gave unsatisfactory results for the study river reach. CSI scores for the hydraulic modelling approaches follow

the same pattern with the DEM accuracy. First in ranking was the two dimensional, second was the coupled and last was the one dimensional modelling approach.
These results indicate the necessity of better spatial resolution accuracies in flood inundation studies and the testing of different modelling approaches in each case before the selection of the most appropriate one for flood modelling and mapping. Furthermore, in complex river and riverine terrain areas, input data with better spatial resolution accuracy are required for successful flood modelling and mapping. Finally, a first indication on the modelling approach shows that more sophisticated models (2D modelling approach) should be used but further research is needed to verify and generalize this finding. Moreover, the use of alternative statistical qualitative criteria such as the Critical Success Index values may provide an indicative verification criterion that considers the spatial distribution of the flood extent and proves to be a useful approach in the application of ungauged watersheds. Application of the proposed techniques in Xerias Watershed showed that a sensitivity analysis should be a mandatory process in flood mapping for ungauged watersheds due to the variation of the results as a result of the DEM accuracy or the modelling approach that is followed. The employed methodology could be applied in ungauged watersheds with limited available information, and/or in areas with compound geomorphology using typical hydrologic and post flood analysis techniques for flood modelling and mapping purposes.

Second level of sensitivity analysis

In Second level of sensitivity analysis, different hydraulic-hydrodynamic models and several configurations for flood analysis and mapping have been examined and compared. The “Second level of sensitivity analysis” methodology is based on the same processes followed in the “First level of sensitivity analysis” (e.g. limited data, typical hydrological and post flood analysis techniques for ungauged catchments, validation of the process using CSI etc.). It was proven that the model structure uncertainty, according to the CSI score, is important concerning the accuracy level that can be achieved (best scores of all approaches have a difference of approximately 19 percent) in this study area. On the other hand, concerning the acceptability of the results, the importance decrease because all models achieved acceptable solutions (CSI value under 0.5). CSI scores pattern was first in the ranking of the two dimensional hydraulic modelling approach, second is the coupled and third the one dimensional. Concerning the simulation time, it was observed that the ranking pattern was reversed compared to the CSI scores. The one dimensional modelling approach ranked first, followed by the coupled and the two dimensional modelling approach was the last. The absence or not of inline hydraulic

structures and the mesh resolution are very important factors concerning the simulation time.

All conclusions are under the assumption that the major factor of uncertainty (accuracy of the river geometry) has been eliminated using an accurate and high resolution DEM. These results indicate that the simplification of a hydraulic-hydrodynamic problem, using simple models (e.g. 1D, 1D/2D) and excluding some structures or using courser mesh elements, should be taken into account in flood risk studies. In floodplain modelling and mapping for engineering purposes the selection of an appropriate model should take into account the availability of models (commercial use or freeware) and the computational cost which must be low, while field measurements are needed in order to minimize the variability of the most sensitive input variables.

A main question that each modeller should ask is whether the use of a more advanced modelling approach will be eventually more advantageous than simplified approaches. The analytical approaches proved very demanding in terms of computational resources and data and imposed several obstacles to their usage in common engineering problems. Once more, it is proven that the use of alternative statistical qualitative criteria such as the Critical Success Index (skill scores) can provide an indicative verification criterion that incorporates the spatial distribution of the flood extent and is very useful in the application of ungauged watersheds. The benchmark analysis conducted in Xerias Watershed showed that a sensitivity analysis should be a mandatory process in flood mapping at ungauged watersheds for engineering purposes due to the variation of the results and the simulation. The employed methodology could be applied in ungauged watersheds with limited available information, and/or in areas with complex geomorphology using typical hydrologic techniques for flood modelling and mapping purposes.

The investigation of the sources of uncertainty in floodplain modelling and mapping can provide supplementary information in order to establish a satisfactory agreement between parsimony and accuracy, which are till know days an unresolved problem in hydraulic modelling (Dimitriadis et al., 2016). Finally it is proposed the use of a simple approach such as the one dimensional hydraulic-hydrodynamic model for calibration and uncertainty analysis investigation (probabilistic flood inundation mapping).

Overall sensitivity analysis

The comparison of the “primary sensitivity analysis” and the “Second level of sensitivity analysis” methodologies presented in this chapter can provide valuable information on how the optimization of the roughness coefficient value affects the overall results. The following comparisons are based on the configurations with the same DEM accuracy

(Processed LIDAR DEM) and mesh resolution. In one dimensional modelling approaches the optimization of roughness coefficient value (increased from 0.035 to 0.07) gave acceptable results according to CSI scores. Specifically, the CSI value of HEC-RAS 1D improved from 0.46 to 0.53, MIKE11 with Interpolated DEM configuration CSI value improved from 0.41 to 0.54 and MIKE11 using DEM configuration CSI value improved from 0.44 to 0.57. The impact of the roughness coefficient value optimization in two dimensional modelling approaches is negligible. Finally, the coupled modelling approaches have a satisfactory improvement with the roughness coefficient change. Therefore, in MIKE11/MIKE21 HD ($25m^2$) CSI score has been improved from 0.55 to 0.64 and in MIKE11/MIKE21 HD FM ($10m^2$) the score has been improved from 0.48 to 0.63.

The comparison of the two systems showed that the roughness coefficient optimization has primarily affected the one dimensional approaches, followed by the coupled dimensional approaches, whereas the response of the two dimensional approaches is almost immune to the change.

Focusing on two study factors (roughness coefficient, DEM accuracy) during the “primary sensitivity analysis” and the “Second level of sensitivity analysis” methodologies presented in this chapter (CHAPTER 5) and implemented on a part of Xerias study area (ungauged catchment, limited data etc.) the following general conclusions can be summarized:

- The input data uncertainty (DEM accuracy) is the most important factor in flood modelling and mapping followed by the roughness coefficient.
- In the DEM accuracy factor first in the ranking is the processed LIDAR, second the Raw LIDAR DEM and the topographical surveying DEM and in the last place is the digitized 1:5000 map that gave unsatisfactory results for the study river reach.
- LIDAR data pre-processing application is a significant process that can affect considerably the outcomes of flood mapping due to the accuracy of the created DEM.
- The topographical surveying configurations gave remarkably better results when compared with the raw lidar results.
- In complex river and riverine landscapes, the use of data with better spatial resolution accuracy is mandatory for successful flood modelling and mapping.
- The improvement of the roughness coefficient value resulted to acceptable solutions for all modelling approaches with significant improvement to the one dimensional and coupled modelling approaches.
- In the selection of different hydraulic modelling configurations, based on CSI score, the two dimensional modelling approach stands first in the rank, followed by the coupled and the one dimensional modelling approach respectively.

- Ranking based on the simulation time shows a reverse pattern compared to hydraulic modelling configurations. Thus, the one dimensional modelling approach ranks first, followed by the coupled and the two dimensional modelling approach respectively.
- The absence or presence of inline hydraulic structures and the mesh resolution severely affect the simulation time.
- The simplification of a hydraulic-hydrodynamic problem, by using simple models (e.g. 1D, 1D/2D) or excluding some structures or using courser mesh elements, should be taken into account in large scale flood risk studies.
- In floodplain modelling and mapping for engineering purposes the availability of the model (commercial use or freeware) and the computational cost must be kept low, while field measurements are needed in order to minimize the variability of the most sensitive input variables.
- The analytical approaches proved very demanding in terms of computational resources, cost, data availability and parameterization and imposed several obstacles to their usage in common engineering problems.
- The use of alternative statistical qualitative criteria such as the Critical Success Index (skill scores) can provide an indicative verification criterion that takes into account the spatial distribution of the flood extent and is very useful when applied at ungauged watersheds.
- The benchmark analysis conducted in Xerias Watershed showed that a sensitivity analysis should be a mandatory process in flood mapping. The variation in the results and the simulation time due to different modelling approach configurations as well as the DEM accuracy proved the benchmark hypothesis.
- The employed methodologies can be applied in ungauged watersheds with limited available information, and/or in areas with complex geomorphology using typical hydrologic and post flood analysis techniques.
- The investigation of the sources of uncertainty in floodplain modelling and mapping can provide supplementary information in order to establish a satisfactory agreement between parsimony and accuracy, which until nowadays remain an unresolved issue in hydraulic modelling (Dimitriadis et al., 2016).
- The use of a simple approach such as the one dimensional hydraulic-hydrodynamic model is proposed for calibration and uncertainty analysis investigation.

CHAPTER 6ο
UNCERTAINTY ANALYSIS COMPONENT

6 Uncertainty analysis component

6.1 Introduction

The largest source of uncertainty in flood inundation modelling is the input data uncertainty. The majority of the studies that deal with flood inundation analysis are based on several assumptions due to the enormous amount of data needed and/or the severe lack of data (quantity and quality). The most common sources of input data uncertainty in flood inundation analysis are: 1) topography data; 2) hydrograph used (rainfall-runoff analysis); 3) roughness coefficient and; 4) hydraulic structures characteristics (Bates et al., 2014). The use of deterministic flood inundation maps involves all the sources of epistemic and natural random uncertainty. All this uncertainties can affect the outcomes of hydraulic-hydrodynamic modelling significantly (Aronica et al., 1998; Aronica et al., 2002; Bates et al., 2004; Pappenberger et al., 2005; Montanari, 2007; Solomatine and Shrestha, 2009; Di Baldassarre et al., 2010; Kiczko et al., 2013; Alfonso et al., 2016; Bellos and Tsakiris, 2016; Fuentes-Andino et al., 2017). Therefore, the deterministic flood maps can provide false information to the policy-makers and lead them to erroneous decisions about the flood risk management strategies and the potential engineering works for flood disaster reduction. Thus, based on the previous findings of this dissertation and the paragraphs mentioned above, the use of Probabilistic Flood Maps (PFMs) can provide a better percentage of certainty in flood inundation analysis to the policy makers.

In this study, a generic procedure for uncertainty analysis of floodplain mapping due to roughness coefficient is developed for the ungauged Xerias stream, Volos, Greece. The HEC-RAS 1D hydraulic-hydrodynamic model is used to assess the uncertainty introduced by the roughness coefficient using Monte-Carlo simulations. Manning's *n* roughness coefficient initial ranges are estimated using several empirical formulas employing pebble count and field survey data, and various theoretical probability distributions are fitted and evaluated using several goodness-of-fit criteria. Latin Hypercube sampling has been used for the generation of different sets of Manning roughness coefficients and several realizations of flood inundation maps are created. The uncertainty is estimated based on a calibration process which is based only on the flood extent derived from historical flood records for an observed extreme flash flood event. Moreover, an extensive sensitivity analysis has been conducted in many factors of Monte Carlo procedure in order to extract the best setup options (e.g. different distance between the cross sections, use of several

realizations sets, use of different acceptable threshold level, and use of different distribution for roughness coefficient generation). Finally, a stability test of the entire component has been applied using the optimized choices.

6.2 Study Area

The study area has been presented in Chapter 2 and it is the ungauged Xerias Watershed, Volos, Greece) (Figure 5.1). The characteristics of the studied extreme flash flood event of the October 9th , 2006, along with the flood estimation using the Clark Instantaneous Unit Hydrograph, the watershed characteristics and the selected stream reach can be found in recent studies (Papaioannou et al., 2015, 2016) and Chapter 2. The validation area is the same as the one presented in Chapter 2 and was carried out with the use of historical data and records (i.e. flood recordings from newspapers, several authorities and local interviews and testimonies) (Papaioannou et al., 2016). A high-resolution DEM created from processed LIDAR point cloud data (see Chapter 3) has been used for the river and riverine geometry configuration. The optimal stationing and digitization of the cross sections in HEC-RAS model have been attained with the use of the high-resolution DEM that was overlaid with local imagery to provide a highly realistic virtual 3-D environment (Figure 5.1).

6.3 Methodology

The main objective of this study is to develop a generic procedure for probabilistic flood inundation mapping at ungauged river reaches. Figure 6.1 presents the flowchart of the recommended procedure and the necessary steps for the estimation and visualization of the uncertainty introduced by the roughness coefficient value. The main structural parts of the suggested methodology are: 1) the Pebble count field survey (see Chapter 3); 2) The use of different Manning's roughness coefficient empirical formulas in order to fit several theoretical probability distributions on the derived empirical one and the generation of different Manning's roughness coefficient data sets using Latin Hypercube Sampling technique; 3) the hydraulic modelling for flood inundation probability mapping using the HEC-RAS 1D model (Figure 6.1). Based on the main structure of the component, several sensitivity analysis scenarios have been conducted in order to examine different configurations of the component and how these affect the outcomes. Finally, the optimal configuration is proposed for probabilistic flood inundation mapping at ungauged watersheds.

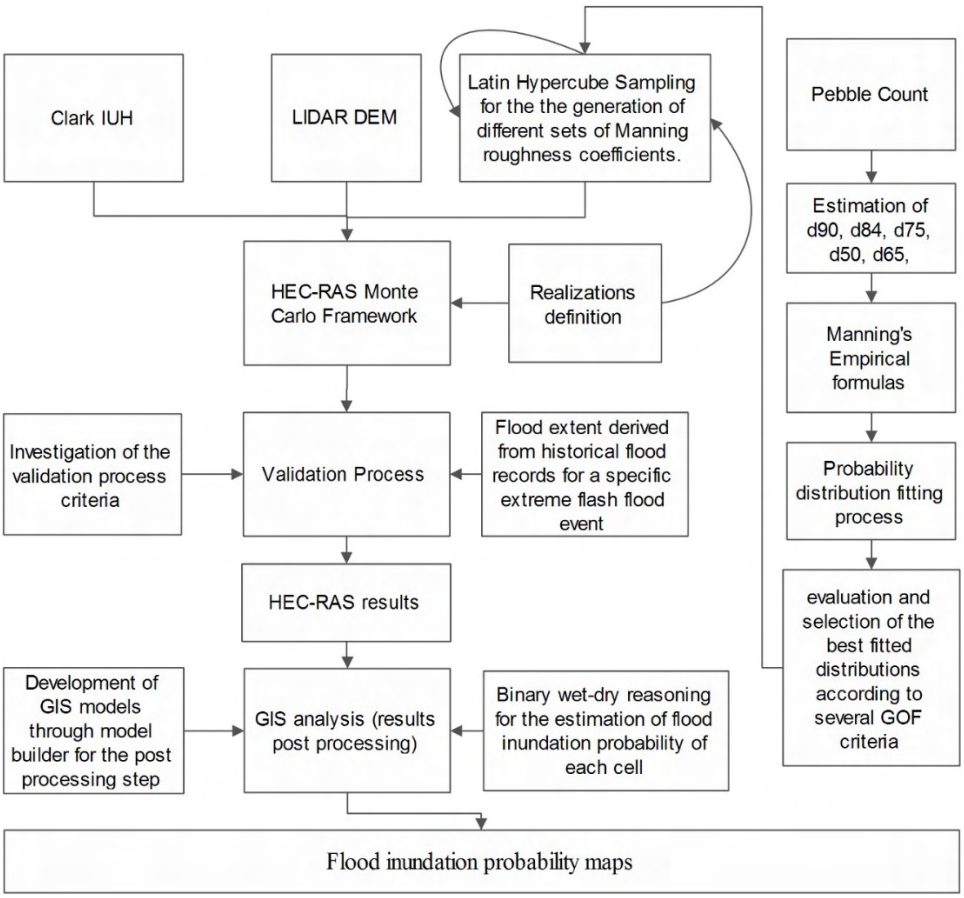

Figure 6.1. Flow diagram of the proposed component.

6.3.1 Hydraulic-hydrodynamic modelling

The main objective of the EU Directive on floods (2007/60) is the production of floodplain maps with the use of hydraulic models that are appropriate and capable for accurate river flood modelling. The use of 1D hydraulic-hydrodynamic model is a common choice in river flood modelling due to its acceptable performance in flood inundation processes, the small input data demands, the low simulation time and the small computing power needed in simulation process (Tsakiris, 2014) (see Chapter 5). However, in the river and riverine areas with complex terrain, the selection of 1D-modelling approach appears to be insufficient and produces erroneous results. Hence, the investigation of different modelling approaches is a mandatory process in order to select the most appropriate modelling approach for flood modelling and mapping (Papaioannou et al., 2016) (see Chapter 5).

Also, new benchmark tests on the evaluation of the modelling approach selection have proved that the combination of complex 2D models with accurate and high-resolution

DEMs can provide a significant improvement in flood inundation modelling and mapping accuracy. However, the use of this modelling configuration can highlight the modelling instabilities due to the grid size selection (Horritt and Bates, 2002; Dimitriadis et al., 2016; Papaioannou et al., 2016) (see Chapter 5). Finally, at ungauged river reaches, the selection of 2-D hydraulic/hydrodynamic models are not favored due to their high data requirements, their complex structure, and the extensive parameterization that is necessary in order to asses accurate results (Tsakiris et al., 2009). Thus, the use of a simple one-dimensional model is proposed for probabilistic flood mapping based on the literature review.

The sensitivity of several parameters such as the use of different hydraulic-hydrodynamic modelling approaches (1D,2D,1D/2D), the use of several river topography spatial resolutions, the use of different mesh/grid resolutions and the use of inline hydraulic structures or not on floodplain mapping and flood inundation modelling at ungauged watersheds, is evaluated and presented in Chapter 5 with respect to the accuracy of the results and other important factors (computational time, computational cost, availability of the models, etc.) that are usually taken into account in typical engineering problems. The evidence from the study presented in Chapter 5 indicates that despite the better results, in terms of accuracy, of two dimensional and coupled hydraulic-hydrodynamic models, all one-dimensional configurations achieved acceptable solutions. Furthermore, the median of the evaluation metric Critical Success Index of 1D modelling approach is included in the range of CSI scores of the other two modelling approaches (2D,1D/2D). Concerning the computational resources, data availability and parameterization, one dimensional models achieved higher scores than the analytical approaches that proved very demanding. Therefore, the use of a simple approach such as the one dimensional hydraulic-hydrodynamic model is proposed for floodplain modelling, for probabilistic flood mapping and mapping for engineering purposes and for calibration and uncertainty analysis investigation.

Moreover, another factor that contributes towards the use of one-dimensional hydraulic hydrodynamic model for probabilistic flood mapping, is the river geomorphology of the study area. The river geomorphology of the selected stream reach is composed of important elevation variations that lead to narrow floodplain. To conclude, the 1-D hydraulic model HEC-RAS is adopted for use on the probabilistic flood inundation mapping component based on the literature review, the results of Chapter 5 and the river and riverine topography of the study area.

The major purpose of the pre-processing stage is to prepare the channel geometry that is going to be imported in the HEC-RAS model. This has been achieved using the HEC-GeoRAS tool in a GIS environment, the high-resolution DEM (LIDAR DEM) and by digitizing all the necessary elements for the accurate representation of the channel geometry and

its characteristics (e.g. stream centerline, flowpaths, cross sections, riverbanks, bridges, etc.). In order to confirm the proper geometry configuration that is ensured by the LiDAR DEM, all cross sections have been manually evaluated for the geometry and the location of the banks.

The initial HEC-RAS configuration consists of cross-sections of variable length (approximately 100m distance) (Figure 5.1) because water surface profiles were found to be highly sensitive to cross-section spacing and DEM accuracy (Sarhadi et al., 2012). Finally, the interpolated cross sections with 1m interval have been created and used for the probabilistic flood hazard mapping at ungauged rivers. This configuration has been applied in order to use the full potential of the LIDAR DEM accuracy in the generated river geometry, to minimize the differences between each cross section and to include the complexity of the river and riverine area in the analysis. Furthermore, this configuration is used due to the nature of the selected hydraulic hydrodynamic model (1D) in order to increase the stability of the system and the accuracy of the outcomes.

Finally, all pre-processed river and floodplain geometry has been inserted to HEC-RAS.

The HEC-RAS modelling stage consists of the flood inundation modelling and mapping using HEAC-RAS model. This stage demands a variety of input data and several parameter configurations such us cross-section and floodplain topography, inflow data, boundary conditions, inline structures configuration (bridges) and the friction parameter determination regarding Manning's roughness coefficient (*n*) values. Many recent studies use 1D hydrodynamic models with steady state flow conditions for probabilistic flood hazard mapping (e.g. Bales and Wagner, 2009; Kizko et. al., 2013; Dimitriadis et. al., 2016; Romanowicz and Kizko, 2016). In the work of Pappenberger et al. (2005), HEC-RAS 1D hydrodynamic model has been used with unsteady state flow conditions but, the iterations where very unstable (only 52,000 were stable from the total 1,600,000 simulations) and several parameters were optimized in order to achieve acceptable results.

In order to achieve consistent unsteady flow simulations, some major modifications in the modelling configurations are: 1) avoidance of "low flow" periods and uneven changes in the hydrograph by adjusting it; 2) changes in river and riverine geometry, i.e. addition of extra cross-sections, deletetion of cross sections, exclusion of irregular geometry points in specific cross sections or, in case of significant drops in elevation, smoothing of the cross sectional geometry by including weirs or by increasing the base flow; 3) implementation of an extensive investigation of the time step in order to achieve the best fit for all possible configurations; 4) application of several parameters optimizations; 5) changes in inline/lateral structures by adjusting the geometry, the wier/gates parameters, and the simulation step; 6) adjustment of the Manning's *n* value since low or high values may result in instabilities, e.g. Manning's *n* value instabilities can affect the modelling

process by providing lower depths, increase of the stage, large attenuation of the hydrograph as it moves downstream, supercritical flows; 7) implementation of an extensive investigation of the initial conditions.

The proposed component deals with the implementation of probabilistic flood inundation mapping at ungauged streams due to roughness coefficient uncertainty in hydraulic modelling. To maximize the usefulness of probabilistic flood hazard assessment, the component is based on a simplified methodology for ungauged catchments and its application is feasible for practical engineering purposes. The applied component uses steady state flow conditions. The selection of steady state flow conditions has been based on the difficulties in the application of unsteady state flow conditions, as described in the previous paragraphs, and the severe lack of data that prevent the use of complex modelling configurations.

In the simulations, the upstream boundary condition has been set to the maximum discharge value (i.e. 490.43 m^3/s) and the downstream boundary conditions where set according to HEC-RAS manual suggestion for ungauged catchments (critical depth is set equal to the friction slope estimated from the LiDAR DEM). The contraction and expansion values have been set equal to the default contraction and expansion coefficients of 0.1 and 0.3 respectively, for the entire channel, except for the bridges openings where the default values of contraction and expansion coefficients are set equal to 0.3 and 0.5, respectively (Brunner, 2016b). The LIDAR DEM has been used for the determination of the topographic characteristics of all cross sections and the floodplain.

An initial approximation of the roughness coefficient values has been carried out based on field evaluation of the size and type of the bed, banks and over-bank material of the channel (Coon, 1998). However, in order to minimize the high uncertainty related to the roughness coefficient values, the pebble count method and several empirical formulas have been used to estimate the final Manning's *n* values. In Xerias stream reach the Wolman pebble count method was conducted by using a zig-zag pattern and by selecting approximately 958 particles with a step-toe procedure (Figure 3.9), as fully described in Chapter 3. Then, the data collected has been used for the statistical analysis of the particle size and the computation of predefined diameters of d_{50}, d_{65}, d_{75}, d_{84}, and d_{94} (Table 3.3). Several empirical formulas recommended in the international literature for the estimation of Manning's roughness coefficient (*n*) values, mainly for gravel and cobble-bed streams (Table 3.2) have defined the choice of the predefined size diameters. The Manning's roughness coefficient has been estimated using these empirical formulas, as described in Chapter 3. Afterwards, the empirical distribution of Manning's roughness coefficient (*n*) estimated values has been used in order to investigate the fitting of several theoretical probability distributions (e.g. Normal, Lognormal, Gamma, Logistic).

The results of the distribution fitting process have been evaluated with the use of many goodness-of-fit statistics and criteria (Table 6.1) (Venables and Ripley, 2002; R Core Team, 2017). Figure 6.2 presents the comparison of the cumulative distribution function of the fitted theoretical probability distributions to the empirical distribution of the estimated Manning's n values. Based on the results presented in Figure 6.2, the Lognormal and Gamma distributions appear to fit better than the other ones and should be used for the simulation of the empirical probability distribution of Manning's values.

Nevertheless, because of the small sample of roughness values, apart from the visual inspection of the fitting of theoretical probability distributions to the empirical distribution, various goodness-of-fit statistics and criteria (Table 6.1) have been used for the non-subjective choice of the "best" fitted distribution. These results indicated that if the judgment of the theoretical distribution is based on the Kolmogorov-Smirnov test, the Logistic and the Weibull distributions should be selected as "best" choices. The Lognormal distribution best fits the empirical derived Manning's *n* distribution based on the goodness of fit criteria of Akaike Information Criterion (AIC) and Bayesian Information Criterion (BIC). Moreover, the Gamma distribution is another possible choice after the Lognormal distribution (Table 6.1).

Finally, based on the optimum theoretical probability distribution (Lognormal) several Manning's (*n*) value data sets have been generated with the use of Latin Hypercube Sampling generator process. The optimum selection of the theoretical distributions has been used for the generic applicability of the proposed component for uncertainty estimation of flood inundation area due to roughness coefficient values. In addition, for sensitivity analysis purposes, the use of Gamma and Weibull probability distributions resulted in acceptable values in the statistical analysis (Table 6.1, Figure 6.2).

The goodness of fit statistics of Cramer-von Mises and Anderson –Darling are alternative tests of the Kolmogorov-Smirnov test. The selected goodness of fit statistics have low performance on small samples but they are extremely precise for large and very large sample sizes (Razali and Wah, 2011; González-Val et al., 2015). However, the goodness of fit criteria of AIC and BIC attempt to resolve a problem by introducing a penalty term for the number of parameters in the model and are based on the whole data sample. Moreover, both goodness of fit criteria implement a trade-off between the goodness of fit of the model and the complexity of the model. Therefore, the selection of the proposed distributions has been based mainly on the goodness of fit criteria AIC and BIC. Finally, the use of Uniform probability distribution has been examined and evaluated for the generation of various roughness coefficient data sets based on findings from other studies (e.g. Di Baldassarre et al., 2010; Kiczko et al., 2013).

Table 6.1. Evaluation criteria of the applied theoretical probability distributions

Distributions	Goodness of fit statistics			Goodness of fit criteria	
	Kolmogorov-Smirnov	Cramer-von Mises	Anderson -Darling	AIC	BIC
Normal	0.1307	0.1008	0.6818	97.5191	-95.337
Lognormal	0.1458	0.0793	0.5153	101.437	-99.2552
Exponential	0.4239	0.8333	4.1749	74.8262	-73.7352
Gamma	0.131	0.08	0.5303	100.762	-98.5796
Beta	0.1304	0.0801	0.5327	100.673	-98.4905
Uniform	0.3358	0.7077	inf	NA	NA
Logistic	0.1292	0.0867	0.625	96.6285	-94.4465
Cauchy	0.2002	0.137	0.9604	87.7592	-85.5771
Weibull	0.1296	0.0848	0.5794	98.6621	-96.48

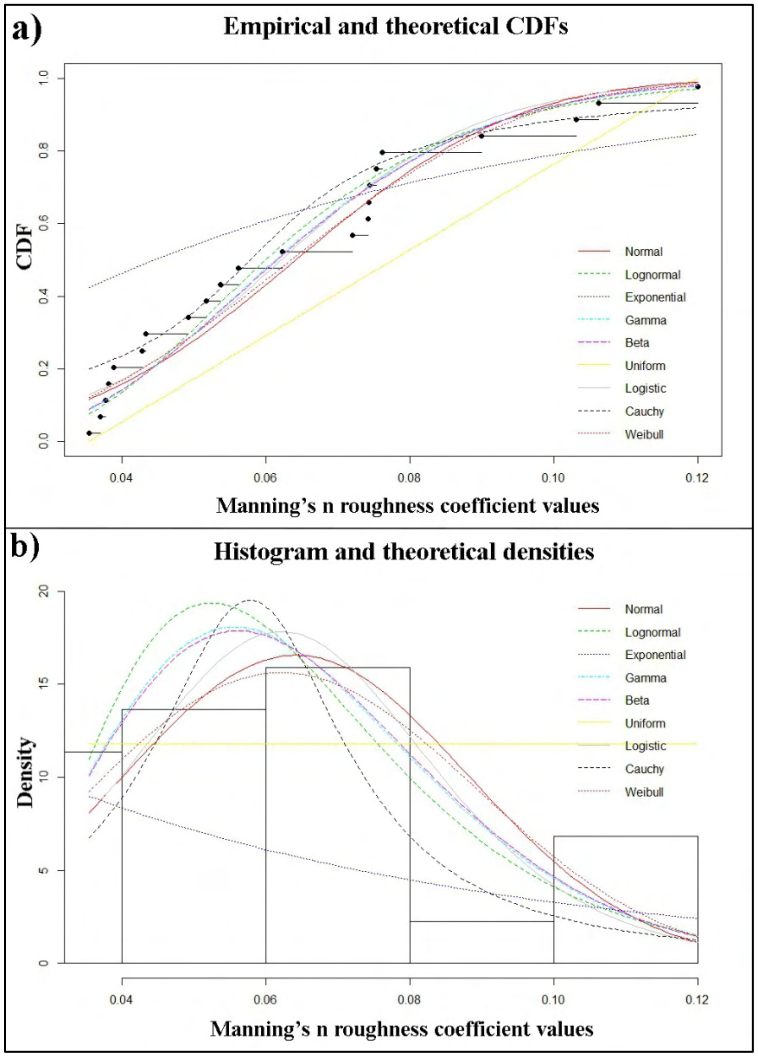

Figure 6.2. Distribution fitting graphs: Empirical and theoretical CDFs (a) and histogram and theoretical densities (b).

6.3.2 HEC-RAS Monte-Carlo component

This study presents an automated HEC-RAS probabilistic flood inundation component for roughness coefficient uncertainty analysis and calibration at ungauged watersheds. The main core of the component is based on the handling of the HEC-RAS model using Excel VBA routines. The outcomes of the hydraulic-hydrodynamic modelling are linked within a GIS environment (in ArcGIS) where several geoprocessing tools combined into model builder platform for the production of the flood probability maps (Figure 6.1). The component is capable of providing Monte-Carlo simulations experiments by operating several processes and using automated data management within HEC-RAS model (Figure 6.1).

The entire code flow, the VBA routines and the architecture of the component have been created by the author with exception on some VBA modules and parts of the code that rely on the work of Goodell (2014). The application of the proposed component is based on the following steps: 1) import the flood extent area; 2) modify the number of the preferred acceptable simulations (realizations) for probabilistic flood inundation mapping; 3) import preferred Manning roughness coefficients data sets; 4) select a favored statistical criterion based on the inherent calibration process for uncertainty analysis due to roughness values; 5) generate flood probability maps using the GIS geoprocessing models.

The flood extent area is imported to the component as values of the wetted area of each cross section. The estimation of each cross section flood extent can be achieved by using simple GIS procedures such as erase or clip. The number of the preferred acceptable simulations (realizations) for probabilistic flood inundation mapping can be adjusted with a simple change in excel environment. The generation of several Manning roughness coefficients data sets is based on Latin Hypercube Sampling (LHS) technique where the best fitted theoretical probability distribution is used. Then, the Manning roughness coefficient data sets are imported into the component for the application of HEC-RAS Monte Carlo simulations. A major advantage of LHS, among other generators used for Monte-Carlo integrations, is that the generated samples are created using all parts of the probability distribution and for n random numbers from the distribution, the distribution is divided into n intervals of equal probability $1/n$ (Millard, 2013). Thus, the use of LHS ensures that the ensemble of random numbers is representative of the real variability. According to McKay et al. (1979), LHS is considered as a stratified sampling method without replacement.

The use of qualitative criteria – skill scores is a typical approach followed at ungauged streams for the evaluation of a simulated area compared to an observed area because of the difficulties generated by the lack of data. The selection of skill scores as evaluation

metrics usually involves the use of 2x2 contingency table (or confusion matrix). Normally, these criteria depend on the contingency table matching agreement by utilizing observed and estimated floodplain areas. The use of such techniques can provide valuable information on how well the simulated flood extent munches the observed one (Horrit and Bates 2001; Horritt and Bates, 2002; Aronica et al., 2002; Alfieri et al., 2014; Nguyen et al., 2015; Papaioannou et al., 2016; Altenau et al., 2017). With the use of the initial HEC-RAS configuration, several statistical quantitative metrics (e.g. as the MSE, RMSE, MAE, Bias, MdAPE, etc) and the qualitative metric of CSI have been examined. All proposed evaluation metrics have been used for the determination of the acceptable simulations and to propose the optimum metric. The application of the metrics is based on the comparison between the simulated and the observed flooded area (Figure 5.1). All the above mentioned metrics have been included in the proposed component for accurate Monte-Carlo experiments.

Based on the presented input data and the settings that the user has selected (e.g. determined observed flood extent, choice of validation criterion), a new roughness coefficient value is selected for iterative modelling. In each iteration, the component accepts or rejects the simulation according to the selected criterion and the determined threshold level. After this process, a new simulation is performed using a new roughness *n* value. Finally, the component terminates the entire process when the number of realizations fulfil the operator's needs and set up criteria for acceptable probabilistic flood inundation mapping realizations (e.g. number of realizations).

In the analysis of the evaluation metrics, it was observed that, the metrics containing median values had a better response compared to the others and, this was also justified by the river and riverine topography and the characteristics of the studied flood event (i.e. small flood extent, small changes in the floodplain, flood inundation in specific areas). The criteria that have been tested are the following: Median absolute percentage error (MdAPE); Mean Square Error (MSE); Median Absolute Error (MdAE); Mean absolute error (MAE); Root Mean Square Percentage Error (RMSPE); Root Median Square Percentage Error (RMdSPE); Symmetric Median Absolute Percentage Error (sMdAPE); Mean absolute percentage error (MAPE) ; symmetric MAPE (sMAPE); Root Mean Square Error (RMSE); Standard Deviation of residuals; Average of residuals; Median of residuals; Total BIAS. Details on the criteria tested and their mathematical expression can be found in the works of Hyndman and Koehler, (2006), Dawson and his associates (Dawson et al., 2007) and Jolliffe and Stephenson, (2011). An example of the sensitivity analysis implementation in order to distinguish the preferred criterion is presented in Table 6.2.

In this study, the unbiased qualitative criterion of Median Absolute Percentage Error (MdAPE) (Hyndman and Koehler, 2006) has been selected for the validation of the component. Accordingly, the selection of the quantitative statistical criterion MdAPE has

been based on several sensitivity analysis tests (e.g. Table 6.2), on "Eyeball" verification (i.e. distribution resemblance) using the CSI qualitative criterion (Figure 6.3), on the characteristics of the selected evaluation metric and the studied flood event, and on the author's personal judgment and experience on the study area characteristics (e.g. parameters, nature of the study event, and lack of data). The MdAPE equation, that is taken into account the simulated and observed flood areal extent, is expressed as follows:

$$\mathrm{MdAPE} = \mathrm{median}\left(\left|\frac{100(\mathrm{Y_t} - \mathrm{F_t})}{\mathrm{Y_t}}\right|\right) \tag{6.1}$$

where Y_t is the observed flood extent; and F_t is the simulated flood extent for all cross-sections.

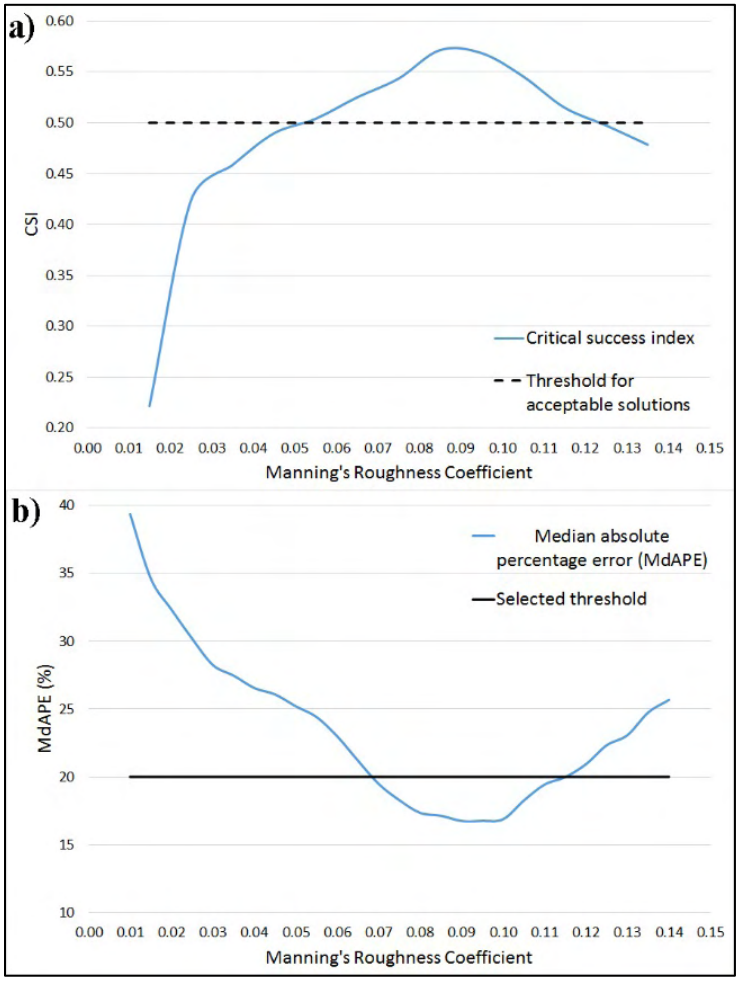

Figure 6.3. HEC-RAS model responses to changes in roughness coefficient values (Manning's n), a) in terms of Critical Succes Index, b) in terms of Median Absolute Percentage Error (MdAPE) and selected threshold for acceptable behavioural models respectively.

Table 6.2. Example of the examined statistical criteria

Manning's n roughness coefficient values	Statistical criteria						
	MdAPE	**MSE**	***MdAE***	***MAE***	***RMSPE***	***RMdSPE***	**MAPE**
0.01	39.4	2504	34.3	39.8	56.7	39.4	45.6
0.02	32.3	1867	24.5	33.3	53.0	32.3	40.2
0.03	28.2	1721	22.0	31.0	54.0	28.2	38.6
0.04	26.5	1769	21.5	30.3	56.2	26.5	38.3
0.05	25.2	1845	21.5	30.3	58.5	25.2	38.7
0.06	23.0	1964	20.0	30.0	62.2	23.0	39.0
0.07	19.5	2091	16.4	29.1	68.0	19.5	39.0
0.08	17.3	2203	15.1	28.8	69.7	17.3	39.1
0.09	16.7	2297	14.3	28.6	71.9	16.7	39.5
0.1	16.9	3269	14.5	35.4	95.8	16.9	52.4
0.11	19.4	3831	16.4	39.4	105.9	19.4	59.0
0.12	20.9	4359	17.9	43.0	114.4	20.9	64.8
0.13	23.1	5284	20.3	49.1	124.7	23.1	73.8
0.14	25.7	7155	25.3	56.9	148.3	25.7	87.0

Manning's n roughness coefficient values	Statistical criteria						
	sMdAPE	**sMAPE**	**RMSE**	***Median of residuals***	***Standard Deviation of residuals***	***Average of residuals***	**Total BIAS**
0.01	47.5	51.2	50.0	34.3	30.3	39.8	0.77
0.02	37.6	42.5	43.2	24.5	27.5	33.3	0.85
0.03	32.3	38.5	41.5	22.0	27.6	31.0	0.90
0.04	30.1	36.4	42.1	21.5	29.2	30.3	0.93
0.05	28.2	35.3	43.0	21.5	30.5	30.3	0.97
0.06	24.8	33.7	44.3	20.0	32.6	30.0	1.01
0.07	20.9	31.2	45.7	16.4	35.2	29.1	1.06
0.08	18.8	29.5	46.9	15.1	37.1	28.8	1.11
0.09	17.7	28.4	47.9	14.3	38.5	28.6	1.15
0.1	17.8	32.8	57.2	14.5	44.9	35.4	1.26
0.11	19.3	35.2	61.9	16.4	47.7	39.4	1.32
0.12	20.9	37.4	66.0	17.9	50.1	43.0	1.37
0.13	23.8	41.3	72.7	20.3	53.7	49.1	1.45
0.14	24.88	45.2	84.6	25.3	62.6	56.9	1.54

The threshold of MdAPE for the acceptable runs was set to 20% (with a best fit to 16%) after First level of sensitivity analysis of the employed statistical criteria (Figure 6.3). Figure 6.3 presents the MdAPE and CSI variation results with the roughness coefficient values (Manning's n) and the selected threshold for acceptable behavioral models. Furthermore, it should be mentioned that the entire validation process is based only on the comparison between simulated flooded areas and historical data of the flood event due to the ungauged nature of the study watershed/stream reach. Unfortunately, the majority of relative data concerning the study flood event are missing (e.g. measured water depth in several locations, flow rate measurements, accurate rainfall data by various meteorological stations, roughness coefficient measurements, etc.). From the data collected concerning the study flood event (see Chapter 2), the only data that can insure appropriate validation of the system is the reconstructed historical flood data.

Finally, in the post-modelling stage, the results of HEC-RAS Monte-Carlo component are imported into a GIS for the generation of the flood extent using specific models-scripts created in the ArcGIS ModelBuilder environment (Figure 6.4). Hence, the graphical representation of the component is achieved through GIS. The main objective was to convert the HEC-RAS outcomes (i.e. flood extent polygons and raster water depth files) into probabilistic flood inundation maps based on (different) roughness values. This was achieved by using a binary wet-dry reasoning in order to estimate the flood inundation probability of each cell (Figure 6.5a). Thus, the modelled probability of inundation is estimated by converting each ensemble member of flood extent to a binary wet–dry map, calculating the number of simulations in which a node is wet, then dividing this by the number of ensemble members (Figure 6.5b) (Horritt, 2006). Eventually, different probability maps have been generated based on the acceptable realizations and the statistical criterion used. For computational purposes the probability maps were classified in 10 probability classes, i.e. 0-10%, 10-20%, 20-30%, 30-40%, 40-50%, 50-60%, 60-70%, 70-80%, 80-90%, 90-100%.

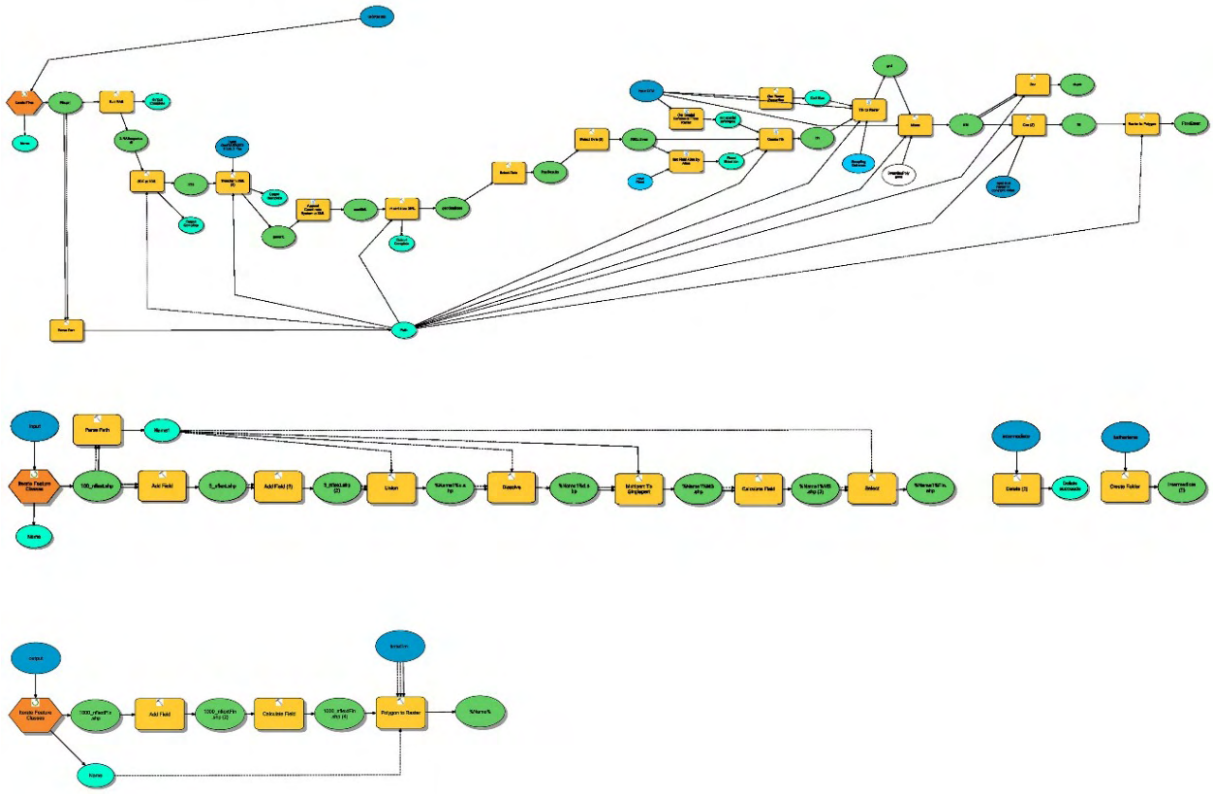

Figure 6.4. GIS geoprocessing models that developed in ArcGIS model builder environment for the production of the flood probability maps.

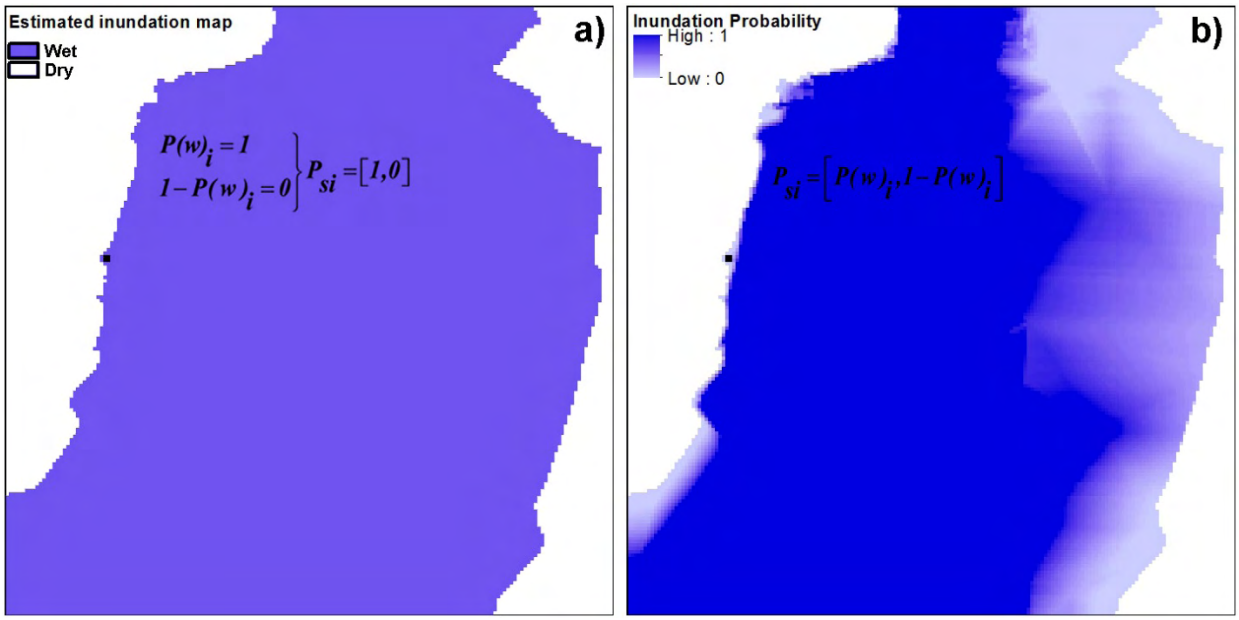

Figure 6.5. Food extent representation with the wet/dry reasoning (a) and the probabilistic (b).

6.3.3 Sensitivity and stability analysis

The sensitivity analysis includes the investigation of several parameters involved in the HEC-RAS Monte-Carlo component to define the best modelling configuration of the component. The different configurations employed for sensitivity analysis purposes are:

1. Different realization sets applied using the best fitted probability distribution (i.e. Lognormal) for Manning's n sampling: 100, 200, 500, 1000, 2000, 5000 realizations,
2. Gamma, Weibull, and Uniform probability distributions for Manning's n sampling have also been examined for 1000 realizations,
3. Three validation threshold values of MdAPE, 22%, 20% and 18% have been examined,
4. Various river cross section spacings have been examined with distance varied from 1 m to 32 m (i.e. 1 m, 2 m, 4 m, 8 m, 16 m and 32 m).

An imperative step in Monte Carlo simulations such as the proposed component is the examination if the component produces reproducible and similar results for the same configuration. Finally, the optimum configuration of the component, derived from the sensitivity analysis, has been then used to test the stability of the component. Five different runs have been employed and the results are compared.

6.4 Results

A HEC-RAS Monte-Carlo component has been developed for flood probability mapping, at ungauged catchments and assesses the uncertainty related to the roughness coefficient. The extreme flash flood event of the October 9th, 2006 has been used for the evaluation of each individual outcome. The comparison of the simulated and the observed flooded area was carried out using MdAPE quantitative statistical criterion (threshold level 20% and best score 16%). The final flood probability maps were classified in 10 probability classes (0-10%, 10-20%, 20-30%, 30-40%, 40-50%, 50-60%, 60-70%, 70-80%, 80-90%, 90-100%) for comparison purposes. All the flood probability results were examined and compared based on their spatial distribution and the proposed probability classes categorization. In order to achieve the optimum configuration of the component, several sensitivity analysis tests have been applied. Finally, the stability of the component has been examined using five different configurations that use the settings of the optimum configuration (1000 realizations, Lognormal distribution, LHS, MdAPE with 20%

threshold) with different seed value in LHS. The majority of the results are based on an ensemble of 1000 simulations.

The first sensitivity analysis is based on the number of realizations (100, 200, 500, 1000, 2000, 5000). In this analysis, the configuration of the component uses the Lognormal distribution for the realization of the Manning's n values; 1m cross section spacing; MdAPE threshold is set to 20% for the selection of acceptable simulations; and acceptable realizations number of 100, 200, 500, 1000, 2000, 5000. The results of the first sensitivity test showed that the selection of the number of realizations affects the flood probability map. The optimum choice of acceptable realizations is 1000 realizations, as the system becomes insensitive for larger number of realizations (Table 6.3, Figure 6.6).

Table 6.3 and Figure 6.6 present the results of the first sensitivity analysis test that take into account the spatial information of each class in comparison to the 5000 realizations results. In particular, the outcomes of the first sensitivity analysis shows that the difference among the flood inundation probability map of 5000 realizations and the 100, 200, 500, 1000 and 2000 realizations is 4.94%, 2.66%, 1.49%, 0.63% and 0.59% respectively. A consistent power pattern is observed between the number of acceptable realizations and the deviation of the results from the 5000 realizations run (Figure 6.6).

Table 6.3. Spatially distributed comparison (sensitivity analysis) based on the number of acceptable realizations.

Number of acceptable realizations	**100**	**200**	**500**	**1000**	**2000**	**5000**
100	0					
200	5.31	0				
500	5.15	1.88	0			
1000	4.71	3.14	1.84	0		
2000	4.57	2.75	1.44	0.60	0	
5000	**4.94**	**2.66**	**1.49**	**0.63**	**0.59**	**0**

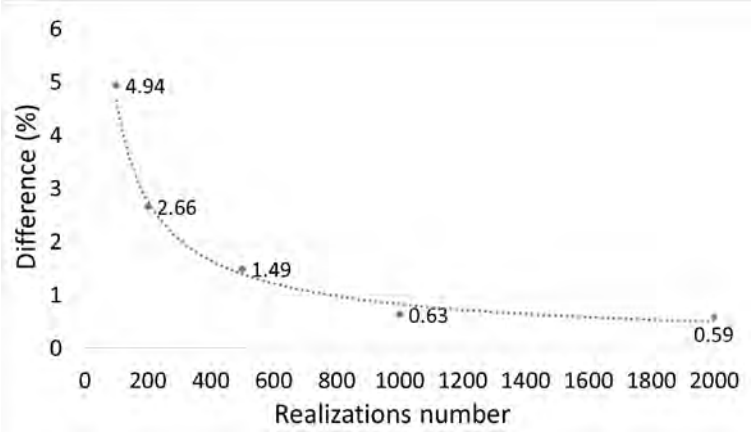

Figure 6.6. Sensitivity analysis on the number of acceptable realizations comparing to the 5000 acceptable realizations based on the spatial distribution.

Additionally, Table 6.4 presents the flood inundation probabilities classes for various number of realizations. These results indicate that the probability classes of 0-10, 10-20, 20-30% have the larger differences varying from 0.78 to 1.42 %. Despite the fact that the total differences, when comparing results only from the tables of distribution classes, vary from 0.68 to 3.65 %, when the spatial distribution of each class is taken into account in the comparison, the total difference is rising and ranges from 0.59 to 4.94 %. Figure 6.7 presents the flood inundation probability map for 1000 realizations and for comparison the "observed" estimated flood inundation area for the studied flood event. Figure 6.8 presents the spatial distributed difference between the flood probabilities of 100 and 5000 acceptable realizations. In the following sensitivity analysis, the optimum number of acceptable realizations (i.e. 1000 realizations) has been used.

Table 6.4. Flood inundation probabilities classes (%) for various realizations.

Flood inundation probabilities classes (%) \Number of acceptable Realizations	**100**	**200**	**500**	**1000**	**2000**	**5000**
100-90	78.72	79.34	78.82	78.87	78.83	78.83
90-80	0.70	0.96	1.06	0.98	1.02	0.93
80-70	0.95	0.97	0.90	0.84	0.83	0.96
70-60	0.81	1.36	1.14	1.23	1.19	1.28
60-50	1.43	1.63	1.49	1.38	1.32	1.29
50-40	1.72	1.29	1.72	1.65	1.73	1.65
40-30	3.16	2.78	3.04	2.72	2.89	2.86
30-20	3.58	2.78	2.45	2.72	2.78	2.65
20-10	5.33	5.74	5.20	5.06	4.84	4.96
10-0	3.61	3.16	4.18	4.56	4.57	4.58

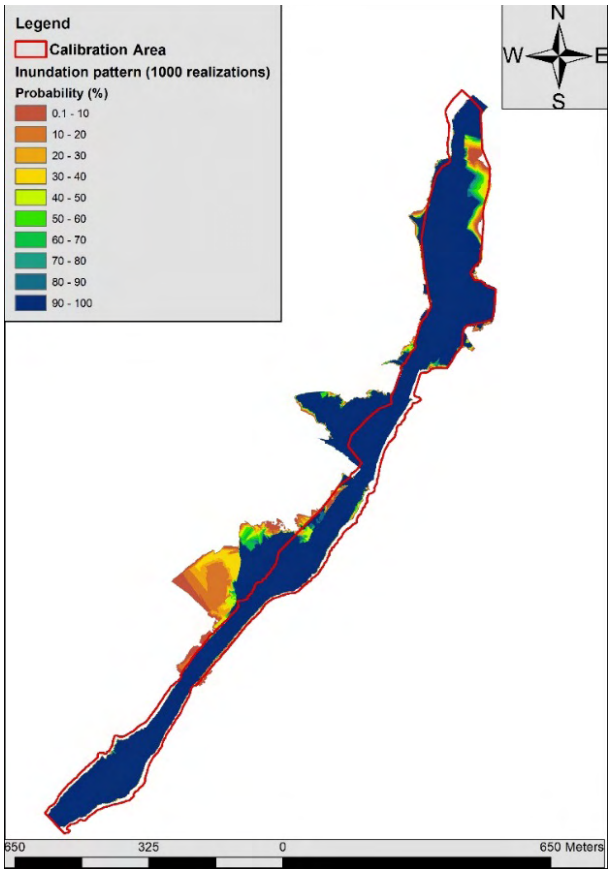

Figure 6.7. Flood inundation probability map for the optimum number of acceptable realizations (i.e. 1000 realizations).

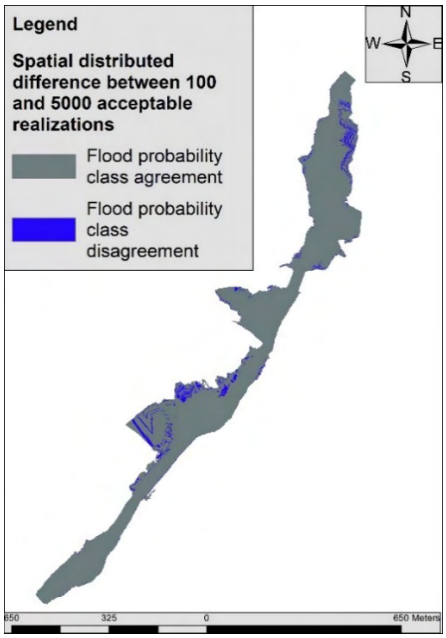

Figure 6.8. Spatial distributed difference between the flood probability maps of 100 and 5000 realizations.

The next sensitivity analysis is using various theoretical probability distributions for the generation of the Manning's n roughness data sets. In this analysis, various theoretical probability distributions have been used and the results have been compared to the results of the simulation using the Lognormal probability distribution. The other elements of the simulation are: 1m cross section spacing; 1000 acceptable realizations and, for validation, the criterion of MdAPE with threshold was set to 20%. Based on the statistical goodness-of-fit criteria, the probability distributions that are satisfactory fitted to the empirical probability distribution, were found to be the Lognormal, Gamma and Weibull probability distributions. Furthermore, a typical probability distribution that has been implemented in similar studies is the Uniform probability distribution (e.g. Dimitriadis et al., 2016) and it is included in the analysis for testing its validity in similar studies. Table 6.5 present the results of the sensitivity analysis based on the choice of theoretical probability distribution compared to the Lognormal theoretical distribution. The outcomes indicate that the flood inundation probability maps using the Gamma, the Weibull and the Uniform probability distributions differ from the flood inundation probability map of the "best-fitted" Lognormal probability distribution by 1.53%, 4.48% and 19.22%, respectively. Hence, the selection of the appropriate theoretical probability distribution for the generation of the Manning's roughness coefficient is a crucial choice that can severely affect the accuracy of the flood probability maps.

Table 6.6 presents the flood inundation probabilities classes (%) of all theoretical probability distributions used in the analysis. The results of Table 6.6 reveal that the largest differences between the maximum differences in the flood inundation probability classes are observed for the probability classes of 0-10, 10-20% with values of 2.88% and 3.71 %, respectively. When comparing the results only from the tables of distribution classes, the total differences vary from 1.59 to 14.03 %. When the spatial distribution of each class is taken into account, the total difference rises and ranges from 1.53 to 19.4 % (Table 6.5). The flood probability distribution maps derived by the Lognormal and the Uniform distributions are presented for comparison in Figure 6.9. Significant differences are shown between all the flood probability classes except for the 90-100% probability class.

Table 6.5. Spatially distributed comparison based on the theoretical probability distribution choice.

Theoretical Probability Distributions differences (%)	**Lnorm**	**Gamma**	**Weibull**	**Uniform**
Lnorm	**0**			
Gamma	**1.53**	0		
Weibull	**4.48**	3.23	0	
Uniform	**19.22**	19.31	18.92	0

Table 6.6. Flood inundation probabilities classes (%) of all theoretical probability distributions.

Flood inundation probabilities classes (%) \ Theoretical Probability Distributions	**Lognormal**	**Gamma**	**Weibull**	**Uniform**
100-90	78.87	78.85	79.16	79.61
90-80	0.98	0.94	1.08	1.85
80-70	0.84	1.01	1.09	2.14
70-60	1.23	1.27	1.46	2.28
60-50	1.38	1.30	1.41	2.84
50-40	1.65	1.73	1.66	2.19
40-30	2.72	3.18	2.72	3.78
30-20	2.72	2.42	2.45	2.29
20-10	5.06	4.69	4.96	1.35
10-0	4.56	4.61	4.01	1.68

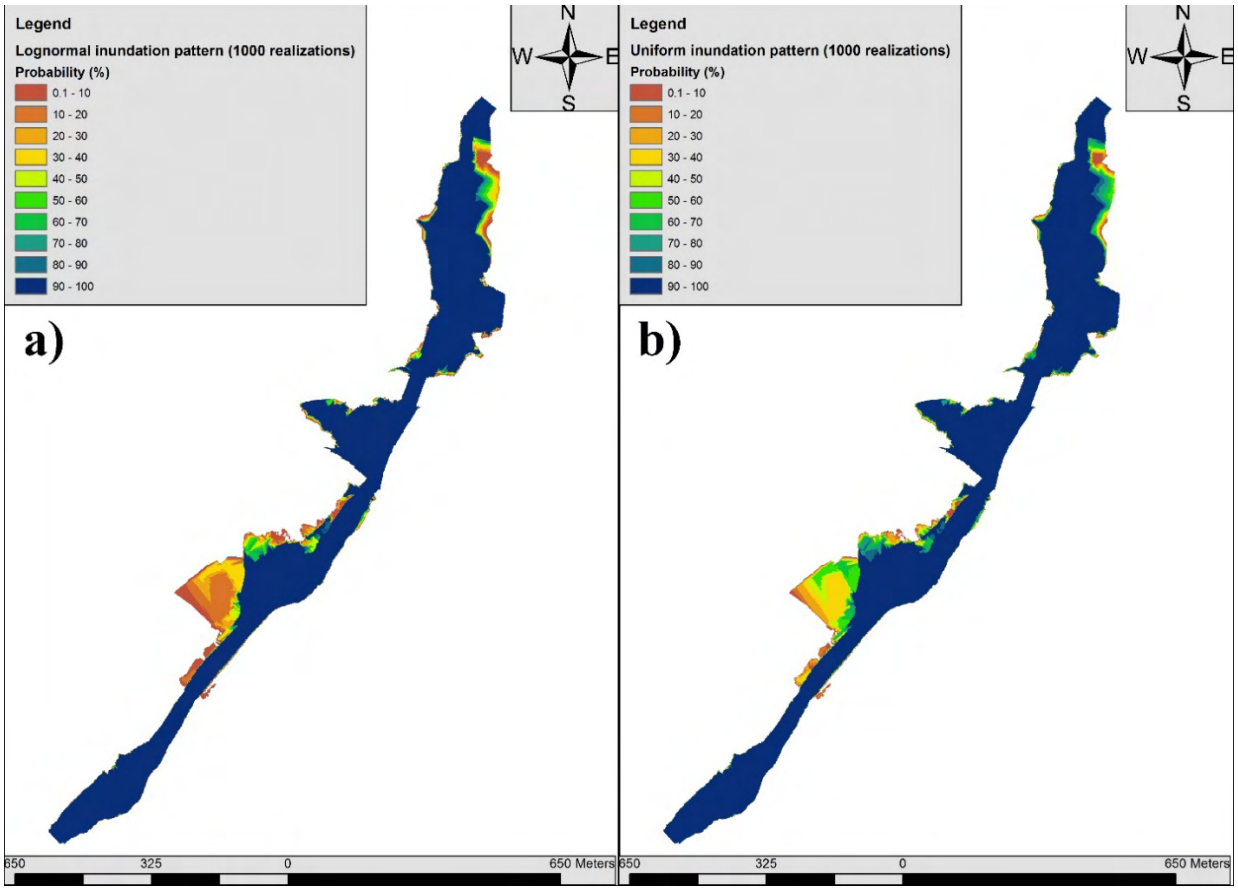

Figure 6.9. Visualization of the flood probability distribution maps derived using the Lognormal and the Uniform distributions.

The next sensitivity analysis is based on the selection of different threshold levels of the statistical criterion MdAPE used for the validation of the acceptable solutions. In this analysis the configuration of the component consists of the Lognormal distribution for the sampling of Manning's roughness coefficient n and have the following elements; 1m cross section spacing; 1000 acceptable realizations and; as validation criterion, the MdAPE with threshold was set to 18%, 20% and 22%. The sensitivity analysis of the threshold level showed that the flood probability maps are sensitive to threshold changes (Table 6.7, Figure 6.10). Specifically, the results of flood inundation probability map using 18% and 22% of MdAPE threshold differ from the respective results using 20% MdAPE threshold by 11.73% and 10.69% , respectively (Table 6.7, Figure 6.10). The results of Table 6.8 indicate that as the threshold level increases the difference in the flood probabilities classes of 0-10, 10-20, 20-30 and 30-40% rises, while the probability class 90-100% decreases. Figure 6.11 illustrates the flood probability distribution maps derived by the threshold level of 18%, 20% and 22%.

Table 6.7. Spatially distributed comparison based on the threshold level.

MdAPE threshold level differences (%)	18	20	22
18	0		
20	11.73	0	
22	15.06	10.69	0

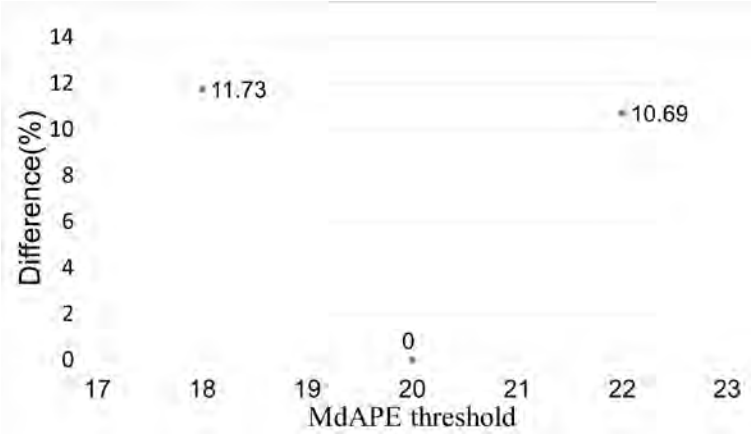

Figure 6.10. Sensitivity analysis on the threshold value of the statistical criterion including the spatial distribution.

Table 6.8. Flood inundation probabilities classes (%) of all threshold value of MdAPE statistical criterion.

Flood inundation probabilities classes (%) \ MdAPE threshold level	MdAPE 18%	MdAPE 20%	MdAPE 22%
100-90	85.02	78.87	75.13
90-80	0.81	0.98	0.88
80-70	0.86	0.84	1.01
70-60	1.02	1.23	1.35
60-50	1.32	1.38	1.44
50-40	1.89	1.65	1.64
40-30	1.39	2.72	2.53
30-20	1.74	2.72	3.82
20-10	3.74	5.06	6.02
10-0	2.20	4.56	6.18

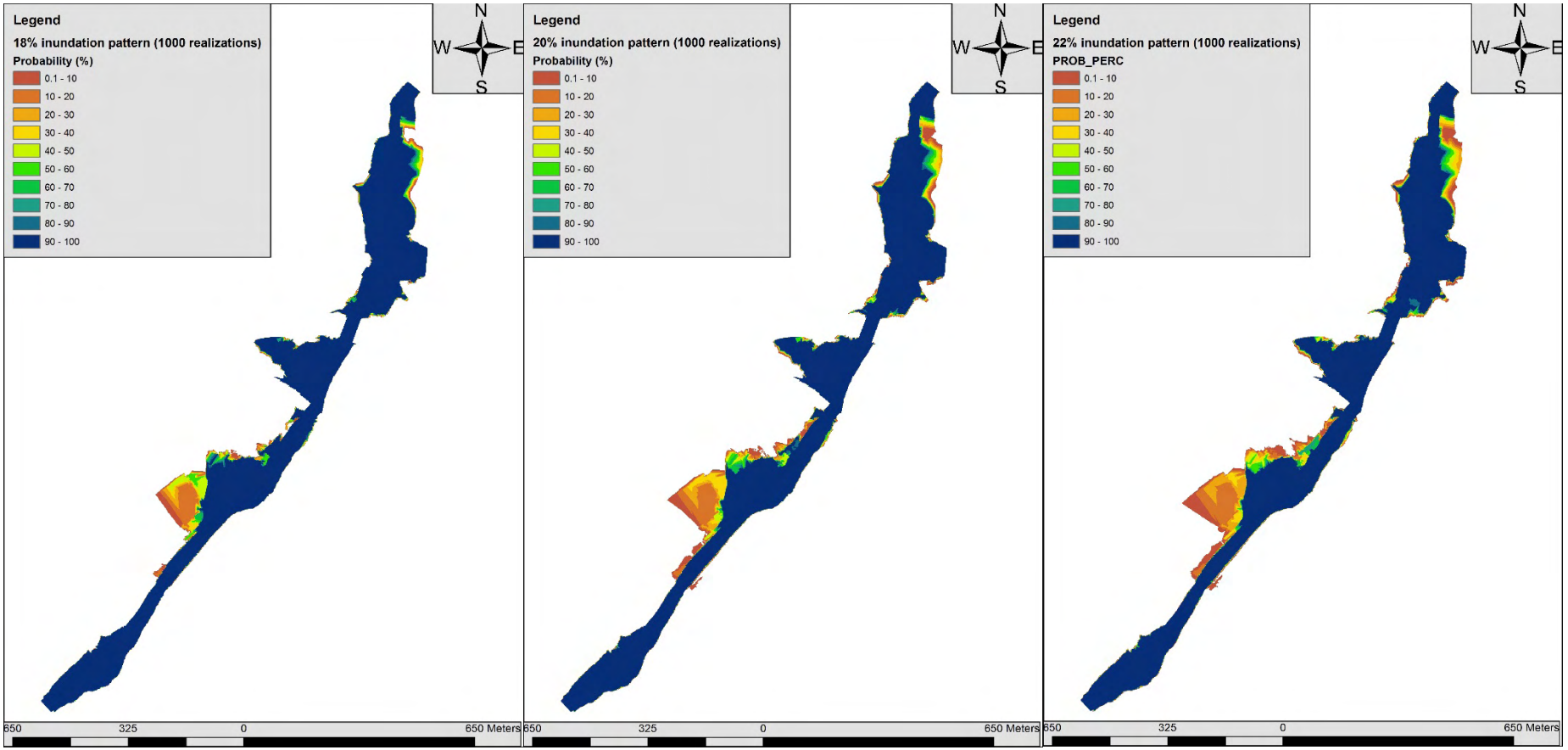

Figure 6.11. Visualization of the flood probability distribution maps derived by the configuration with a threshold level of 18%, 20% and 22% respectively from left to right.

The last sensitivity analysis is based on the selection of different cross section distance intervals (2m, 4m, 8m, 16m, and 32m). In this analysis, the configuration of the component consists of the Lognormal distribution; 1m, 2m, 4m, 8m, 16m and 32m cross section spacing; as validation criterion the MdAPE with threshold was set to 20%; and 1000 acceptable realizations are used. The results indicate that the river cross section distance interval has a significant effect in the flood inundation probability mapping when the distance between the cross sections is equal or larger than 16 m (Figure 6.12). In more detail, the spatial distributed differences between the flood probability map of 1m and the configurations of 2 m, 4 m, 8 m, 16 m, and 32 m are 2.07%, 3.69%, 3.20%, 8.43% and 13.29%, respectively (Figure 6.12). A consistent linear pattern is observed in Figure 6.12 due to the effect of the river cross section spacing in flood probability mapping. The results of Table 6.9 reveal that the largest differences between the maximum values of the flood inundation probability classes are observed at the classes of 0-10, 10-20, 20-30 and 90-100% with values 1.25, 2.53, 1.58 and 1.9%, respectively. When comparing results only from the tables of distribution classes, the total differences vary from 0.8 to 8.22%. If the spatial distribution of each class is taken into account, then, the total probability difference increases from 2.07 to 13.29 %. Finally, Figure 6.13 illustrates the flood probability maps of the configuration that uses 1m cross-section interval comparing to the configuration that uses 32m cross-section interval.

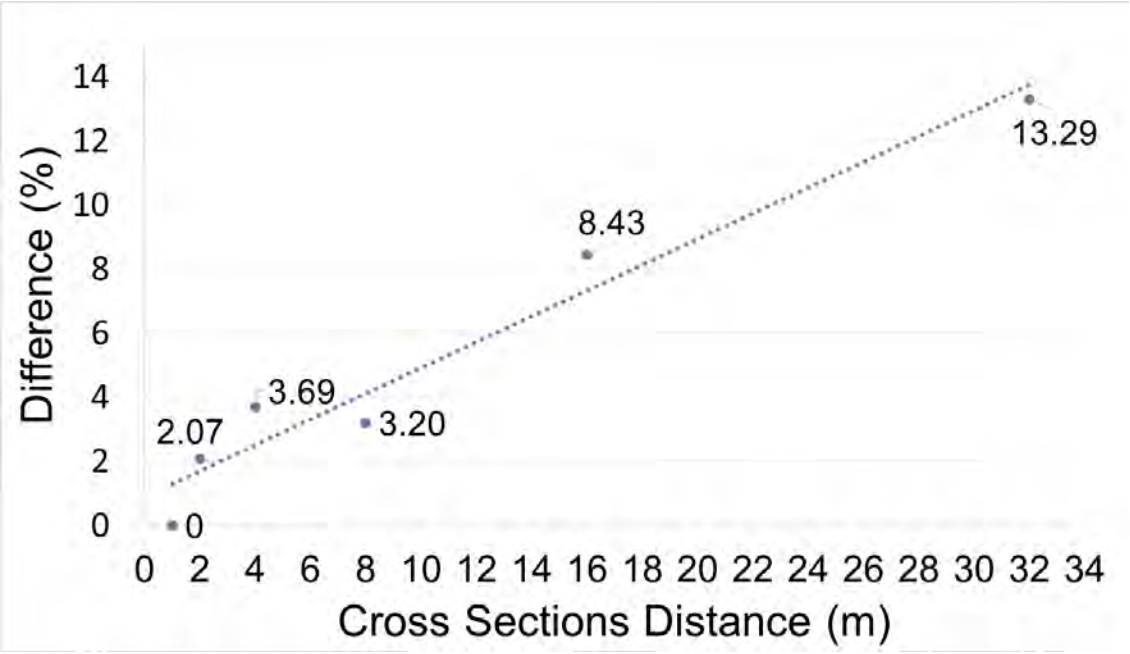

Figure 6.12. Sensitivity analysis on the cross section distance interval including the spatial distribution.

Table 6.9. Flood inundation probabilities classes (%) of all cross section distance intervals.

Flood inundation probabilities classes (%) \ Cross Sections Distance interval	1m	2m	4m	8m	16m	32m
100-90	78.87	79.08	80.31	79.02	80.04	80.77
90-80	0.98	1.02	0.96	0.97	0.95	0.84
80-70	0.84	0.92	0.82	0.87	1.12	1.08
70-60	1.23	1.18	1.21	1.26	1.06	1.08
60-50	1.38	1.38	1.25	1.21	1.46	1.40
50-40	1.65	1.56	1.51	1.58	1.83	2.01
40-30	2.72	2.75	2.37	2.87	2.99	2.69
30-20	2.72	2.77	2.95	2.59	2.64	4.30
20-10	5.06	4.97	4.93	5.27	4.56	2.53
10-0	4.56	4.39	3.70	4.35	3.35	3.31

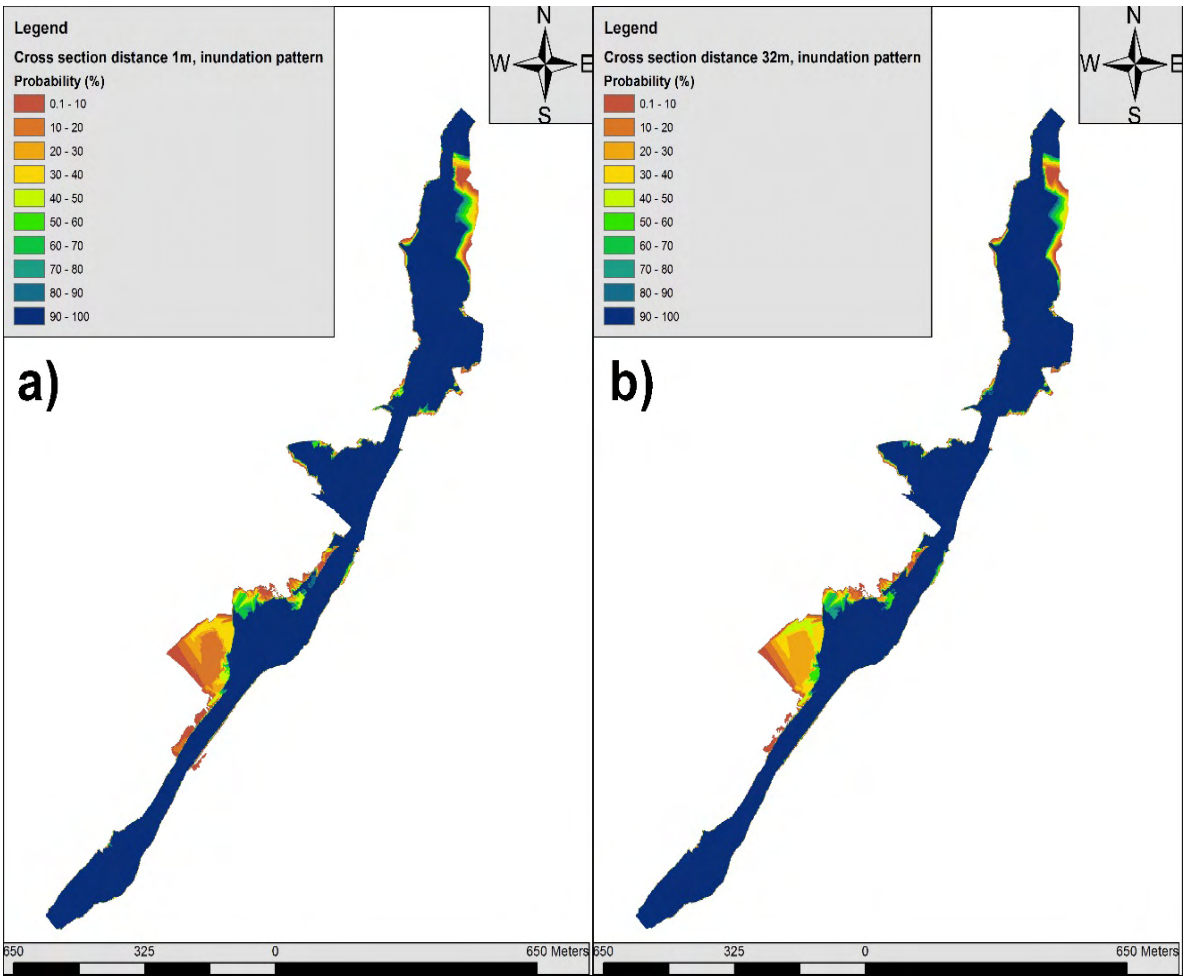

Figure 6.13. Visualization of the flood probability distribution maps derived by the configuration with cross-section spacing of 1m and 32m.

For better understanding of the flood hazard, Figure 6.14 illustrates the flood inundated areas presented in various probabilistic classes overlaid with a high resolution aerial orthophoto in order to emphasize the spatial extension of the flooded areas. The same figure also depicts, for comparison purposes, the optimum deterministic simulation of

HEC-RAS with a red line (Figure 6.14). The distinction of the floodplains in two regions, a wet area (flooded) and a dry area is usually implemented with the use of deterministic flood inundation maps. This binary map is produced by calibration of the HEC-RAS model. The trial and error manual calibration process has been used for the simulation of the examined historical flood inundation event in order to estimate the optimum Manning's n value for the study river reach. As mentioned before, there were neither a water depth data nor official flood extent data or detailed records available from the study event. The only evidence that could be used for calibration purposes was the inundation extent map estimated by the limited data found in public organizations records and the responses of local people during the field survey described in Chapter 2 (black boundary area in Figure 6.14).

Kiczko et al. (2013) claim that the stochastic maps cannot be directly compared with the deterministic maps. Nevertheless, for comparison purposes, the deterministic flood inundation map is assumed to represent flooded areas with a probability of exceedance of 0.9 (Figure 6.15). The optimum estimated Manning's n value based on calibration process using deterministic simulation was 0.09 (Table 3.2, Figure 6.15) and the estimated MdAPE value achieved was approximately 16%. Moreover, in Figure 6.14 each pixel expresses the probability of flooding and incorporates the uncertainty derived by the selection of Manning's n roughness values. In order to generate the specific flood probability map, the optimum configuration has been used (i.e. use of 1000 realizations, use of the Lognormal probability distribution for Manning's n sampling, a threshold of 20% value for the MdAPE criterion, and river cross section spacing of 1m).

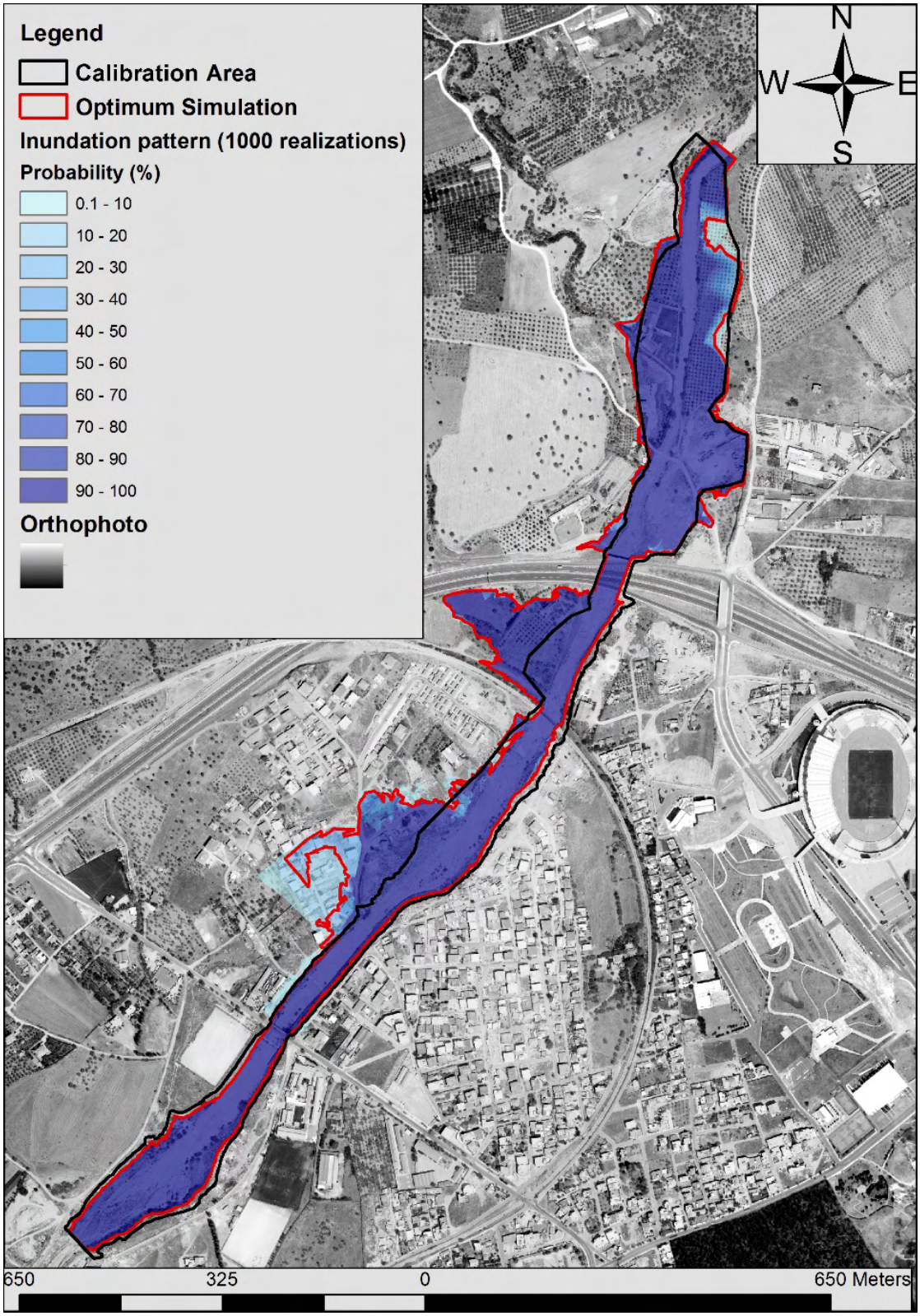

Figure 6.14. Flood inundation map for the best component configuration (i.e. using 1000 realizations, lognormal probability distribution for roughness coefficient generation, MdAPE threshold 20% and 1 m cross section spacing).

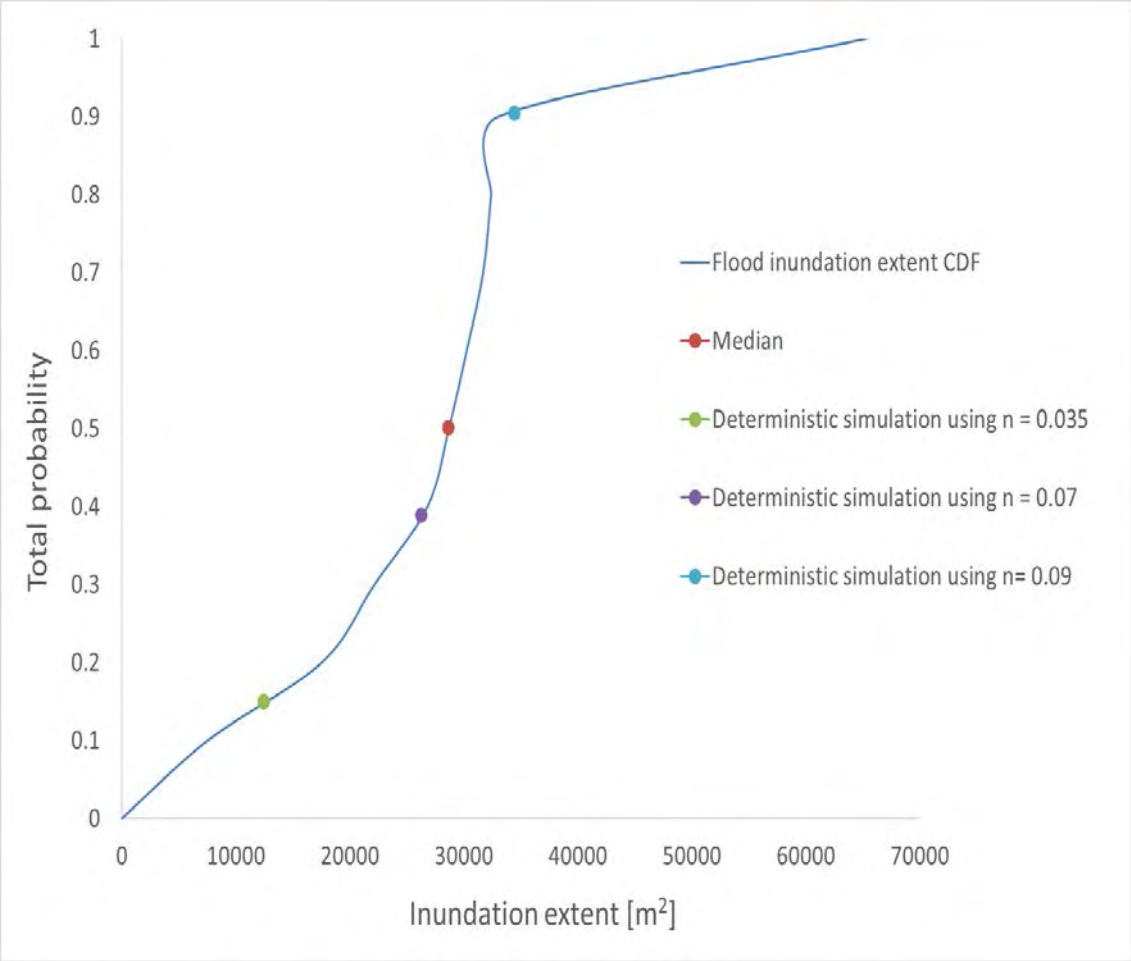

Figure 6.15. Comparison of several deterministic flood extent results based on the cumulative distribution function of the flood extent.

Based on the results of the sensitivity analysis, the optimum configuration of the HEC-RAS Monte Carlo component is the one that uses 1000 relations, Lognormal probability distribution for Manning's n value sampling, the threshold of 20% value of MdAPE, and river cross section spacing of 1m. In order to investigate the stability of the proposed HEC-RAS component configuration, the suggested configuration five different runs have been performed and five flood probability maps have been generated (Table 6.10).
For comparison purposes, the already presented optimum configuration has been used as a base scenario in order to check the spatial distributed differences of the five generated flood probabilities maps. The results that include the spatial distribution of the flood probability classes showed that the proposed configuration deviates from 0.82 to 1.65 % for the five different runs (Table 6.10). These findings suggest that the proposed HEC-RAS Monte Carlo component is stable and gives reproducible results.

Table 6.10. Stability of the proposed HEC-RAS Monte Carlo component. Spatial distributed differences among the five cases and the base scenario.

Number of simulation	Differences with the Base scenario (%)
1st	1.25
2nd	1.07
3rd	1.65
4th	0.82
5th	0.99

6.5 Conclusions

A probabilistic procedure for floodplain inundation mapping was developed and analysed for a reach of the ungauged Xerias stream, Volos, Greece. The developed process evaluated the uncertainty introduced by the roughness coefficient values in flood inundation modelling and mapping. The well-established hydraulic model, HEC-RAS 1D was selected and used with in a Monte-Carlo simulation component. Terrestrial Laser Scanner data had been used to produce a high quality DEM for input data uncertainty minimization and to improve representation accuracy of stream channel topography required by the hydraulic model. Manning's n roughness coefficient values were estimated using pebble count field surveys and empirical formulas. Various theoretical probability distributions were fitted and evaluated on their accuracy to represent the estimated roughness values. Moreover, Latin Hypercube Sampling had been used for generation of different sets of Manning roughness values and finally, flood inundation probability maps had been created with the use of Monte Carlo simulations. Historical flood extent data, from an extreme historical flash flood event, were used for the validation of the method. The calibration process was based on a binary wet-dry reasoning with the use of Median Absolute Percentage Error evaluation metric. The proposed component was based on limited data (ungauged catchments) using only flood extent data. Several sensitivity analysis tests had been conducted in order to justify the structure of the proposed floodplain mapping uncertainty component. The sensitivity analysis tests were based on: 1) the determination of the realization number; 2) the selection of the theoretical distribution for the generation of several roughness value data sets; 3) the threshold determination of the MdAPE statistical criterion used to accept or reject the hydraulic –hydrodynamic modelling results; 4) the cross section interval. The results of this study support the probabilistic flood hazard mapping and can provide water resources managers with valuable information for planning and implementing flood risk mitigation strategies.

Finally, deterministic and probabilistic approaches for flood inundation mapping at ungauged rivers were compared and evaluated in this study. The simulated flood

hydrograph which corresponds to a specific return period and the Manning's roughness values used to map the flooded spatial extent are affected by significant uncertainty in their estimation. Based on these conditions, visualizing flood hazard in a study reach as a probability map seems to be more correct than a deterministic assessment. Hence, probability maps for mapping flood extent are attractive ways of flooding likelihood visualization and add extra credibility in their estimation. Flood inundation prediction under different probabilistic scenarios could assist in floodplain risk management and to minimize the social and economic impacts of floods.

Furthermore, the application of deterministic and probabilistic approaches in the same study area highlights and exemplifies the pros and cons of the two methods for floodplain mapping at ungauged watersheds. For more details, the reader is referred to recent studies and references therein (Di Baldassarre et al., 2010; Dottori, et al., 2013; Alfonso et al., 2016). These studies showed that the calibration process of a hydraulic model on a historical event with a specified return period could give poor results in flood inundation mapping due to the uncertainty in model parameters when applied in other synthetic design flood hydrographs. Therefore, probabilistic approaches should be followed which are less sensitive to the non-stationarity of model parameters (Di Baldassarre et al., 2010). The generalized nature of the proposed component is justified by the fact that the operator is able to:

- apply the component to other study areas and especially at ungauged catchments
- use several types of inline and parallel structures
- modify the number of the preferred acceptable simulations (realizations) for probabilistic flood inundation mapping according to the needs
- import different preferred Manning roughness coefficients data sets of variable range
- use alternate proposed technique for the roughness coefficient generation
- select a favored statistical criterion based on the inherent calibration process for uncertainty analysis due to roughness values or even to use alternate proposed statistical criteria by importing the new criterion to the component

Based on the results of the sensitivity analysis the optimum configuration of the proposed component consist of the:

- use of Lognormal probability distribution for Manning's n roughness coefficient sampling generation
- use 1000 realizations
- use of MdAPE statistical criterion equal to 20% for the selection of the acceptable simulations
- use of 1 m cross sections spacing.

The proposed component could be further investigated. Possible areas of investigation are:

- Application/verification of the proposed component to other stream reaches.
- Application/verification of the proposed component using spatial distributed roughness coefficient values or different values for the channel and the floodplain.
- Further investigation of the proposed statistical criterion MdAPE.
- Evolution of the proposed component in order to implement stochastic discharge values. This analysis could be achieved by fitting probability distributions on the estimated discharge values and performing Monte Carlo simulations.
- Evolution of the proposed component in order to investigate possible relationship between roughness coefficient and discharge values. Estimate the combined uncertainty derived by the roughness coefficient and the discharge values.

CHAPTER 7ο
CONCLUSIONS AND RECOMMENDATIONS

7 Conclusions and recommendations

In this dissertation, several methodologies for ungauged streams and watersheds have been investigated, produced and proposed. They are mainly targeting at: 1) the improvement in identifying and mapping flood prone areas and/or flood hazard mapping, 2) the investigation of specific parameters that affect the process of flood modelling and mapping and 3) the investigation of the uncertainty introduced in flood inundation modelling due to roughness coefficient. This Chapter presents the conclusions drawn from this research, the innovative elements of the dissertation, limitations and recommendations for future research and development in the field of flood hazard and risk modelling for ungauged streams and watersheds.

7.1 Flood Hazard and Risk Modelling framework for Ungauged Streams and Watersheds

This study has developed new methodologies and contributed in three flood modelling and mapping research areas: a) identification of flood prone areas (Identification and mapping of flood prone areas component/ first component); b) sensitivity analysis of flood modelling and mapping due to various hydraulic-hydrodynamic modelling approaches in combination with several types of river and riparian areas spatial resolutions (Sensitivity analysis component/ second component); c) estimation of the uncertainty involved in flood modelling and mapping due to roughness coefficient (Uncertainty analysis component/ third component). Therefore, the flood hazard and risk modelling framework for ungauged streams and watersheds has been developed and composed of the above mentioned three components. The basic characteristic of all methodologies developed and examined is the nature of the study areas which are characterized by insufficient records of various hydrometeorological elements and flow observations regarding both quantity and quality (ungauged watershed/stream). Typical methods and techniques have been used for flood data collection and the hydrometeorological analysis at ungauged catchments. Several field measurements have been performed for the collection of accurate topographic data of the entire flood routing stream reach, accurate topographic data for specific river cross sections and data concerning the river bed particle size. A specific extreme flash flood event has been examined due to the severity of the event that caused serious damages all over the city of Volos. The methodologies have been applied at Xerias Watershed (stream watershed), at the upper Xerias Watershed and a specific flood routing stream reach of Xeria that is located at the outflow point of the upper Xerias Watershed.

The study watershed of Xerias has been used for the development of an objective flood prone areas identification and mapping component. The architecture of the component is based on a GIS-based spatial multi-criteria analysis and the evaluation structure. The primary objective of the first component is to identify potential flood prone areas. The upper watershed of Xerias and the selected flood routing stream reach have been used for the sensitivity and uncertainty analysis of specific parameters that affect the flood inundation modelling and mapping. Therefore, a sensitivity analysis component has been developed to investigate the use of different hydraulic-hydrodynamic modelling approaches in combination with several types of river and riparian areas spatial resolutions on floodplain mapping and flood inundation modelling at ungauged watersheds. Finally, an uncertainty analysis component has been developed for uncertainty analysis of floodplain mapping due to roughness coefficient. All proposed components developed and analyzed within this dissertation are based on limited data (ungauged watersheds/streams) and use a generalised architecture that provide their users the freedom to implement them in other study areas with similar hydrometeorological and geomorphological conditions.

7.1.1 Identification and mapping of flood prone areas component

In this dissertation, there has been developed, examined and validated a flood prone areas identification and mapping component applied at catchment scale. The proposed component can be a valuable tool for decision makers to produce potential flood prone areas maps. The component is based on typical GIS applications, common multi-criteria methods and the use of alternative clustering techniques than the ones provided in several GIS packages. The criteria have been selected based on literature review and the use of Pearson correlation coefficient.

The component structure that has been examined and validated consists of the following methodologies - configurations:

- Selected Criteria: 1) DEM= Elevation, 2) Slope 3) Aspect = Modified aspect according to the direction of storms, 4) Flow Ac = Flow Accumulation , 5) Flow Dir = Flow Direction, 6) Fill = depressionless DEM, 7) Hillshade = surface representation, 8) HOFD = Horizontal Overland Flow Distance, 9) VOFD = Vertical Overland Flow Distance, 10) OFD = Overland Flow Distance, 11) VDCN = Vertical Distance to Channel Network, 12) SPI = Stream Power Index, 13) TPI = Topographic Position Index (implemented with different pixel sampling perimeter of 3,5,10,20,30,40,50,75,100), 14) WI = Wetness Index (modified wetness index from SAGA GIS software), 15) TWI = Topographic Wetness Index, 16) CN = Curve Number (SCS method), 17) WE = Wind Effect (implemented with different grid directions of 0,360,45,90,135,180,225,270,315), 18) MFI = Modified Fournier Index.

- Framework configuration: first approach, second approach.
- MCA methods: AHP, FAHP.
- Pairwise comparison matrix: “expert knowledge”, “group of experts”.
- Clustering techniques: Natural Breaks (Jenks), K-mean (using ‘sqEuclidean’ and ‘cityblock’ distance configuration), Fuzzy c-mean, GMMC, CLARA.

The sensitivity analysis of the component has been based on different combinations of the above-mentioned methodologies and the two different component configurations (first and second approach). The credibility of the proposed component has been validated against historical flood event and flood inundation modelling data. The proposed component has been applied at the ungauged Xerias Watershed. The main conclusions derived from the flood prone areas identification and mapping component are presented in the following paragraph.

A key element of all the flood prone areas identification and mapping frameworks and/or flood hazard mapping frameworks is the selection of the criteria and should be based on specific evaluation processes, on the flood generation mechanism and should have simple interpretability and estimation process. In the majority of the related studies the selection of the criteria is based only on literature review and/or on the authors’ choice according to the respective study area (e.g. Gigovic et al., 2017; Xiao et al., 2017). Thus, this study presents a methodology in which the selection of the criteria has been based not only on literature review but also with the use of Pearson correlation coefficient on several criteria that are related to the flood mechanism.

Another common disadvantage, based on the general applicability of the proposed frameworks, of some related studies is that the flood hazard of each criterion is specified using fixed classes and the separation of these classes depends on subjective factors such as the knowledge of the specific study area and/or literature reviews and/or typical classification approach provided within GIS packages (e.g. Kourgialas et al., 2011; Rahmati et al., 2016; Gigovic et al., 2017). The component developed in this dissertation overcomes all previous mentioned limitations accounted for the criteria and flood hazard classification by classifying the selected criteria and the flood hazard with the use of several clustering-classification techniques. The outcomes of the present study proved that the use of alternate clustering methods could optimize the outcomes of a flood hazard mapping framework and evaluate their associated flood hazard degree. Hence, the use of alternate clustering methods should be a mandatory step in all GIS-MCA frameworks for flood-prone areas recognition.

Furthermore some studies use classified criteria based on a specified number of flood hazard classes at the beginning and before the application of merging (Boolean algebra) where the final flood hazard maps are produced (e.g. Park et al., 2013; Radmehr and Araghinejad, 2015). In this study there has been examined the effect of classifying or not the criteria at the beginning of the framework using different framework configurations (First approach, Second approach). Therefore, based on the results of this study, the

normalization of all criteria from the beginning of the processes can provide better results concerning the Very High hazard class and increase the subjectivity and the generalized nature of the flood hazard mapping framework (e.g., first approach).
Moreover, the results of this study support the use of a reliability measurement such as CR and suggest its obligatory use when decision maker's involved in the process of flood hazard mapping estimation. Sensitivity analysis conducted in this study proved that many framework configurations that have already been used by many authors can be optimized using different approaches and other configurations. Thus, the application of a sensitivity analysis should be an essential process in order to achieve the optimum configuration of a proposed framework. Moreover, the use of the proposed GIS-MCA framework for flood-prone areas recognition can be a valuable and low-cost tool for detection surveys and decision makers. Policy makers can use the proposed component for flood hazard estimation at ungauged areas and/or in areas that luck of preliminary flood hazard information and/or at operational level and large scale applications (e.g. estimation of potential flooded areas for the entire Greece). The use of all recommended component configurations have increased the subjectivity of the proposed flood prone areas identification and mapping component and establish the generalized applicability of the framework. Finally, for accurate investigation of flood hazard and risk characteristics (e.g., flood extent, water depth, etc.) the use of flood inundation modelling is mandatory.

The optimum component configuration that highlighted consist of:

- Selected Criteria: 1) DEM, 2) Slope, 3) Aspect, 4) Flow Ac., 5) HOFD, 6) VOFD, 7) TPI, 8) WI, 9) CN, 10) MFI.
- Framework configuration: First approach (1st approach).
- MCA methods: AHP.
- Pairwise comparison matrix: "expert knowledge" or "group of experts".
- Clustering techniques: K-mean (using 'cityblock' distance configuration), CLARA.

7.1.2 Sensitivity analysis component

In this dissertation, a sensitivity analysis component has been developed, examined and validated based on the selection of different hydraulic-hydrodynamic modelling approaches in combination with several types of river and riparian areas spatial resolutions on flood inundation modelling and mapping. The sensitivity analysis in flood inundation modelling and mapping has been applied at an ungauged Xerias flood routing stream reach (see Chapter 2). The sensitivity analysis has been separated in two levels (first and second sensitivity analysis level).
In the first level of sensitivity analysis different hydraulic-hydrodynamic models and several DEMs with varying level of accuracy for flood analysis and mapping have been

examined and compared. The river and riverine geomorphologies used in this analysis are: a) Digital Terrain Model (DTM) created from TLS data, b) Digital Surface Model (DSM) created from TLS data, c) topographic land survey data and d) typical digitized contours from 1:5000 scale topographic maps. The estimation of the flood hydrograph has been based on CIUH. Typical post flood analysis techniques have been used for the roughness coefficient determination and the validation of the flood hydrograph. The validation of the flooded area has been based only on the flood extent against historical flood extent data and the objective qualitative criterion of CSI. All the methods mentioned above have been followed due to insufficient records of various hydrological observations regarding both quantity and quality. The First level of sensitivity analysis that has been examined and validated consists of the following methodologies-configurations:

- Hydrograph generation: IUH generation based on typical hydrological processes and the use of meteorological and geomorphology data. The validation CIUH and the estimation of the roughness coefficient have been based on post flood analysis.
- River and riverine area topography preparation: Four different DEM has been used in combination with several packages such us MIKE ZERO, MIKE GIS and HEC-GeoRAS for the topography generation.
- One dimensional hydraulic-hydrodynamic models: HEC-RAS, MIKE-11 (applying two configurations).
- Two-dimensional hydraulic-hydrodynamic models: MIKE 21 HD and MIKE 21 HD FM.
- Coupled (1D/2D) hydraulic-hydrodynamic models: MIKE11/MIKE21 HD and MIKE11/MIKE21 HD FM through MIKE FLOOD platform.

In the Second level of sensitivity analysis a bigger number of hydraulic-hydrodynamic models and several different configurations for flood analysis and mapping have been examined and compared. The riverine geomorphology and the hydrograph used are based on the previous analysis (First level of sensitivity analysis) and consists of the LIDAR high-resolution DEM and the CIUH, respectively. The validation of the results has been performed using the same criterion (SCI) with the First level of sensitivity analysis. The Second level of sensitivity analysis that has been examined and validated consists of the following methodologies-configurations:

- Hydrograph generation: IUH generation based on typical hydrological processes and the use of meteorological and geomorphology data. The roughness coefficient estimation has been based on an empirical formula.
- River and riverine area topography preparation: Processed LIDAR DEM has been used in combination with several packages such us MIKE ZERO, MIKE GIS/MIKE HYDRO, HEC-GeoRAS, LISFLOOD-FP/ArcGIS and Flo2d for the topography generation.

- One-dimensional hydraulic-hydrodynamic models: HEC-RAS, MIKE 11 (applying two configurations) and XPSTORM.
- Quasi-2D and two-dimensional hydraulic-hydrodynamic models: MIKE 21 HD, MIKE 21 HD FM (applying two configurations), XPSTORM (applying two configurations), LISFLOOD-FP, HEC-RAS (applying three configurations), and FLO2D.
- Coupled (1D/2D) hydraulic-hydrodynamic models: MIKE11/MIKE21 HD and MIKE11/MIKE21 HD FM (applying two configurations) through MIKE FLOOD platform, XPSTORM, HEC-RAS, and LISFLOOD-FP (applying two configurations).

In the following paragraphs the main conclusions derived from the Sensitivity analysis component are presented.

The main evidence from this study suggests that the sensitivity analysis should be a mandatory process followed in all flood risk modelling and mapping applications. The outcomes of the sensitivity analysis highlighted that the DEM accuracy and spatial resolution play a key role in flood inundation modelling and mapping. Thus, the use of high spatial resolution accuracies should be followed in flood inundation studies, especially in complex river and riverine terrain areas. The determination of the spatial resolution accuracy should be based on specific characteristics of the study area (river complexity, river length and width, floodplain length and width) and the purpose of the analysis (flood hazard mapping, flood risk mapping, flood early warning system, flood forecasting, etc.).

Moreover, it is interesting to note that the model structure uncertainty may be significant based on the accuracy level that can be attained. Despite the fact that the model structure (1D, 2D, 1D/2D) can affect the accuracy, in this study all models achieved acceptable solutions by using an optimized roughness coefficient value. Thus, another crucial parameter that should be carefully investigated in this kind of studies is the roughness coefficient. Additionally, the sensitivity analysis proves that the estimation of roughness coefficient and its optimization can severely affect the estimated flood inundation area, especially in one-dimensional hydraulic hydrodynamic models. As expected the two-dimensional modelling approach stands first in the rank based on the accuracy of the results, followed by the coupled and the one-dimensional modelling approach respectively. A reverse pattern compared to hydraulic modelling configurations is followed when the simulation time is taken into account. Also, the simulation time is seriously affected by the presence or absence of inline hydraulic structures and the mesh resolution.

Our findings appear to be well supported by many other studies (e.g. Bates and De Roo, 2000; Horritt and Bates, 2002; Pappenberger et al., 2005; Merz and Thieken, 2005; Dutta et al., 2007; Apel et al., 2009; Cook and Merwade, 2009; Neelz and Pender, 2009, 2010,2013; Tsubaki and Fujita, 2010; Neal et al., 2010; Grimaldi et al., 2013; Freer et al.,

2013; Tsakiris and Bellos, 2014; Kourgialas and Karatzas, 2014; Shen et al., 2015; Liu et al., 2015; Dimitriadis et al., 2016; Bellos and Tsakiris, 2016; Teng et al., 2017; Altenau et al., 2017).

In summary, the evidence from this study indicates that the input data uncertainty prevails over the model structure. Last but not least, this analysis supports the use of probabilistic approaches in flood inundation modelling and mapping for ungauged stream reaches due to the significant input data uncertainty. This conclusion is consistent with previous studies (e.g., Di Baldassarre et al., 2010; Domeneghetti et al., 2013; Alfonso et al.; 2016, Dimitriadis et al., 2016), where the use of probabilistic approaches in flood inundation modelling and mapping is suggested. Therefore, there is evidence to suggest the use of a simple approach such as the one dimensional hydraulic-hydrodynamic model for calibration and uncertainty analysis investigation (probabilistic flood inundation mapping).

7.1.3 Uncertainty analysis component

In this dissertation, a probabilistic procedure for floodplain inundation mapping has been developed, examined and validated in order to determine the uncertainty introduced by the roughness coefficient values. The probabilistic procedure is based on HEC-RAS 1D hydraulic model and a Monte-Carlo simulation framework. The riverine geomorphology and the hydrograph that have been used are based on the previous analysis and consist of the LIDAR high-resolution DEM and the CIUH, respectively. The basic assumption of the uncertainty analysis component is that the precision of the riverine geomorphology and the hydrograph are unquestioned. In addition, the estimation of Manning's n roughness coefficient has been based on pebble count field surveys and empirical formulas. Then, various theoretical probability distributions were fitted and evaluated on their accuracy to represent the estimated roughness values. Furthermore, different sets of Manning roughness values have been generated using Latin Hypercube Sampling technique in order to implement Monte Carlo simulations for the production of PFMs.

The same validation data (historical flood extent data, from an extreme historical flash flood event) with the previous analysis of the dissertation has been used in the PMF production. A binary wet-dry reasoning has been applied in the calibration process using the Median Absolute Percentage Error evaluation metric. The proposed component was based on insufficient records of various hydrological observations in terms of quantity and quality and by using only flood extent data. The component justification has been achieved using several sensitivity analysis tests. All sensitivity analysis tests concern several parameters and setups of the component such as the choice of realization number, the selection of the theoretical distribution that used for the roughness value data sets generation, the determination of Median Absolute Percentage Error (MdAPE) statistical criterion threshold and, the cross section interval. This analysis compares and

evaluates the use of deterministic and probabilistic approaches for flood inundation modelling and mapping at the ungauged stream reach of Xerias.

The analysis confirms previous findings in the recent literature (e.g., Di Baldassarre et al., 2010; Kiczko et al., 2013; Alfonso et al., 2016; Dimitriadis, 2016; Fuentes-Andino et al., 2017) that support the use of probabilistic flood hazard maps. The majority of these studies proved that the investigation of a historical flood event with the use of a hydraulic model could produce erroneous results in flood inundation mapping due to the big input data uncertainty. Moreover, PFMs can be valuable information for water resources managers and policy makers to develop accurate and acceptable flood risk mitigation strategies and planning. In conclusion, the use of probabilistic approaches in floodplain analysis should be followed because they are less sensitive to the non-stationarity of model parameters (Di Baldassarre et al., 2010).

The proposed uncertainty analysis component can be applied to other study areas and especially at ungauged catchments. The user of the component has the ability to use all types of inline and parallel structures and to modify according to his needs, the number of the preferred, acceptable simulations (realizations). Moreover, the user can generate and/or import alternate Manning roughness coefficients data sets. Finally, the user can implement probabilistic flood inundation analysis using the proposed statistical criterion and/or other criterions tested and/or new criterion by importing it to the component. All these facts strengthen and support the generalized nature of the proposed component.

The optimum configuration of the uncertainty analysis component has been based on the results of the sensitivity analysis. This configuration consists of the following setups:

- use of Lognormal probability distribution for Manning's n roughness coefficient sampling generation
- use 1000 realizations
- use of MdAPE statistical criterion equal to 20% for the selection of the acceptable simulations
- use of 1 m cross-sections spacing.

7.2 Dissertation Innovative Elements

This dissertation has proposed a holistic approach (framework) to investigate flood hazard and risk modelling for ungauged streams and watersheds. The use MCDA-GIS technique is a common procedure followed in the last decade for flood prone areas recognition. This study has examined and produced an objective GIS-based flood prone areas identification and mapping component for ungauged catchments. The entire methodology is based on limited data and information with minimum subjectivity in the multicriteria analysis. Several sensitivity analysis scenarios have been examined for the configuration of the optimum flood prone areas identification and mapping component.

An innovative characteristic of the flood prone areas identification and mapping component that has never been tested in other related studies is the examination of the impact of the selected clustering techniques (e.g. Chen et al., 2011; Manfreda et al., 2011; Tehrany et al., 2013; Rahmati et al., 2016; Khosravi et al., 2016; Tang et al., 2017; Gigovic et al., 2017; Xiao et al., 2017). Furthermore, the selection of the criteria has been based on statistical examination and not only in the literature review. New criteria have been developed and used for flood prone areas recognition and/or flood hazard mapping such as the criterion of aspect that is based on historical extreme meteorological events at the study area. Moreover, it is the first time that specific topographic, hydrologic and meteorological criteria have been combined and used in such a way to identify potential flooded areas. In this study two MCA methods have been examined while many of the related studies examine only one MCA method and/or not both methods used in this analysis (e.g. Chen et al., 2011; Stefanidis and Stathis, 2013; Radmehr and Araghinejad, 2015; Gigovic et al., 2017). Evaluation of the MCA methods has been achieved using the Consistency Ratio approach. Another innovation of the developed flood prone areas identification and mapping component is the examination of the impact of using normalized or clustered criteria (first and second approach comparison).

Finally, all results have been evaluated based on historical flood events and flood inundation modelling data. The proposed flood prone areas identification and mapping component can be an important tool that can provide to policy makers valuable information for flood risk management mitigation strategies and planning. A major conclusion from the previous analysis is that for accurate investigation of the flood extent it is mandatory to use hydraulic-hydrodynamic models. Hence, a sensitivity analysis component has been examined and developed for the estimation of the impact involved in flood modelling and mapping due to several important factors that affect the entire process. The factors that have been examined are the DEM resolution and accuracy, the modelling approach (1D,2D,1D/2D), the simulation time, and the existence or not of inline hydraulic structures. An innovative characteristic of this analysis is that it has examined several DEM accuracies and resolutions and several hydraulic-hydrodynamic models of approximately all possible modelling approach combinations (1D,2D,1D/2D). Moreover, the entire methodology has been applied to a study area with limited hydrometeorological data in terms of quantity and quality. Thus, the validation of the sensitivity analysis component has been based only on the flood extent using a binary wet/dry reasoning.

A major conclusion from the previous analysis is that for accurate calibration and uncertainty analysis investigation, a simple approach should be used, such as the one-dimensional hydraulic-hydrodynamic model. Therefore, there has been examined and developed a probabilistic procedure for floodplain inundation mapping for ungauged streams.

The main novelty of the uncertainty analysis component developed for ungauged streams is that, within the proposed component, it is included a specific methodology

for the estimation of Manning's n values with the use of field measurements, empirical equations and a statistical method for generating samples based on specific distributions. An innovation of the proposed probabilistic procedure is that the applied methodology is based only on historical flood extent data and not on flood peak watermarks like similar studies (e.g. Aronica et al., 2002; Pappenberger et al., 2005; Aronica et al., 2012; Kiczko et al., 2013). Furthermore, the new qualitative evaluation metric, MdAPE, is proposed for the generation of PFMs. The optimum component configuration has been achieved using several sensitivity analysis tests. Unlike other studies such as Aronica et al. (2002), Pappenberger et al. (2005), Mukolwe et al. (2014), Kim et al. (2012), Domeneghetti et al. (2013), Neal et al. (2015), Dimitriadis et al. (2016), this study examined and evaluated the use of different theoretical distributions for the generation of various roughness coefficient data sets. The use of probabilistic approaches is recommended because they are less sensitive to the non-stationarity of model parameters. Finally, the proposed floodplain inundation uncertainty analysis component can be a valuable tool in floodplain risk management and to minimize the social and economic impacts of floods.

7.3 Limitations

The main limitation of all the results of this dissertation is that all the applications concern one case study. Another weakness of the dissertation is that due to the lack of data, too many assumptions have been taken into account. First, all cases presented in this study are based on a single historical flood event. Yet, changes in land use and in hydrological regimes may result in additional uncertainties. Thus, it is expected that the prediction of uncertainties will increase significantly when the input data certainty increase. Another limitation of the study is that the accuracy of the generated DEMs and the CIUH is taken into account as unquestioned. Surface changes were not tested in this dissertation. Catchment surface infiltration rates have a substantial role in run-off generation. The catchment response and runoff generation rate depend on the percentage of paved surfaces. Despite the importance of surface changes in runoff generation, surface changes were not tested in this dissertation. Though, during flood flows, infiltration rates have been assumed to be negligible during floodplain inundation. Another limitation of the study is that all flood inundation modelling and mapping applications have been implemented only at the specific flood routing stream reach of certain length where no buildings are affected by the flood event. Moreover, within this dissertation, the only input data uncertainty that was taken into account is the roughness coefficient that has been used by setting a single value for the entire stream routing reach. Thus, this assumption may have led to an overestimation of the channel roughness coefficient, though the scope of the proposed component fulfill their purpose for ungauged catchments/streams. Finally, other epistemic and/or natural random

uncertainties were not considered, but could significantly affect the flood inundation maps (probabilistic and deterministic). Lastly, with regards to the proposed evaluation criterion (MdAPE) used in the production of the PFMs, further investigation should be made on its applicability to other study areas with variable flood extents.

7.4 Summary of conclusions

The aim of this research is to investigate and develop new tools and techniques for the generation of a new flood hazard and risk modelling framework for ungauged streams and watersheds. This research explores several methodologies for flood prone areas recognition and for sensitivity and uncertainty analysis in flood inundation modelling. In this dissertation, three components have been developed, namely Identification and Mapping of Flood Prone Areas Component, Sensitivity Analysis Component, and Uncertainty Analysis Component. The Flood Prone Areas Identification and Mapping Component uses typical GIS-MCA techniques for flood prone areas recognition. The Sensitivity Analysis Component uses several hydraulic models in combination with several modelling configurations for sensitivity analysis of specific parameters introduced in flood inundation modelling. The Uncertainty Analysis Component uses Monte Carlo simulations methodology for uncertainty analysis in flood inundation modelling due to roughness coefficient. This research has demonstrated that typical hydrological and hydraulic methods for ungauged catchments and streams are able to build reasonably accurate and efficient models for predicting flood hazard and flood risk modelling sensitivity and uncertainty. Finally, all proposed components can be valuable tools for policy makers to produce acceptable and accurate planning and implementing flood risk mitigation strategies.

7.5 Thoughts for future further work and investigation

This research has raised many questions in need for further investigation. The proposals for further investigations are presented in the following paragraphs based on the three developed frameworks:

- **<u>Identification and mapping of flood prone areas component: Chapter 3</u>**

Future work should focus on the applicability of the proposed flood prone areas identification and mapping component to other river watersheds and/or to areas were the flood extent has been estimated using remote sensing techniques or other advanced methods. Moreover, the prospect of being able to investigate other MCA techniques (e.g., rough number theory in MCA analysis) and/or perform uncertainty analysis based on the pairwise comparison tables, urge for future research. The uncertainty analysis could be implemented by fitting several theoretical probability distributions on demand

of the experts for each criterion and performing Monte Carlo simulations by checking the sum of weights (it should be equal to 1).

- **Sensitivity analysis component: Chapter 5**

Future studies should aim at the applicability of the proposed sensitivity analysis component to other stream reaches. Furthermore, the use of different hydrographs and/or spatial distributed roughness coefficient values and/or several alternate evaluation criteria should be investigated.

- **Uncertainty analysis component: Chapter 6**

A vital issue for further research is the application of the proposed uncertainty analysis component to other stream reaches. Also, future research should be undertaken using the proposed uncertainty analysis component inside urban areas and/or using several or spatial distributed roughness coefficient values and/or using the two-dimensional solver (2D approach) and/or using unsteady flow conditions. Additional work on the applicability of MdAPE statistical criterion should be made in order to enforce its usage in flood inundation modelling and mapping. Moreover, the proposed component can be evolved by including other sources of input data uncertainty such as discharge values or hydrographs. This analysis could be achieved by fitting several theoretical probability distributions to the estimated discharge values and performing Monte Carlo simulations. Also, another important issue for future research is the expansion of the proposed component in order to examine the relation, if any, between the roughness coefficient and discharge values. The aim of this research is to estimate the combined uncertainty from the two main factors of input data uncertainty. Furthermore the evolved component uncertainty (combined roughness coefficient – discharge uncertainty) can be examined for application inside urban areas and/or using several or spatial distributed roughness coefficient values and/or using the two-dimensional solver (2D approach) and/or using unsteady flow conditions (entire hydrograph).

Finally, another important issue for future research is the use of state of the art processes for the estimation of Manning's *n* roughness coefficient. The proposed processes involves the use of several methodologies and field measurement such as:

1. Use of Unmanned Aerial Vehicle with high resolution camera to build orthophoto mosaic of the main channel and the floodplain.
2. Use of the high resolution orthophoto data in combination with several automated algorithms for grain sizing to estimate the bed load sample size-frequency distribution.
3. The validation of the proposed methodology can be achieved by comparing the results of the proposed method against traditional methods used for bed material size estimation (e.g. using typical sample grids in many locations).
4. Estimation of roughness coefficient using several empirical equations and generation of spatial distributed roughness coefficient maps.

References

Abbott, M., & Ionescu, F. (1967). On The Numerical Computation Of Nearly Horizontal Flows. *Journal Of Hydraulic Research*, *5*(2), 97-117. http://dx.doi.org/10.1080/00221686709500195

Aggett, G., & Wilson, J. (2009). Creating and coupling a high-resolution DTM with a 1-D hydraulic model in a GIS for scenario-based assessment of avulsion hazard in a gravel-bed river. *Geomorphology*, 113(1-2), 21-34. http://dx.doi.org/10.1016/j.geomorph.2009.06.034

AghaKouchak, A., Easterling, D., Hsu, K., Schubert, S., & Sorooshian, S. (Eds.). (2013). *Extremes in a changing climate: Detection, analysis and uncertainty*. Dordrecht: Springer.

Ahmadisharaf, E., Kalyanapu, A., & Chung, E. (2016). Spatial probabilistic multi-criteria decision making for assessment of flood management alternatives. *Journal Of Hydrology*, *533*, 365-378. http://dx.doi.org/10.1016/j.jhydrol.2015.12.031

Ahmed, F. (2010). Numerical modeling of the Rideau Valley Watershed. *Natural Hazards*, *55*(1), 63-84. http://dx.doi.org/10.1007/s11069-010-9588-4

Akram, F., Rasul, M., Khan, M., & Amir, M. (2014). Comparison of Different Hydrograph Routing Techniques in XPSTORM Modelling Software: A Case Study. *World Academy Of Science, Engineering And Technology, International Science Index 87, International Journal Of Environmental, Chemical, Ecological, Geological And Geophysical Engineering*, *8*(3), 213 - 223.

Alata, M., Molhim, M., & Ramini, A. (2008). Optimizing of Fuzzy C-Means Clustering Algorithm Using GA. *World Academy of Science, Engineering and Technology*, *2*(3), 224–229.

Alfieri, L., Salamon, P., Bianchi, A., Neal, J., Bates, P., & Feyen, L. (2013). Advances in pan-European flood hazard mapping. *Hydrological Processes*, *28*(13), 4067-4077. http://dx.doi.org/10.1002/hyp.9947

Alfonso, L., Mukolwe, M., & Di Baldassarre, G. (2016). Probabilistic Flood Maps to support decision-making: Mapping the Value of Information. *Water Resources Research*, *52*(2), 1026-1043. http://dx.doi.org/10.1002/2015wr017378

Alonso, J. A., & Lamata, M. T. (2006). Consistency in the analytic hierarchy process: a new approach. *International Journal of Uncertainty, Fuzziness and Knowledge-Based Systems*, *14*(04), 445–459. doi:10.1142/s0218488506004114

Altenau, E., Pavelsky, T., Bates, P., & Neal, J. (2017). The effects of spatial resolution and dimensionality on modeling regional-scale hydraulics in a multichannel river. *Water Resources Research*, *53*(2), 1683-1701. http://dx.doi.org/10.1002/2016wr019396

AMS. (2017). *Flash flood – American Meteorological Society (AMS) Glossary*. *Glossary.ametsoc.org*. Retrieved 2 August 2017 *(Term updated 24 April 2017)*, from http://glossary.ametsoc.org/wiki/Flash_flood

Anane, M., Bouziri, L., Limam, A., & Jellali, S. (2012). Ranking suitable sites for irrigation with reclaimed water in the Nabeul-Hammamet region (Tunisia) using GIS and AHP-multicriteria decision analysis. *Resources, Conservation and Recycling*, *65*, 36–46. doi:10.1016/j.resconrec.2012.05.006

Apel, H., Aronica, G.T., Kreibich, H., & Thieken, A. (2009). Flood risk analyses—how detailed do we need to be?. *Natural Hazards*, *49*(1), 79-98. http://dx.doi.org/10.1007/s11069-008-9277-8

Apel, H., Thieken, A., Merz, B., & Blöschl, G. (2004). Flood risk assessment and associated uncertainty. *Natural Hazards And Earth System Science*, 4(2), 295-308. http://dx.doi.org/10.5194/nhess-4-295-2004

Arnoldus, H. (1980). An approximation of the rainfall factor in the universal soil loss equation. In M. De Boodt & D. Gabriels (Eds.), *Assessment of erosion* (pp. 127–132). Chichester: Wiley.

Aronica, G.T., Bates, P., & Horritt, M. (2002). Assessing the uncertainty in distributed model predictions using observed binary pattern information within GLUE. *Hydrological Processes*, *16*(10), 2001-2016. http://dx.doi.org/10.1002/hyp.398

Aronica, G.T., Brigandí, G., & Morey, N. (2012). Flash floods and debris flow in the city area of Messina, north-east part of Sicily, Italy in October 2009: the case of the Giampilieri catchment. *Natural Hazards And Earth System Science*, *12*(5), 1295-1309. http://dx.doi.org/10.5194/nhess-12-1295-2012

Aronica, G.T., Hankin, B., & Beven, K. (1998). Uncertainty and equifinality in calibrating distributed roughness coefficients in a flood propagation model with limited data.

Advances In Water Resources, *22*(4), 349-365. http://dx.doi.org/10.1016/s0309-1708(98)00017-7

Arthur, D., & Vassilvitskii, S. (2007). *K-means++: The Advantages of Careful Seeding*. Eighteenth annual ACM-SIAM symposium on Discrete algorithms, New Orleans, LA.

Asare-Kyei, D., Forkuor, G., & Venus, V. (2015). Modeling flood hazard zones at the sub-district level with the rational model integrated with GIS and remote sensing approaches. *Water*, *7*(7), 3531–3564. doi:10.3390/w7073531

Babaei, H., Araghinejad, S., & Hoorfar, A. (2013). Developing a new method for spatial assessment of drought vulnerability (case study: Zayandeh-Rood river basin in Iran). *Water and Environment Journal*, *27*(1), 50–57. doi:10.1111/j.1747-6593.2012.00326.x

Bales, J., & Wagner, C. (2009). Sources of uncertainty in flood inundation maps. *Journal Of Flood Risk Management*, 2(2), 139-147. http://dx.doi.org/10.1111/j.1753-318x.2009.01029.x

Baltsavias, E. (1999). A comparison between photogrammetry and laser scanning. ISPRS Journal Of Photogrammetry And Remote Sensing, 54(2-3), 83-94. http://dx.doi.org/10.1016/s0924-2716(99)00014-3

Basaran, B. (2012, March). *A Critique on the Consistency Ratios of Some Selected Articles Regarding Fuzzy AHP and Sustainability*. 3rd International Symposium on Sustainable Development (ISSD'12), Sarajevo, Bosnia-Herzegovina.

Bates, P., & De Roo, A. (2000). A simple raster-based model for flood inundation simulation. *Journal Of Hydrology*, *236*(1-2), 54-77. http://dx.doi.org/10.1016/s0022-1694(00)00278-x

Bates, P., Horritt, M., Aronica, G.T., & Beven, K. (2004). Bayesian updating of flood inundation likelihoods conditioned on flood extent data. *Hydrological Processes*, *18*(17), 3347-3370. http://dx.doi.org/10.1002/hyp.1499

Bates, P., Pappenberger, F., & Romanowicz, R. (2014). Uncertainty in Flood Inundation Modelling. *Applied Uncertainty Analysis For Flood Risk Management*, 232-269. http://dx.doi.org/10.1142/9781848162716_0010

Bates, P., Trigg, M., Neal, J., & Dabrowa, A. (2013). *LISFLOOD-FP User's Manual* (1st ed.). School of Geographical Sciences, University of Bristol.

Bates, P., Wilson, M., Horritt, M., Mason, D., Holden, N., & Currie, A. (2006). Reach scale floodplain inundation dynamics observed using airborne synthetic aperture radar imagery: Data analysis and modelling. *Journal Of Hydrology*, 328(1-2), 306-318. http://dx.doi.org/10.1016/j.jhydrol.2005.12.028

Bellos, V., & Tsakiris, G. (2016). A hybrid method for flood simulation in small catchments combining hydrodynamic and hydrological techniques. *Journal Of Hydrology*, *540*, 331-339. http://dx.doi.org/10.1016/j.jhydrol.2016.06.040

Besl, P., & McKay, N. (1992). A method for registration of 3-D shapes. *IEEE Transactions On Pattern Analysis And Machine Intelligence*, 14(2), 239-256. http://dx.doi.org/10.1109/34.121791

Bezdek, J. C. (1981). *Pattern recognition with fuzzy objective function algorithms*. Netherlands: Kluwer Academic / Plenum Publishers.

Bhaskar, N., Parida, B., & Nayak, A. (1997). Flood Estimation for Ungauged Catchments Using the GIUH. *Journal Of Water Resources Planning And Management*, *123*(4), 228-238. http://dx.doi.org/10.1061/(asce)0733-9496(1997)123:4(228)

Bhushan, N., & Rai, K. (2004). *Strategic decision making: Applying the analytic hierarchy process*. London: Springer London.

Bishop, C. M. (2008). *Pattern recognition and machine learning (information science and statistics)*. New York: Springer-Verlag New York.

Bohner, J., & Selige, T. (2006). Spatial prediction of soil attributes using terrain analysis and climate regionalisation. In J. Bohner, K. R. McCloy, & J. Strobl (Eds.), *SAGA Analysis and Modelling Applications* (pp. 13–27). Göttinger Geographische Abhandlungen.

Bohner, J., Koethe, R., Conrad, O., Gross, J., Ringeler, A., & Selige, T. (2002). Soil regionalisation by means of terrain analysis and process parameterisation. In E. Micheli, F. Nachtergaele, & L. Montanarella (Eds.), *Soil classification 2001* (pp. 213–222). Luxembourg: European Soil Bureau.

Boroushaki, S., & Malczewski, J. (2010). Using the fuzzy majority approach for GIS-based multicriteria group decision-making. *Computers & Geosciences*, *36*(3), 302–312. doi:10.1016/j.cageo.2009.05.011

Brocca, L., Melone, F., Moramarco, T., & Singh, V. (2009). Assimilation of Observed Soil Moisture Data in Storm Rainfall-Runoff Modeling. *Journal Of Hydrologic Engineering*, *14*(2), 153-165. http://dx.doi.org/10.1061/(asce)1084-0699(2009)14:2(153)

Brodu, N., & Lague, D. (2012). 3D terrestrial lidar data classification of complex natural scenes using a multi-scale dimensionality criterion: Applications in geomorphology. *ISPRS Journal Of Photogrammetry And Remote Sensing*, *68*, 121-134. http://dx.doi.org/10.1016/j.isprsjprs.2012.01.006

Brunner, G. (2016a). *HEC-RAS River Analysis System: Hydraulic Reference Manual*, Version 5.0 (5th ed.). US Army Corps of Engineers – Hydrologic Engineering Center. Retrieved from http://www.hec.usace.army.mil/software/hec-ras/documentation/HEC-RAS%205.0%20Reference%20Manual.pdf

Brunner, G. (2016b). *HEC-RAS River Analysis System: User's Manual*, Version 5.0 (5th ed.). US Army Corps of Engineers – Hydrologic Engineering Center. Retrieved from http://www.hec.usace.army.mil/software/hec-ras/documentation/HEC-RAS%205.0%20Users%20Manual.pdf

Buckley, J. J. (1985). Fuzzy hierarchical analysis. *Fuzzy Sets and Systems*, *17*(3), 233–247. doi:10.1016/0165-0114(85)90090-9

Bulut, E., Duru, O., Keçeci, T., & Yoshida, S. (2012). Use of consistency index, expert prioritization and direct numerical inputs for generic fuzzy-aHP modeling: A process model for shipping asset management. *Expert Systems with Applications*, *39*(2), 1911–1923. doi:10.1016/j.eswa.2011.08.056

Bunte, K., & Abt, S.R. (2001). Sampling surface and subsurface particle-size distributions in wadable gravel- and cobble-bed streams for analyses in sediment transport, hydraulics, and streambed monitoring. Gen. Tech. Rep. RMRS-GTR-74. Fort Collins, CO: U.S. Department of Agriculture, Forest Service, Rocky Mountain Research Station. 428 p. https://www.fs.fed.us/biology/nsaec/assets/rmrs-gtr-74samplingsurfandsubsufpartszdist.pdf

Bunte, K., Abt, S., Potyondy, J., & Swingle, K. (2009). Comparison of Three Pebble Count Protocols (EMAP, PIBO, and SFT) in Two Mountain Gravel-Bed Streams. *JAWRA Journal Of The American Water Resources Association*, 45(5), 1209-1227. http://dx.doi.org/10.1111/j.1752-1688.2009.00355.x

Burrough, P., McDonnell, R., & Lloyd, C. (2015). *Principles of Geographical Information Systems* (3rd ed.). Oxford: OXFORD UNIVERSITY PRESS.

Casulli, V. (2009). A high-resolution wetting and drying algorithm for free-surface hydrodynamics. *International Journal For Numerical Methods In Fluids*, *60*(4), 391-408. http://dx.doi.org/10.1002/fld.1896

Chandio, I. A., Matori, A. N. B., WanYusof, K. B., Talpur, M. A. H., Balogun, A. L., & Lawal, D. U. (2013). GIS-based analytic hierarchy process as a multicriteria decision analysis instrument: A review. *Arabian Journal of Geosciences*, *6*(8), 3059–3066. doi:10.1007/s12517-012-0568-8

Chang, D. Y. (1996). Applications of the extent analysis method on fuzzy AHP. *European Journal of Operational Research*, *95*(3), 649–655. doi:10.1016/0377-2217(95)00300-2

Chang, M. (2012). *Forest hydrology: An Introduction to Water and Forests* (3rd ed.). Boca Raton, FL: CRC Press.

Chang, T., & Wang, T. (2009). Using the fuzzy multi-criteria decision making approach for measuring the possibility of successful knowledge management. *Information Sciences*, *179*(4), 355–370. doi:10.1016/j.ins.2008.10.012

Chen, C., Meselhe, E., & Waldon, M. (2012). Assessment of mineral concentration impacts from pumped stormwater on an Everglades Wetland, Florida, USA – Using a spatially-explicit model. *Journal Of Hydrology*, *452-453*, 25-39. http://dx.doi.org/10.1016/j.jhydrol.2012.05.016

Chen, H., Ito, Y., Sawamukai, M., & Tokunaga, T. (2015). Flood hazard assessment in the Kujukuri plain of Chiba prefecture, Japan, based on GIS and multicriteria decision analysis. *Natural Hazards*, *78*(1), 105–120. doi:10.1007/s11069-015-1699-5

Chen, Y. R., Yeh, C. H., & Yu, B. (2011). Integrated application of the analytic hierarchy process and the geographic information system for flood risk assessment and flood plain management in Taiwan. *Natural Hazards*, *59*(3), 1261–1276. http://dx. doi. org/10.1007/s11069-011-9831-7

Chow, W. (1959). *Open-channel hydraulics* (1st ed.). New York [etc.]: McGraw-Hill.

Chowdary, V. M., Chakraborthy, D., Jeyaram, A., Murthy, Y. V. N. K., Sharma, J. R., & Dadhwal, V. K. (2013). Multi-criteria decision making approach for watershed Prioritization using analytic hierarchy process technique and GIS. *Water Resources Management*, *27*(10), 3555–3571. doi:10.1007/s11269-013-0364-6

Clark, C. O. (1945). *Storage and the unit hydrograph*. Trans., ASCE, 110, 1419-1446.

Cook, A., & Merwade, V. (2009). Effect of topographic data, geometric configuration and modeling approach on flood inundation mapping. *Journal Of Hydrology*, *377*(1-2), 131-142. http://dx.doi.org/10.1016/j.jhydrol.2009.08.015

Coon, W. (1998). Estimation of roughness coefficients for natural stream channels with vegetated banks. Denver, CO: U.S. Geological Survey.

Costabile, P., & Macchione, F. (2015). Enhancing river model set-up for 2-D dynamic flood modelling. *Environmental Modelling & Software*, *67*, 89-107. http://dx.doi.org/10.1016/j.envsoft.2015.01.009

Danish Hydraulic Institute. (2014a). *MIKE11 A Modelling System for Rivers and Channels. Reference Manual*. MIKE by DHI 2014.

Danish Hydraulic Institute. (2014b). *MIKE21 Flow Model FM. User Guide*. MIKE by DHI 2014.

Danish Hydraulic Institute. (2014c). *MIKE 21 & MIKE 3 FLOW MODEL FM. Hydrodynamic and Transport Module Scientific Documentation*. MIKE by DHI 2014.

Danish Hydraulic Institute. (2014d). *MIKE21 Flow Model. User Guide*. MIKE by DHI 2014.

Danish Hydraulic Institute. (2014e). *MIKE21 Flow Model. Hydrodynamic Module Scientific Documentation*. MIKE by DHI 2014.

Danish Hydraulic Institute. (2014f). *MIKEFLOOD 1D-2D Modelling. User Guide*. MIKE by DHI 2014.

Dawson, C., Abrahart, R., & See, L. (2007). HydroTest: A web-based toolbox of evaluation metrics for the standardised assessment of hydrological forecasts. *Environmental Modelling & Software*, *22*(7), 1034-1052. http://dx.doi.org/10.1016/j.envsoft.2006.06.008

de Moel, H., van Alphen, J., & Aerts, J. C. J. H. (2009). Flood maps in Europe – methods, availability and use. *Natural Hazards and Earth System Science*, *9*(2), 289–301. doi:10.5194/nhess-9-289-2009

de Smith, M. J., Goodchild, M. F., Longley, P. A., & Smith, M. J. (2015). *Geospatial analysis: A comprehensive guide to principles, techniques and software tools* (5th ed.). Winchelsea, UK: Winchelsea Press.

Delrieu, G., Nicol, J., Yates, E., Kirstetter, P., Creutin, J., Anquetin, S., Obled, C., & Saulnier, G. M. (2005). The Catastrophic Flash-Flood Event of 8–9 September 2002 in the Gard Region, France: A First Case Study for the Cévennes–Vivarais Mediterranean Hydrometeorological Observatory. *Journal Of Hydrometeorology*, *6*(1), 34-52. http://dx.doi.org/10.1175/jhm-400.1

Dempster, A. P., Laird, N. M., & Rubin, D. B. (1977). Maximum Likelihood from Incomplete Data via the EM Algorithm. *Journal of the Royal Statistical Society. Series B (Methodological)*, *39*(1), 1–38.

Di Baldassarre, G., Schumann, G., Bates, P., Freer, J., & Beven, K. (2010). Flood-plain mapping: a critical discussion of deterministic and probabilistic approaches. *Hydrological Sciences Journal*, *55*(3), 364-376. http://dx.doi.org/10.1080/02626661003683389

Diakakis, M. (2011). A method for flood hazard mapping based on basin morphometry: Application in two catchments in Greece. *Natural Hazards*, *56*(3), 803–814. doi:10.1007/s11069-010-9592-8

Diakakis, M., Mavroulis, S., & Deligiannakis, G. (2012). Floods in Greece, a statistical and spatial approach. *Natural Hazards*, *62*(2), 485-500. http://dx. doi. org/10. 1007/s11069-012-0090-z

Dimitriadis, P., Tegos, A., Oikonomou, A., Pagana, V., Koukouvinos, A., Mamassis, N., Koutsoyiannis, D., & Efstratiadis, A., (2016). Comparative evaluation of 1D and quasi-2D hydraulic models based on benchmark and real-world applications for uncertainty assessment in flood mapping. *Journal Of Hydrology*, *534*, 478-492. http://dx.doi.org/10.1016/j.jhydrol.2016.01.020

Domeneghetti, A., Vorogushyn, S., Castellarin, A., Merz, B., & Brath, A. (2013). Probabilistic flood hazard mapping: effects of uncertain boundary conditions. *Hydrology And Earth System Sciences*, *17*(8), 3127-3140. http://dx.doi.org/10.5194/hess-17-3127-2013

Dottori, F., Di Baldassarre, G., & Todini, E. (2013). Detailed data is welcome, but with a pinch of salt: Accuracy, precision, and uncertainty in flood inundation modeling. *Water Resources Research*, 49(9), 6079-6085. http://dx.doi.org/10.1002/wrcr.20406

Duc Tran, D., van Halsema, G., Hellegers, P., Phi Hoang, L., Quang Tran, T., Kummu, M., & Ludwig, F. (2017). Assessing impacts of dike construction on the flood dynamics in the Mekong Delta. *Hydrology And Earth System Sciences Discussions*, 1-41. http://dx.doi.org/10.5194/hess-2017-141

Dunning, D. J., Ross, Q. E., & Merkhofer, M. W. (2000). Multiattribute utility analysis for addressing section 316(b) of the clean water act. *Environmental Science & Policy*, *3*, 7–14. doi:10.1016/s1462-9011(00)00022-8

Dutta, D., Alam, J., Umeda, K., Hayashi, M., & Hironaka, S. (2007). A two-dimensional hydrodynamic model for flood inundation simulation: a case study in the lower Mekong river basin. *Hydrological Processes*, *21*(9), 1223-1237. http://dx.doi.org/10.1002/hyp.6682

Efstratiadis, A., Koussis, A., Koutsoyiannis, D., & Mamassis, N. (2014). Flood design recipes vs. reality: can predictions for ungauged basins be trusted?. *Natural Hazards And Earth System Science*, *14*(6), 1417-1428. http://dx.doi.org/10.5194/nhess-14-1417-2014

Erensal, Y. C., Öncan, T., & Demircan, M. L. (2006). Determining key capabilities in technology management using fuzzy analytic hierarchy process: A case study of turkey. *Information Sciences*, *176*(18), 2755–2770. doi:10.1016/j.ins.2005.11.004

European Environment Agency (EEA) (2010). *Mapping the impacts of natural hazards and technological accidents in Europe: An overview of the last decade.* Report 13/2010. Luxembourg: European Environment Agency.

European Environment Agency (EEA) (2012). *Urban adaptation to climate change in Europe - Challenges and opportunities for cities together with supportive national and European policies*. Report 02/2012. Copenhagen: European Environment Agency.

Faccini, F., Luino, F., Sacchini, A., & Turconi, L. (2015). Flash Flood Events and Urban Development in Genoa (Italy): Lost in Translation. In: Lollino G., Manconi A., Guzzetti F., Culshaw M., Bobrowsky P., Luino F. (eds) *Engineering Geology For Society And Territory - Volume 5*, 797-801. Springer, Cham. http://dx.doi.org/10.1007/978-3-319-09048-1_155

Fechner, G. (1860). *Elemente der Psychophysik* (Vol. 1). Leipzig: Breitkopf und Härtel. https://archive.org/details/elementederpsych001fech

Feizizadeh, B., & Blaschke, T. (2013). GIS-multicriteria decision analysis for landslide susceptibility mapping: Comparing three methods for the Urmia lake basin, Iran. *Natural Hazards*, *65*(3), 2105–2128. doi:10.1007/s11069-012-0463-3

Fels, J. E., & Zobel, R. (1995). *Landscape position and classified landtype mapping for statewide DRASTIC mapping project*. North Carolina State University.

Fisher, W. D. (1958). On grouping for maximum homogeneity. *Journal of the American Statistical Association*, *53*(284), 789–798. doi:10.2307/2281952

Flo-*2d*. (2017). *Flo-2d.com / FLO-2D Reference Manual 2009*. Retrieved 19 May 2017, from http://www.flo-2d.com/wp-content/uploads/2014/04/Manuals-Pro.zip

Foudi, S., Osés-Eraso, N., & Tamayo, I. (2015). Integrated spatial flood risk assessment: The case of Zaragoza. *Land Use Policy*, *42*, 278-292. http://dx.doi.org/10.1016/j.landusepol.2014.08.002

Fournier, F. (1960). *Climate and Erosion*. Paris, France: University of Paris.

Fread, D. L., (1976). *Theoretical Development of an Implicit Dynamic Routing Model*. Hydrologic Research Laboratory, Office of Hydrology, U.S. Department of Commerce, NOAA, NWS, Silver Spring, MD., presented at Dynamic Routing Seminar, Lower Mississippi River Forecast Center, Slidell, LA., 13-17 Dec 1976.

Freeman, T. G. (1991). Calculating catchment area with divergent flow based on a regular grid. *Computers & Geosciences*, *17*(3), 413–422. doi:10.1016/0098-3004(91)90048-i

Freer, J., Beven, K., Neal, J., Schumann, G., Hall, J., & Bates, P. (2013). Flood risk and uncertainty. In J. Rougier, S. Sparks, & L. Hill (Eds.), *Risk and Uncertainty Assessment for Natural Hazards*. Cambridge: Cambridge University Press. http://dx.doi.org/10.1017/cbo9781139047562.008

Fuentes-Andino, D., Beven, K., Halldin, S., Xu, C., Reynolds, J., & Di Baldassarre, G. (2017). Reproducing an extreme flood with uncertain post-event information. *Hydrology And Earth System Sciences*, *21*(7), 3597-3618. http://dx.doi.org/10.5194/hess-21-3597-2017

Gain, A., Mojtahed, V., Biscaro, C., Balbi, S., & Giupponi, C. (2015). An integrated approach of flood risk assessment in the eastern part of Dhaka City. *Natural Hazards*, *79*(3), 1499-1530. http://dx.doi.org/10.1007/s11069-015-1911-7

Gaume, E., Livet, M., Desbordes, M., & Villeneuve, J. (2004). Hydrological analysis of the river Aude, France, flash flood on 12 and 13 November 1999. *Journal Of Hydrology*, *286*(1-4), 135-154. http://dx.doi.org/10.1016/j.jhydrol.2003.09.015

Giandotti, M. (1937). Idrologia. Barbera Ed., Firenze, 107 p.

Gigović, L., Pamučar, D., Bajić, Z., & Drobnjak, S. (2017). Application of GIS-Interval Rough AHP Methodology for Flood Hazard Mapping in Urban Areas. *Water*, *9*(6), 360. http://dx.doi.org/10.3390/w9060360

Golden, B. L., Wasil, E. A., & Harker, P. T. (1989). *The analytic hierarchy process applications and studies*. Berlin, Heidelberg: Springer Berlin Heidelberg.

González-Val, R., Ramos, A., Sanz-Gracia, F., & Vera-Cabello, M. (2015). Size distributions for all cities: Which one is best?. *Papers In Regional Science*, *94*(1), 177-197. http://dx.doi.org/10.1111/pirs.12037

Goodell, C. (2014). *Breaking the HEC-RAS code*. Portland, Oregon: H21s.

Grimaldi, S., Petroselli, A., Arcangeletti, E., & Nardi, F. (2013). Flood mapping in ungauged basins using fully continuous hydrologic–hydraulic modeling. *Journal Of Hydrology*, *487*, 39-47. http://dx.doi.org/10.1016/j.jhydrol.2013.02.023

Gruntfest, E., & Handmer, J. (2001). *Coping with Flash Floods* (1st ed.). Dordrecht: Springer Netherlands.

Gu, J., Hu, C., Kuang, C., Kolditz, O., Shao, H., Zhang, J., & Liu, H. (2016). A water quality model applied for the rivers into the Qinhuangdao coastal water in the Bohai Sea, China. *Journal Of Hydrodynamics, Ser. B*, *28*(5), 905-913. http://dx.doi.org/10.1016/s1001-6058(16)60691-1

Gupta, V., Waymire, E., & Wang, C. (1980). A representation of an instantaneous unit hydrograph from geomorphology. *Water Resources Research*, *16*(5), 855-862. http://dx.doi.org/10.1029/wr016i005p00855

Gwinn, W., & Ree, W. (1980). Maintenance Effects on the Hydraulic Properties of A Vegetation-Lined Channel. *Transactions Of The ASAE*, 23(3), 636-642. http://dx.doi.org/10.13031/2013.34637

Hajkowicz, S., & Collins, K. (2007). A review of multiple criteria analysis for water resource planning and management. *Water Resources Management*, *21*(9), 1553–1566. doi:10.1007/s11269-006-9112-5

Hall, J., Arheimer, B., Borga, M., Brázdil, R., Claps, P., Kiss, A., Kjeldsen, T., Kriauciuniene, J., Kundzewicz, Z., Lang, M., Llasat, M., Macdonald, N., McIntyre, N., Mediero, L., Merz, B., Merz, R., Molnar, P., Montanari, A., Neuhold, C., Parajka, J., Perdigao, R., Plavcova, L., Rogger, M., Salinas, J., Sauquet, E., Schar, C., Szolgay, J., Viglione, A., & Bloschl, G. (2014). Understanding flood regime changes in Europe: a state-of-the-art assessment. *Hydrology And Earth System Sciences*, 18(7), 2735-2772. http://dx.doi.org/10.5194/hess-18-2735-2014

Hall, M., Zaki, A., & Shahin, M. (2001). Regional analysis using the Geomorphoclimatic Instantaneous Unit Hydrograph. *Hydrology And Earth System Sciences*, *5*(1), 93-102. http://dx.doi.org/10.5194/hess-5-93-2001

Hallema, D., & Moussa, R. (2014). A model for distributed GIUH-based flow routing on natural and anthropogenic hillslopes. *Hydrological Processes*, *28*(18), 4877-4895. http://dx.doi.org/10.1002/hyp.9984

Han, J., Lee, J. G., & Kamber, M. (2009). An Overview of Clustering Methods in Geographic Data Analysis. In H. J. Miller & J. Han (Eds.), *Geographic Data Mining and Knowledge Discovery* (Second edition ed.) (pp. 149–187). CRC press.

Harats, N., Ziv, B., Yair, Y., Kotroni, V., & Dayan, U. (2010). Lightning and rain dynamic indices as predictors for flash floods events in the Mediterranean. *Advances In Geosciences*, *23*, 57-64. http://dx.doi.org/10.5194/adgeo-23-57-2010

Harker, P. T., & Vargas, L. G. (1987). The theory of ratio scale estimation: Saaty's analytic hierarchy process. *Management Science*, *33*(11), 1383–1403. doi:10.1287/mnsc.33.11.1383

Harrelson, C.C., Rawlins, C.L., & Potyondy, J.P. (1994). Stream channel reference sites: an illustrated guide to field technique. Gen. Tech. Rep. RM-2 Fort Collins, CO: U.S. Department of Agriculture, Forest Service, Rocky Mountain Forest and Range Experiment Station. 61 p. https://watershed.ucdavis.edu/education/classes/files/content/page/rm_gtr245.pdf

Hazarika, N., Barman, D., Das, A., Sarma, A., & Borah, S. (2016). Assessing and mapping flood hazard, vulnerability and risk in the Upper Brahmaputra River valley using

stakeholders' knowledge and Multi-Criteria Evaluation (MCE). *Journal Of Flood Risk Management*. http://dx.doi.org/10.1111/jfr3.12237

Herschy, R. (2009). *Streamflow measurement* (1st ed.). London: Taylor & Francis.

Ho, C., & Huang, H. (1992). Manning's roughness coefficient of mountainous streams in Taiwan. In B. Yen, *Channel flow resistance: centennial of Manning's formula*. (1st ed., pp. 299-308). Littleton: Water Resources Publications.

Horritt, M. (2006). A methodology for the validation of uncertain flood inundation models. *Journal Of Hydrology*, 326(1-4), 153-165. http://dx.doi.org/10.1016/j.jhydrol.2005.10.027

Horritt, M., & Bates, P. (2001). Predicting floodplain inundation: raster-based modelling versus the finite-element approach. *Hydrological Processes*, *15*(5), 825-842. http://dx.doi.org/10.1002/hyp.188

Horritt, M., & Bates, P. (2002). Evaluation of 1D and 2D numerical models for predicting river flood inundation. *Journal Of Hydrology*, 268(1-4), 87-99. http://dx.doi.org/10.1016/s0022-1694(02)00121-x

Horritt, M., Di Baldassarre, G., Bates, P., & Brath, A. (2007). Comparing the performance of a 2-D finite element and a 2-D finite volume model of floodplain inundation using airborne SAR imagery. *Hydrological Processes*, 21(20), 2745-2759. http://dx.doi.org/10.1002/hyp.6486

Hosseini, S., Mahjouri, N., & Riahi, S. (2016). Development of a Direct Geomorphologic IUH Model for Daily Runoff Estimation in Ungauged Watersheds. *Journal Of Hydrologic Engineering*, *21*(6), 05016008. http://dx.doi.org/10.1061/(asce)he.1943-5584.0001333

Howard, A. F. (1991). A critical look at multiple criteria decision making techniques with reference to forestry applications. *Canadian Journal of Forest Research*, *21*(11), 1649–1659. doi:10.1139/x91-228

Huang, P.-H., Tsai, J.-S., & Lin, W.-T. (2010). Using multiple-criteria decision-making techniques for eco-environmental vulnerability assessment: A case study on the Chi-Jia-Wan stream watershed, Taiwan. *Environmental Monitoring and Assessment*, *168*(1-4), 141–158. doi:10.1007/s10661-009-1098-z

Hyndman, R., & Koehler, A. (2006). Another look at measures of forecast accuracy. International *Journal Of Forecasting*, 22(4), 679-688. http://dx.doi.org/10.1016/j.ijforecast.2006.03.001

IATE. (2017). *Inter-Active Terminology for Europe. Iate.europa.eu*. Retrieved 2 August 2017, from http://iate.europa.eu

Jarrett, R. (1984). Hydraulics of High-Gradient Streams. *Journal Of Hydraulic Engineering*, *110*(11), 1519-1539. http://dx.doi.org/10.1061/(asce)0733-9429(1984)110:11(1519)

Jarrett, R. (1985). *Determination of roughness coefficients for streams in Colorado*, Water Res. Investigations Report 85-4004. Lakewood, Colorado, USA: Geological Survey (U.S.).

Javan, M., McKeogh, E., & Kiely, G. (1992). Field evaluation of Manning's n in gravel rivers. In B. Yen, *Channel flow resistance: centennial of Manning's formula* (1st ed., pp. 318-327). Littleton: Water Resources Publications.

Jeefoo, P., & Tripathi, N. K. (2011). Dengue risk zone index (DRZI) for mapping dengue risk areas. *International Journal of Geoinformatics*, *7*(1), 53–62.

Jena, P., Panigrahi, B., & Chatterjee, C. (2016). Assessment of Cartosat-1 DEM for Modeling Floods in Data Scarce Regions. *Water Resources Management*, *30*(3), 1293-1309. http://dx.doi.org/10.1007/s11269-016-1226-9

Jenks, G. F. (1967). The Data Model Concept in Statistical Mapping. *International Yearbook of Cartography*, *7*, 186–190.

Jenks, G. F., & Caspall, F. C. (1971). Error on choroplethic maps: Definition, measurement, reduction. *Annals of the Association of American Geographers*, *61*(2), 217–244. doi:10.1111/j.1467-8306.1971.tb00779.x

Jenson, S. K., & Domingue, J. O. (1988). Extracting Topographic Structure from Digital Elevation Data for Geographic Information System Analysis. *Photogrammetric Engineering and Remote Sensing*, *54*(11), 1593–1600.

Jolliffe, I., & Stephenson, D. (2011). *Forecast Verification: A Practioner's Guide in Atmospheric Science, 2nd Edi* (1st ed.). John Wiley & Sons.

Karim, F., Dutta, D., Marvanek, S., Petheram, C., Ticehurst, C., & Lerat, J. et al. (2015). Assessing the impacts of climate change and dams on floodplain inundation and wetland

connectivity in the wet–dry tropics of northern Australia. *Journal Of Hydrology*, *522*, 80-94. http://dx.doi.org/10.1016/j.jhydrol.2014.12.005

Kaufman, L., & Rousseeuw, P. J. (1986). Clustering large data sets. In E. S. Gelsema & L. N. Kanal (Eds.), *Pattern Recognition in Practice II* (pp. 425–437). Amsterdam: North-Holland.

Kaufman, L., & Rousseeuw, P. J. (1990). *Finding groups in data: An introduction to cluster analysis* (3rd ed.). New York: Wiley-Interscience, Hoboken, New Jersey, U.S.A.

Kazakis, N., Kougias, I., & Patsialis, T. (2015). Assessment of flood hazard areas at a regional scale using an index-based approach and analytical hierarchy process: Application in Rhodope–Evros region, Greece. *Science of The Total Environment*, *538*, 555–563. doi:10.1016/j.scitotenv.2015.08.055

Khaleghi, M., Gholami, V., Ghodusi, J., & Hosseini, H. (2011). Efficiency of the geomorphologic instantaneous unit hydrograph method in flood hydrograph simulation. *CATENA*, *87*(2), 163-171. http://dx.doi.org/10.1016/j.catena.2011.04.005

Khosravi, K., Nohani, E., Maroufinia, E., & Pourghasemi, H. (2016). A GIS-based flood susceptibility assessment and its mapping in Iran: a comparison between frequency ratio and weights-of-evidence bivariate statistical models with multi-criteria decision-making technique. *Natural Hazards*, *83*(2), 947-987. http://dx.doi.org/10.1007/s11069-016-2357-2

Kiczko, A., Romanowicz, R., Osuch, M., & Karamuz, E. (2013). Maximising the usefulness of flood risk assessment for the River Vistula in Warsaw. *Natural Hazards And Earth System Science*, *13*(12), 3443-3455. http://dx.doi.org/10.5194/nhess-13-3443-2013

Kim, Y., Tachikawa, Y., Shiiba, M., Kim, S., Yorozu, K., & Noh, S. (2012). Simultaneous estimation of inflow and channel roughness using 2D hydraulic model and particle filters. *Journal Of Flood Risk Management*, *6*(2), 112-123. http://dx.doi.org/10.1111/j.1753-318x.2012.01164.x

King, H.W., (1918). *Handbook of Hydraulics for the solution of Hydraulic problems*. New York: McGraw-Hill Book Company.

Kirkby, M. J. (1975). Hydrograph modelling strategies. In R. F. Peel, M. D. Chisholm, & P. Haggett (Eds.), *Progress in physical and human geography* (pp. 66–69). London: Heinemann.

Kourgialas, N., & Karatzas, G. (2011). Flood management and a GIS modelling method to assess flood-hazard areas—a case study. *Hydrological Sciences Journal*, *56*(2), 212–225. doi:10.1080/02626667.2011.555836

Kourgialas, N., & Karatzas, G. (2012). A hydro-economic modelling framework for flood damage estimation and the role of riparian vegetation. *Hydrological Processes*, *27*(4), 515-531. http://dx.doi.org/10.1002/hyp.9256

Kourgialas, N., & Karatzas, G. (2014). A hydro-sedimentary modeling system for flash flood propagation and hazard estimation under different agricultural practices. *Natural Hazards And Earth System Science*, *14*(3), 625-634. http://dx.doi.org/10.5194/nhess-14-625-2014

Kourgialas, N., & Karatzas, G. (2016). A flood risk decision making approach for Mediterranean tree crops using GIS; climate change effects and flood-tolerant species. *Environmental Science & Policy*, *63*, 132–142. doi:10.1016/j.envsci.2016.05.020

Kourgialas, N., & Karatzas, G. (2017). A national scale flood hazard mapping methodology: The case of Greece – Protection and adaptation policy approaches. *Science Of The Total Environment*, *601-602*, 441-452. http://dx.doi.org/10.1016/j.scitotenv.2017.05.197

Koutsogiannis, D., and Markonis, I., (2010). *Hydrological analysis of Xerias river basin, Magnesia - Flood works report of Xerias, Seskouliotis and Kakaviotis streams*. Assignments: Magnesia Prefectural Authority, Concessionaire: Mahairas Technical Consultant Company, Athens (in Greek).

Kringer, K. S. (2010). *Geomorphometric Analysis of Airborne Laserscanning data for Soil Mapping in an Alpine Valley Bottom* (MSc Dissertation). Institute of Geography, University of Innsbruck.

Kumar, A. (2015). Geomorphologic Instantaneous Unit Hydrograph Based Hydrologic Response Models for Ungauged Hilly Watersheds in India. *Water Resources Management*, *29*(3), 863-883. http://dx.doi.org/10.1007/s11269-014-0848-z

Kumar, R., Chatterjee, C., Singh, R., Lohani, A., & Kumar, S. (2007). Runoff estimation for an ungauged catchment using geomorphological instantaneous unit hydrograph (GIUH) models. *Hydrological Processes*, *21*(14), 1829-1840. http://dx.doi.org/10.1002/hyp.6318

Kunzler, M., Huggel, C., & Ramírez, J. (2012). A risk analysis for floods and lahars: case study in the Cordillera Central of Colombia. *Natural Hazards*, *64*(1), 767-796. http://dx.doi.org/10.1007/s11069-012-0271-9

Lee, A. H. I., Chen, W.-C., & Chang, C.-J. (2008). A fuzzy AHP and BSC approach for evaluating performance of IT department in the manufacturing industry in Taiwan. *Expert Systems with Applications*, *34*(1), 96–107. doi:10.1016/j.eswa.2006.08.022

Lee, M. C. (2010). The Analytic Hierarchy and the Network Process in Multicriteria Decision Making: Performance Evaluation and Selecting Key Performance Indicators Based on ANP Model. In M. Crisan (Ed.), *Convergence and Hybrid Information Technologies* (pp. 125–148). INTECH.

LISFLOOD-FP (2017). *Bris.ac.uk*. *School of Geographical Sciences. University of Bristol*. Retrieved 18 May 2017, from http://www.bris.ac.uk/geography/research/hydrology/models/lisflood/

Liu, Q., Qin, Y., Zhang, Y., & Li, Z. (2015). A coupled 1D–2D hydrodynamic model for flood simulation in flood detention basin. *Natural Hazards*, *75*(2), 1303-1325. http://dx.doi.org/10.1007/s11069-014-1373-3

Liu, X. (2008). Airborne LiDAR for DEM generation: some critical issues. *Progress In Physical Geography*, 32(1), 31-49. http://dx.doi.org/10.1177/0309133308089496

Liu, X., & Lim, S. (2017). Flood Inundation Modelling for Mid-Lower Brisbane Estuary. *River Research And Applications*, *33*(3), 415-426. http://dx.doi.org/10.1002/rra.3078

Llasat, M., Llasat-Botija, M., Petrucci, O., Pasqua, A., Rosselló, J., Vinet, F., & Boissier, L. (2013). Towards a database on societal impact of Mediterranean floods within the framework of the HYMEX project. *Natural Hazards And Earth System Science*, *13*(5), 1337-1350. http://dx.doi.org/10.5194/nhess-13-1337-2013

Lloyd, S. (1982). Least squares quantization in PCM. *IEEE Transactions on Information Theory*, *28*(2), 129–137. doi:10.1109/tit.1982.1056489

Loukas, A., & Quick, M. (1996). Physically-based estimation of lag time for forested mountainous watersheds. *Hydrological Sciences Journal*, 41(1), 1-19. http://dx.doi.org/10.1080/02626669609491475

Loukas, A., Quick, M., & Russell, S. (1996). A physically based stochastic-deterministic procedure for the estimation of flood frequency. *Water Resources Management*, *10*(6), 415-437. http://dx.doi.org/10.1007/bf00422548

Machiwal, D., Jha, M. K., & Mal, B. C. (2011). Assessment of groundwater potential in a Semi-Arid region of India using remote sensing, GIS and MCDM techniques. *Water Resources Management*, *25*(5), 1359–1386. doi:10.1007/s11269-010-9749-y

Maechler, M., Rousseeuw, P., Struyf, A., Hubert, M., Hornik, K. (2016). *cluster: Cluster Analysis Basics and Extensions*. R package version 2.0.5.

Magnusson, M., Nuchter, A., Lorken, C., Lilienthal, A., & Hertzberg, J. (2009). Evaluation of 3D registration reliability and speed - A comparison of ICP and NDT. 2009 *IEEE International Conference On Robotics And Automation*. http://dx.doi.org/10.1109/robot.2009.5152538

Maimon, O., & Rokach, L. (2005). *Clustering methods, Data Mining and Knowledge Discovery Handbook*. New York: Springer.

Malczewski, J. (2006). GIS-based multicriteria decision analysis: A survey of the literature. *International Journal of Geographical Information Science*, *20*(7), 703–726. doi:10.1080/13658810600661508

Manfreda, S., Di Leo, M., & Sole, A. (2011). Detection of flood-prone areas using digital elevation models. *Journal of Hydrologic Engineering*, *16*(10), 781–790. doi:10.1061/(asce)he.1943-5584.0000367

Marcus, W., Roberts, K., Harvey, L., & Tackman, G. (1992). An Evaluation of Methods for Estimating Manning's n in Small Mountain Streams. *Mountain Research And Development*, 12(3), 227. http://dx.doi.org/10.2307/3673667

MathWorks (2013) *Statistics Toolbox User's Guide*. MATLAB.

McKay, M., Beckman, R., & Conover, W. (1979). Comparison of Three Methods for Selecting Values of Input Variables in the Analysis of Output from a Computer Code. *Technometrics*, 21(2), 239-245. http://dx.doi.org/10.1080/00401706.1979.10489755

McKay, S., & Fischenich, J. (2011). *Robust prediction of hydraulic roughness*. Vicksburg, Miss: US Army Engineer Research and Development Center.

Md Ali, A., Solomatine, D., & Di Baldassarre, G. (2015). Assessing the impact of different sources of topographic data on 1-D hydraulic modelling of floods. *Hydrology And Earth System Sciences*, *19*(1), 631-643. http://dx.doi.org/10.5194/hess-19-631-2015

Merz, B., & Thieken, A. (2005). Separating natural and epistemic uncertainty in flood frequency analysis. *Journal Of Hydrology*, *309*(1-4), 114-132. http://dx.doi.org/10.1016/j.jhydrol.2004.11.015

Meyer, V., Scheuer, S., & Haase, D. (2009). A multicriteria approach for flood risk mapping exemplified at the Mulde river, Germany. *Natural Hazards*, *48*(1), 17–39. doi:10.1007/s11069-008-9244-4

Mikhailov, L. (2003). Deriving priorities from fuzzy pairwise comparison judgements. *Fuzzy Sets and Systems*, *134*(3), 365–385. doi:10.1016/s0165-0114(02)00383-4

Miliani, F., Ravazzani, G., & Mancini, M. (2011). Adaptation of Precipitation index for the estimation of antecedent moisture condition in large mountainous basins. *Journal of Hydrologic Engineering*, *16*(3), 218–227. doi:10.1061/(asce)he.1943-5584.0000307

Millard, S. (2013). *EnvStats: An R Package for Environmental Statistics* (1st ed.). Springer.

Molinari, D., Menoni, S., Aronica, G.T., Ballio, F., Berni, N., & Pandolfo, C. et al. (2014). Ex post damage assessment: an Italian experience. *Natural Hazards And Earth System Science*, *14*(4), 901-916. http://dx.doi.org/10.5194/nhess-14-901-2014

Montanari, A. (2007). What do we mean by 'uncertainty'? The need for a consistent wording about uncertainty assessment in hydrology. *Hydrological Processes*, *21*(6), 841-845. http://dx.doi.org/10.1002/hyp.6623

Mukolwe, M., Baldassarre, G., Werner, M., & Solomatine, D. (2014). Flood modelling: parameterisation and inflow uncertainty. *Proceedings Of The Institution Of Civil Engineers - Water Management*, *167*(1), 51-60. http://dx.doi.org/10.1680/wama.12.00087

Nandi, A., Mandal, A., Wilson, M., & Smith, D. (2016). Flood hazard mapping in Jamaica using principal component analysis and logistic regression. *Environmental Earth Sciences*, *75*(6). http://dx.doi.org/10.1007/s12665-016-5323-0

Neal, J., Fewtrell, T., Bates, P., & Wright, N. (2010). A comparison of three parallelisation methods for 2D flood inundation models. *Environmental Modelling & Software*, *25*(4), 398-411. http://dx.doi.org/10.1016/j.envsoft.2009.11.007

Neal, J., Odoni, N., Trigg, M., Freer, J., Garcia-Pintado, J., Mason, D., Wood, M., & Bates, P. (2015). Efficient incorporation of channel cross-section geometry uncertainty into

regional and global scale flood inundation models. *Journal Of Hydrology*, *529*, 169-183. http://dx.doi.org/10.1016/j.jhydrol.2015.07.026

Neal, J., Schumann, G., & Bates, P. (2012). A subgrid channel model for simulating river hydraulics and floodplain inundation over large and data sparse areas. *Water Resources Research*, *48*(11). http://dx.doi.org/10.1029/2012wr012514

Neelz, S., & Pender, G., (2009). *Desktop Review of 2D Hydraulic Modelling Packages*. DEFRA/Environment Agency, UK. http://evidence.environment-agency.gov.uk/FCERM/Libraries/FCERM_Project_Documents/SC080035_Desktop_review_of_2D_hydraulic_packages_Phase_1_Report.sflb.ashx.

Neelz, S., & Pender, G., (2010). *Benchmarking of 2D Dyfraulic Modelling Packages*. DEFRA/Environment Agency, UK. https://www.gov.uk/government/uploads/system/uploads/attachment_data/file/290884/scho0510bsno-e-e.pdf.

Neelz, S., & Pender, G., (2013). *Benchmarking the Latest Generation of 2D Hydraulic Modelling Packages*. DEFRA/Environment Agency, UK. http://evidence.environment-agency.gov.uk/FCERM/Libraries/FCERM_Project_Documents/SC120002_Benchmarking_2D_hydraulic_models_Report.sflb.ashx.

Negi, P., & Jain, K. (2008). Spatial Multicriteria analysis for siting groundwater polluting industries. *Journal of Environmental Informatics*, *12*(1), 54–63. doi:10.3808/jei.200800124

Ng, R. T., & Han, J. (1994). *Efficient and effective clustering methods for spatial data mining*. 20th International Conference on Very Large Data Bases, Santiago, Chile.

Nguyen, P., Thorstensen, A., Sorooshian, S., Hsu, K., & AghaKouchak, A. (2015). Flood Forecasting and Inundation Mapping Using HiResFlood-UCI and Near-Real-Time Satellite Precipitation Data: The 2008 Iowa Flood. *Journal Of Hydrometeorology*, *16*(3), 1171-1183. http://dx.doi.org/10.1175/jhm-d-14-0212.1

Nock, R., & Nielsen, F. (2006). On weighting clustering. *IEEE Transactions on Pattern Analysis and Machine Intelligence*, *28*(8), 1223–1235. doi:10.1109/tpami.2006.168

Noman, N. S., Nelson, J., & Zundel, A. K. (2001). Review of Automated Floodplain Delineation from Digital Terrain Models. *Journal of Water Resources Planning and Management*, *127*(6), 394–402. doi:10.1061/(ASCE)0733-9496(2001)127:6(394)

Noman, N., Nelson, E., & Zundel, A. (2003). Improved Process for Floodplain Delineation from Digital Terrain Models. *Journal Of Water Resources Planning And Management*, 129(5), 427-436. http://dx.doi.org/10.1061/(asce)0733-9496(2003)129:5(427)

Olaya, V. (2004). *A gentle introduction to SAGA GIS* (1.1 ed.)

Pal, I., Nath, S. K., Shukla, K., Pal, D. K., Raj, A., Thingbaijam, K. K. S., & Bansal, B. K. (2008). Earthquake hazard zonation of Sikkim Himalaya using a GIS platform. *Natural Hazards*, *45*(3), 333–377. doi:10.1007/s11069-007-9173-7

Papagiannaki, K., Lagouvardos, K., & Kotroni, V. (2013). A database of high-impact weather events in Greece: a descriptive impact analysis for the period 2001–2011. *Natural Hazards And Earth System Science*, *13*(3), 727-736. http://dx.doi.org/10.5194/nhess-13-727-2013

Papaioannou, G., & Loukas, A., (2010). Flood inundation mapping uncertainty introduced by topographic data accuracy, geometric configuration and modeling approach. *EGU General Assembly*, 02-07 May 2010, Vienna, Austria. Geophysical Research Abstracts, 12. EGU2010-14805.

Papaioannou, G., Loukas, A., & Georgiadis, C. (2013). The effect of riverine terrain spatial resolution on flood modeling and mapping. *First International Conference On Remote Sensing And Geoinformation Of The Environment (Rscy2013)*, *SPIE Proceedings, 8795*. http://dx.doi.org/10.1117/12.2028218

Papaioannou, G., Loukas, A., Vasiliades, L., & Aronica, G.T. (2016). Flood inundation mapping sensitivity to riverine spatial resolution and modelling approach. *Natural Hazards*, *83*(S1), 117-132. http://dx.doi.org/10.1007/s11069-016-2382-1

Papaioannou, G., Loukas, A., Vasiliades, L., & Aronica, G.T., (2011). Flood prone areas mapping through GIS and Multi-Criteria Analysis, *EGU Leonardo Conference: Floods in 3D: Processes, Patterns, Predictions*, 23-25 November 2011, Bratislava, Slovakia.

Papaioannou, G., Vasiliades, L., & Loukas, A. (2015). Multi-Criteria Analysis Framework for Potential Flood Prone Areas Mapping. *Water Resources Management*, *29*(2), 399-418. http://dx.doi.org/10.1007/s11269-014-0817-6

Papaioannou, G., Vasiliades, L., Loukas, A., & Aronica, G.T. (2017). Probabilistic flood inundation mapping at ungauged streams due to roughness coefficient uncertainty in hydraulic modelling. *Advances In Geosciences*, *44*, 23-34. http://dx.doi.org/10.5194/adgeo-44-23-2017

Pappenberger, F., & Beven, K. (2006). Ignorance is bliss: Or seven reasons not to use uncertainty analysis. *Water Resources Research*, 42(5). http://dx.doi.org/10.1029/2005wr004820

Pappenberger, F., Beven, K., Horritt, M., & Blazkova, S. (2005). Uncertainty in the calibration of effective roughness parameters in HEC-RAS using inundation and downstream level observations. *Journal Of Hydrology*, *302*(1-4), 46-69. http://dx.doi.org/10.1016/j.jhydrol.2004.06.036

Park, S., Choi, C., Kim, B., & Kim, J. (2013). Landslide susceptibility mapping using frequency ratio, analytic hierarchy process, logistic regression, and artificial neural network methods at the Inje area, Korea. *Environmental Earth Sciences*, *68*(5), 1443–1464. doi:10.1007/s12665-012-1842-5

Parry, M., Canziani, O., Palutikof, J., van der Linden, P., & Hanson, C. (2007). *Climate change 2007 - impacts, adaptation and vulnerability - Contribution of Working Group II to the Fourth Assessment Report of the Intergovernmental Panel on Climate Change.* (1st ed., p. 976). New York: Cambridge Univ Press.

Pawattana, C., & Tripathi, N. K. (2008). Analytical hierarchical process (AHP)-based flood water retention planning in Thailand. *GIScience & Remote Sensing*, *45*(3), 343–355. doi:10.2747/1548-1603.45.3.343

Polyworks, (2007). PolyWorks® V10 Beginner's Guide. InnovMetric Software Inc. Retrieved from: https://www.unavco.org/projects/project-support/polar/support/TLS/PolyWorksBeginnersGuide.pdf

Qi, H., Qi, P., & Altinakar, M. (2013). GIS-Based Spatial Monte Carlo Analysis for Integrated Flood Management with Two Dimensional Flood Simulation. *Water Resources Management*, *27*(10), 3631-3645. http://dx.doi.org/10.1007/s11269-013-0370-8

Quinn, P., Beven, K., Chevallier, P., & Planchon, O. (1991). The prediction of hillslope flow paths for distributed hydrological modelling using digital terrain models. *Hydrological Processes*, *5*(1), 59–79. doi:10.1002/hyp.3360050106

R Core Team (2017). R: A language and environment for statistical computing. R Foundation for Statistical Computing, Vienna, Austria. URL https://www.R-project.org/.

Radmehr, A., & Araghinejad, S. (2015). Flood Vulnerability Analysis by Fuzzy Spatial Multi Criteria Decision Making. *Water Resources Management*, *29*(12), 4427-4445. http://dx.doi.org/10.1007/s11269-015-1068-x

Rahmati, O., Zeinivand, H., & Besharat, M. (2016). Flood hazard zoning in Yasooj region, Iran, using GIS and multi-criteria decision analysis. *Geomatics, Natural Hazards And Risk*, *7*(3), 1000-1017. http://dx.doi.org/10.1080/19475705.2015.1045043

Razali, N., & Wah, Y. (2011). Power comparisons of Shapiro-Wilk, Kolmogorov-Smirnov, Lilliefors and Anderson-Darling tests. *Journal Of Statistical Modeling And Analytics*, *2*(1), 21-33.

Renard, K. G., & Freimund, J. R. (1994). Using monthly precipitation data to estimate the r-factor in the revised USLE. *Journal of Hydrology*, *157*(1-4), 287–306. doi:10.1016/0022-1694(94)90110-4

Resource Assessment Commission (RAC) (1992). *Multi-criteria analysis as a resource assessment tool*. Canberra: Published for the Resource Assessment Commission by the Australian Govt. Pub. Service.

Rodríguez-Iturbe, I., & Valdés, J. (1979). The geomorphologic structure of hydrologic response. *Water Resources Research*, *15*(6), 1409-1420. http://dx.doi.org/10.1029/wr015i006p01409

Roe, P. (1981). Approximate Riemann solvers, parameter vectors, and difference schemes. *Journal Of Computational Physics*, *43*(2), 357-372. http://dx.doi.org/10.1016/0021-9991(81)90128-5

Romanowicz, R., & Kiczko, A. (2016). An event simulation approach to the assessment of flood level frequencies: risk maps for the Warsaw reach of the River Vistula. *Hydrological Processes*, 30(14), 2451-2462. http://dx.doi.org/10.1002/hyp.10857

Romero, C., & Rehman, T. (1987). Natural resource management and the use of multiple criteria decision-making techniques: A review. *European Review of Agricultural Economics*, *14*(1), 61–89. doi:10.1093/erae/14.1.61

Romero, M., Revollo, N., & Molina, J. (2010). Flow resistance in steep mountain rivers in Bolivia. *Journal Of Hydrodynamics*, Ser. B, 22(5), 702-707. http://dx.doi.org/10.1016/s1001-6058(10)60018-2

Rutkowska, A., Kohnová, S., Banasik, K., Szolgay, J., & Karabová, B. (2015). Probabilistic properties of a curve number: A case study for small polish and Slovak Carpathian basins. *Journal of Mountain Science*, *12*(3), 533–548. doi:10.1007/s11629-014-3123-0

Saaty, R. W. (1987). The analytic hierarchy process—what it is and how it is used. *Mathematical Modelling*, *9*(3-5), 161–176. doi:10.1016/0270-0255(87)90473-8

Saaty, T. L. (1980). *The analytic hierarchy process: Planning setting priorities, resource allocation* (2nd ed.). New York: McGraw-Hill International Book Co.

Saaty, T. L. (1986). Axiomatic foundation of the analytic hierarchy process. *Management Science*, *32*(7), 841–855. doi:10.1287/mnsc.32.7.841

Samantaray, D., Chatterjee, C., Singh, R., Gupta, P., & Panigrahy, S. (2014). Flood risk modeling for optimal rice planning for delta region of Mahanadi river basin in India. *Natural Hazards*, *76*(1), 347-372. http://dx.doi.org/10.1007/s11069-014-1493-9

Sampson, C., Fewtrell, T., Duncan, A., Shaad, K., Horritt, M., & Bates, P. (2012). Use of terrestrial laser scanning data to drive decimetric resolution urban inundation models. *Advances In Water Resources*, 41, 1-17. http://dx.doi.org/10.1016/j.advwatres.2012.02.010

Sarhadi, A., Soltani, S., & Modarres, R. (2012). Probabilistic flood inundation mapping of ungauged rivers: Linking GIS techniques and frequency analysis. *Journal Of Hydrology*, 458-459, 68-86. http://dx.doi.org/10.1016/j.jhydrol.2012.06.039

Sharma, M., Paige, G., & Miller, S. (2010). DEM Development from Ground-Based LiDAR Data: A Method to Remove Non-Surface Objects. *Remote Sensing*, 2(11), 2629-2642. http://dx.doi.org/10.3390/rs2112629

Shen, D., Wang, J., Cheng, X., Rui, Y., & Ye, S. (2015). Integration of 2-D hydraulic model and high-resolution lidar-derived DEM for floodplain flow modeling. *Hydrology And Earth System Sciences*, *19*(8), 3605-3616. http://dx.doi.org/10.5194/hess-19-3605-2015

Sithole, G., & Vosselman, G. (2004). Experimental comparison of filter algorithms for bare-Earth extraction from airborne laser scanning point clouds. *ISPRS Journal Of Photogrammetry And Remote Sensing*, 59(1-2), 85-101. http://dx.doi.org/10.1016/j.isprsjprs.2004.05.004

Smith, R.H., (1978). Development of a Flood Routing Model for Small Meandering Rivers, *Ph.D. Dissertation*, Department of Civil Engineering, University of Missouri at Rolla, MO.

Soil Conservation Service (SCS). (1956). *Hydrology, National Engineering Handbook, Section 4*. Washington, D.C.: Soil Conservation Service, U.S.D.A..

Solomatine, D., & Shrestha, D. (2009). A novel method to estimate model uncertainty using machine learning techniques. *Water Resources Research*, *45*(12). http://dx.doi.org/10.1029/2008wr006839

Sowmya, K., John, C., & Shrivasthava, N. (2015). Urban flood vulnerability zoning of Cochin City, southwest coast of India, using remote sensing and GIS. *Natural Hazards*, *75*(2), 1271-1286. http://dx.doi.org/10.1007/s11069-014-1372-4

Special Secretariat for Water, Ministry of Environment, Energy and Climate Change (SSW-MEECC) (2012). *Preliminary assessment of the flood directive*. Athens: Ministry of Ministry of Environment, Energy and Climate Change Retrieved from http://www.ypeka.gr/LinkClick.spx?fileticket=T4DDG1hqQMY%3d&tabid=252&language=el-GR

Stefanidis, S., & Stathis, D. (2013). Assessment of flood hazard based on natural and anthropogenic factors using analytic hierarchy process (AHP). *Natural Hazards*, *68*(2), 569–585. doi:10.1007/s11069-013-0639-5

Stelling, G. (1983). *On the construction of computational methods for shallow water flow problems*. *Ph.D. Dissertation*, Applied Sciences, TU DELFT.

Syme, W. (1991). *Dynamically Linked Two-Dimensional / One-Dimensional Hydrodynamic Modelling Program for Rivers, Estuaries and Coastal Waters* (M.Eng.Sc Dissertation). Department of Civil Engineering, The University of Queensland.

Syme, W. (2001). TUFLOW – *Two & one - dimensional Unsteady FLOW Software for Rivers, Estuaries and Coastal Waters*. Sydney: IEAust Water Panel Workshop on 2D Models.

Tagil, S., & Jenness, J. (2008). GIS-Based automated Landform classification and topographic, Landcover and geologic attributes of Landforms around the Yazoren Polje, turkey. *Journal of Applied Sciences*, *8*(6), 910–921. doi:10.3923/jas.2008.910.921

Tang, Z., Yi, S., Wang, C., & Xiao, Y. (2017). Incorporating probabilistic approach into local multi-criteria decision analysis for flood susceptibility assessment. *Stochastic Environmental Research And Risk Assessment*. http://dx.doi.org/10.1007/s00477-017-1431-y

Tehrany, M. S., Pradhan, B., & Jebur, M. N. (2013). Spatial prediction of flood susceptible areas using rule based decision tree (DT) and a novel ensemble bivariate and multivariate statistical models in GIS. *Journal of Hydrology*, *504*, 69–79. doi:10.1016/j.jhydrol.2013.09.034

Teng, J., Jakeman, A., Vaze, J., Croke, B., Dutta, D., & Kim, S. (2017). Flood inundation modelling: A review of methods, recent advances and uncertainty analysis. *Environmental Modelling & Software*, *90*, 201-216. http://dx.doi.org/10.1016/j.envsoft.2017.01.006

Teng, J., Vaze, J., Dutta, D., & Marvanek, S. (2015). Rapid Inundation Modelling in Large Floodplains Using LiDAR DEM. *Water Resources Management*, *29*(8), 2619-2636. http://dx.doi.org/10.1007/s11269-015-0960-8

Thurstone, L. L. (1927). A law of comparative judgements. *Psychological Reviews*, *34*(4), 273–286. doi:http://dx.doi.org/10.1037/h0070288

Ticehurst, C., Dutta, D., Karim, F., Petheram, C., & Guerschman, J. (2015). Improving the accuracy of daily MODIS OWL flood inundation mapping using hydrodynamic modelling. *Natural Hazards*, *78*(2), 803-820. http://dx.doi.org/10.1007/s11069-015-1743-5

Tramblay, Y., Bouvier, C., Martin, C., Didon-Lescot, J., Todorovik, D., & Domergue, J. (2010). Assessment of initial soil moisture conditions for event-based rainfall–runoff modelling. *Journal Of Hydrology*, *387*(3-4), 176-187. http://dx.doi.org/10.1016/j.jhydrol.2010.04.006

Trigg, M., Wilson, M., Bates, P., Horritt, M., Alsdorf, D., Forsberg, B., & Vega, M. (2009). Amazon flood wave hydraulics. *Journal Of Hydrology*, *374*(1-2), 92-105. http://dx.doi.org/10.1016/j.jhydrol.2009.06.004

Tsakiris, G. (2014). Flood risk assessment: concepts, modelling, applications. *Natural Hazards And Earth System Science*, *14*(5), 1361-1369. http://dx.doi.org/10.5194/nhess-14-1361-2014

Tsakiris, G., & Bellos, V. (2014). A Numerical Model for Two-Dimensional Flood Routing in Complex Terrains. *Water Resources Management*, 28(5), 1277-1291. http://dx.doi.org/10.1007/s11269-014-0540-3

Tsakiris, G., Nalbantis, I., & Pistrika, A. (2009). Critical Technical Issues on the EU Flood Directive. *European Water*, 25/26, 39-51. Retrieved from http://www.ewra.net/ew/pdf/EW_2009_25-26_04.pdf

Tsubaki, R., & Fujita, I. (2010). Unstructured grid generation using LiDAR data for urban flood inundation modelling. *Hydrological Processes*, *24*(11), 1404-1420. http://dx.doi.org/10.1002/hyp.7608

Tung, Y. & Yen, B. C., (1993). Some recent progress in uncertainty analysis for hydraulic design. In B. C. Yen and Y. Tung, *Reliability and uncertainty analyses in hydraulic design* (1st ed., pp. 17-34). New York, N.Y.: American Society of civil engineers.

Ugarte, A., & Madrid-Aris, M. (1994). Roughness Coefficient in mountain river. In G. Cotroneo & R. Rumer, *Hydraulic Engineering '94 Volume1.* (1st ed., pp. 652–656). New York: American Society of Civil Engineers.

USDA-SCS (1985): *National Engineering Handbook, Section 4, Hydrology*, Washington, DC: USDA.

van Laarhoven, P. J. M., & Pedrycz, W. (1983). A fuzzy extension of Saaty's priority theory. *Fuzzy Sets and Systems*, *11*(1-3), 229–241. doi:10.1016/s0165-0114(83)80082-7

Venables, W., & Ripley, B. (2002). *Modern applied statistics with S* (1st ed.). New York: Springer.

Vosselman, G., & Maas, H. (2014). *Airborne and Terrestrial Laser Scanning*. Dunbeath: Whittles Publishing.

Vozinaki, A., Karatzas, G., Sibetheros, I., & Varouchakis, E. (2015). An agricultural flash flood loss estimation methodology: the case study of the Koiliaris basin (Greece), February 2003 flood. *Natural Hazards*, *79*(2), 899-920. http://dx.doi.org/10.1007/s11069-015-1882-8

Ward, A., Trimble, S., Burckhard, S., & Lyon, J. (2016). *Environmental hydrology* (3rd ed.). Boca Raton: CRC Press.

Weiss, A. (2001). *Topographic position and landforms analysis*. ESRI User Conference, San Diego, CA.

Wen, L., Macdonald, R., Morrison, T., Hameed, T., Saintilan, N., & Ling, J. (2013). From hydrodynamic to hydrological modelling: Investigating long-term hydrological regimes

of key wetlands in the Macquarie Marshes, a semi-arid lowland floodplain in Australia. *Journal Of Hydrology*, *500*, 45-61. http://dx.doi.org/10.1016/j.jhydrol.2013.07.015

Werner, M. (2004). A comparison of flood extent modelling approaches through constraining uncertainties on gauge data. *Hydrology And Earth System Sciences*, *8*(6), 1141-1152. http://dx.doi.org/10.5194/hess-8-1141-2004

Werner, M., Hunter, N., & Bates, P. (2005). Identifiability of distributed floodplain roughness values in flood extent estimation. *Journal Of Hydrology*, 314(1-4), 139-157. http://dx.doi.org/10.1016/j.jhydrol.2005.03.012

Xiao, Y., Yi, S., & Tang, Z. (2017). Integrated flood hazard assessment based on spatial ordered weighted averaging method considering spatial heterogeneity of risk preference. *Science Of The Total Environment*, *599-600*, 1034-1046. http://dx.doi.org/10.1016/j.scitotenv.2017.04.218

XP2d. (2017). *Xpsolutions.com / XP2d Manual*. Retrieved 19 May 2017, from http://xpsolutions.com/assets/dms/xp2d_manual.pdf

XPSTORM. (2017a). *http://xpsolutions.com*. Retrieved 10 May 2017, from http://xpsolutions.com/assets/dms/xpstorm-tech-desc.pdf

XPSTORM. (2017b). *Analytical Engine - xpswmm/xpstorm Resource Center - XP Solutions Resource Center*. *Help.xpsolutions.com*. Retrieved 10 May 2017, from https://help.xpsolutions.com/display/xps/Analytical+Engine

Yair, Y., Lynn, B., Price, C., Kotroni, V., Lagouvardos, K., Morin, E., Mugnai, A., & Llasat, M. (2010). Predicting the potential for lightning activity in Mediterranean storms based on the Weather Research and Forecasting (WRF) model dynamic and microphysical fields. *Journal Of Geophysical Research*, *115*(D4). http://dx.doi.org/10.1029/2008jd010868

Yalcin, A., & Bulut, F. (2007). Landslide susceptibility mapping using GIS and digital photogrammetric techniques: A case study from Ardesen (nE-turkey). *Natural Hazards*, *41*(1), 201–226. doi:10.1007/s11069-006-9030-0

Yang, Y., & Huang, S. (2007). Image segmentation by Fuzzy C-means clustering algorithm with a novel penalty term. *Computing and Informatics*, *26*(1), 17–31.

Yazdi, J., & Salehi Neyshabouri, S. (2012). A Simulation-Based Optimization Model for Flood Management on a Watershed Scale. *Water Resources Management*, *26*(15), 4569-4586. http://dx.doi.org/10.1007/s11269-012-0167-1

Younis, J., Anquetin, S., & Thielen, J. (2008). The benefit of high-resolution operational weather forecasts for flash flood warning. *Hydrology And Earth System Sciences*, *12*(4), 1039-1051. http://dx.doi.org/10.5194/hess-12-1039-2008

Zhou, X. (2012). Fuzzy Analytical Network Process Implementation with Matlab. In V. N. Katsikis (Ed.), *MATLAB - A Fundamental Tool for Scientific Computing and Engineering Applications - Volume 3* (pp. 133–160). INTECH.

Zou, Q., Zhou, J., Zhou, C., Song, L., & Guo, J. (2013). Comprehensive flood risk assessment based on set pair analysis-variable fuzzy sets model and fuzzy AHP. *Stochastic Environmental Research and Risk Assessment*, *27*(2), 525–546. doi:10.1007/s00477-012-0598-5